THE BEHAVIOUR OF COMPOSITE WALLS WITH PROFILED STEEL SHEETING

A DISSERTATION SUBMITTED TO THE DEPARTMENT OF CIVIL ENGINEERING AND THE COMMITTEE FOR POSTGRADUATE STUDIES OF THE UNIVERSITY OF STRATHCLYDE, GLASGOW, IN PARTIAL FULFILMENT OF THE REQUIREMENTS FOR THE DEGREE OF DOCTOR OF PHILOSOPHY

By

Stewart Craik Gallocher

1993

I certify that I have read this thesis and that in my opinion it is fully adequate, in scope and in quality, as a dissertation for the degree of Doctor of Philosophy.

(Principal Adviser)

I certify that I have read this thesis and that in my opinion it is fully adequate, in scope and in quality, as a dissertation for the degree of Doctor of Philosophy.

I certify that I have read this thesis and that in my opinion it is fully adequate, in scope and in quality, as a dissertation for the degree of Doctor of Philosophy.

Approved for the University Committee on Graduate Studies:

Dean of Graduate Studies and Research

Abstract

During the 1980's the application of composite slabs with profiled steel decking grew rapidly replacing reinforced concrete flooring systems. Reductions in construction time and costs assisted in this rapid shift in building practice away from more traditional methods towards the currently popular "Fastrack" construction. It is therefore a logical extension to investigate the possible use of profiled steel decking as composite walling.

This thesis investigates the possible application of double-skin composite walls with a concrete core through experimental and theoretical studies of the behaviour. The experimental investigations focus on a series of four full-scale pilot tests where the performance at the wet concrete stage before curing and the behaviour under a concentric axial load is studied. Various boundary and end reinforcement details are tried. Analytical equations based on one-dimensional analysis techniques are derived to give linear elastic solutions to the stresses and strains formed in each layer. The critical buckling load is also calculated. Further materially non-linear equations including the P-Δ effect are generated.

The profiled steel sheeting is shown to be effective formwork, resisting the lateral pressures developed by the wet concrete.

The critical nature of the interface bond behaviour between the steel and concrete faces is shown to be of prime importance in determining the axial capacity of the walls. Local buckling of the steel sheeting is considered of secondary importance being easier to predict and control.

The problems associated with the possible design of double-skin composite walls are discussed concluding that the axial capacity at present should be based on the capacity of the concrete alone. Further research directions are also outlined.

Acknowledgements

I would like to thank my supervisor, Professor Howard Wright, for his support and encouragement throughout this project. His guidance and encouragement were invaluable in focusing the project on achievable goals.

I also greatly appreciate the contributions of the technical staff whose helpful and practical assistance enabled the smooth running of the laboratory experiments.

Finally, I would like to thank my family, for their moral and financial support throughout the 'whole' period of my studies.

Contents

Notation

Unless otherwise stated the following notation applies

A_1 area of lower steel sections

A_2 area of concrete section

A_3 area of upper steel section

A_r area of bar reinforcement

E_1 Young's modulus for steel sections

E_2 Young's Modulus for concrete section

I_1 second moment of area of steel sections

I_2 second moment of area of concrete section

k linear elastic slip constant

L length of beam/column

M_1 moment in the lower steel

M_2 moment in the central concrete

M_3 moment in the upper steel

N_1 force in the lower steel

N_2 force in the central concrete

N_3 force in the upper steel

P axial point load

p udl loading on the element

r distance from steel to concrete centroid

r_1 distance from lower steel to concrete centroid

r_2 distance from upper steel to concrete centroid

r_b distance from bar reinforcement to concrete centroid

d_1 depth of lower steel

d_2 depth of concrete

d_3 depth of upper steel

u_1 axial displacement of the lower steel

u_2 axial displacement of the concrete

u_3 axial displacement of the upper steel

ε_1 axial strain of lower steel

ε_2 axial strain of concrete

ε_3 axial strain of upper steel

Δu_1 horizontal interface slip between lower steel and concrete

Δu_2 horizontal interface slip between upper steel and concrete

w_1 displacement of lower steel in the z direction

w_2 displacement of central concrete in the z direction

w_3 displacement of upper steel in the z direction

w displacement of element in the z direction

γ_1 variable modelling the axial displacements

γ_2 variable modelling the bending displacements

ΣEI_o $2E_1I_1+E_2I_2$ non-composite bending stiffness

EI_∞ $\Sigma EI_c+2r^2E_1A_1$ fully composite bending stiffness

$\sigma(\Delta u)$ non-linear interface stress-slip relationship

b breadth of interface connection

ε_b strain in lower concrete fibre

h distance from lower concrete fibre, or depth of form (m)

$\sigma_1(\varepsilon)$ steel stress/strain function

$\sigma_2(\varepsilon)$ concrete stress/strain function

σ_r bar reinforcement stress/strain relationship

n_i number of divisions of layer i

Chapter 1 General Introduction

1.1 The Concept of Composite Walling

The development of composite walling using profiled steel sheeting, is a logical progression from the current popular and economic use of profiled steel sheets in floors.

Since the early 1980's the use of composite slabs in the construction industry has grown rapidly, replacing traditional reinforced concrete flooring systems. For the historical development the reader is referred to papers by Viest (1960), Schuster (1976) and more recently Wright (1987). Their present widespread popularity in "Fastrack" construction arises from the advantages of this type of construction:

- **Decreased construction time.** The decking can be quickly installed (approximately 800m^2 per person per day) and easily poured, providing a temporary working platform that eliminates or reduces the need for temporary supports.

- **Reinforcement.** The decking acts as tensile reinforcement on the soffit of the slab, reducing substantially the overall requirements. The mesh reinforcement normally required can be easily fixed in position.

- **Services.** The geometry of the re-entrant decking ribs allows simple installation of suspended ceilings and ventilation.

- **Wind Bracing.** Once the decking is fixed in position it provides plan stability to the frame.

- **Weight Reductions.** Composite slabs are normally lighter than the equivalent reinforced flooring providing savings in material, and reductions

in foundation and column costs.

The decking geometries can be divided into two types, those possessing re-entrant ribs and those with trapezoidal ribs (see figure 1.1). The thickness of the decks range from 0.75mm to 1.5mm protected on both faces by a 20 micron zinc coating.

A number of the decks are also provided with embossments, pressed into the surface of the ribs and upper flanges, which provide longitudinal shear resistance at the steel concrete interface (see figure 1.2). The embossments should in all cases project into the concrete.

Composite Slabs are most commonly used in multi-storey steel-framed buildings although they may be incorporated in concrete, masonry or wood framed structures. They are normally located internally where corrosion is unlikely to occur under normal conditions. Maximum spans range from 2m to over 4m with deep profiles or where temporary supports are provided.

Based on these advantages a system of composite walling has therefore been proposed utilising two layers of profiled steel sheeting infilled with concrete to provide a load bearing element. The basic system is illustrated in figure 1.3.

The external profiled steel sheets act as permanent formwork reducing the need for extensive temporary formwork during construction and casting of the composite wall. Temporary vertical supports and transverse intermediate ties may be required depending on the height of wall. The vertical spacing of the ties will depend on the bending resistance of the sheeting to lateral loading.

Once the concrete has cured the ties and supports can be removed and the steel sheets may act with the concrete to form a composite section. To ensure a composite interaction at the steel concrete interface embossments may be used to prevent premature failure.

The advantages of this system are thought similar to those of composite slabs

- Temporary formwork avoided and formwork reduced.
- Internal bar reinforcement and its fixing avoided.
- The profiling of the steel sheets results in less concrete required for the same inertia, with a consequential weight saving, especially where slenderness is a factor.
- The sheeting allows simple fixing of support brackets and finishing panels.
- Overall construction costs, as in composite slabs are reduced.
- Before casting the steel sheets will supply in-plane shear resistance.

There are some disadvantages that may affect the performance and feasibility of this composite walling system such as fire resistance and corrosion but these are considered avoidable by suitable protection and finishes.

The application of such systems are, for instance, in shear walls for steel framed buildings to provide lateral stability and in blast resistance, stopping spalling of concrete when impact occurs.

1.2 Aims of Thesis

It is the intention of this thesis to investigate the wet concrete and ultimate axial behaviour of composite walls where cold formed steel sheets are provided as permanent formwork and external reinforcement. The particular aspects of behaviour requiring close attention are the interface bond behaviour under axial compression, the resistance of the steel sheets to lateral concrete pressure and whether the walls may be designed according to the current codes of practice. It is hoped that the walls may be shown to provide similar benefits to composite flooring systems.

The design and construction of a loading frame built in the Heavy Structures Laboratory of Strathclyde University is given in Chapter 2. The frame has been

constructed to provide an axial capacity of 3000kN capable of crushing the four full-scale composite walls. Different arrangements were investigated and accepted, or rejected, based on the flexibility and cost effectiveness of the particular design.

The lateral pressure developed behind the steel sheets during casting of the composite walls, and the profile deflections are described in Chapter 3. A full review of the major research and code recommendations is also discussed with a comparison between the current recommendations and the test results.

After curing of the walls the axial capacity under concentric axial loading was determined with measurements taken of the resulting strains and deflections up to failure. Chapter 4 describes these experimental investigations along with a review of associated work. It should be noted that, at present, little research has been carried out on the performance of composite structures with external cold formed steel sheets.

In parallel with the experimental work analytic and numerical studies were performed to model the behaviour of the composite walls under various loading conditions. In Chapter 5 analytic equations are derived and studied to investigate the response of the composite walls with partial interaction including the second-order P-Δ effect and assuming linear material properties. This work focuses on the critical buckling load of the walls and the load transfer at the boundaries of the walls.

The limitations of assuming a linear material response and the complicated response at the interface observed in the results from Chapter 5 led to the development of a finite difference model described in Chapter 6. Previous work by various authors applying various approaches is reviewed. The one-dimensional model assumed non-linear material, steel and interface behaviour with inclusion of the P-Δ effect in the analysis. The Double Skin Composite Wall (DSCW) model, coded in Pascal, is validated by comparison with the analytic results of Chapter 5, and other simple

linear cases.

In Chapter 7 the performance of non-linear material and interface models are verified by comparison to tests on double skin composite beams, columns and beam/columns. A study is then performed on the axial behaviour of the composite walls with several types of interface model.

Chapter 8 has a review of composite column design with some additional recommendations for the design of double skin composite columns at the connections and in slender situations.

In Chapter 9 a design method, based on the information from the ultimate tests, analytic studies and numerical work, is proposed for the design of the composite walls. These design proposals were devised, wherever possible, to be in accordance with the methods of the current code of practice BS 8110.

Chapter 10 summarises the major finding of the thesis and the feasibility of applying composite walls in modern construction projects.

1.3 Research Funding

Finances to study the series of four full-scale pilot tests were provided by the Steel Construction Institute (SCI) in order to experimentally investigate the wet concrete and ultimate axial behaviour of composite walls.

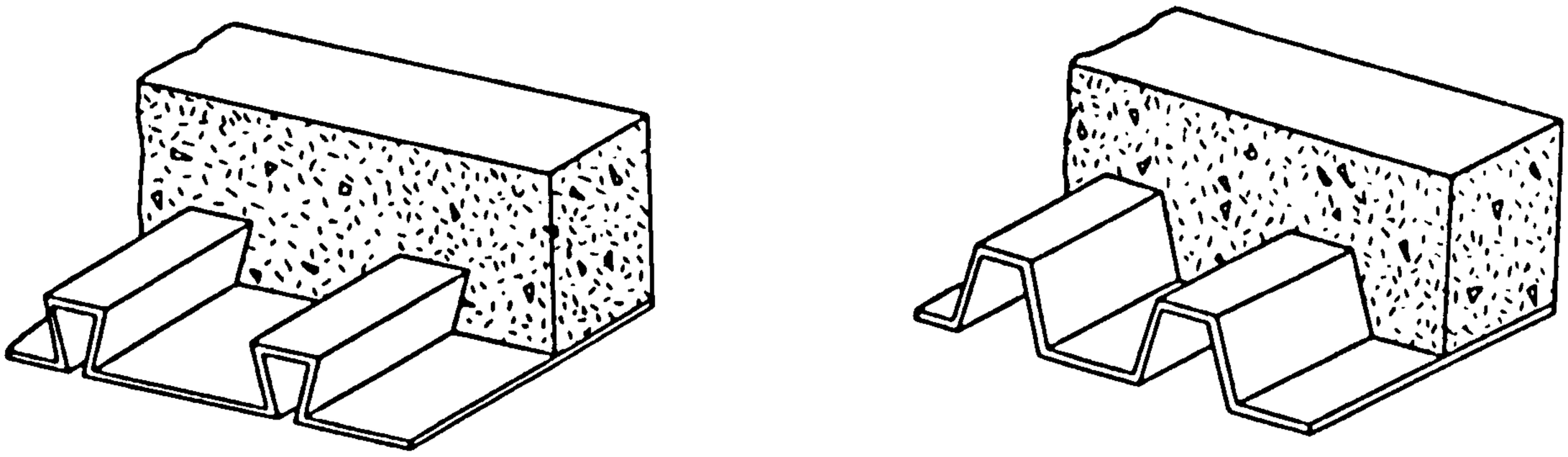

Figure 1.1 Re-entrant and Trapezoidal Rib Geometries

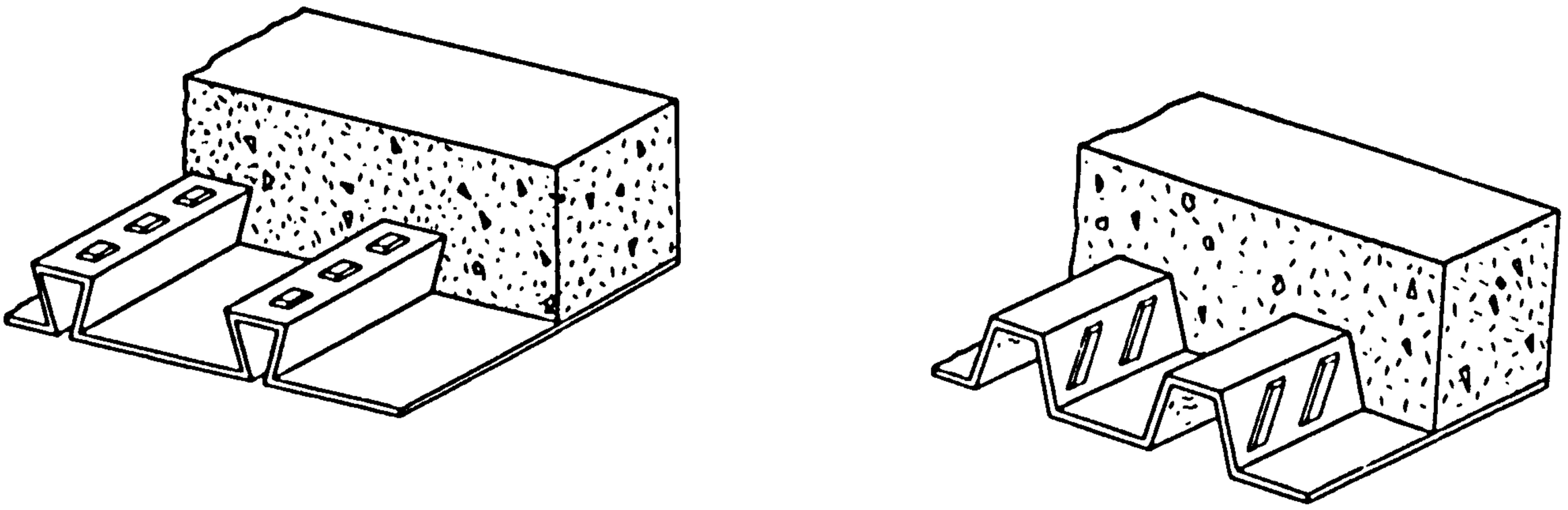

Figure 1.2 Embossment Details

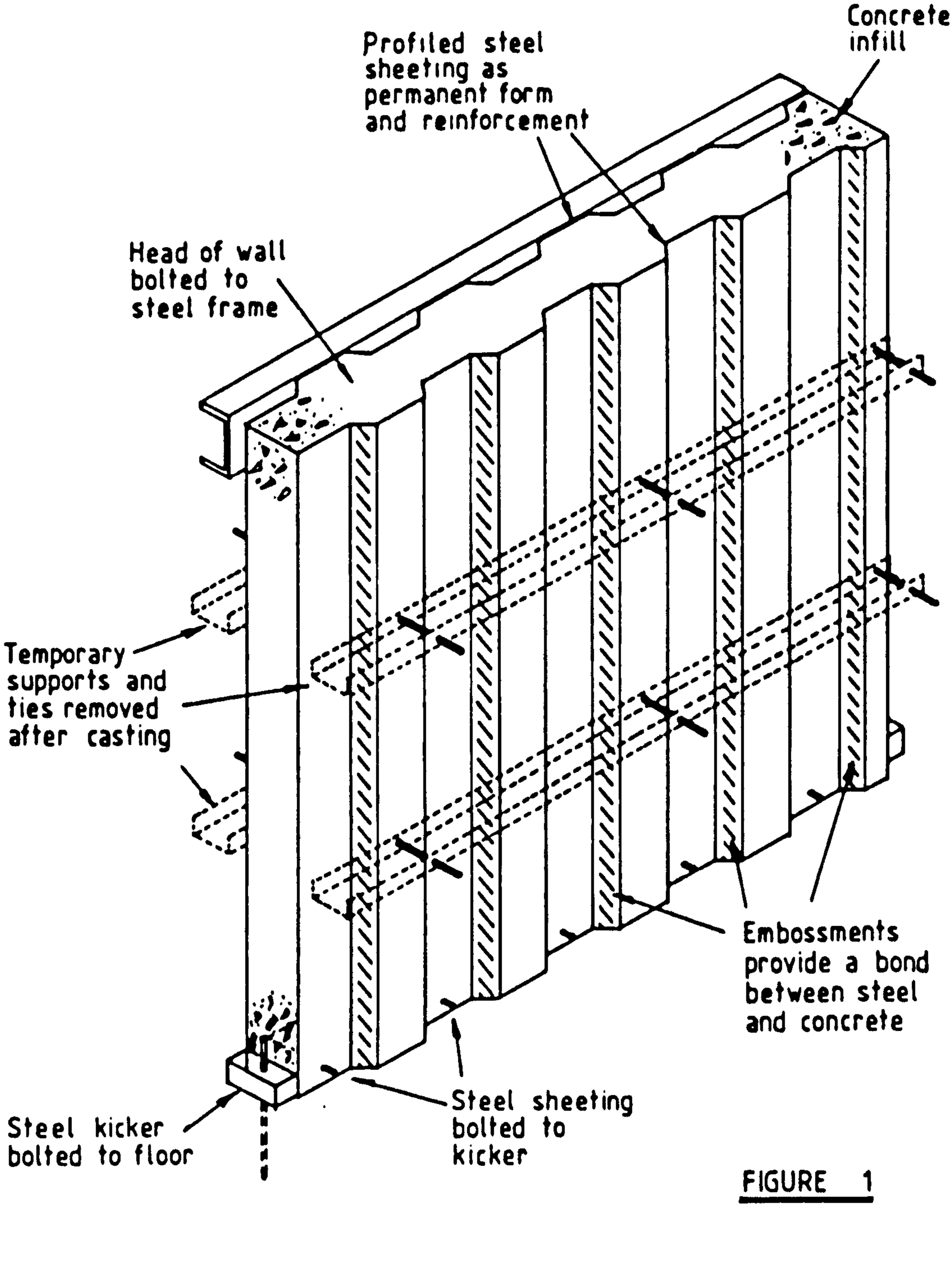

FIGURE 1

Figure 1.3 Basic Composite Walling System

Chapter 2 Design of Loading Frame

2.1 Introduction

The design of the loading frame required early attention in order to allow the experimental investigation to proceed on schedule.

The Heavy Structures Laboratory located in the Anderson Building at Strathclyde University already possessed a loading rig capable of applying a 500kN compressive load to specimens. Unfortunately, the project funded by the Steel Construction Institute (SCI) required the testing of four full-scale walls with an estimated maximum axial capacity of 2700kN. It was therefore necessary to consider the construction of a new loading frame in the laboratory capable of supplying sufficient axial load to fail the walls.

Various configurations were considered for the loading frame with each subjected to a critical analysis primarily based on cost, performance and adaptability for future requirements.

2.2 Specification of Loading Frame

Three major design criteria were required to be incorporated in the loading frame.

The first criteria was that the frame be capable of supplying an axial load of 3000kN to the test specimen. This allowed the composite walls of cross-section approximately 1000mm x 150mm to be failed in the subsequent ultimate tests with sufficient capacity for other types of experiments, such as push-out test on shear studs.

As the heavy structures laboratory floor could only sustain an imposed load of 100kN/m^2 it was also necessary that the frame be self straining, imposing no direct loading on the laboratory floor. The load would be supplied by specified number of

hydraulic jacks and measured by a similar number of loads cells.

The second criteria related to the dimesions of the rig. The plan width was specified as 2m without any restriction on the length, as the frame would consist of detachable bays. The maximum specimen height in the rig was not to exceed approximately 6.5m for overhead travelling crane clearance and for safe access adjustments. This height would permit a study on the effects of slenderness of composite walls.

The third criteria was that the loading frame be allowed to separate into a number of bays in order to test long sections.

2.3 Costs

An initial investigation showed the largest equipment costs were in the purchasing and fabrication of the steelwork, the hydraulic jacks, the load cells and the high pressure cabling. As the total cost of the loading frame was restricted to approximately £15,000, this imposed severe restrictions on the choice of design for the loading frame. In order to control costs section sizes were frequently standardized in the designs proposals, reducing the overall cost. To reduce the cost of the hydraulic jacks spring and gravity return as well as more expensive push-pull systems were considered.

2.4 Design Alternatives

Different systems of applying load to the composite walls were proposed before a choice of loading frame was finalised. The main selection criteria were the total cost and flexibility of the loading frame.

The design alternatives considered differed in

a. **Individual Member Construction**

It was possible for the loading frame to be assembled from plate girders or

universal sections. Employing plate girders reduced the overall depth of the members, by increasing web thickness, with a corresponding rise in the maximum element height tested in the loading frame. The major drawback was the rise in fabrication cost compared to frames with universal sections.

b. **Number of Hydraulic jacks**

In some proposals a single hydraulic jack was positioned around the centre line of each bay, while in other arrangements a symmetric double jacking arrangement was employed. Two hydraulic jacks allowed end moments to be established at the ends of the element without the eccentric loading system required with a single hydraulic jack. The main disadvantage was the increased number of hydraulic jacks required a pressure control system to create the required moment at the end of the test specimen.

c. **Number of Load Cells**

The load cells may have been attached to hydraulic jacks or positioned over the loading beam. The large cost of these elements (£825 each) forced down the amount to the minimum required for the design.

d. **Design of Crushing Surface**

The crushing surface on which the specimens were to be tested could be formed from built up sections or by a single beam with web and bearing stiffeners along the length.

e. **Position of Hydraulic jacks**

The location of the hydraulic jacks on the loading frame was a choice between supplying the load from above or beneath the test specimen. Supplying the axial load from beneath allowed easy access to the hydraulic jacks, with the jacks returning through gravity to the unloaded position after testing. The disadvantage of supplying the load from below was the resulting increase in height from the base of the loading frame to the top of the loading

beam above the hydraulic jacks. By loading the test specimen from above placing the test specimen would be simplified, although spring or hydraulic return jacks would be needed.

Various alternatives were considered for the loading system and construction of the frame which are shown in figures 2.1 - 2.3.

In figure 2.1 three self straining bays were proposed, tied together by bracing. The vertical sections were constructed from channels with plate girders forming the top and bottom cross-beams. Loads were applied by two 500kN hydraulic jacks placed symmetrically around the centre-line with a centrally located 20kN Hydraulic jack to lift the loading beam prior to placing the test specimen.

In the second arrangement shown in figure 2.2 the beams below the hydraulic jacks were replaced by a stiff decking constructed from beams and flat plate sections. The deck was raised and lowered by two push-pull hydraulic jacks also capable in combination of supplying direct end moments. As before channels sections were used for the columns with universal column sections for the cross-beams, on the top and bottom of each bay.

The third arrangement in figure 2.3 shows a system where the load is supplied from the base by two gravity return hydraulic jacks. In order to increase the maximum specimen height the jacks were located within the depth of the beam, with the load applied to the upper flange section. A similar arrangement could have been positioned to load the test specimens from above.

Unfortunately, having twin hydraulic jacks in each bay doubled the number of hydraulic jacks and load cells from three to six increasing the total cost of the loading frame by £4,000, exceeding the available equipment budget. As a result the number of jacks and load cells were restricted to one each per bay producing a total of 3 jacks and load cells in the loading rig. This also allowed removal of the cross-

beam positioned below the hydraulic jacks (see figure 2.1) with the force passed directly to the loading beam. Other cost reductions were accomplished by bolting the channel sections together at the flanges, eliminating the need for bracing between the bays, and using spring return hydraulic jacks.

2.5 Design

The general arrangement of the final design is given in figure 2.4 with section and cross-section details in figures 2.5-2.9. The steelwork was fabricated from 2 types of section, the beams from 356 x 406 x 235kg/m Universal Column Sections and the columns from 432 x 102 x 65kg/m Channel Sections. A column section with a thick web was chosen over the short 2m span between the bays as vertical shear was the critical design factor. By stiffening the flanges the same sections were also employed as load spreading beams, above and below the test specimen.

The vertical sections were only required to resist the tensile forces developed by the hydraulic jacks, as only a small unstable load was developed by the dead load. Therefore, channel sections were chosen with the advantage of reducing the floor space, and not developing significant moments at the connection to the cross-beams.

Single 1000 kN hydraulic jacks were located centrally in each bay, with a load cell fixed to the base providing direct bearing onto the loading surface. The hydraulic jacks were spring return and capable of delivering a load of approximately 1400kN in direct compression at 700 Bar. This allowed the maximum load of 1000kN to be achieved as the Reihle compressor could only deliver 600 Bar. The hydraulic jacks were individually connected to a manifold to ensure no variations in the supply of fluid pressure. The base of the frame was secured by tie rods through 1 metre spaced holes in the reinforced concrete floor, to provide uplift resistance and overall stability (see figure 2.9).

The design was carried out at the ultimate limit state according to the recommendations of BS5950: 1984 with a serviceability check performed at working

load levels to ensure that the yield was not reached. Grade 43C steel was specified throughout with Grade 8.8 bolts at the connections. A breakdown of the various costs incurred is given in Table 2.1.

2.6 Shakedown Trial

The loading frame was constructed in the heavy structures laboratory and lifted into position by an overhead travelling crane.

In order to check the performance the frame was loaded to its maximum working load of 3000kN with the load cell reading and overall behaviour closely monitored. Two heavy steel column sections were used for this purpose with cross bracing to tie them together. As expected some 'settling in' was notice at the connections as the load was raised on the first cycle of loading.

2.7 Discussion

The main consideration in the design of the loading frame was the total cost limit of £15000. This prevented application of some of the possible arrangements, especially those involving two or more hydraulic jacks in each bay.

At present, the frame can provide concentric and eccentric axial loads up to a maximum of 3000kN to specimens approximately 5m in height and 1200mm in length. This is adequate for the current and future axial tests on composite walls.

In future work, further modification may be carried out such as adding hydraulic jacks to provide lateral, in addition to the present axial loads to the test specimens, or adding instrumentation to obtain stroke control of the hydraulic jacks.

Table 2.1 Equipment Costs

Equipment	Manufacturer	Quantity	Cost (£)
Frame Fabrication and Steelwork	Ward Ltd	1	6500
Hydraulic Jacks CLS 1506	Enerpac Ltd	3	1995
Load Cells LC 131	Vibrometer Ltd	3	2475
High Pressure Cabling	British Ropes Ltd	-	1499
Saddle Cat 200	Enerpac Ltd	3	444
		VAT@17.5%	2260
		Total Cost	**15173**

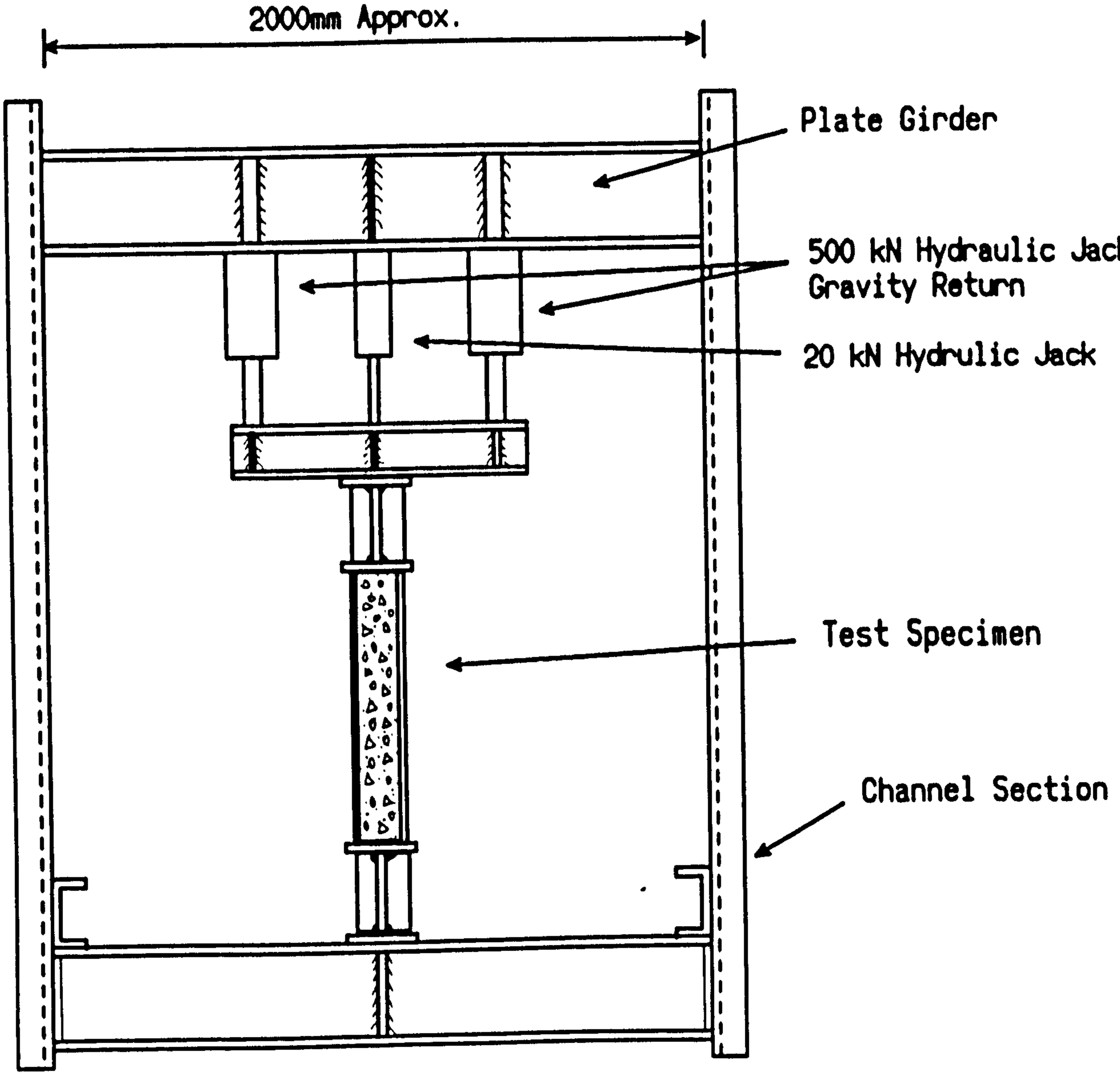

Figure 2.1 Frame Arrangement No. 1

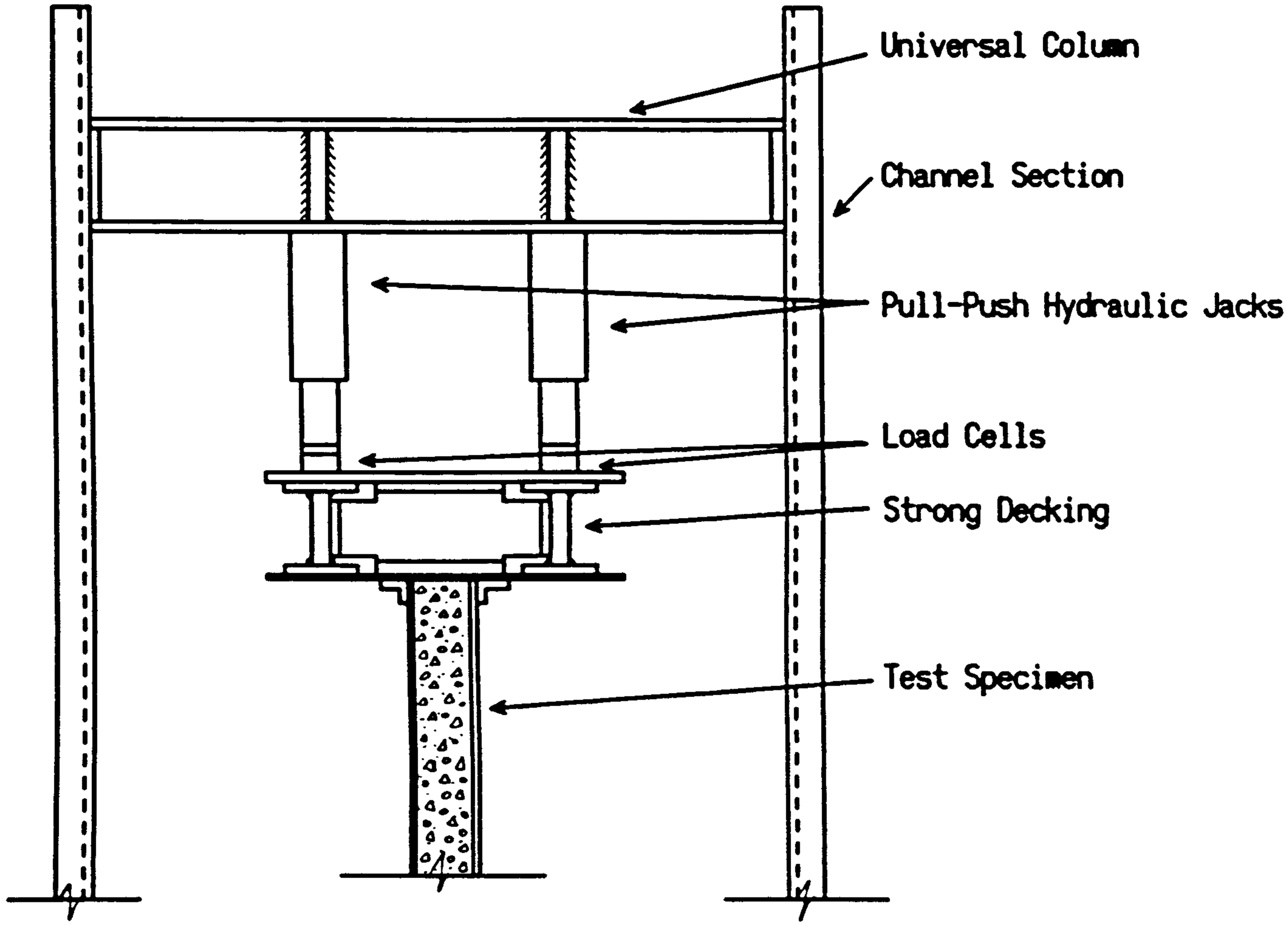

Arrangement 2

Figure 2.2 Frame Arrangement No. 2

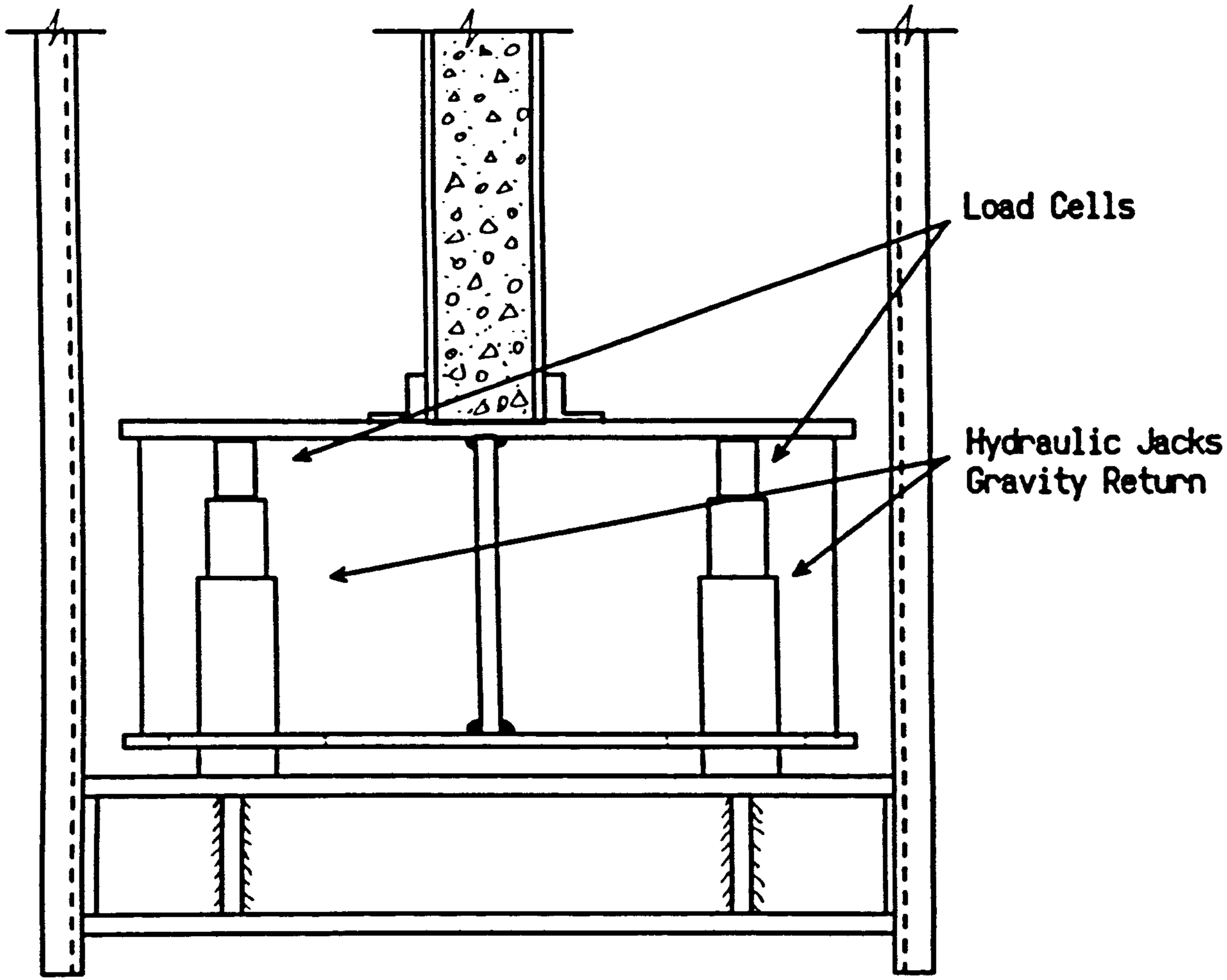

Figure 2.3 Frame Arrangement No. 3

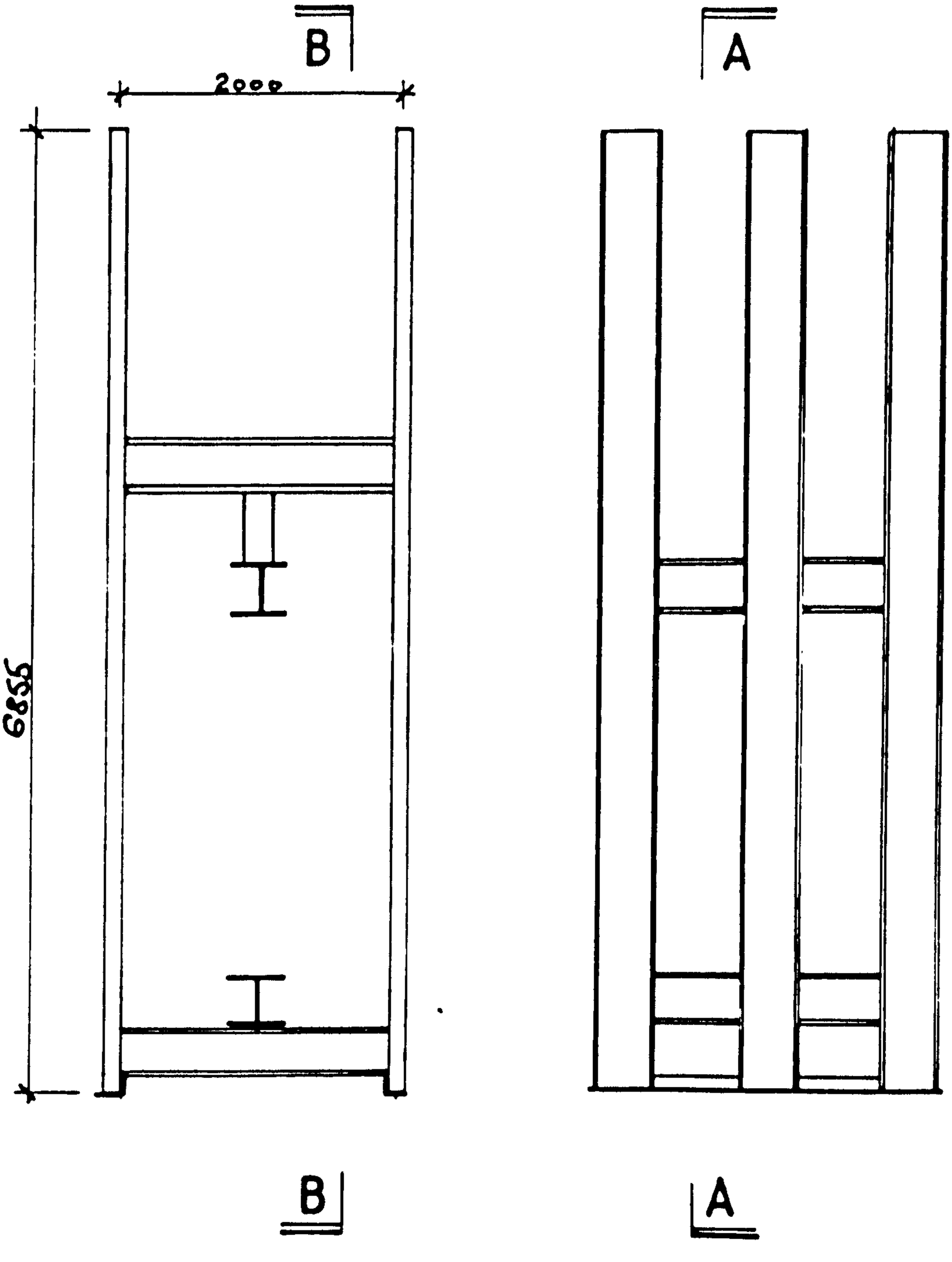

Figure 2.4 General Arrangement

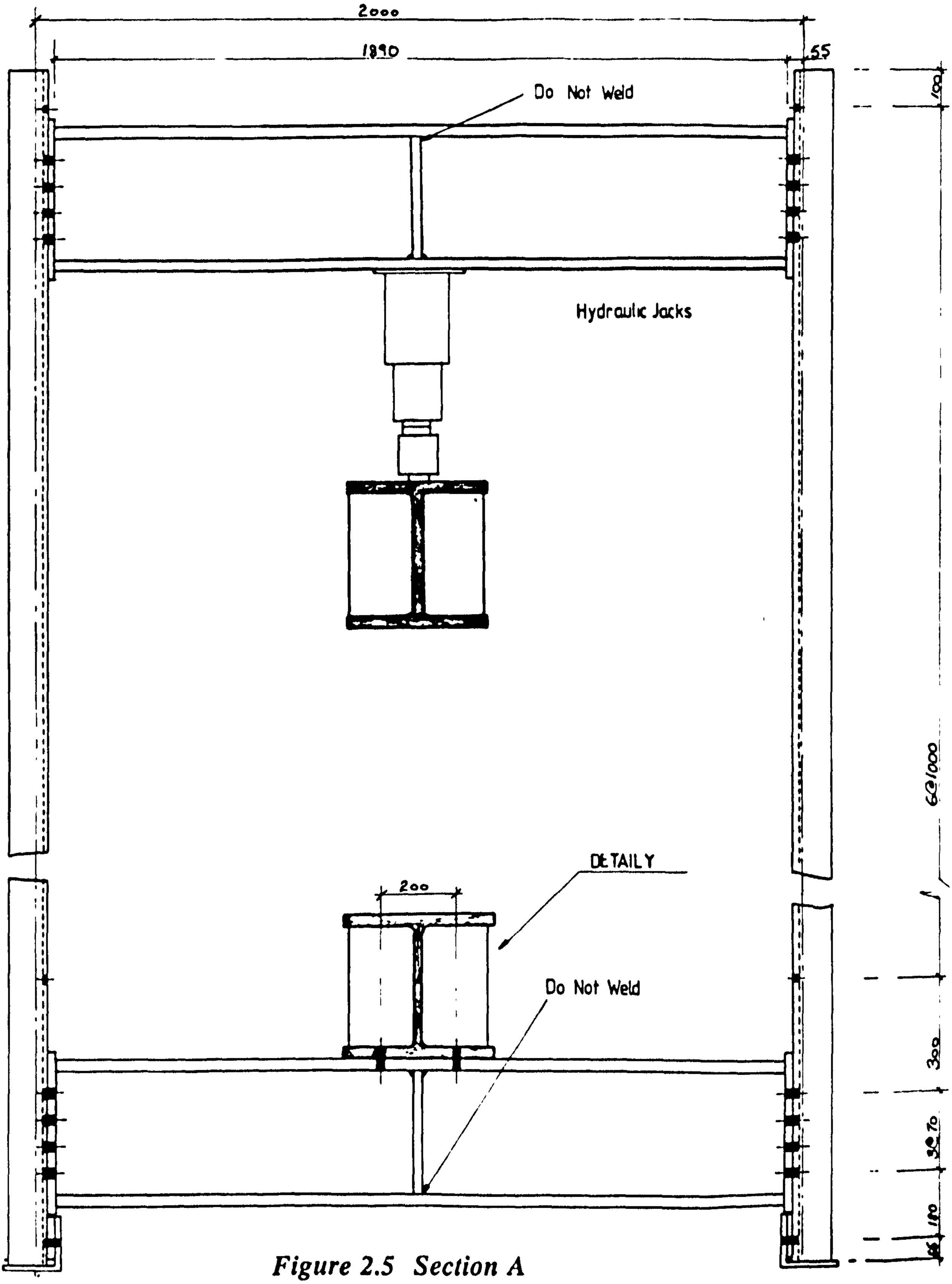

Figure 2.5 Section A

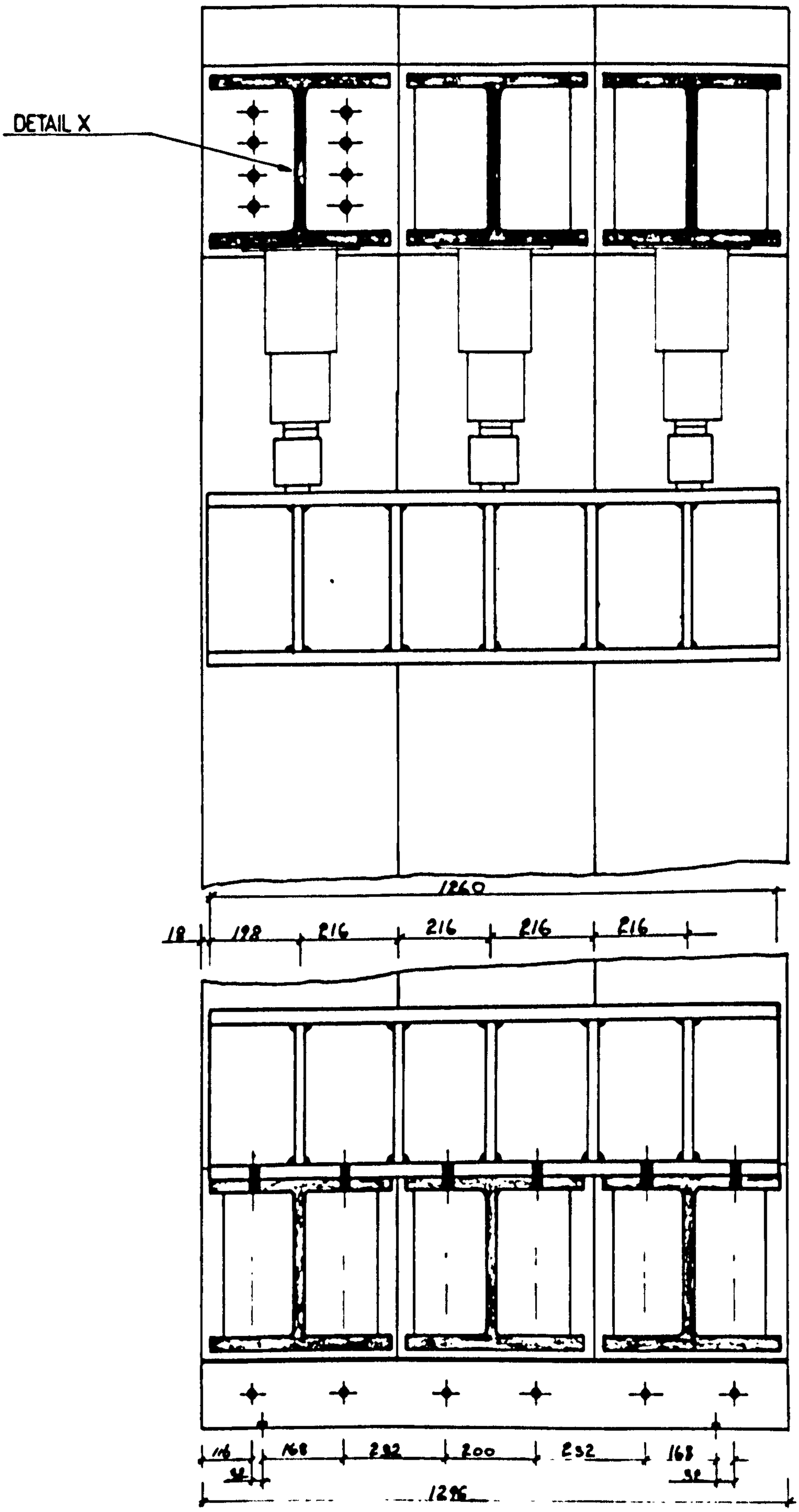

Figure 2.6 Section B

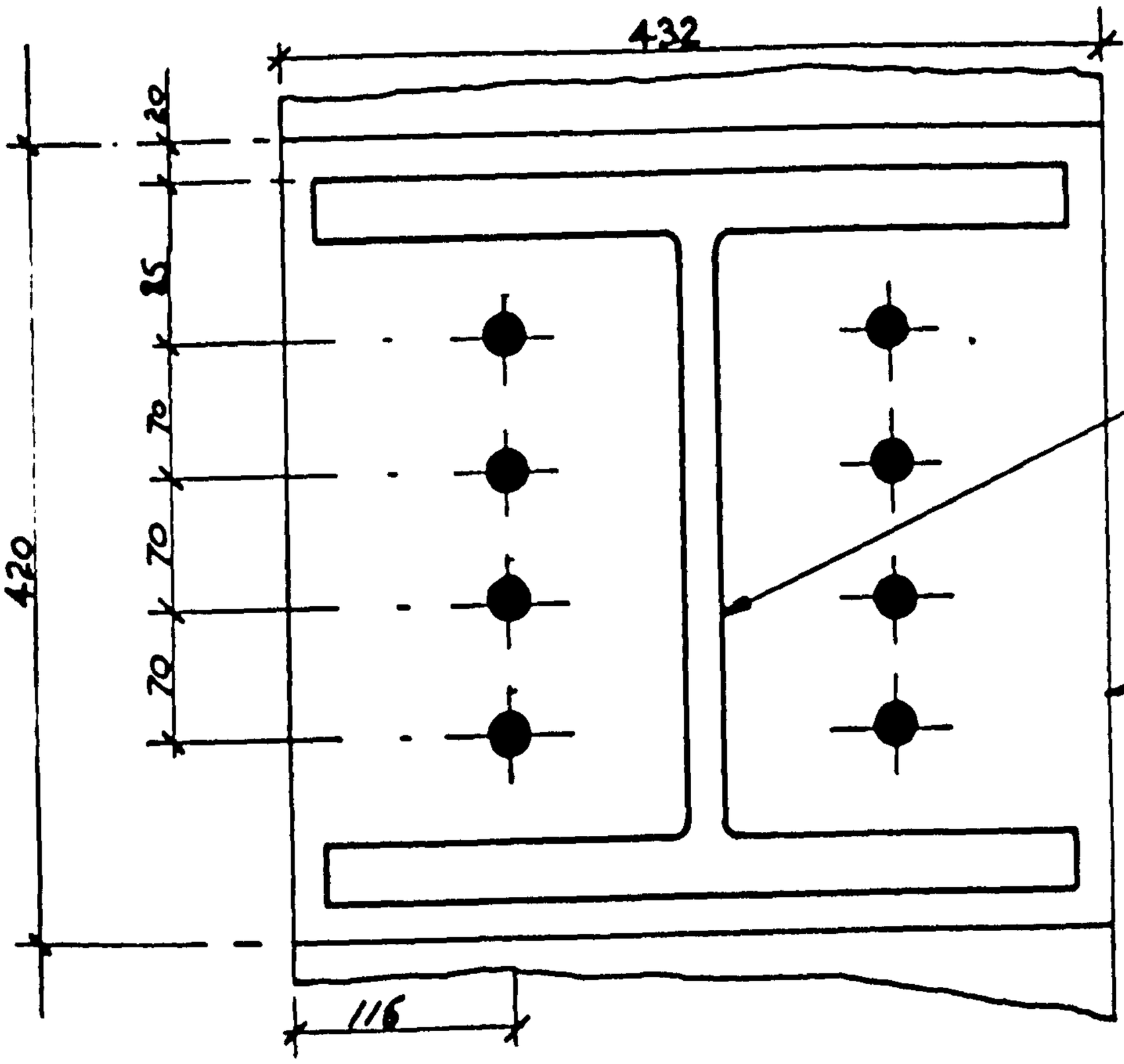

DETAIL X

Figure 2.7

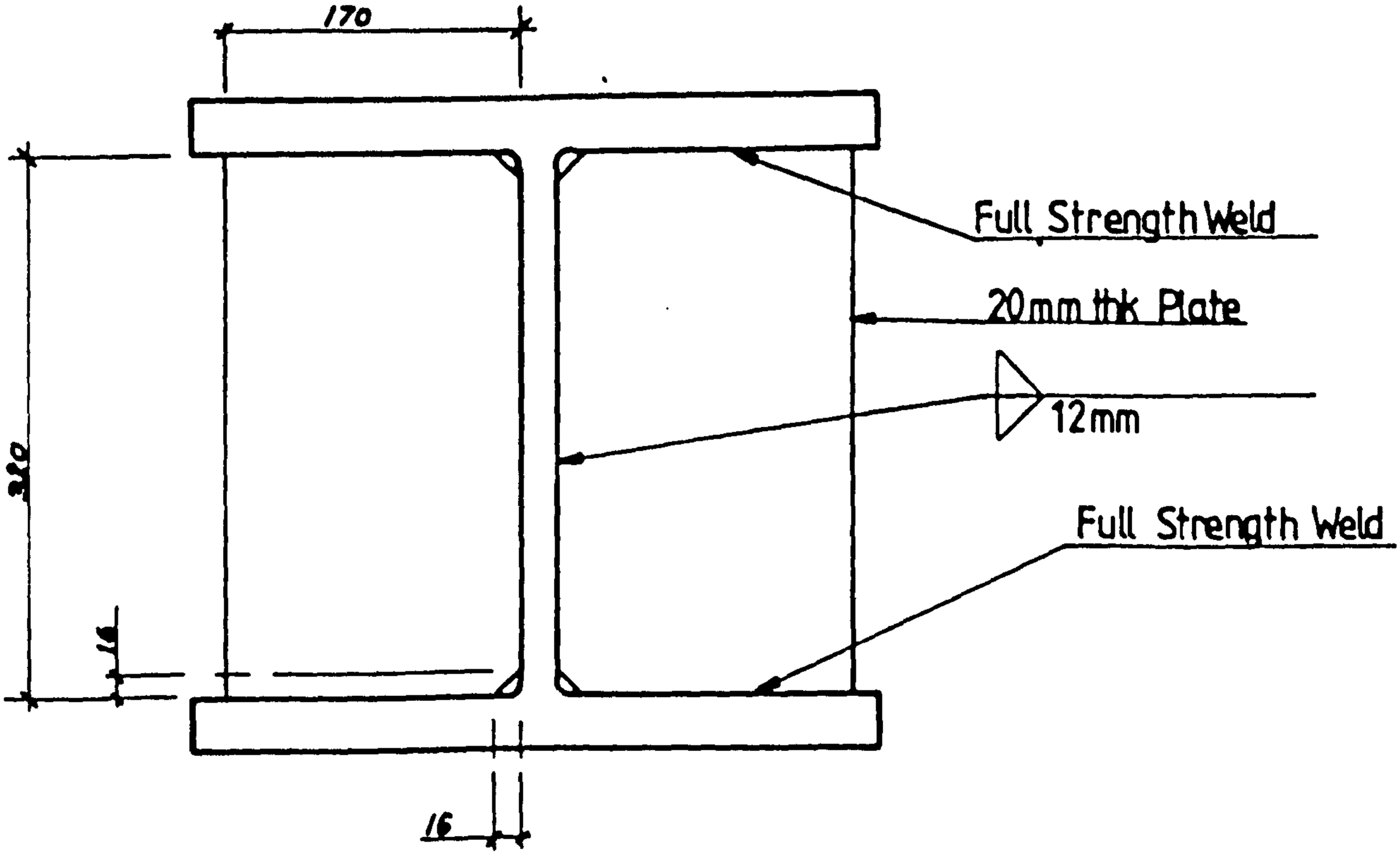

DETAIL Y

Figure 2.8

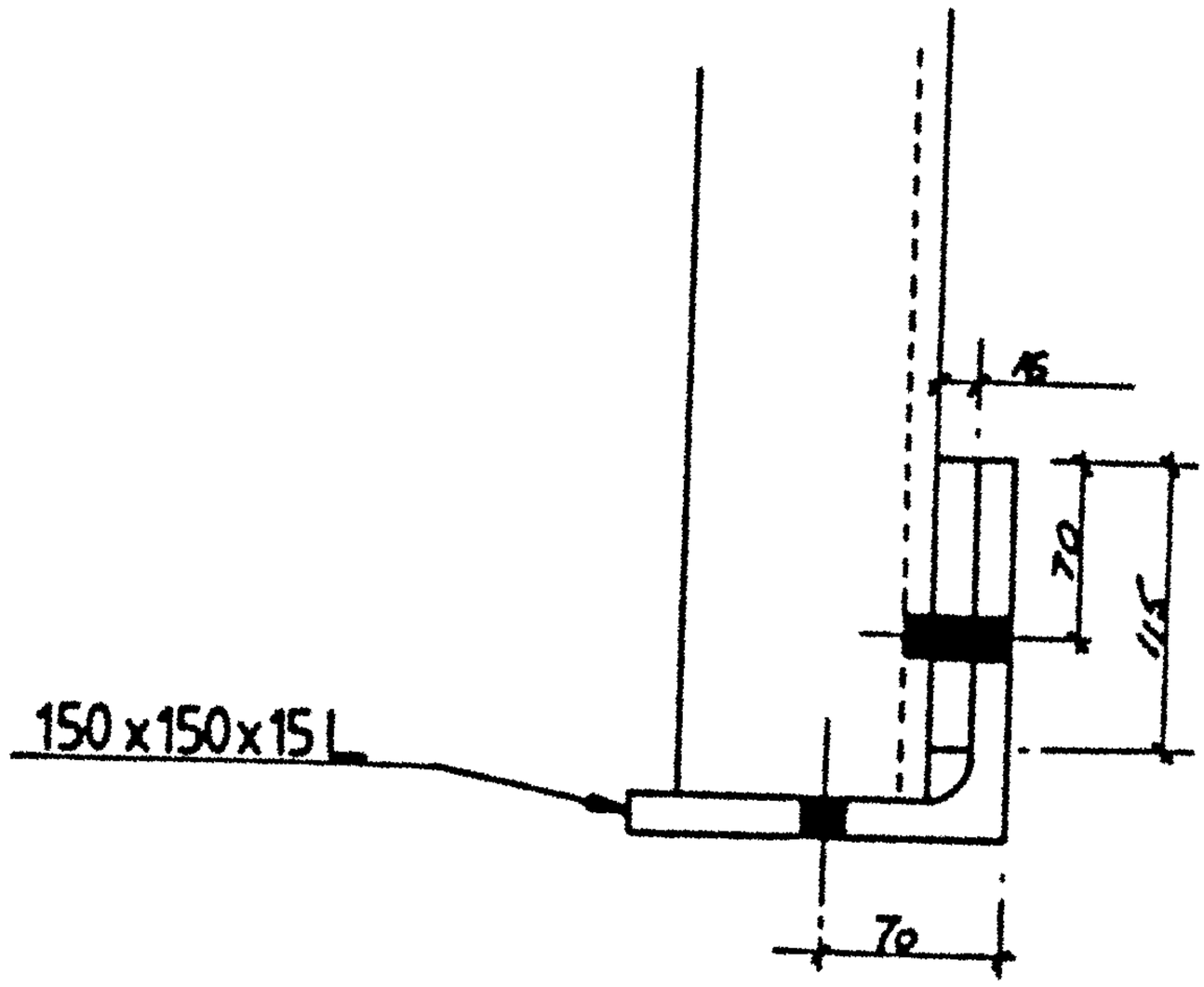

DETAIL Z

Figure 2.9

Chapter 3 Wet Concrete Tests

3.1 Introduction

The lateral pressure exerted by fresh concrete, on the sides of permanent formwork, determines the spacing and number of lateral ties required to give an adequate factor of safety when designing the walls. Underestimating pressures would result in deformed faces and unsafe forms.

The purpose of measuring the lateral pressure was to assemble some measurements of expected values for these form types with narrow and smooth surfaces. Comparisons could then be made with current design recommendations.

3.2 Review

The investigation of formwork pressures began with Rodin (1952) who reviewed existing experimental data on the lateral pressure of wet concrete against formwork. He suggested that the major factors affecting the maximum concrete pressure were the rate of pour, vibration, mix consistency and proportion, concrete temperature, concrete setting time and the dimensions and shape of the form. For internally vibrated mixes a pressure envelope was proposed derived from the following equations based on a 1:2:4 concrete mix at 21°C with a 150mm slump (figure 3.1a)

$$H_{max} = 1.63R^{1/3} \quad (m) \qquad ..3.1$$

$$P_{max} = 23.5H_{max} \quad (kN/m^2) \qquad ..3.2$$

The assumed concrete density was 2400kg/m^3 with R the rate of pour (m/hr) and H_{max} the depth at which P_{max}, the maximum lateral concrete pressure, occurred. For externally vibrated concrete Rodin suggested that the concrete would be fluidized and therefore should be designed for the hydrostatic pressure. In order to deal with other mix proportions, temperatures and slumps Rodin adjusted the calculated values with correction curves.

Schojdt (1955) proposed a theoretical model for the lateral pressure envelope including the effect of pore pressure and introducing a lateral pressure coefficient based on Soil Mechanics concepts. Other factors taken account of were rate of pour, depth of vibration, slump, setting time and the permeability and shape of the form. Gardner (1986) notes that the method did not gain wide acceptance due to the method's complexity and the problem of determining the strength properties of fresh concrete.

ACI committee 347 (1958) assembled the test reports and existing literature on the subject and suggested that the lateral pressure should increase hydrostatically up to a calculated limiting value and then remain constant thereafter (see figure 3.1b). For walls the proposals suggested that for the rate of placing R < 2.14 m/hr

$$P_{max} = 7.19 + \frac{785R}{17.78 + T} \quad kN/m^2 \qquad ..3.3$$

with P_{max} not greater than 23.5h or 95.8 kN/m^2. For walls with 2.14 < R < 3m/hr then

$$P_{max} = 7.19 + \frac{1155}{17.78 + T} + \frac{244R}{17.78 + T} \quad kN/m^2 \qquad ..3.4$$

For columns they proposed

$$P_{max} = 7.19 + \frac{785R}{17.78 + T} \quad kN/m^2 \qquad ..3.5$$

P_{max}, the maximum value of lateral pressure, was not to exceed 23.5h or 143.7 kN/m^2. h is the depth of the form (m), R is the rate of pour (m/hr) and T is the temperature in °C.

The ACI committee considered that slump, aggregate size and water cement ratio had a minimal effect on the maximum pressure.

The first proposals in the United Kingdom came from the Construction Industry

Research and Information Association (CIRIA) (1965) who funded a large experimental study of formwork pressures by the Cement and Concrete Association (CACA). The resulting design method included rate of pour, concrete temperature, slump, minimum form dimension and vibration duration as variables in empirical relations. Upper bounds on the maximum pressure were calculated taking account of arching

$$P_{max} = 14.37 + 0.094d + 3.14R \quad kN/m^2 \qquad ..3.6$$

and concrete stiffening

$$P_{max} = \frac{\gamma_c R t}{1 + c(\frac{t}{t_{max}})} + (4.6 - 1.89R) \quad kN/m^2 \qquad ..3.7$$

with P_{max} also limited to 24h or 143.7 kN/m^2. d is the minimum form dimension, t the time from the start of the pour (hr), t_{max} the setting time, γ_c the concrete density (kN/m^3), c a vibration constant and h the height of the concrete in the form. The values of t_{max} and c were empirically derived from existing data.

The effect of relaxation of the formwork under lateral concrete pressure was reported by Levitsky (1975) who suggested that there was a very rapid initial set in the concrete mix after pouring which determined the maximum form pressure and the depth at which it occurred. A viscoelastic solid model was derived based on an instantaneous transition of the concrete from a liquid state into a rigid solid which showed good qualitative agreement with test results. Levitsky also suggested that the reduction in maximum concrete pressure was due to relaxation in the formwork.

The effect of internal vibration was considered by Gardner and Queresh (1979) who investigated the effect of the power of the vibrator, duration and the depth of immersion of the vibrator on the lateral concrete pressure. Their tests involved pouring concrete into a rigid form 4.6m deep with 5 pressure cells at various depths and vibrating for set times and depths in eight stages. They concluded that the power

of the vibrator had a major effect on the lateral pressure. In contrast the duration was of minor importance which could be ignored provided that the level of consolidation was adequate. It was also noted that both the CIRIA (1965) and ACI (1958) design methods gave extremely conservative results for the design of formwork and suggested that the CIRIA (1965) arching criterion should only be used where the formwork was rough and the concrete temperature above 15°C.

Gardner and Ho (1979) carried out an experimental investigation to determine the variation of envelope of lateral pressure exerted by fresh concrete with rate of placing, strength of concrete, slump and consistency of concrete, formwork size and yielding of concrete. They concluded, as had previous authors, that the envelope was essentially hydrostatic up to a limiting value and constant thereafter. Also, increase of slump and rate of placing raised the lateral pressure significantly but aggregate size and concrete strength only had minor effects.

Measurements of Concrete pressures on wall forms were carried out by Douglas *et al* (1981) who measured tie forces instrumented with electric resistance strain gauges as an indirect method in estimating the lateral concrete pressure. The tests, carried out in the field, also suggested the conservative nature of the CIRIA (1965) and ACI (1985) design methods. It was observed that the effect of revibration on the mix was to increase formwork pressures by up to 40%.

Harrison (1983 A) tested and reported on the application of the ACI method to concretes containing water reducers, slag and superplasticisers. The effect on the concrete pressure of water reducers was small although they left the particle structure prone to impact for longer periods. For concretes with a high proportion of slag higher concrete pressures were obtained to the effect that it was recommended that the ACI (1958) method not be applied. The work on superplasticisers suggested little difference in the lateral pressure distribution to that of normal concrete.

A pore pressure model of the concrete behaviour was also proposed to obtain a better

theoretical understanding, therefore increasing the scope and range of tests carried out. The horizontal pressure on the formwork p comprised of the porewater pressure u and the particle structure stress σ ie.

$$p = u + \lambda \sigma \qquad ..3.8$$

where λ is a constant less than unity governing the proportion of the particle stress acting horizontally. The high proportion of the pore-water pressure (90% of the formwork pressure was due to the pore-water) contributing to the total lateral pressure suggested to Harrison that the main fundamental factors in controlling the maximum concrete pressure were the rate of dispersal of the pore-water pressure and the distance that the particles would have to move in order to establish contact with a neighbouring particle. An important finding was that for narrow sections the proportion of the pore-water contribution to the total pressure remained the same as in wide sections indicating that arching was not the cause of the reduction in lateral pressure.

Harrison (1983 B) noted that the need to update and revise current methods of estimating formwork pressure to take account of increases in the rate of placement. He stated that there was no evidence to suggest that the maximum pressure for columns of 144 kN/m^2 was inadequate although some doubt remained for walls with a limiting pressure of 96kN/m^2. The change from skip and crane to the pumping of concrete did not increase the formwork pressures according to Harrison as the tendency to bleed is significantly reduced in mixes suitable for pumping.

He suggested that the viability of a purely mathematical approach to calculating formwork pressures was reduced because of the problem of impact fluidizing the concrete giving higher than expected concrete pressures.

Gardner (1984) examined the effect of partial cement replacement by fly ash and found an increase in the lateral concrete pressure proportional to the percentage of fly ash present. This increase was due to an increase in the mobility of the concrete and

a decrease in the early age strength. Modifications to previously suggested design equations were suggested to take account of this effect.

In 1985 CIRIA updated their original recommendations in order to cover concretes which contained admixtures and blended cements. The method of estimating and calculating concrete pressures on formwork was also improved to take account of recent test information. The maximum concrete pressure is calculated from the equation

$$P_{max} = D(C_1\sqrt{R} + C_2K\sqrt{H - C_1\sqrt{R}}) \quad kN/m^2 \qquad ..3.9$$

or from

$$P_{max} = Dh \quad kN/m^2 \qquad ..3.10$$

whichever is smaller. The coefficient C_1 is dependant on the size and shape of the formwork with the value of C_2 dependant on the constituent materials of the concrete. The term $C_1R^{0.5}$ incorporates the effects of vibration and workability as these factors depend on the dimensions of the form and rate of rise of the concrete. The contributions from cement type , admixtures, height of discharge and temperature are contained in the term

$$C_2K(H - C_1R^{0.5})^{0.5} \qquad ..3.11$$

The coefficient K is calculated from

$$K = \left(\frac{36}{T + 16}\right)^2 \qquad ..3.12$$

The governing equations were incorporated in separate tables for walls and bases. No change in the original design pressure envelope was proposed to take account of rigid forms. According to Harrison, a reduction occurs in the pressure against rigid forms after the maximum is reached.This is not true for flexible forms as some stress remains between the form and the concrete. The would appear to contradict previous

work by Levitsky (1979) and Gardner and Ho (1979) who suggested that more flexible forms gave lower pressures.

ACI Committee 347 (1988) suggested that because of insufficient test data, forms containing cement other than Type I should be designed for the hydraulic pressure although provisions are made for the use of other design procedures such as the CIRIA 1985 method where adequate experimental data is available.

3.3 Review Conclusions

The design of formwork for lateral concrete pressure remains empirically based due to the complexity and number of factors affecting the maximum concrete pressure. The pressure affecting narrow forms is not fully understood with the original reductions in pressure attributed to arching challenged by pore pressure results from Harrison (1983 A). There would also appear to be some confusion over the effect of form stiffness on the design pressure. The addition of additives to mixes and increases in pour rates from the pumping of concrete in recent years has led to a requirement for further extensive testing.

From existing work performed to date the parameters that appear to have a significant affect are :-

Rate of Placing - The greater the rate of placing the higher the maximum concrete pressure developed behind the formwork.

Slump - The higher the slump the higher the workability and lateral pressure.

Temperature - The lower the concrete temperature then the slower the concrete hydrates and consequently the slower the material properties of the concrete develop. Therefore the lower the temperature the higher the lateral pressure developed.

Minimum Dimension - The larger the size of the minimum form dimension the greater the lateral concrete pressure developed as the proportion of side frictional resistance reduces.

Vibration - The depth of immersion of the vibrator can effect the maximum pressure if vibration of previously settled mix occurs.

The work of this study will generate more experimental data to compare with the existing design approaches as they apply to narrow walls.

3.4 Experimental Investigation

The lateral pressure formed behind the profiles and the resulting deflections were recorded on the four pilot tests performed in this study. The instrumentation, assembly and pouring of the tests are described followed by discussion and conclusions based on the results obtained.

3.4.1 Instrumentation

Instrumentation was provided on the walls to measure the concrete pressure, lateral deflections and strains during the pouring of the walls and subsequent ultimate testing. Details of the instrumentation and setup are given below.

3.4.1.1 Concrete Pressure

In order to monitor the resulting lateral concrete pressure produced during casting of the 1.9m and 3.4m walls a vibrating wire pressure cell was attached between the ribs of the profiled steel sheet with a rubber seal and 4 securing bolts. The basic principle behind the cell is based on a pressure applied to the plate producing a deflection which causes a change in the period of the vibrating wire gauge. This change in period is electronically measured by the magnetic plucking and counting of the wire cycles at resonance. Having measured the period the change in length of the wire corresponding to the deflection of the plate can be calculated and therefore the

applied pressure on the cell face.

For these tests a Gage Technique Ltd. Boundary Soil Pressure gauge was fixed and connected to a single channel vibrating-wire strain meter to monitor the gauge output frequency. A calibration was also provided to convert the output value to pressure.

3.4.1.2 Measurement of Lateral Deflections

The measurement of lateral deflections of the profiled steel sheet for the monitoring of lateral deflections due to concrete pressures and those under increasing load to ultimate failure needed a system where small changes such as local buckling of the profiled steel sheet as well as large changes such as global buckling could be measured. Dial gauges or single LVDT's, while offering adequate monitoring of large movements of the wall when placed at strategic locations could not pick up small local buckles or deformations of the form. Obviously a system capable of monitoring the deflections over the whole height of the wall on both sides was required to obtain as much information as possible during each test.

Measurements of lateral deflections and heights at which they occurred were carried out by two LVDT's carried on a trolley and lifted by a screwed rod powered from an electric motor at the base. Figure 3.2 shows the system details and important features. As the carriage moved up and down an LVDT monitored the deflection of the wall from an assumed zero at 100mm from the base of the wall and another measured the vertical height from this datum by means of an inclined angle. Using inclined angles allowed a specific value of voltage output to be calibrated to a specific height above the datum. By continuously monitoring the values of height and displacement on each side of the wall the displaced profile of the sheeting on either side of the wall could be assembled using a SPECTRA data acquisition system and SPECTRA-DAS computer program and writing the output produced to computer disk for later analysis. A useful feature of the system was that although the aluminium angles were not exactly vertical during the tests the error in gradient was easily subtracted during the data processing as long as the lateral supports were

assumed undeflected at the end of casting.

3.4.1.3 Measurement of Strain

The steel strains on each of the four tests were monitored by approximately 20 electric resistance strain gauges. In general the locations of the strain gauges were such that the strains on the faces and the re-entrant sections at the top, middle and bottom of the sections were measured on both sides of the each wall. All gauges were fixed to measure vertical strain and were only located on one half of the walls. For tests 3 and 4 concrete embedment strain gauges became available and these were used to monitor the concrete strains during the ultimate testing. Unfortunately because of the height the mix was dropped the gauges at the bottom of the walls were damaged during casting.

The locations of the strain gauges are shown in figures 3.3 - 3.6.

3.4.2 Profiled Steel Permanent Formwork

The permanent formwork was a Super Holorib deck supplied by Richard Lees Ltd shown in figure 3.18. The decking had a gauge thickness of 0.9mm with an Area of 1550 mm^2 per m width. Located at the centre of each side was a joint as the cover width of 610mm was not sufficient for the length of wall required. The only embossments on the sheeting were on the re-entrants portions.

3.4.3 Lateral Support Spacing

The design of the lateral support spacing was based on the CIRIA (1985) recommendations as these were the most applicable to the current investigation. A rate of placement of 5m/hr was assumed although this was conservative and led to a full hydrostatic head for the design. The criteria considered were limiting the maximum profile deflection to an acceptable value and checking the bending moments developed were within the working load limits of the sheeting. This resulted in a spacing of 0.9m on the short 1.9m walls between the ties. This distance

would be significantly increased by employing a deeper profile with a higher Inertia.

3.4.4 Construction of Permanent Wall Forms

The construction of the wall forms was performed when the instrumentation was completed. Initially the two sides were placed back to back and the 8mm diameter tie rod holes drilled at the locations shown in figures 3.3 - 3.6. Hollow 50mm spacers were placed between the sheets at the tie rod positions and the threaded tie rods were pushed through the sheet (see figure 3.7). External 10mm square and 1mm thick longitudinal supports were fixed on the outside of each side of the tie rods and the bolts were tightened. The narrow re-entrant space prevented screwing up of the bolts when the form was stripped and the external supports removed. It was therefore necessary to have additional spacers fitted inside the re-entrant gaps to allow tightening of the bolts. The permanent form was then placed on a flat channel section with temporary forms secured to either end and to the channel for stability. In the initial test the end form fixed against the flat was secured using an industrial tape. Subsequent tests 2,3 and 4 had a foam rubber tape attached to the end forms, to allow for irregularities in the cutting of the profiles, pressed against cut re-entrant sections. A cross-sectional plan of the form during casting and before final testing is shown in figure 3.7.

3.4.5 Casting Process

The system used for pouring the walls involved batches of approximately 100kg of concrete being lifted by an overhead travelling crane to the top of the walls and manual scooping of the mix into the form. The 1.9 metre walls required 6 batches of concrete while the 3.4 metre walls needed 10 batches. The placement rates achieved were around 1 metre per hour for all tests. In general 2 cubes were taken with each batch of concrete with 3 cylinders in total for each test. This allowed frequent checking of the mix strength from the cube strength which was necessary as testing was carried out at 7 days instead of the normal 28 days. After each batch was poured the concrete pressure, monitored by the pressure cell, and the height of

the mix above the pressure cell were recorded, prior to and after vibration of the mix at that level. The level of vibration was limited to the height of the previous batch in order to reduce likelihood of possible segregation of the mix from excess vibration. For the same reason the duration of the vibration over the length of the wall was restricted to approximately 40 seconds.

The concrete mix was of high workability with a collapse slump and proportions :

Water Content	225 kg/m^3
Cement	409 kg/m^3
Sand	889 kg/m^3
10mm Crushed Gravel Agg.	788 kg/m^3

For tests 2, 3 and 4 the final 10 millimetres of form height was left to enable a concrete cap (1 part high alumina cement : 2 parts sharp sand) to be placed at a later stage. In test 1 the concrete was taken to the full height and a plywood cap placed between the wall and the loading beam during the final testing of the wall to give a smooth loading surface.

During the casting of the walls the pressure was primarily monitored by the pressure cell located at 210mm from the base but the strain gauges were also monitored to observe the changes in vertical and bending moment at different points on the profile. These readings were also useful to indicate the amount of shrinkage between casting and the final testing 7 days later when the gauge readings were repeated.

3.4.6 Test Observations during Casting

It was noted during the pouring of the first wall that the end forms needed modification in subsequent tests as the sealant tape had insufficient strength to prevent substantial warping of the free profile edges by the concrete pressure. This resulted in some leakage of the mix and slight honeycombing at the base where the lateral pressure was highest. To prevent this problem in later tests an adjustment of

a half re-entrant section at the edges, to resist bowing of the form, was devised. In addition, side forms had a 5mm foam rubber tape fixed which sealed any irregularities in the cutting of the steel sheets. Another source of leakage at the drilled tie rod holes gave some leakage but this was minimal. To prevent leakage at the bottom of the walls a 10mm deep concrete mortar was placed 1 day prior to pouring of the main mix.

The lack of space between the faces of the wall especially at the ribs with only a 50mm gap did not present any problem for compaction vibrator access. Unfortunately in tests 3 and 4 where steel mesh and reinforcement were fixed to the profiles access became more difficult especially with concrete gauges fixed on the mesh. The high workability of the mix aided the compaction especially in later tests when dropped from 3.4m.

During pouring it was observed that the profiled steel sheeting visibly deformed between the longitudinal supports. The supports themselves appeared relatively stable under the concrete pressure showing little signs of stress.

3.4.7 Discussion of Results

The results taken by the pressure cell and the lateral displacement system are given below.

3.4.7.1 Pressure Cell Readings

The readings taken by the vibrating wire pressure cell were recorded and plotted against

a) head of concrete, and

b) time

a) Pressure vs Head of Concrete

Figure 3.8 shows the results of pressures obtained in testing the four walls. All the pressures follow a similar pattern with the pressure increasing linearly following the

hydrostatic pressure until a maximum and then decreasing slightly with greater depths. The obvious difference in maximums between walls 1 and 2 in comparison with 3 and 4 is due to the inclusion of mesh between the ribs of the profiles in walls 3 and 4. To be stable the concrete had to resist the effects of increasing vertical load and vibration. The mesh had the effect of reducing the pressure at the cell by passing some of the pressure directly to the ribs and by allowing a more rapid formation of a stable crystal structure than if no mesh had been present.

b) Pressure vs Time

Figure 3.9 shows the Pressure against time results obtained from the four tests. It can be seen at the end of each batch that there is a decline in pressure before the next batch is placed. This reduction in pressure is disturbed by the addition of further mixes and by the affects of vibration. Eventually a pressure is reached where the addition of further batches does not increase the pressure at that level as a stable structure has formed.

3.4.7.2 Lateral Displacements

The initial lateral displacements taken after removal of the lateral supports and before ultimate testing are given in figures 3.10 - 3.13. Each graph clearly shows the position of the tie rods on the surface of the wall with the displacement measured at regular intervals up both sides of the walls. In walls 1 and 2 the distribution was as expected with displacements of 4mm in the bottom section reducing to 2mm in the top where the lateral pressure had not reached a maximum. In walls 3 and 4 where reinforcement was provided in the lower and upper 600mm there would appear to be reduced displacements. This suggests that the main reduction in pressure was due to the mesh lowering the maximum pressure rather than shedding the load onto the ribs - if the load had been passed to the ribs then the value of lateral displacement would not have been greatly affected. To investigate the acceptability of the results the pressure distributions were compared with the design pressure envelopes proposed by CIRIA, ACI and Rodin. Table 3.1 contains the design pressure recommendations by these authors using the experimental rates of pour and temperature. The

CIRIA(1965) values are based on the narrow section equation although 47.9 kN/m^2 is the minimum design value. Figures 3.14 to 3.17 show each of the four experimental results compared with the design envelopes calculated using experimental rates of pour and temperature in the CIRIA (1985). The results suggest the current UK design method is valid for pressure distribution calculations on this profile cross-section.

3.5 Conclusions

The results of the lateral pressure distribution tests suggest the following :-

1. The current CIRIA (1985) design method is valid for those type of sections where profiled steel sheeting is used as permanent formwork. The high workability of the concrete mix would suggest the experimental pressures provide an upper bound on possible results.

2. The system of ties between the support faces provides adequate fixing for the lateral supports.

3. The variation of width along the wall length increases the formwork perimeter per m length and may reduce the maximum concrete pressure achieved.

4. The leakage of concrete at profile joins is minimal as concrete pressure causes self-sealing at these locations.

5. Reinforcement substantially reduces the level of the maximum pressure at the cell by allowing rapid formation of a stable concrete structure.

The most recent version of the ACI committee 347 guide would imply that for walls of this type with a high workability then the hydraulic pressure would be the design pressure. Application of this method would have led to high design pressures and very conservative spacing of the lateral supports. It would be of interest to observe

the changes in lateral pressure with a trapezoidal profile where wall thickness varies along the wall length.

3.6 Summary

This chapter has considered the lateral concrete pressure and the profile displacements resulting from the casting of the composite walls. Satisfactory results were obtained in line with the current CIRIA recommendation with no detrimental effects. The following chapter investigates the behaviour of the composite walls under concentric axial loads.

Table 3.1 Maximum Experimental and Design Pressures

	Wall No.1	Wall No.2	Wall No.3	Wall No.4
R m/hr	1.14	1.14	0.91	1.17
T °C	19	20	19	18
h m	1.9	1.9	3.4	3.4
Density kN/m^3	24	24	24	24
Rodin (1952)	40.9	40.9	37.9	41.2
CIRIA (1965)	32.0	32.0	31.3	32.1
CIRIA (1985)	32.6	32.2	34.8	38.2
ACI (1978)	31.5	30.9	26.1	32.9
ACI (1988)	45.6	45.6	81.6	81.6
Experiment	31.9	33.1	23.0	22.5

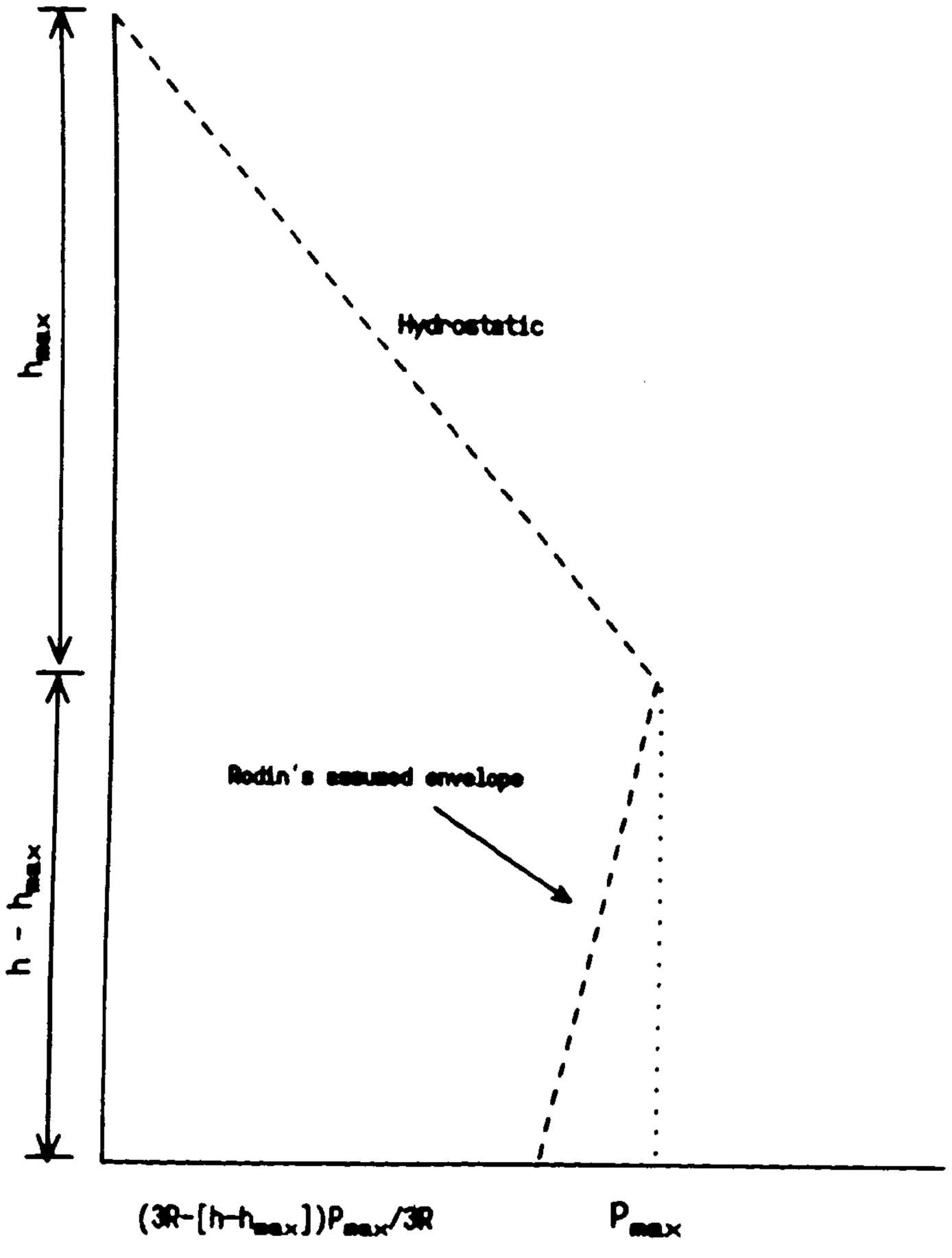

3.1a

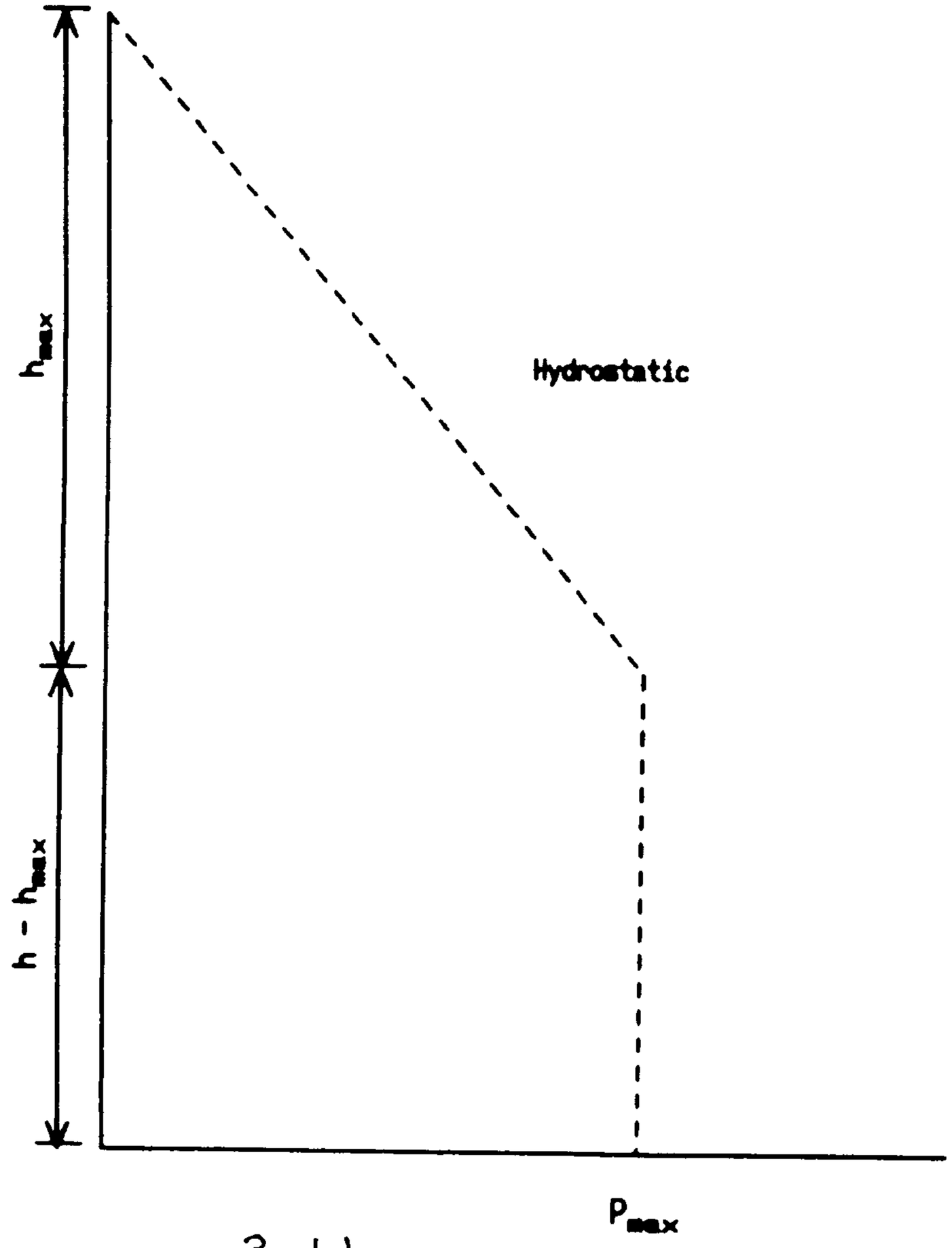

3.1b

Lateral Pressure Envelopes

Figure 3.1

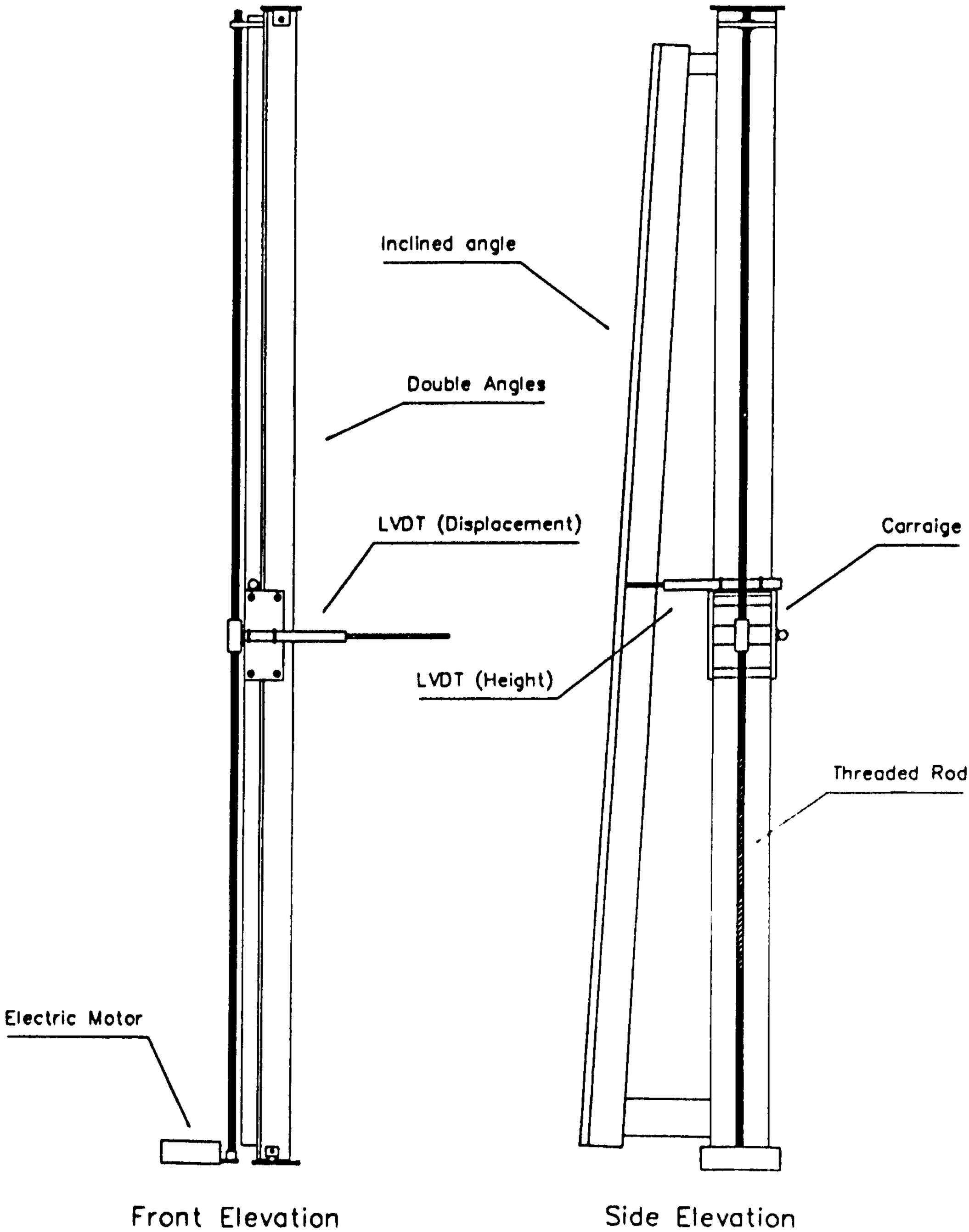
Inclined angle
Double Angles
LVDT (Displacement)
Carraige
LVDT (Height)
Threaded Rod
Electric Motor
Front Elevation
Side Elevation
LVDT DISPLACEMENT SYSTEM

Figure 3.2

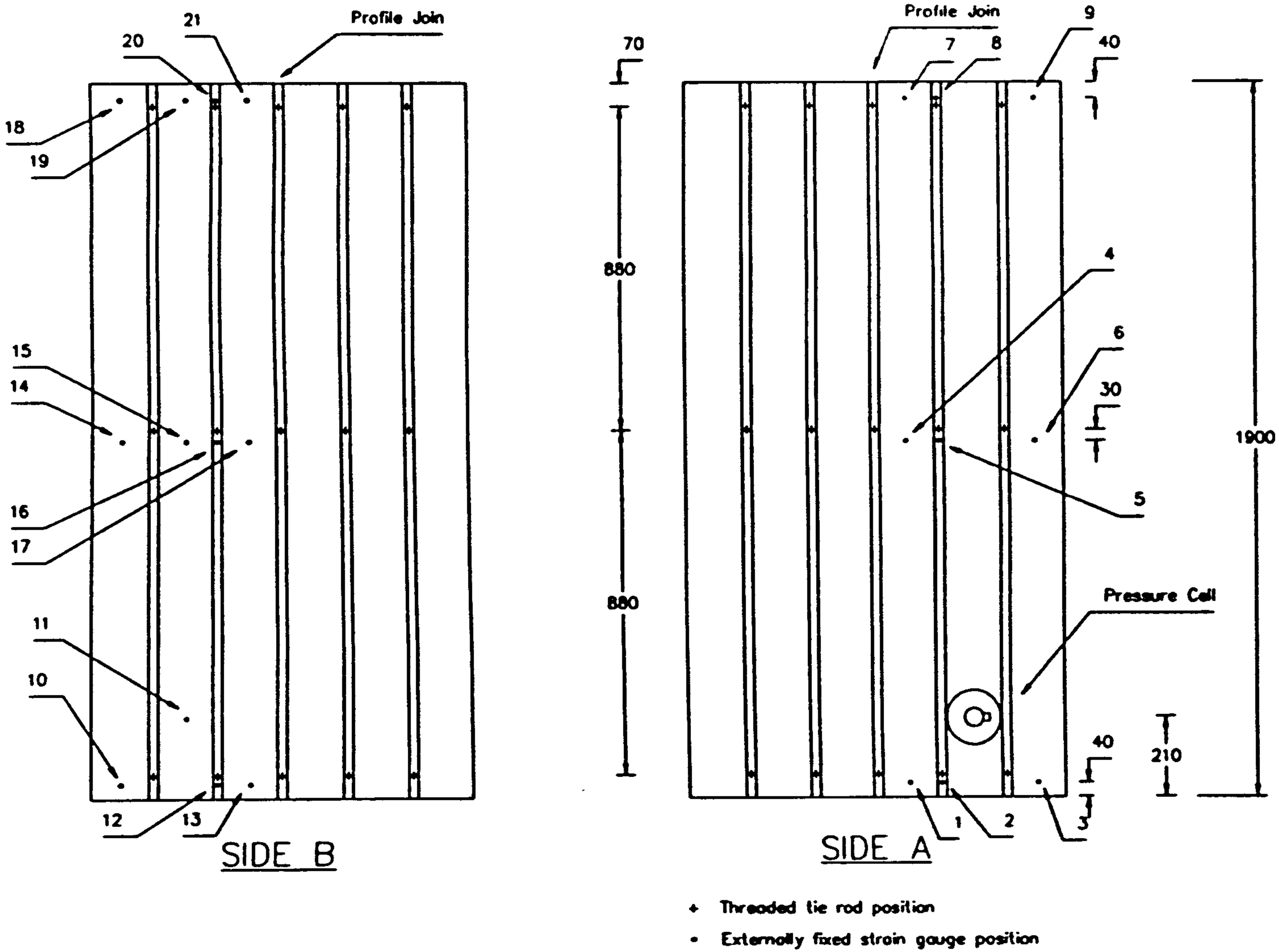

Figure 3.3 Wall 1 : Dimensions and Instrumentation

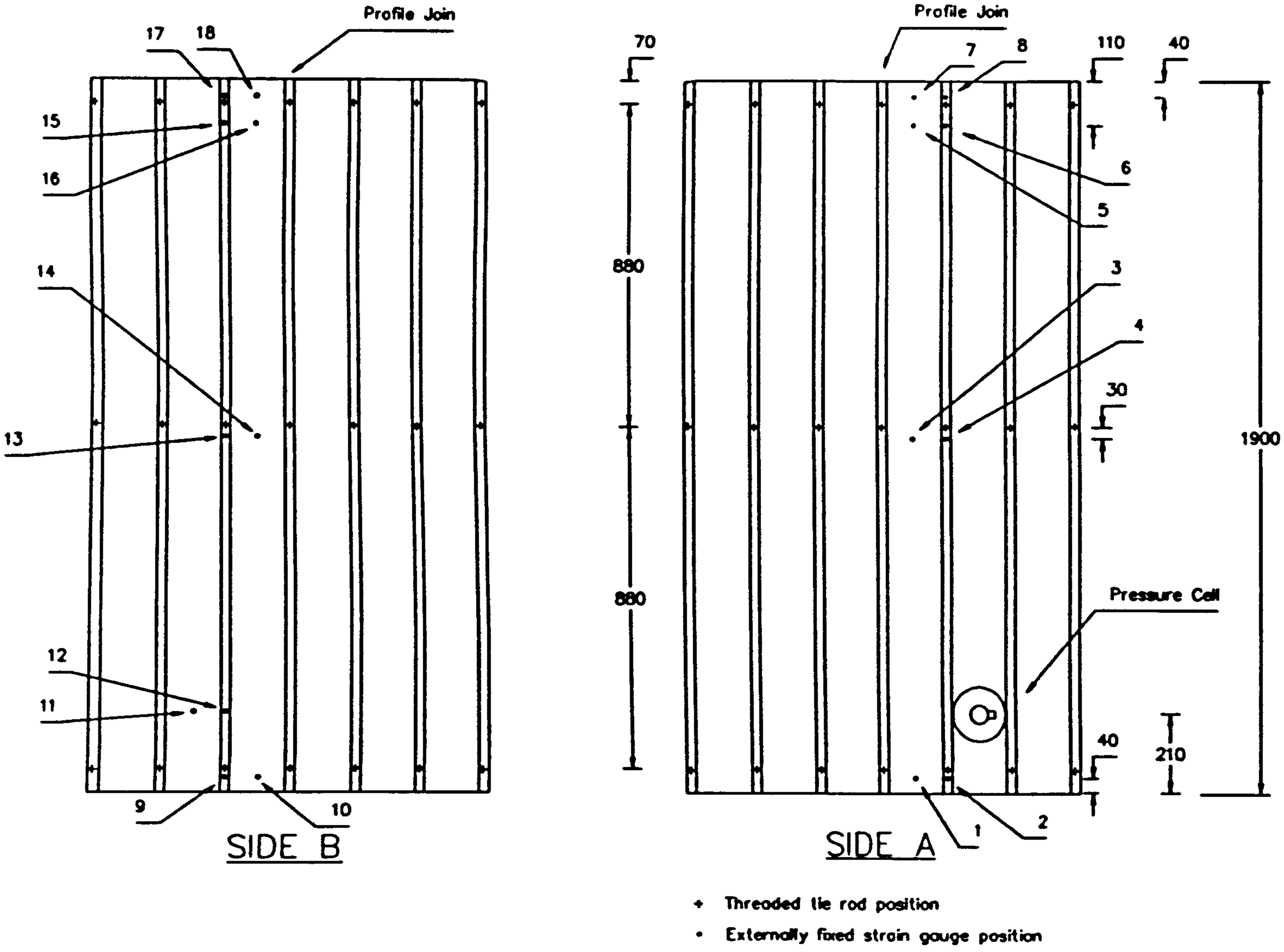

Figure 3.4 Wall 2 : Dimensions and Instrumentation

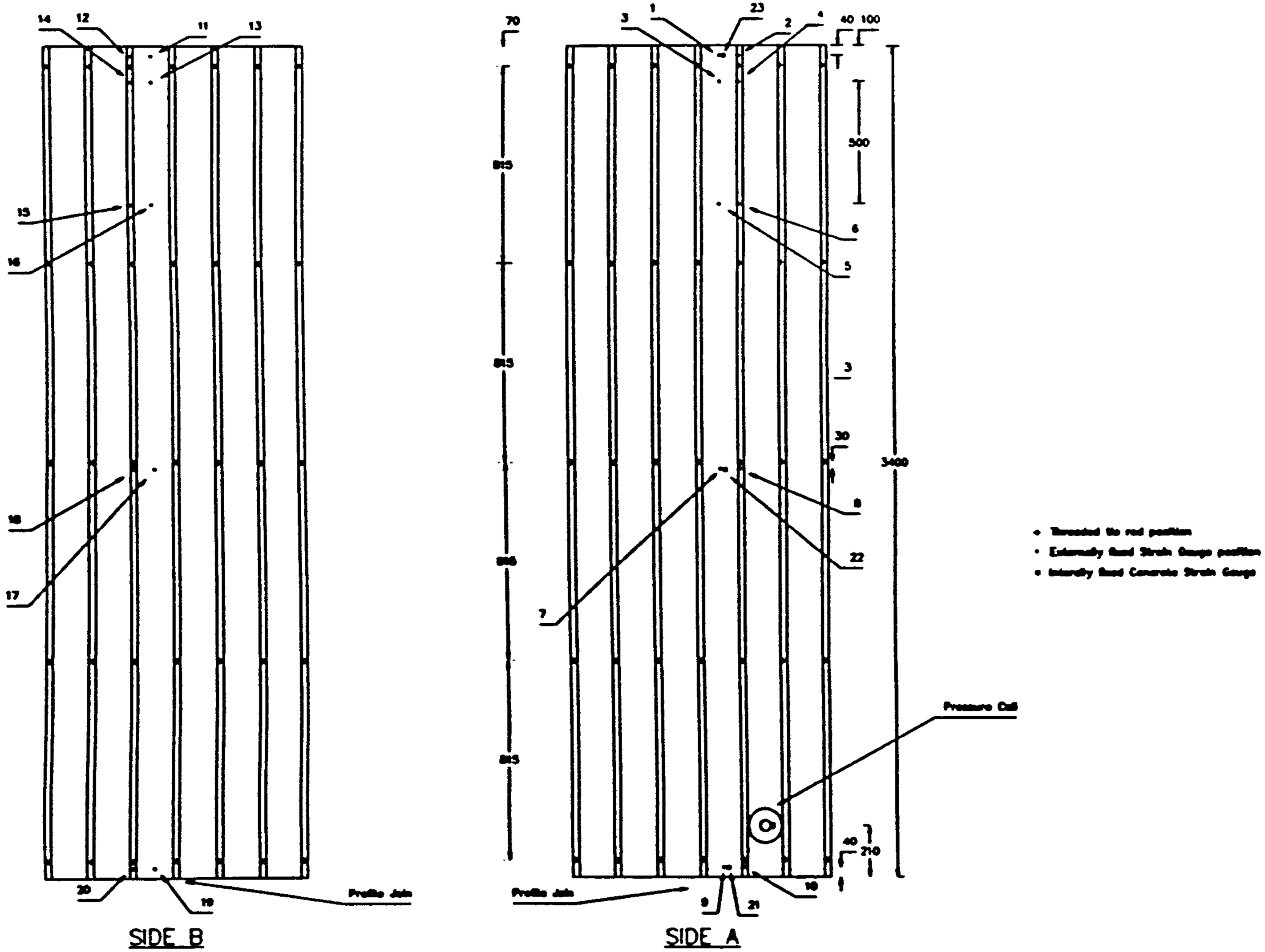

Figure 3.5 Wall 3 : Dimensions and Instrumentation

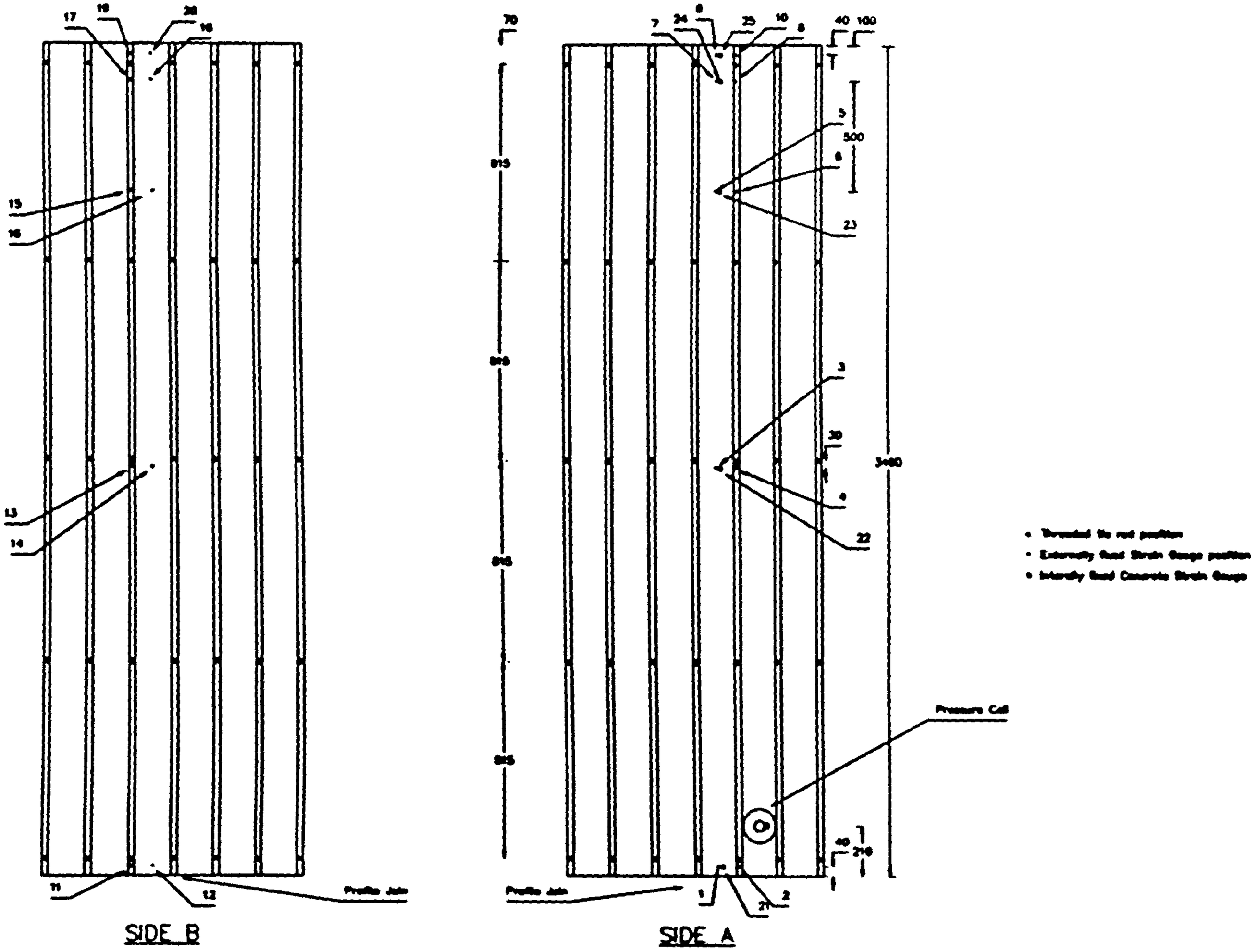

Figure 3.6 Wall 4 : Dimensions and Instrumentation

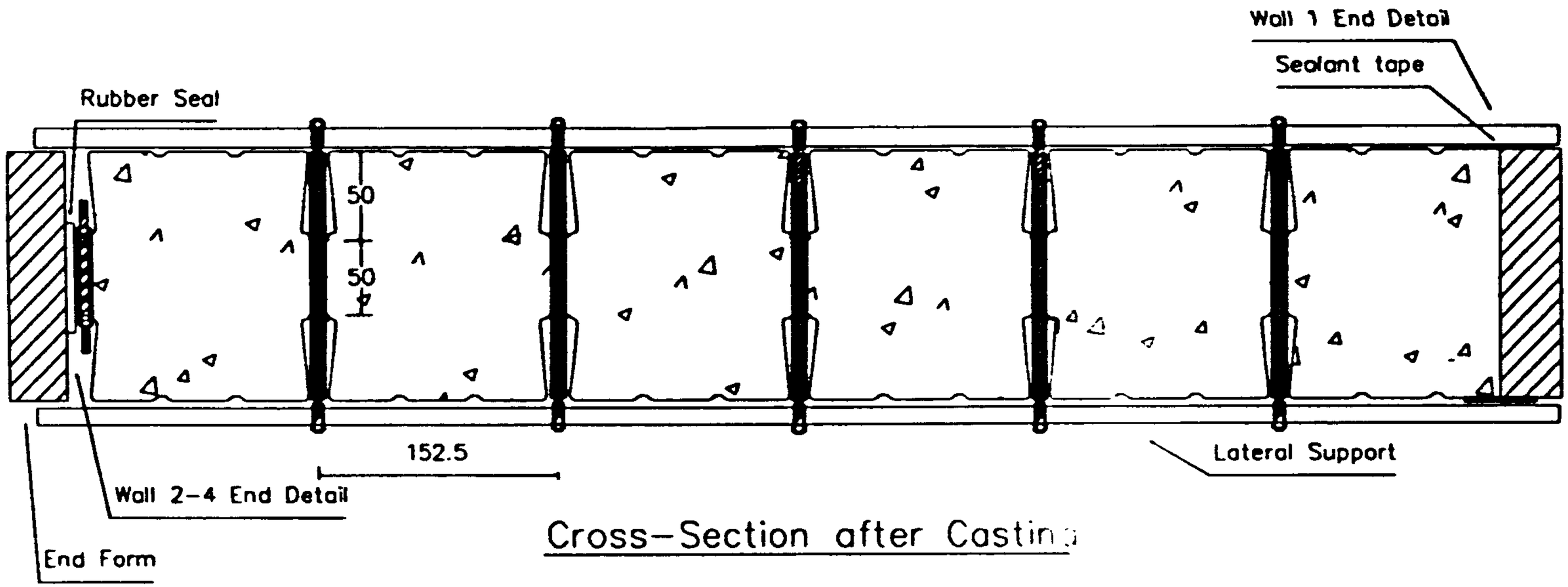

Cross–Section after Casting

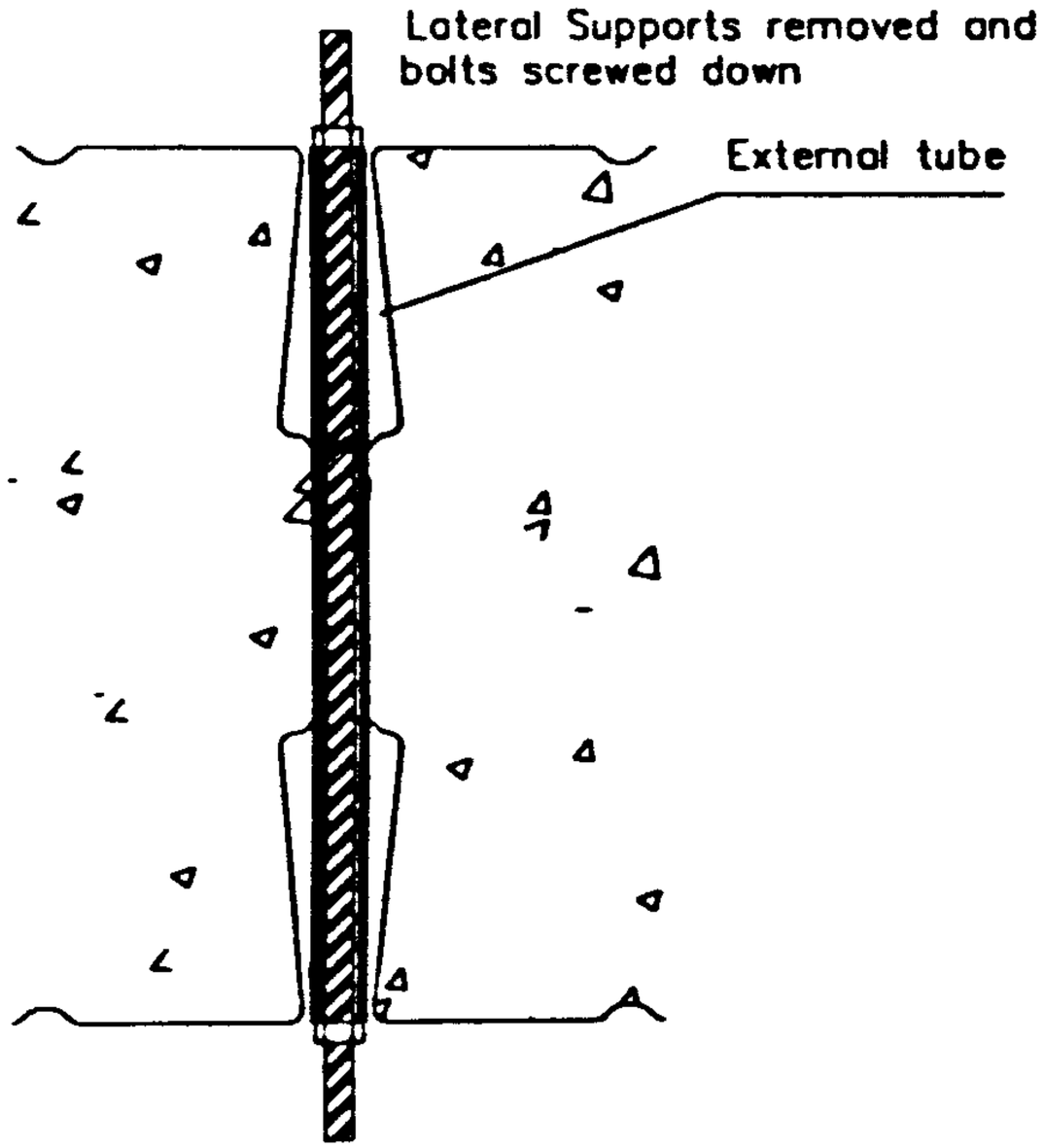

Typical Section before Testing

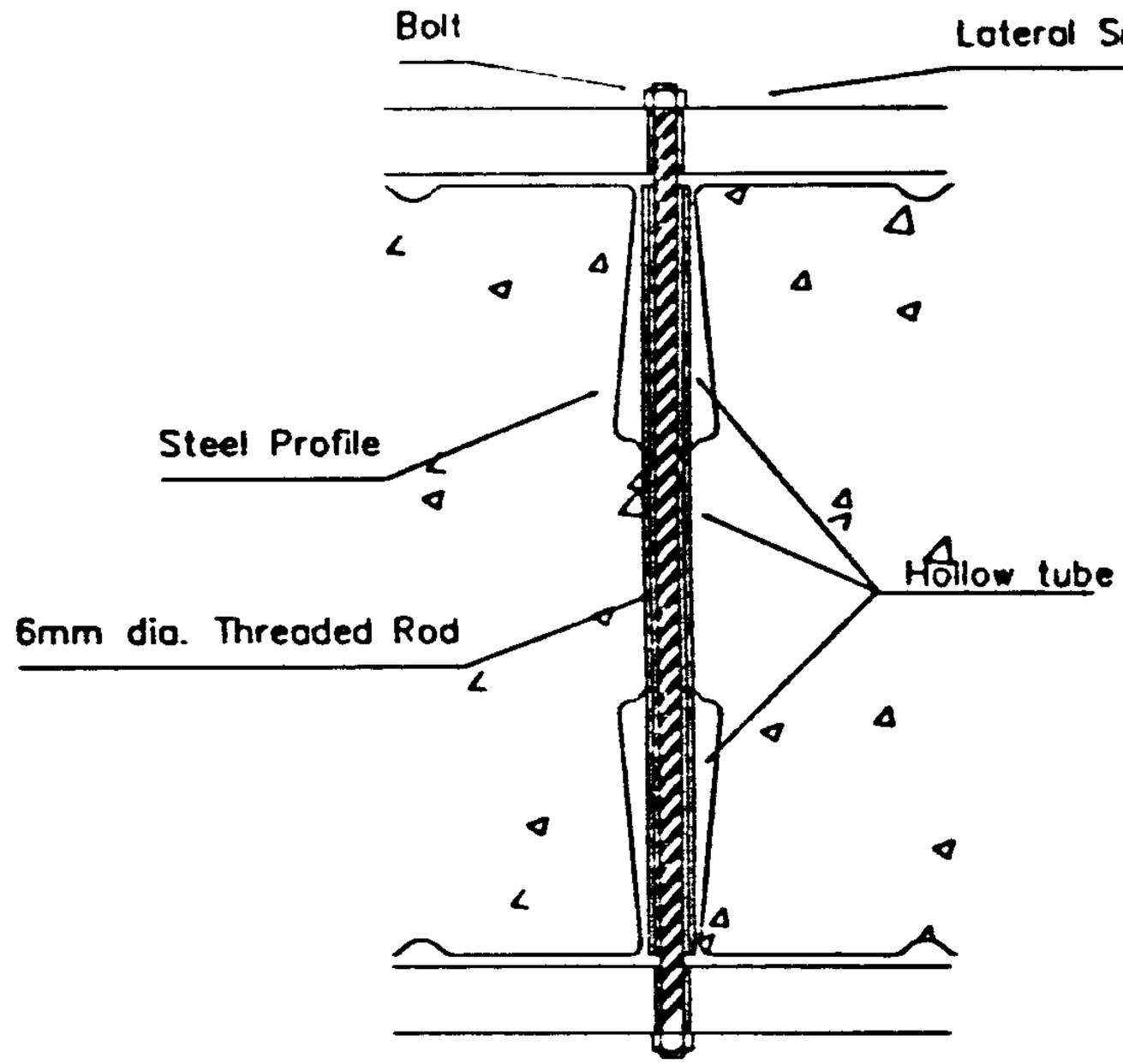

Typical Section after Casting

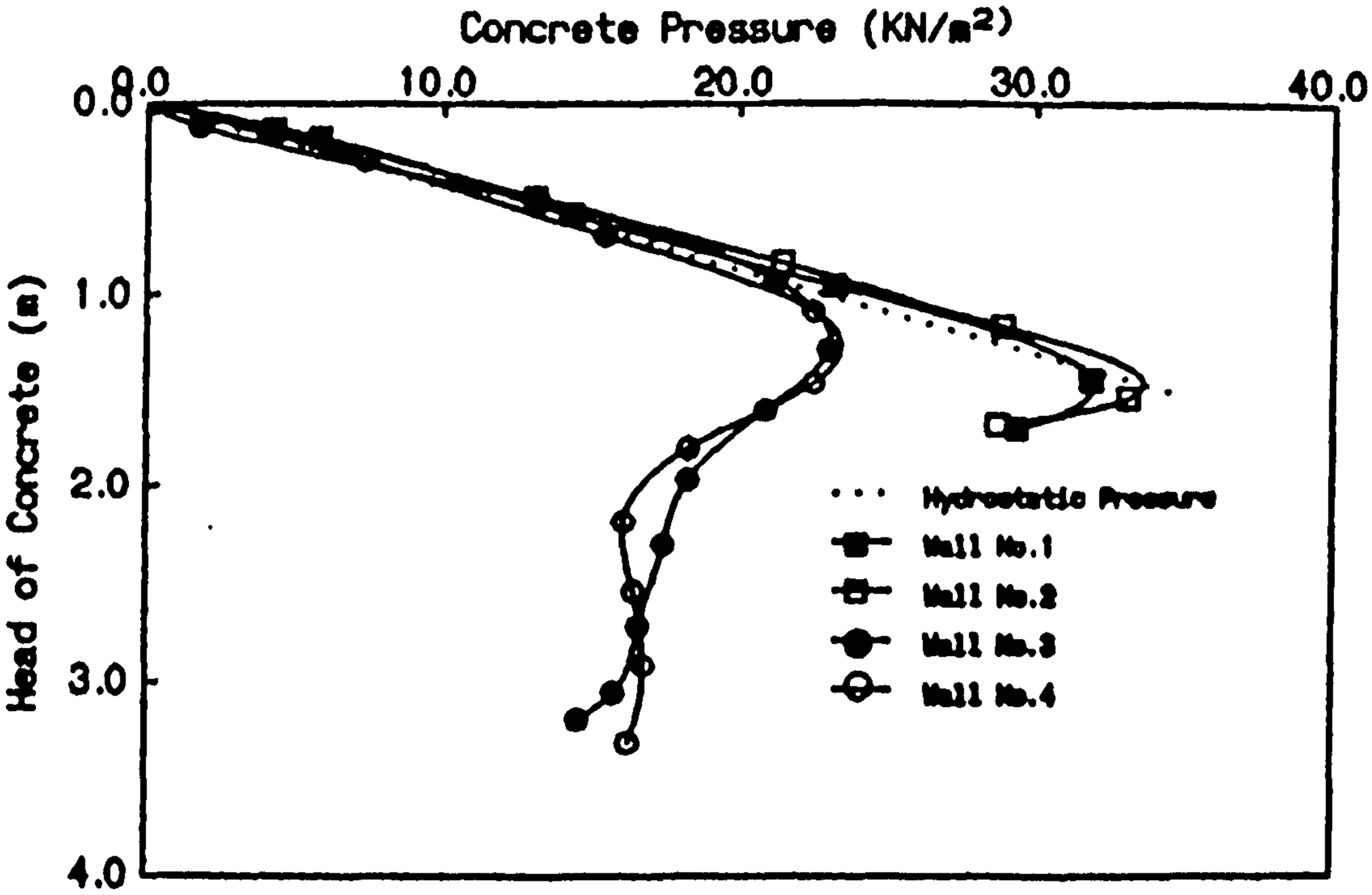

Figure 3.8 Concrete Pressures during Casting

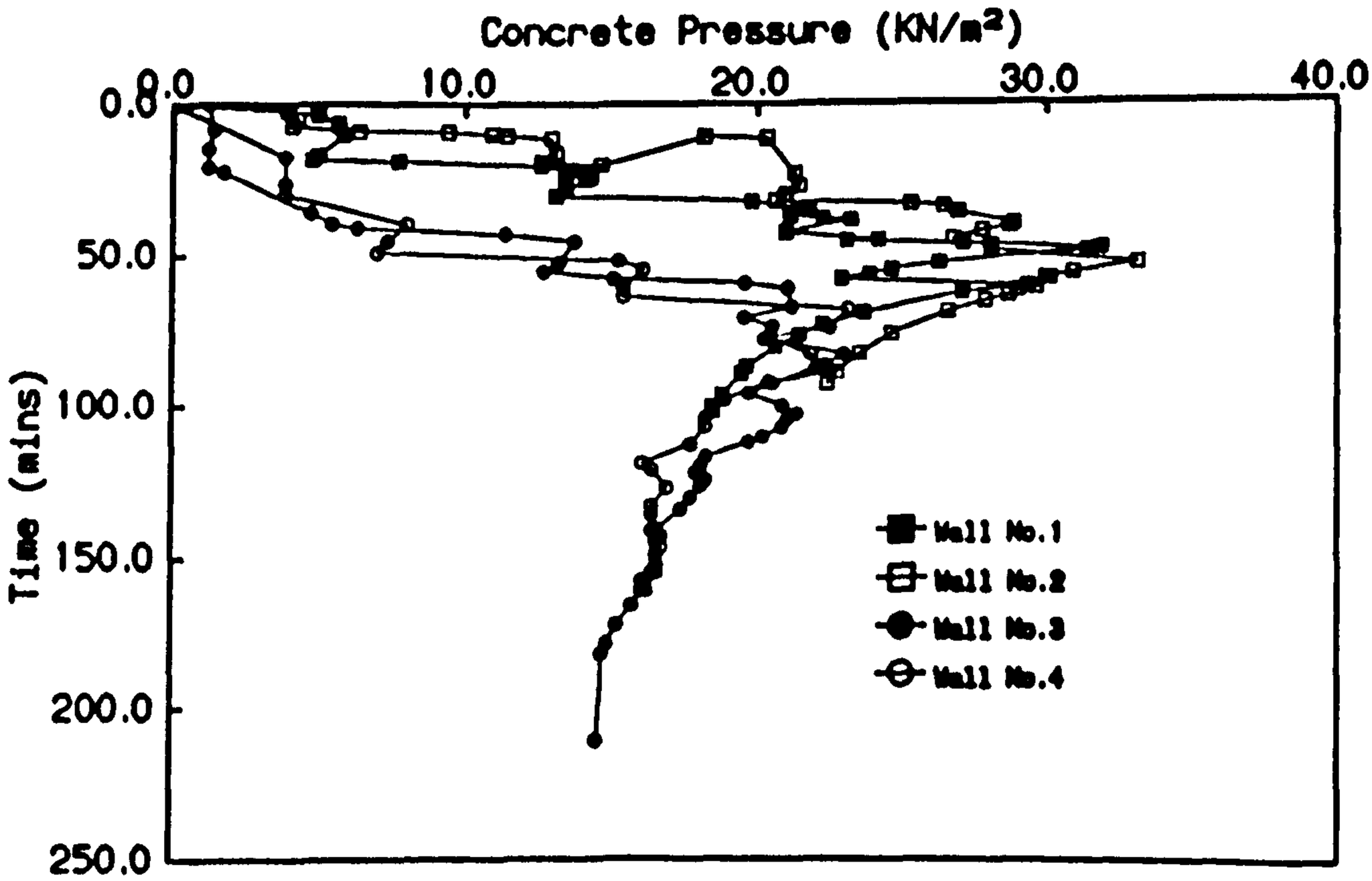

Figure 3.9 Concrete Pressures during Casting

Wall 1

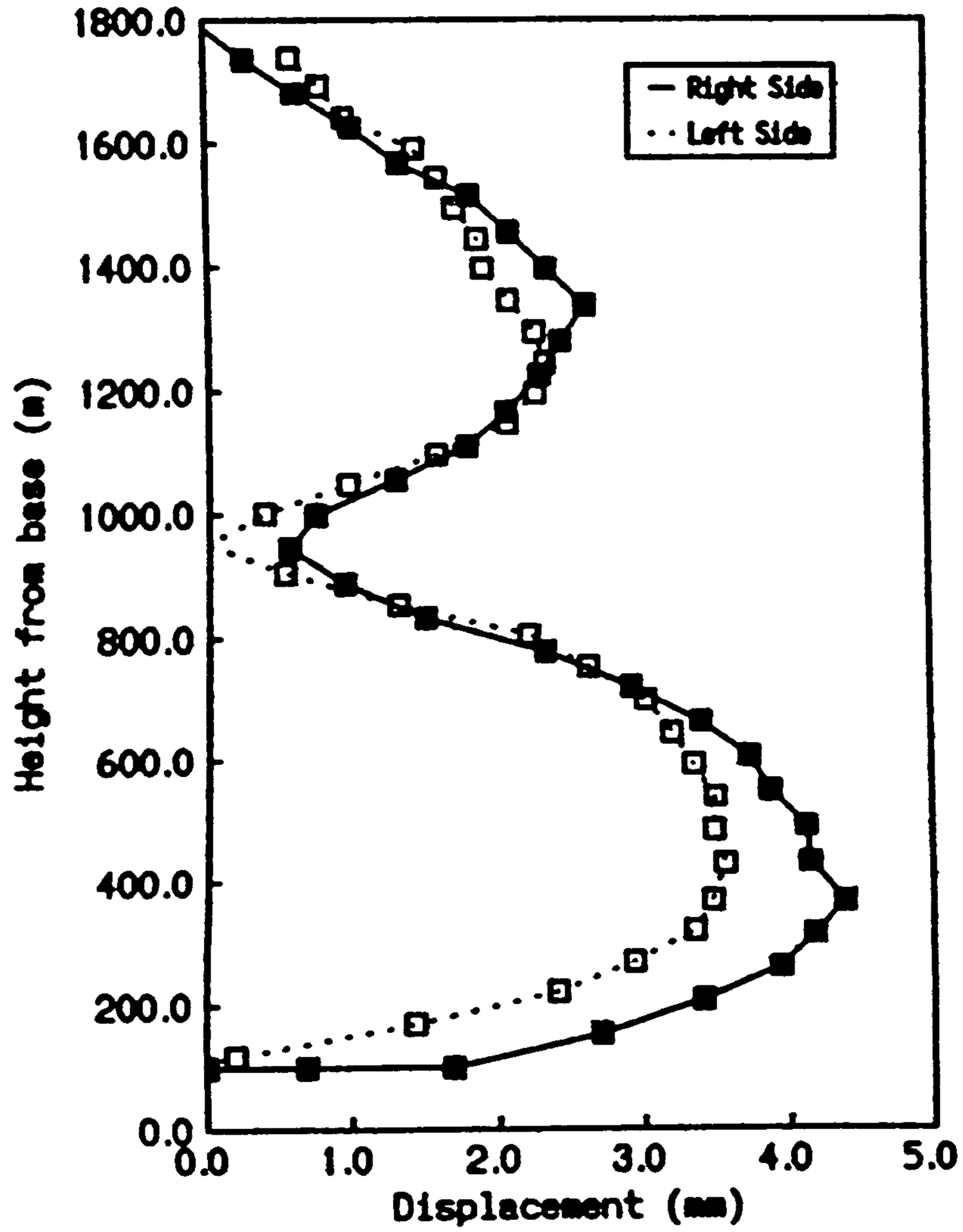

Figure 3.10

Wall 2

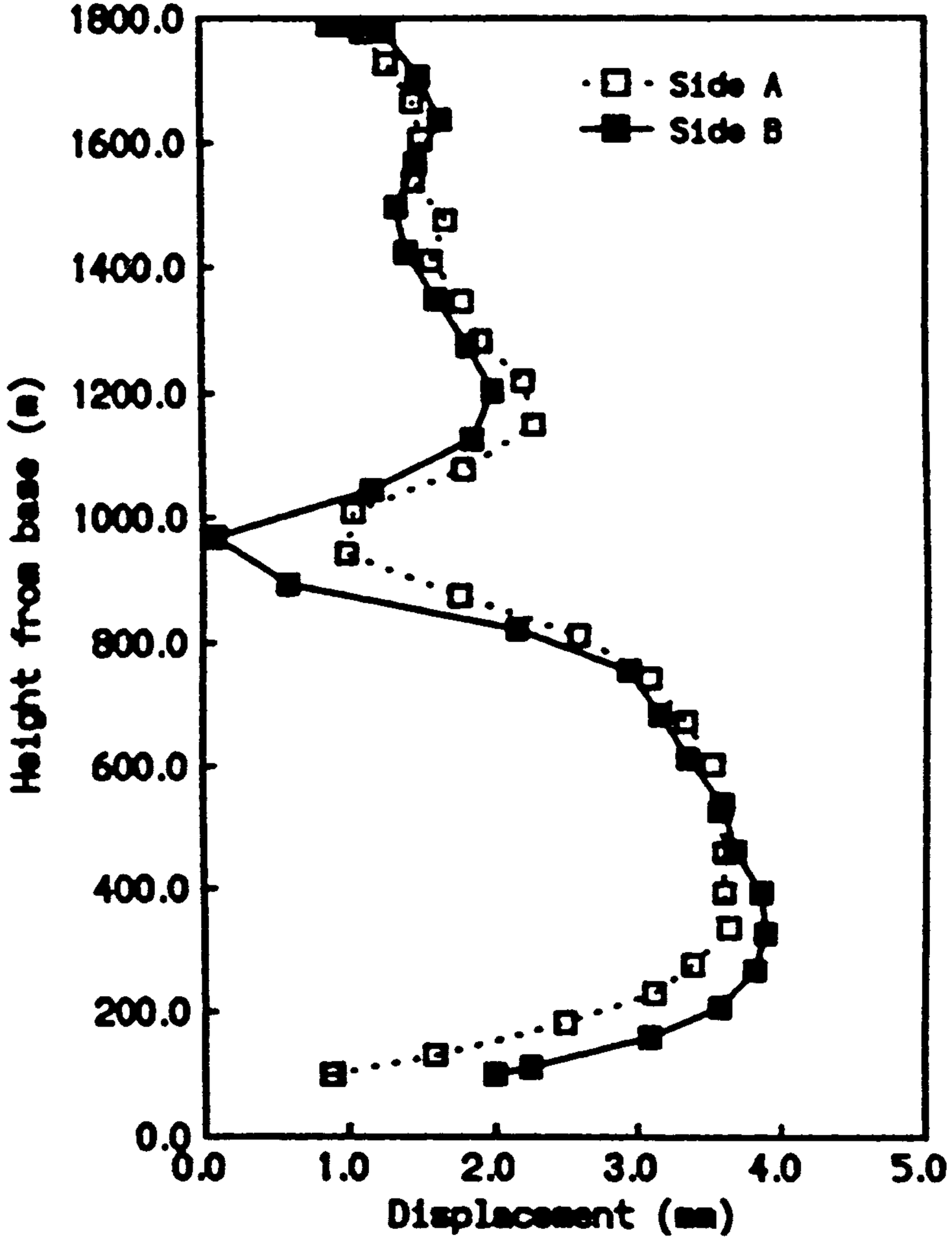

Figure 3.11

Wall 3

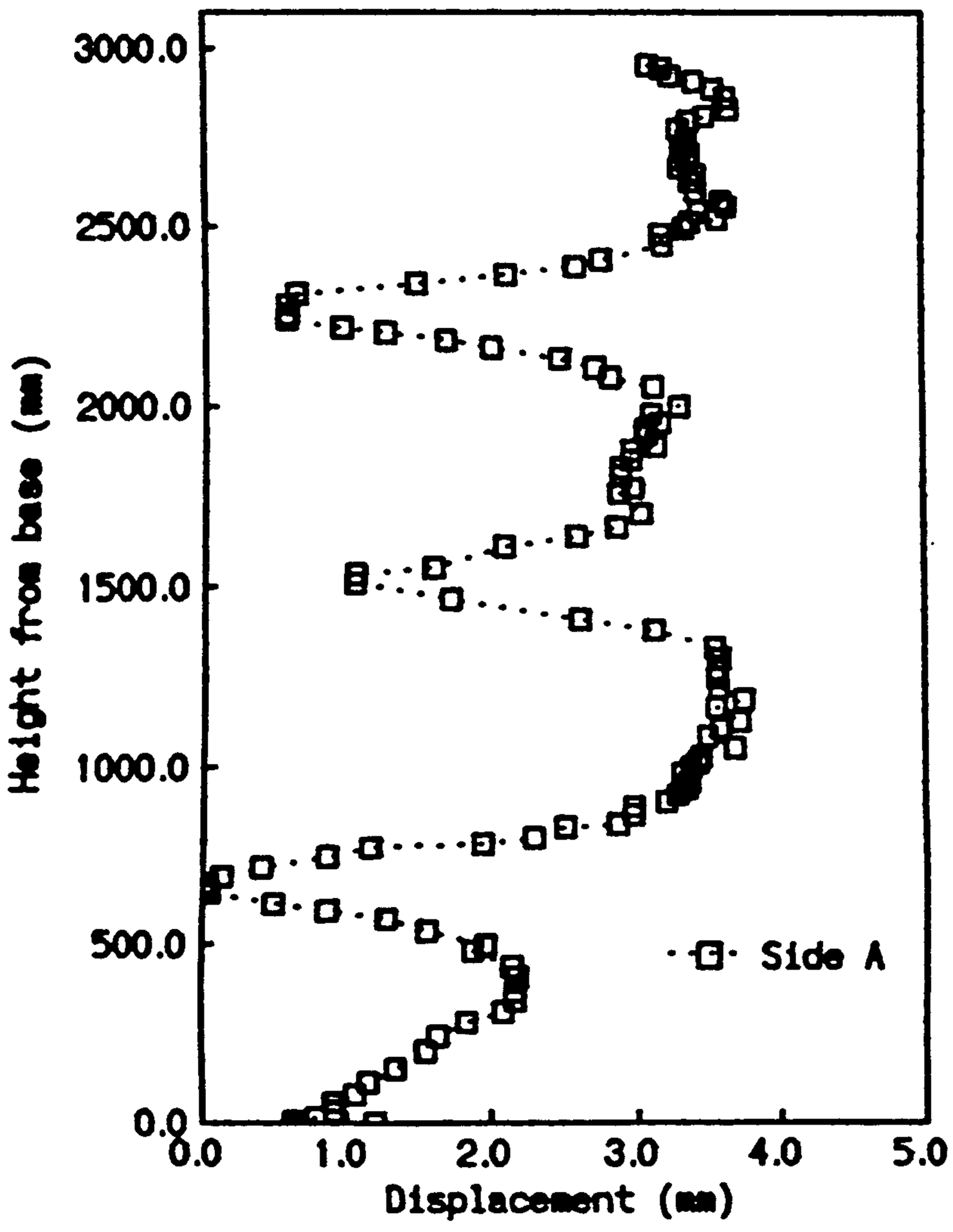

Figure 3.12

Wall 4

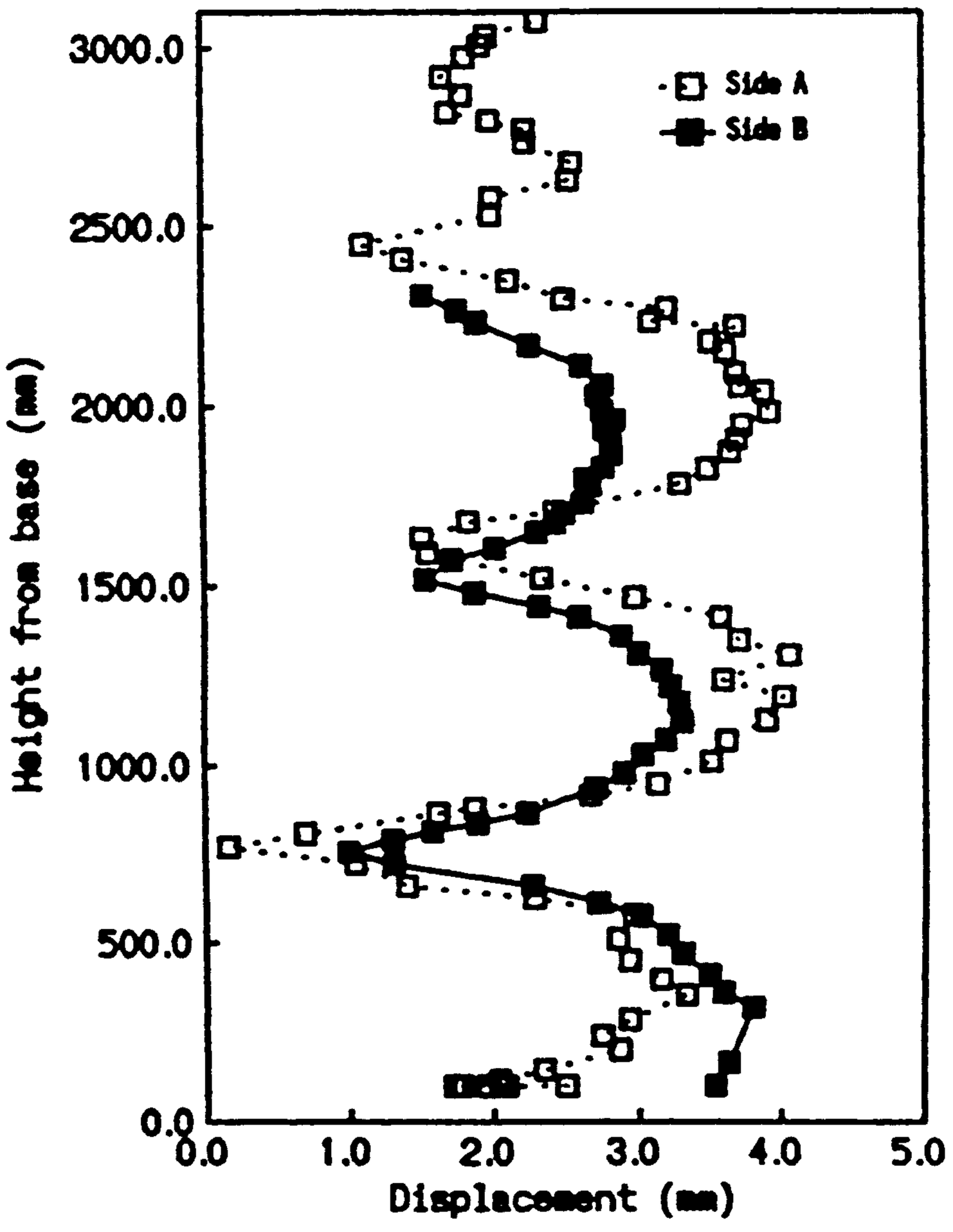

Figure 3.13

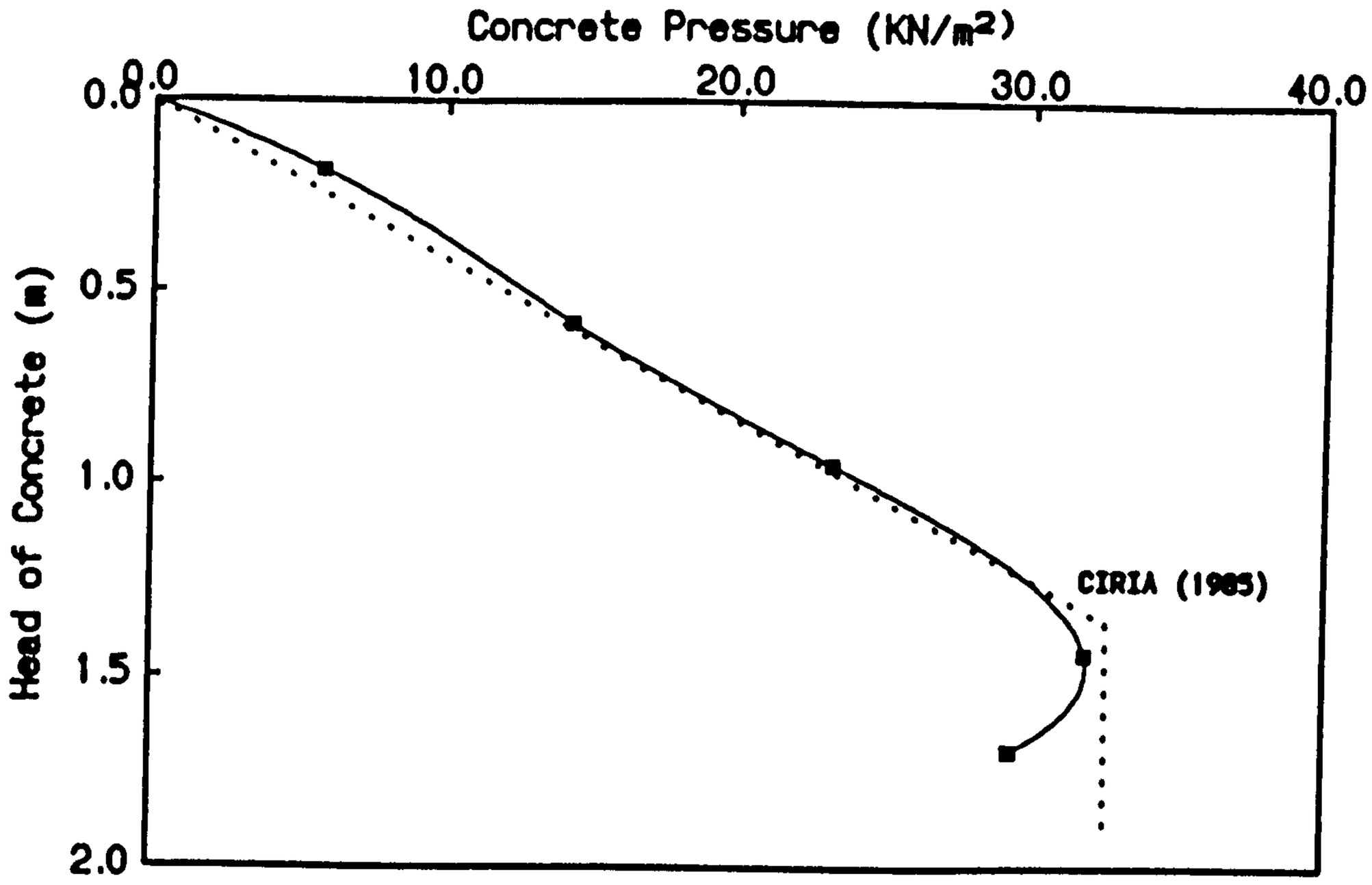

Figure 3.14 Wall 1 : Comparisons with CIRIA Recommendations

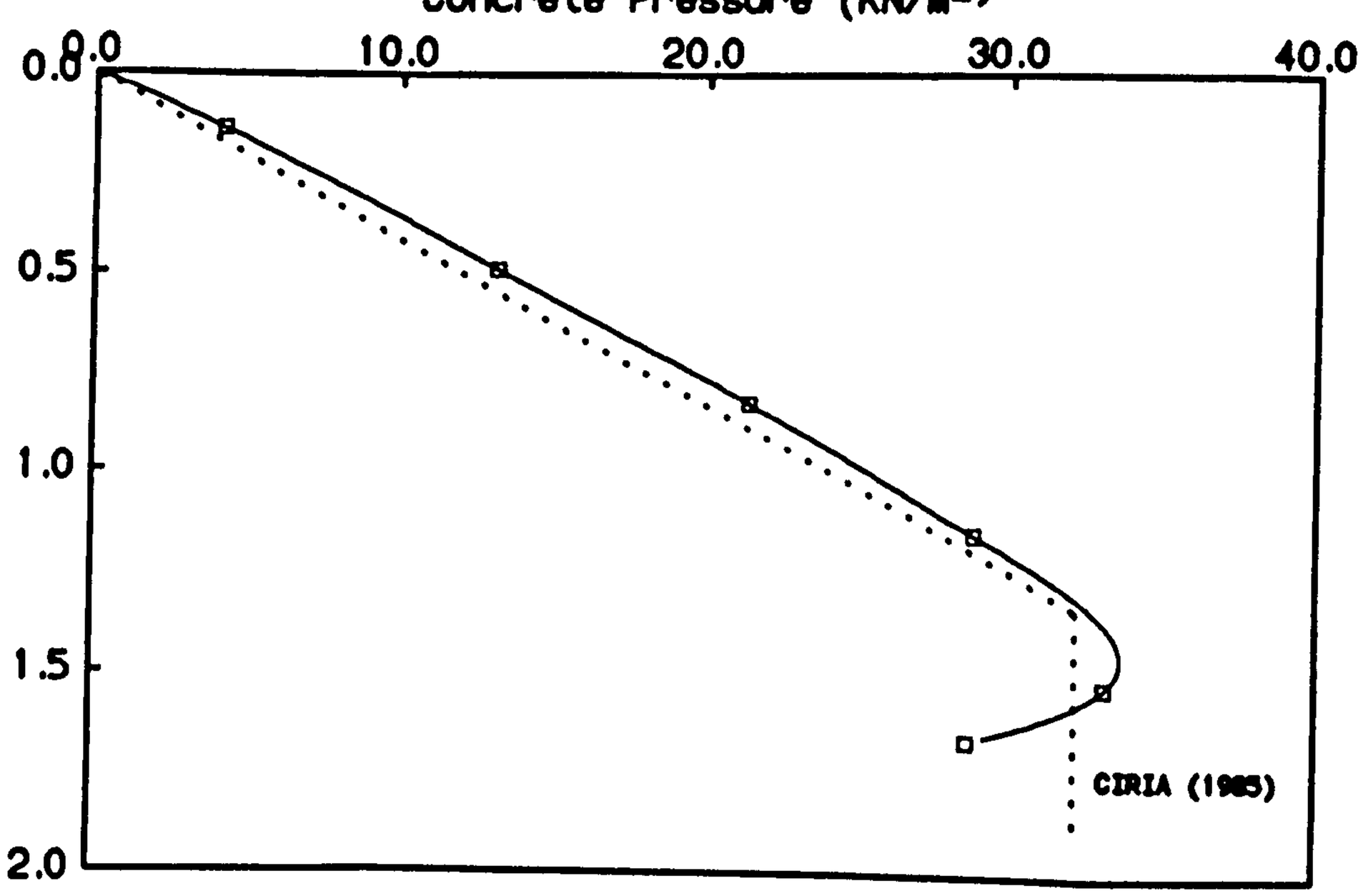

Figure 3.15 Wall 2 : Comparisons with CIRIA Recommendations

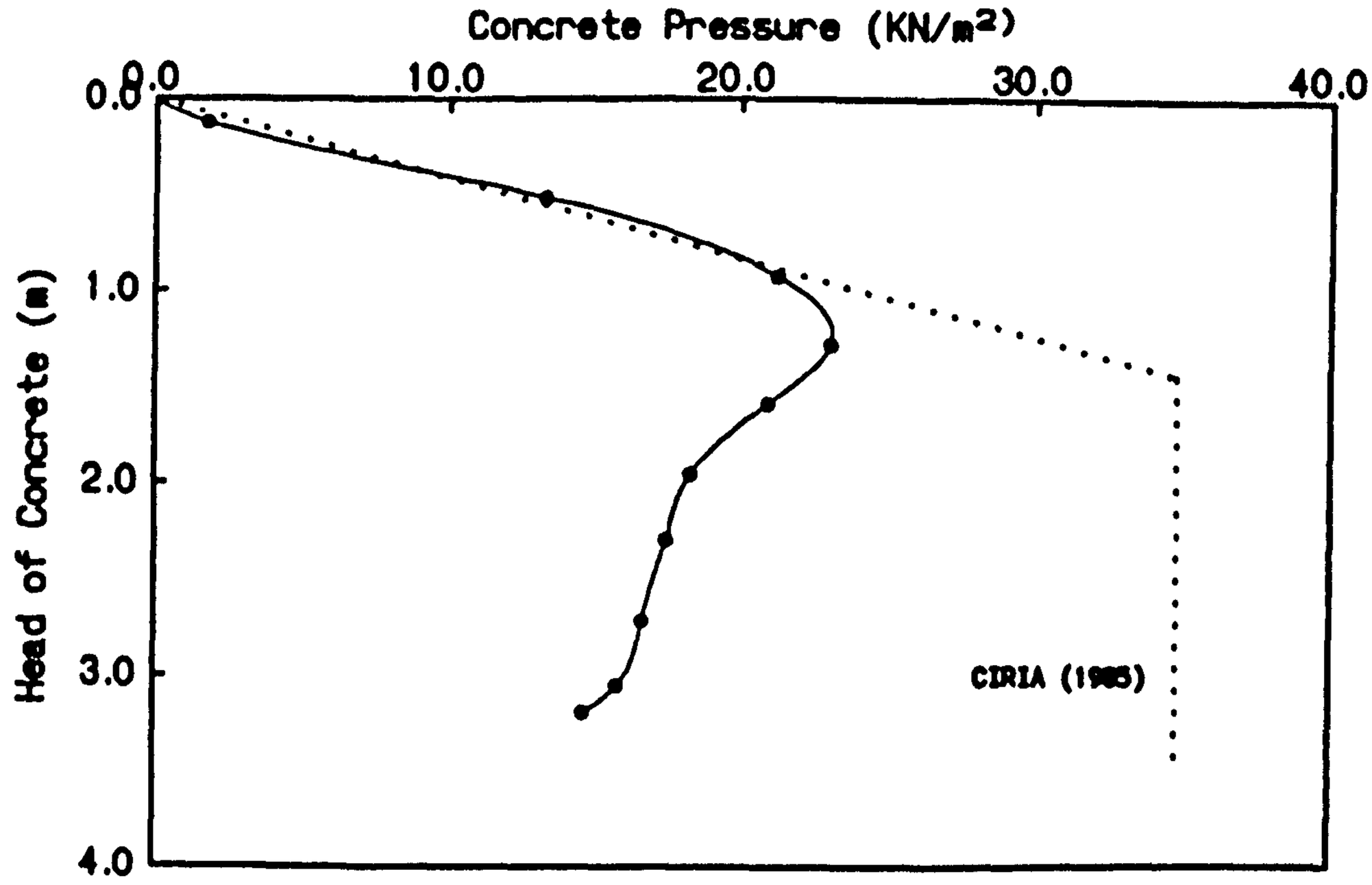

Figure 3.16 Wall 3 : Comparisons with CIRIA Recommendations

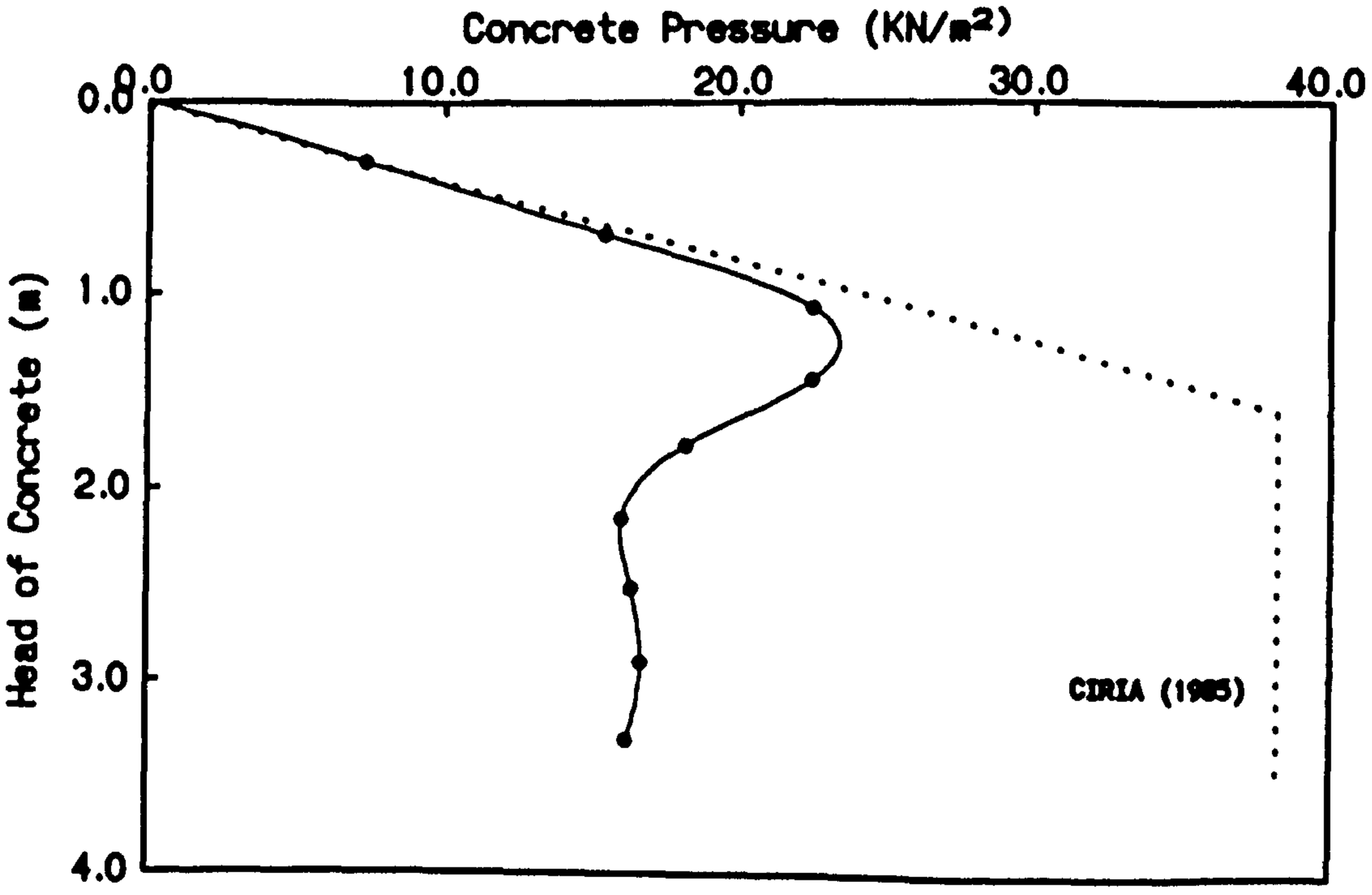

Figure 3.17 Wall 4 : Comparisons with CIRIa Recommendations

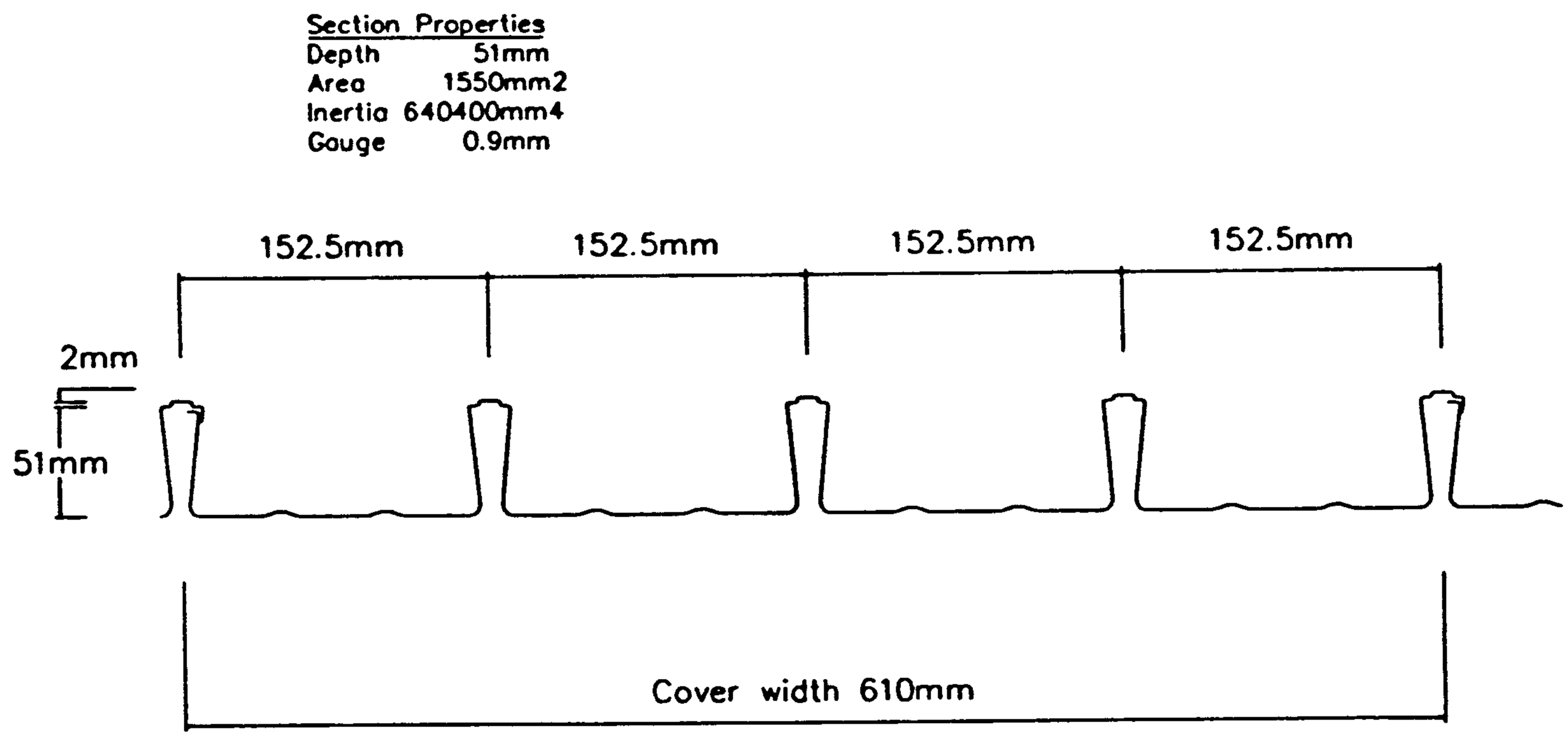

Figure 3.18 Profile Cross-Section

Chapter 4 Ultimate Testing

4.1 Introduction

The four initial pilot tests investigated the axial behaviour of the composite walls, in particular examining the local buckling and loss of bond at the steel concrete interface.

The ultimate experiments on the walls were performed on the loading frame in the Heavy Structures Laboratory at Strathclyde University. After casting the walls were lifted into the loading frame where they were axially tested to failure by 3 hydraulic jacks capable of applying a maximum load of 3000kN in compression. The object of the tests was to determine the maximum axial capacity of the walls and study the interface bond and local buckling behaviour of the profiled steel sheeting under loading.

4.2 Review

The previous research work relating to plain concrete reinforced with external flat steel plates, possibly bonded to the surface with epoxy resins or fixed with shear studs, was investigated. Both single and double steel skinned systems were examined for information that would prove useful in determining the possible behaviour.

L'Hermite and Bresson (1967) carried out tests on concrete beams with steel plate bonded by epoxy resin to the tension surface. Tests were also performed on beams with vertical sides which led to the formation of U-shaped permanent forms coated with epoxy resin into which the concrete was poured. The beams were loaded with the resulting performance characteristics monitored over a period of time.

Subsequently Bresson (1971) performed tests to determine the characteristics of the epoxy resin joint between the steel and the concrete.

Lerchenthal (1967) described a series of tests on two way spanning slabs with steel sheets bonded to the tension face of the concrete by epoxy resin. The biaxial strength of the sheet was expected to reduce the weight by as much as 50% compared to an equivalent traditional two-way reinforced slab. Interestingly examination of the cost savings of the proposed system were restricted to the structural efficiency of the slab, by reducing reinforcing material and overall slab thickness, rather than potential labour and formwork savings.

Solomon, Smith and Cusens (1976) working at the Wolfson Bridge Unit at Dundee University performed a series of flexural tests on double skin elements and investigated the suitability of the accepted design procedures. The main purpose of the work, carried out as a possible alternative to the standard slab design in medium and long span composite bridges, was to obtain knowledge of the structural behaviour and ultimate strength under loading of slab and beam specimens.

Two techniques were used to manufacture the slabs. In the first method the concrete core was cast and steel facing plates were glued onto both surfaces after the concrete had hardened. The second involved coating the plates with adhesive and casting the concrete directly against them in the mould.

All the tests beams were 2m long with tests 1-15 using the precast technique and tests 16 and 17 cast in place. The beams were loaded with two loads placed symmetrically about the mid-span. Deflections and Longitudinal strains were measured during the tests with the location and inclination of cracks also noted. The failure of all beams took place after slippage between the tensile plate and the concrete core. Most of the beams failed at the interface before yield occurred in the steel except for 4 tests in which the yield stress was achieved. The strain in the upper steel plate remained well below the yield strength with no indication of buckling prior to failure reported. Two double skinned slabs were also tested with failure resulting from punching of the slab due to shear failure around a load patch. During punching the lower steel plate was pushed down and peeled of the concrete

with the top plate bent upwards around the load patch. Based on the experiments an empirical equation was proposed for design purposes.

Taylor (1976) and Taylor, Mills and Rankin (1978) described a series of tests on T-beams where the reinforcement consisted of high strength reinforcement and a channel secured by shear studs to the base of the web (see figure 4.1). A total of 25 beams were tested in flexural and shear tests with variation in the distribution and type of reinforcement.

In the flexural tests all beams failed as a result of crushing of the concrete between or adjacent to the load points. The beams deflected up to 15% more than would have been expected from the equivalent reinforced concrete section because of the loss of stress at the channel/concrete interface. It was therefore suggested that some adjustment to the serviceability requirements would be required if this system was designed in practice.

Following from previous work Solomon and Goplani (1979) described a series of 5 tests on beams externally reinforced by a single steel sheet. In these tests it was decided not to use epoxy adhesives to attach the steel sheets to the concrete as adequate bond was expected by the casting process itself. The external reinforcement consisted of a 1.84mm thick mild steel sheet of 4m length and 0.36m width. Stirrups were also provided, the same thickness as the sheet, and welded to the surface of the sheet.

The loading of each test was carried out in increments to failure by applying two point loads through a loading beam. The deflection of the beams, and strains in the concrete and steel under the loading were recorded.

All beams collapsed due to failure of the upper concrete in flexural compression following tension yielding of the lower steel sheet. No bond failure at the steel concrete interface was observed during the tests or indication of shear cracking within

the shear span. The calculated ultimate loads based on steel yielding were close to the observed values indicating failure soon after yield.

They concluded that the beams satisfied the ultimate and serviceability requirements and that the main economies of this approach would be in ease of construction and reduction in reinforcing steel and formwork.

Mays and Smith (1980) updated work carried out at the Wolfson Bridge Research Unit and confirmed the viability of bonded steel plates as a viable structural option but suggested further work was required on the long term durability and performance under actual traffic conditions.

Ong and Cusens (1982) at the Wolfson Bridge Research Unit noting the low stresses obtained on the upper flanges in the work of Solomon *et al* (1976) carried out a series of tests using the cast-in-place technique - applying the adhesive to the steel and casting the concrete on top. Different adhesive and mix types were tried on the 38 beams and 6 slabs cast.

The authors concluded that provided an efficient bond existed between the concrete and steel both slabs and beams behaved compositely. The long span tests failed in bending with the short span tests from shear slip with collapse after detachment of the concrete from the steel. For optimum strength and ductility a 1mm minimum adhesive thickness was suggested.

MacDonald (1978) reported on a series of four tests on reinforced concrete beams with steel plates bonded to their tension flanges. The tests related to the possible use for increasing the load capacity of existing bridges. He noted that existing on-site work had been performed to improve the serviceability in terms of crack control and deflection rather than to increase the ultimate capacity of particular bridges.

The factors considered in the tests were the resin type, the number of steel plates, the

thickness of the plates and the effect of load cycling. The strains and deflections were monitored with the vertical and horizontal slip between the steel and the concrete also measured. An interesting result of the experiments was the failure of the beams at a load similar to that of the unplated beams because of horizontal shear forces removing the steel plate at loads below the ultimate unplated beam strength. The variables tested also had little effect on the load causing plate separation as this was according to MacDonald more a function of the concrete strength.

Harmoush and Ahmad (1990) examined the debonding of concrete beams strengthened with steel plates applying linear elastic fracture mechanics and the finite element method. The conservation laws were applied to determine the energy release rate at which the crack would propagate and beam failure occur. One result of the tests was that for undamaged concrete beams the strain energy release rate was negligibly small giving a high interface debonding load. Also, the strain energy release rate reached a maximum value when the length of the interface crack was equal to the length of the flexural cracks the adhesive thickness had little effect on the failure load.

One of the largest bodies of work investigating the application of double skin beams and columns has been performed at the University of Wales College of Cardiff. The system was originally devised for submerged tube tunnels by a team of consultants in Cardiff (Messrs Tomlinson and Partners with Sir Alexander Gibb and Partners). The system proposed by Narayanan *et al* (1987) consisted of a double-skin steel-plated construction secured by welding headed studs at suitable intervals anchored in a concrete infill (see figure 4.2). The spacing of the studs was used to control local buckling of the steel sheets under loading.

The advantages suggested over conventional reinforced concrete tunnels included fabrication in sections, allowing speedier construction and better quality control. Also, in conventional concrete tube tunnels an outer steel layer is required to ensure watertightness but with external skin reinforcement this would not be required.

Tests were performed on full- and half-scale models of the tunnel sections. The half-scale tests with a rectangular cross-section 250mm deep x 800mm wide and 4m long had steel plates 6mm and 3mm thick secured to the outside and inside of the concrete by 6mm diameter mild steel bolts. The failure of the beams in simply supported and cantilevered tests was exhibited by shear cracks developing in the concrete at the quarter span positions with steel plate buckling and yielding accompanied by stud shearing. The ultimate observed experimental loads agreed with the theoretical loads based on a fully composite action. The full scale tests shown in figure 4.3 had full size stud connections spaced at 300mm centres. The type of failure, as before, occurred from shear failure at the quarter-span position. Narayanan *et al* concluded the applications of the system were not restricted to submerged tunnels but had wider general applications in construction.

Following from this initial work Oduyemi and Wright (1989) reported on an investigation into the behaviour of double-skin sandwich beams. The tests on eighteen model beams of dimension 150mm x 150mm x 1500mm were loaded by a symmetrical two-point load as shown in figure 4.4. The factors investigated were:

- overlapping of shear studs
- steel skin thickness
- spacing of top shear connector
- amount of bottom shear connection
- low concrete strength

The beams were expected to fail in either flexural, horizontal slip or vertical shear failure. The bond between the steel plate and the concrete was removed by greasing the inside faces allowing the studs alone to take the interface shear forces produced.

When flexural failure of the beams occurred the deflection was linear up to tensile yielding of the lower steel. After yielding the beams behaved with a large amount of ductility until collapse produced by concrete crushing.

Horizontal slip failure occurred after the flexural cracking of the concrete and an increasing rate of bottom slip. The failure was sudden with shearing of the bottom plate from the concrete caused by stud failure.

Vertical shear failure occurred in the 'diagonal tension' manner with final collapse when the dowel action capacity of the steel plates was reached. This type of failure was prevented by introducing long studs to provide shear reinforcement.

Local buckling of the compression plate reduced the value of ultimate load in some tests and so a maximum stud spacing/plate thickness ratio of 30 was proposed.

Oduyemi and Wright concluded that flexural failure of the beams could be realised by providing adequate short studs to transfer shear bond and long studs to carry diagonal tension stresses. In order to take account of the effects of combined shear, axial and bending stresses the design strength of the shear studs was recommended to be 55% in the tension zone and 80% in the compression zone of the ultimate strength obtained from push-out tests.

Subsequently Wright and Oduyemi (1989) published work on double skin composite columns. The work examined 23 small scale columns considering

- steel area
- concrete strength
- ratio of shear connector spacing/steel thickness
- shear connector length

for 10 concentric tests and

- load eccentricity ratio
- tension and compression steel thickness
- amount of shear connectors under compression and tension

for the eccentrically loaded tests.

Push out tests were performed to obtain a load-slip characteristic for the shear studs. The concentrically loaded tests (see figure 4.5) all failed by crushing with plate buckling occurring prior to failure in one test where the ratio of stud spacing/steel thickness was 50. In another test where the stud length/stud diameter ratio was 6 gradual pull-out of the studs occurred followed by immediate collapse.
Based on the test observations recommendations were made restricting the stud spacing/steel thickness ratio to 33 and the stud length/stud diameter to a minimum of 6. Also suggested for sufficient anchorage was a stud head/shank diameter ratio of 2 and a minimum size of stud equal to the plate thickness.

Most of the columns tested in the eccentric tests failed in compression with the others failing by 'interface shear bond failure' at either the compression or the tension plate.

A theoretical study was also performed with a squash load for a short column assuming full connection given by :

$$N_u = 0.67 f_{cu} A_c + A_s f_s + A_r f_r \qquad ..4.1$$

where

A_c	=	Area of concrete
A_s	=	Area of steel
A_r	=	area of reinforcement
$0.67f_{cu}$	=	strength of concrete in compression
f_s	=	yield strength of steel
f_r	=	yield strength of reinforcement

This equation showed good agreement ranging between 90 and 110% of the experimental values. For design purposes BS 8110 and BS 5400, Part 5 partial safety factors were introduced.

In order to examine the theoretical columns a small program was written assuming full interaction between the steel and concrete portions. Where flexural failure occurred the calculated failure loads were reasonably close to the experimental values but in the case of shear slip failure an overestimation of the collapse load resulted. Upon adjusting the ultimate collapse loads to take account of this effect it was noticed that lower failure values occurred than expected suggesting :

- a reduction in the capacity of tension zone shear connectors
- a reduction in the capacity of all the connectors due to the existence of a connector axial load
- an increase in the force transmitted by the connectors due to strain hardening after yield

Where slender column effects are present the approach from BS8110 was recommended, over that of BS 5400 Part 5, treating the plate as reinforcement.

Oduyemi and Wright (1990) continued the previous investigations by testing 12 scale model beam/column elements. The factors considered were :

- magnitude of axial load
- amount of shear connection between the layers
- thickness of the steel plates

The test elements of dimension 150mm and 150mm in cross-section and 2.3m in length with mild steel plates, 2 to 6 mm thick, on the top and bottom surfaces. There were 3 groups of 4 tests cast varying the factors already mentioned above.

The first group of tests investigating variations in the axial load failed in a flexural manner with flexural cracks appearing at higher load levels for greater axial loads.

In the second group, where the spacing between the connectors varied, those tests

with the studs closely spaced failed in flexure while the later tests with studs further apart collapsed due to longitudinal shear.

In the final group looking at the effect of thickness, the initial tests with thin plates failed in flexure because of yielding of the steel. In the final test with the thickest plate the shear studs failed, before yield, at the steel/concrete interface.

The authors concluded that the shear connection at the tension plate was critical in determining the behaviour of the element but with correct design predictable critical loads could be achieved.

Kountoris (1990) produced design charts for the double skin composite elements based on the requirements of BS8110 with modifications to take account of failure at the steel/concrete interface. The design curves showed greater convergence to experimental results as the load eccentricity increased probably because flexural rather than axial failure occurred. When the degree of interaction fell below 60% of the ultimate plate capacity the experimental load was less than the predicted design load.

Wright, Oduyemi and Evans (1991) described design developments based on the series of tests on double skin beams, columns and beam/columns. The design basis applied was similar to that of reinforced concrete but with the additional considerations of the possibility of plate buckling and adequate provision of shear connectors. The ultimate strength in bending was based on the BS 8110 stress block with a partial safety factor of 1.5 on the concrete and 1.15 of the steel strength. These equations assumed full connection between the steel plate and the concrete which to be achieved required sufficient shear connectors capable of transferring the full yield load to the steel. The correct number of shear connectors was evaluated and found to be 0.5 for the tensile area and 0.8 for the compression area. The reason for the difference is the severe cracking of the concrete in the tensile area causing a reduction in the stiffness. The section could therefore be designed for stud failure.

To ensure that buckling of the compression plate does not occur where double studs are used a stud spacing to plate thickness ratio of 67.5 based on work by Wright (1989).

In shear the basic design strength, not including the effect of long shear studs, was recommended to be that of BS 8110 table 3.9 with a reduction of 20% to allow for the crack inducing effect of the shear studs.

For elements under only axial compression, short braced elements were recommended designed from equation (39) in BS 8110 assuming that no plate buckling or connection problems.

When combined axial load and bending forces act on the element the forces were resolved to give two equations solved by iteration and based on an unknown depth of neutral axis and bending moment capacity. Design charts were also produced dependant on variations in plate thickness. The actual thickness of the steel plate is reduced to an equivalent thickness if the number of shear studs is insufficient to transfer the full yield load. Although different thicknesses and degree of connection were possible on each side it was thought safe to design for the thinnest plate and degree of connection on the tension face as tests showed that the connection strength on the compression face did not greatly effect the strength.
For serviceability requirements the span/depth ratio given in Table 3.10 of BS 8110 were thought sufficient for most cases with a transformed section analysis possible although full connection may not be achieved.

The design proposals were validated by performing 11 full scale tests on beam, column and beam/column elements.

In concluding the authors noted the need for slender column behaviour to be investigated as partial interaction may have a significant effect where buckling is likely to occur.

Perhaps the closest program to the proposed use of profiled sheets in Composite Walling is the development of the ASP Construction System proposed by Yerushalmi (1988) in the United States. The development of the system was primarily for use in protective structures from blast resistance and weapons.

The proposed wall element consists of exterior steel panels and diagonal interior steel lacing panels with a concrete fill. The ASP wall is erected on conventional concrete foundations with roof slabs constructed using a bottom ASP exterior panel in manner similar to floor decking. The walls vary in thickness from 8 to 16 inches and can be filled with concrete, crushed stones or sand. The main advantages of the ASP system according to Yerushalmi are:

- the potential cost savings compared to equivalent reinforce concrete systems.
- ASP walls are approximately half as thick as reinforced concrete alternatives.
- the higher factor of safety compared to reinforced concrete
- reinforcement, formwork and anti-spalling protection and RF shielding provided in one system.
- increase in speed of construction and reduction in falsework requirements.

The system has been proposed for blast resistance in the chemical industry, military structures capable of withstanding near miss and localised effects of air bombs, and protective structures and walls effective against terrorist car bomb and demolition attacks.

The testing programs have involved four different types of tests have been performed to assess the ASP performance. Israeli Defence Force tests assessed ASP against fragments generated by near miss air bombs. High resistance to penetration was achieved as spalling of the inside surfaces was prevented by the inner steel surface.

Further tests investigated the systems dynamic response, protection against chain detonations and the effects of direct rockets hits where 50 percent less penetration

occurred than in massive concrete.

Details of the system and the applications are sensitive and detailed results are classified because of the military applications.

The review carried out was based on work with flat steel sheets although the tests recently performed employed profiled steel sheeting with a variable geometry. Also, the bond in the current tests was established by mechanical rather than by epoxy resin or shear studs. The effect of these changes may have a significant effect on the performance of composite walls.

4.3 Material Tests

Concrete tests were performed according to BS 1881:Parts 103,106,108 and 121 with 100 mm cubes and cylinders to establish the cube strength, compaction factor (wet density) and Young's modulus of the concrete. The cube tests were performed after 7 days at the time of testing and at 28 days. The results of the tests performed are given in tables 4.1 and 4.2.

4.4 Composite Wall Dimensions and Features

The basic features of each wall are given in figures 3.3 - 3.6 and in table 4.3.

4.5 Transfer of Walls to Loading Frame

In order to transfer the walls to the loading rig a lifting frame was constructed from steel channels and angles present in the laboratory. This system worked, as shown in plate 1, by counterbalancing the weight of the walls with steel weights on an additional channel section bolted to the end of the existing channel. This system allowed the wall to be placed directly between the loading beams without the crane cable being restricted by the upper cross-beam on the test rig. Once each wall was in place the channels were unbolted and the rear section removed. No problems were encountered using this method of lifting the walls which proved extremely effective

and greatly reduced manual time and handling.

4.6 Composite Wall 1

The wall shown in figure 3.3 was cast to the top of the profiled steel sheet. A 5mm plywood spreading plate was located between the top of the wall and the loading beam for a smooth transfer of load. At the top and bottom of the wall a light steel cage was placed to prevent local concrete cracking. As the wall was located directly on a channel section which acted as a base during the casting and transfer, there was no need for a spreading plate on the base. With the wall in the test rig the lateral supports and threaded rod ties were removed.

4.6.1 Instrumentation

Having set the wall in the correct central position the LVDT instrumentation was set up to measure the lateral deflection established during casting and for the subsequent load testing. The LVDT positions for the lateral deflection have already been mentioned in section 3.6 but three addition LVDT's were added to record the overall shortening of the wall under the vertical load. The LVDT's were attached to the unstressed lateral deflection rail as to attach to the loading rig columns would have produced significant errors in the readings during the test. The reason for the two upper LVDT's as opposed to the single LVDT, at the base, was to check that no significant rotation of the walls occurred at the top before failure. Rotation at the base was restricted by the lower loading beam bolted to the cross-beams. All LVDT's were calibrated and read into the SPECTRA-DAS recording system as were the strain gauges.

The strain gauges shown in figure 3.3 were positioned at strategic locations on one half and each side of the wall. Gauges were placed on a re-entrant rib, at the centre of a flat and on an outer flat at the top, middle and bottom of each side of the wall. The gauges placed on the re-entrant ribs were fixed from the inside with a small hole drilled to connect the wiring. It was hoped that by placing the gauges on the re-entrant ribs and the central flat sections at each level, stress differences caused by

local buckling and reduced interface shear transfer on the flats would be apparent. It was also expected that transfer of load from the concrete to profiled steel sheet would occur between the top and centrally located gauges, further from the point of load.

4.6.2 Loading

The axial loading of the walls, applied by the three hydraulic jacks through the load cells, proceeded in 250 kN stages up to 2000 kN where an unloading re-loading cycle was performed with loading continuing in 100 kN stages up to failure. At each loading stage (including no applied load) readings were taken of the deflected profile of the steel sheeting, the strain gauges and the LVDT's measuring vertical deflection. The LVDT's recording the deflected profile were positioned to run along the centre of the profile where local buckling was most likely to occur.

4.6.3 Results

Visual observation of cracking on the wall faces was obviously impossible during the loading sequence. At the wall edges some cracking was seen on the concrete surface at the top of the wall. As the wall was loaded the load spreading plywood plate was crushed under the increasing load with bearing on the profiled steel sheet occurring at higher levels. The sheeting at the edges, with no re-entrant along the outer edge, buckled at a load below the final ultimate load. The effect of the bearing load on the steel profile was to buckle the profile locally between the ribs at the top and crush the ribs. Upon failure, which took place without warning at 2100 kN, some bursting at the top of the wall occurred accompanied by concrete crushing.

Figures 4.6 - 4.9 show the steel strains at the top, middle and bottom of the profiled steel sheets on the re-entrant and flat portions of each face. The gauge locations are given in figure 3.3. The Lateral displacement of the profiled steel sheeting found using the LVDT displacement system is shown in figure 4.10 and 4.11. Each line represents a sweep of the system across the profile for a particular level of load. The diagrams also show the initial deflection at the start of the tests from the lateral

concrete pressure.

4.6.4 Discussion of Results

As can be seen from the strain diagrams, at no time does the steel sheeting obtain a yield stress under the applied axial load, with a maximum of 1100 microstrain recorded. Generally, the strain recorded on the flat sections between the ribs was similar to those on the re-entrant portions. This was probably because the sheeting was bearing on the steel beam once the plywood loading plate crushed and was not relying on the steel concrete bond. At about 1300 kN the sheet slipped under the loading as can seen from loss of stress in gauge 7 of figure 4.6. The load was probably shed into the concrete as there is no indication of any transfer to the re-entrant portions or elsewhere. After slip occurred little load capacity was left in the steel central sections although the re-entrants continued to pick up load. The values of strain recorded in the middle of the wall are higher than those at the top or bottom (gauges 7 and 4). This indicates a gradual transfer of the load through the interface bond from the concrete to the steel away from the loading points. Figure 4.12 shows the load plotted against the axial displacement but is unreliable as crushing of the plywood plate contributed to the displacement. The lateral displacement system indicated some movement at the top of the wall during the loading sequence but this was small in comparison to the height. As the wall neared failure there is some indication on figures 4.10 and 4.11 of local buckling near the tie rod positions. This suggests the lateral displacement from the concrete pressure may produce instabilities that lead to local buckling of the sheeting.

4.7 Composite Wall 2

4.7.1 Introduction

The results of the first test suggested some changes to the construction of the second short wall (figure 3.4). These consisted of:

1. The wall was constructed with an additional half re-entrant at the ends in order to prevent warping during casting (see figure 3.7) and to increase the

buckling capacity at the ends under axial loading.

2. The tie rods linking the profiled steel faces were left in place after casting to resist shear forces and bursting forces at the top of the wall.

3. The plywood plate at the top of the wall was replaced by a concrete cap using a 1:2 mix of high alumina cement and sand.

4. The light mesh cage at the top and bottom was not installed for the second test. The loading regime remained the same as the initial test although the LVDT system failed during the test and therefore no lateral displacement data was available.

4.7.2 Results

Similarly to Wall 1, during loading of the wall there was little indication of the approach of failure. The failure occurred by crushing of the concrete at the top of the wall accompanied by buckling of the steel sheeting. At the top of the wall the concrete cap was about 5mm above the top of the profiled steel sheeting allowing slippage between the profiled steel sheet and the concrete without the steel sheeting bearing on the loading beam.

The strain gauge results for sides A and B are given in figures 4.13 – 4.16 with the vertical displacement under loading in figure 4.12

4.7.3 Discussion of Results

It can be seen from the strain gauge results in figure 4.13 that between 1000 kN and 1500 kN bond failure occurred at the top of the wall. The bond failure, evident on the flat sections between the ribs (gauges 7, 5 and 3), was reduced slightly on the re-entrant sections where a stronger bond existed. Leaving the threaded rods in the steel prevented bursting at the top of the wall.

4.8 Composite Wall 3

This test (figure 3.5) was the first of two, 3.4m high wall experiments. The details were similar to the previous test but A198 mesh was welded to the top and bottom 600mm of the profiled steel sheet across the re-entrant portions (see figure 4.17) to increase the bond.

4.8.1 Instrumentation

The addition of concrete embedment strain gauges at the top, middle and bottom of the wall allowed monitoring of the concrete strains during the loading of the tests.

4.8.2 Results

The behaviour of this wall was similar to the previous tests with failure occurring at close to the top. The effect of the mesh was to increase the rate of load transfer, from the concrete to the steel sheeting. This increase in steel strain resulted in local buckling between the re-entrant portions further from the wall than the failure location. Despite the increased bond, failure of the wall occurred by crushing at the top of the wall.

The strain gauge results for the concrete and the steel sheeting are given in figures 4.18 - 4.21 and 4.22. The displacement under the axial load is given in figure 4.12 and the lateral displacements in figure 4.24.

4.8.3 Discussion of Results

It was apparent from the results that the mesh had increased the bond strength between the steel and concrete surfaces with no bond failure evident from the results of the strain gauges. This allowed a better distribution of strain between the steel and the concrete further down the wall.

As the loading increased local buckling of the profiled sheeting was observed and measured by the lateral displacement system (figure 4.24). The buckles appeared slightly above the tie level, showing the significance of the initial sinusoidal

displacement, due to the lateral concrete pressure in the formation of local buckles. The wall failed close to 2000 kN which was similar to the previous experiments. Although the bond strength and rate of stress transfer were increased, the steel sheeting close to the top of the wall was only slightly stressed. As a consequence only concrete at the top was loaded and therefore the wall failed by concrete failure. There was no evidence of global buckling of the wall probably because the wall never achieved a fully composite ultimate load.

4.9 Composite Wall 4

4.9.1 Introduction

The second of the 3.4m walls (figure 3.6) was similar to the previous test with the addition of deformed bar reinforcement to the top of the wall (see figure 4.17). The reinforcement was added to prevent concrete crushing of the wall at the top and force failure to occur further down the wall, where a greater proportion of load had passed from the concrete to the steel sheeting. The bar reinforcement had an approximately equal area to the steel sheeting.

4.9.1 Results

The behaviour of the wall was similar to the previous test with buckling of the steel sheeting prior to failure. By introducing bar reinforcement at the top, ultimate failure was shifted to a position lower down the wall.

The steel and concrete strain gauge results on the final wall are given in figures 4.25-4.26 and 4.23 respectively with the lateral displacements in figure 4.29 and 4.30.

4.9.2 Discussion of Results

The strain gauge results were similar to the previous wall. There was a loss of bond at gauge 16 on side B which may have been caused by the buckling of the profile at the same position near gauge 5 on side A. The gradual loss of stress on gauge 5 after 1500 kN was due to increasing buckling of the sheet at this point.

Figure 4.30 shows local buckling deformation before failure near gauge 5. The buckles are shown on plates 4 and 5. The wall failed above 2000 kN below the area of the bar reinforcement at the local buckling position.

4.10 Comparison of Experimental/Theoretical Results

An initial comparison of the results with those suggeted from the theoretical capacities, with various assumptions, is given in Table 4.4.

- the concrete capacity
- the ultimate capacity
- the concrete capacity + the buckled steel capacity

4.10.1 Concrete Capacity

The concrete capacity is based only on the capacity of the concrete in the walls and was found from the equation

$$N_{conc} = 0.67 f_{cu} A_c \qquad ..4.2$$

where A_c = Area of concrete

$0.67f_{cu}$ = strength of concrete in compression

The empirical 0.67 factor reduces the cube strength obtained from tests to the compressive capacity in the element under test and contains no partial safety factors. The load obtained from this equation is that expected where bond failure and slippage occur before failure with no load transferred from the concrete to the steel surfaces.

4.10.2 Ultimate Capacity

The ultimate capacity assumes the steel reaches yield and sustains this stress until concrete failure occurs. The expected failure load in this case is

$$N_u = 0.67 f_{cu} A_c + A_s f_s + A_r f_r \qquad ..4.3$$

where A_s = Area of steel

A_r = Area of reinforcement

f_s = Yield strength of steel

f_r = Yield strength of reinforcement

The load capacity produced by this equation would be that expected where full interaction occurred throughout the height of the wall with the steel sheeting obtaining yield.

4.10.3 Concrete Capacity + Buckled Steel Capacity

This equation considers the possibility of buckling of the thin outer skin of steel occurring before the yield stress is achieved. The method of BS 5950 Pt 4 is applied to reduce the area of steel in sections where buckling is likely to occur.

$$N_{buck} = 0.67 A_c f_{cu} + f_s A_{sr} \qquad ..4.4$$

where A_{sr} = reduced area of steel

4.10.4 Discussion

Table 4.4 shows that the ultimate experimental loads obtained are close to the concrete crushing loads with no reinforcement present. The results suggested that no composite action was mobilised with the bond unable to effectively transfer load between the steel and concrete at failure.

4.11 Slenderness of Walls

There was no evidence of global buckling in tests 3 and 4 as the loads necessary to produce instability could not be achieved before concrete crushing resulted in failure. It may be possible to apply the method BS 8110 to take account of slender elements by modifying the technique for composite decks where shear bond failure is an additional likely failure mode.

4.12 Conclusions

The results of the ultimate testing of the short 1.9m and more slender 3.4m walls have highlighted the advantages and problems associated with composite walls using profiled steel sheeting.

The two main factors affecting the performance of the walls are the interface bond strength between the steel and the concrete and the local buckling capacity of the steel sheeting.

4.12.1 Interface Bond Strength

The structural action of composite walls is different under bending and axial loads. Under the action of bending forces, in simply supported loading conditions, the maximum tensile force occurs at the centre of the member where the bending moment is greatest gradually reducing to zero at the supports. As a result the tensile force produced at the centre can be distributed to areas nearer the supports that are less highly stressed. The effect in axially loaded columns is different. In the case of columns where the steel and concrete are loaded together then interface shear is not a factor as both materials are under similar strains. If the concrete alone is loaded at the top, as was the case in tests 2 - 4, then the load must be transferred rapidly into the steel or concrete failure will occur at the top. The action of axially loading the concrete causes steel slippage towards the top (or bottom) of the member, the reverse of the bending action. The solution to this problem is either to reinforce the top of the wall with bar reinforcement, to force failure further down where load transfer has occurred, or to have a very strong bond at the top to pass load rapidly to the steel.

The steel profile used in the series of tests showed good bond on the re-entrant portions which had embossments but poor bond on the flat sections which had no mechanical transfer mechanism. By adding a light mesh the bond was increased but not sufficiently to prevent concrete crushing at the top.

4.12.2 Local Buckling

Having achieved a better interface bond in tests 3 and 4 local buckling of the sheeting between the re-entrants became a problem as higher stress levels were achieved in the sheeting (plate 4 and 5).

4.13 Summary

This chapter completed the experimental work on the four pilot tests performed under the SCI contract. The main difficulty encountered during in the tests was the brittle failure of the bond between the concrete and steel surface before the ultimate load was reached, and local buckling of the steel sheeting between the re-entrant ribs.

In the following chapter an analytic model of the walls is derived from one-dimensional beam theory to obtain a better understanding of the load transfer process and the effect of partial interaction on the buckling capacity of the composite walls.

Table 4.1 Material Tests at 7 Days

Wall No.	Cube Str No.1 (N/mm^2)	Cube Str No.2 (N/mm^2)	Cube Str No.3 (N/mm^2)	Cube Str Av. (N/mm^2)	Comp Fac.	Wet Density (kN/m^2)	Young's Modulus (kN/mm^2)
1	27.7	24.9	25.1	25.9	0.98	24.0	17.5
2	26.6	24.6	25.8	25.7	0.98	24.0	16.8
3	22.6	23.8	24.6	23.7	0.98	24.0	18.4
4	30.7	26.8	26.5	28.0	0.98	24.0	19.0

Table 4.2 Material Tests at 28 Days

Wall No.	Dry Cube No.1 (N/mm^2)	Dry Cube No.2 (N/mm^2)	Dry Cube No.3 (N/mm^2)	Wet Cube No.1 (N/mm^2)	Wet Cube No.2 (N/mm^2)	Wet Cube No.3 (N/mm^2)
1	34.8	35.0	-	42.4	40.9	42.2
2	43.0	43.2	44.0	-	-	-
3	-	-	-	-	-	-
4	36.0	33.6	36.2	43.0	49.0	44.0

Table 4.3 Wall Dimensions and Features

Wall No.	Height (mm)	Thickness (mm)	Ties	Length (mm)
1	1900	150	removed	845
2	1900	150	retained	900
3	3400	150	retained	900
4	3400	150	retained	900

Note: Only in test 1 were the ties removed before testing.

Table 4.4 Comparison of Theoretical and Experimental Failure Loads

Wall No.	Concrete Crushing Load	Fully Composite Failure Load	BS 5950 Pt.4 Buckling	**Experimental Load**
1	2168	2927	2463	**2150**
2	2176	2971	2618	**2000**
3	2007	2802	2618	**1950**
4	2372	3166	2618	**2100**

Note: All loads shown are in kN.

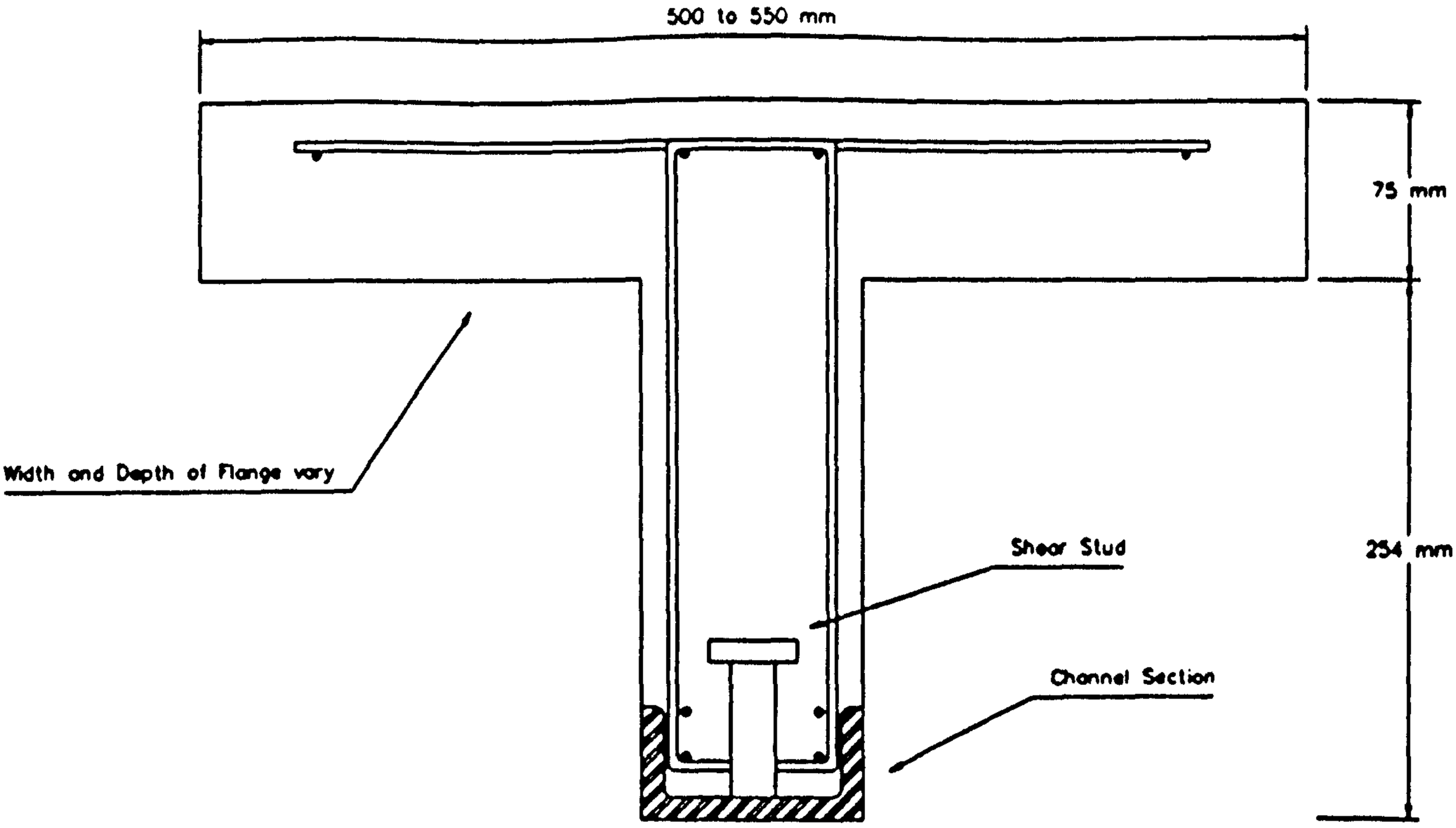

Cross–Section of Type of Beam tested

Figure 4.1

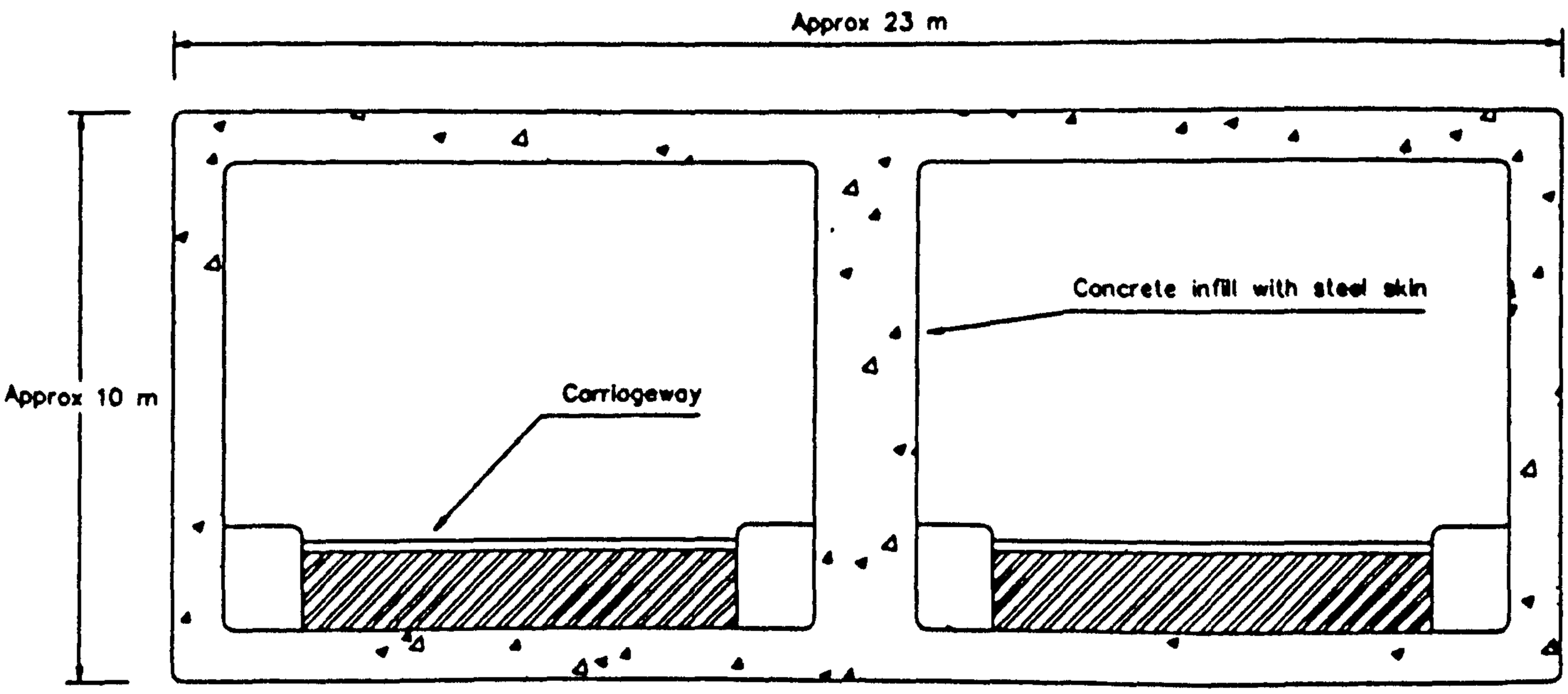

Typical Tunnel Section

Figure 4.2

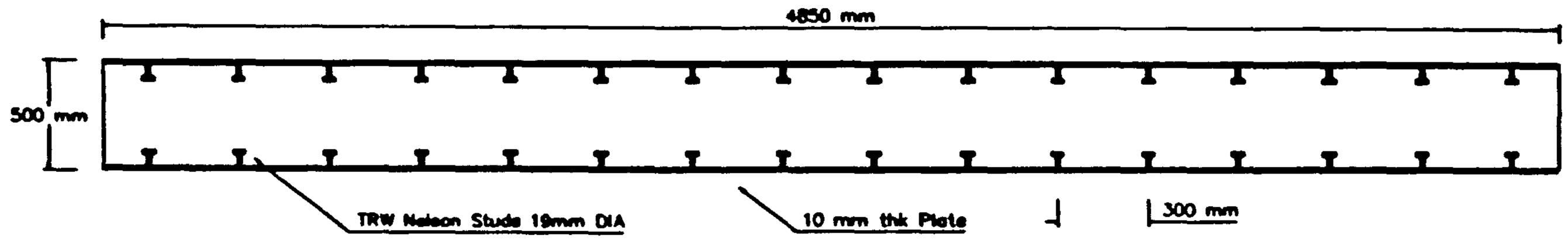

Elevation of Full Scale Test Beam

Figure 4.3

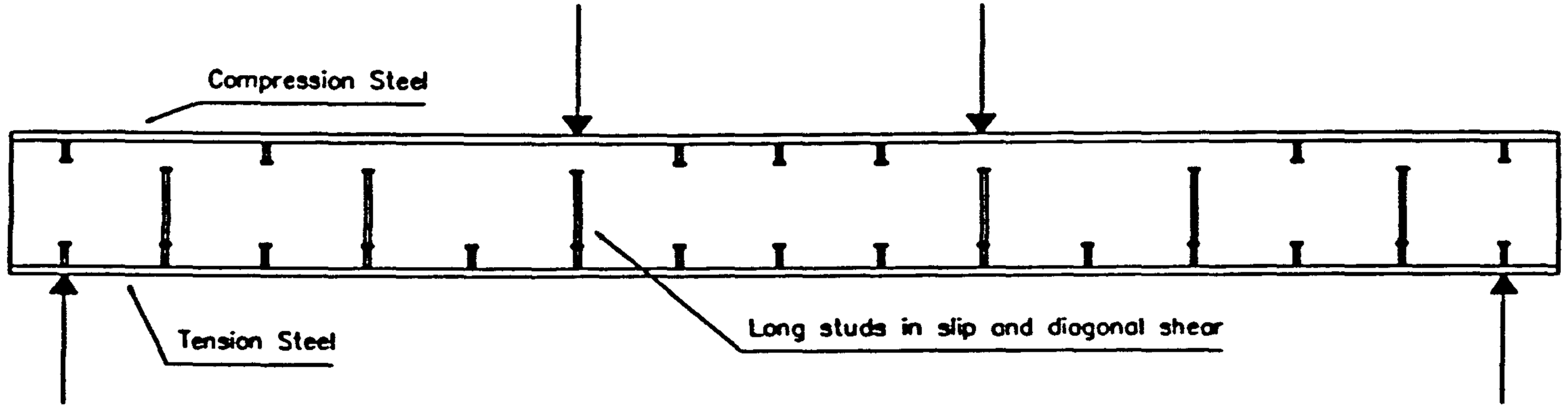

Double–skin Composite Beam

Figure 4.4

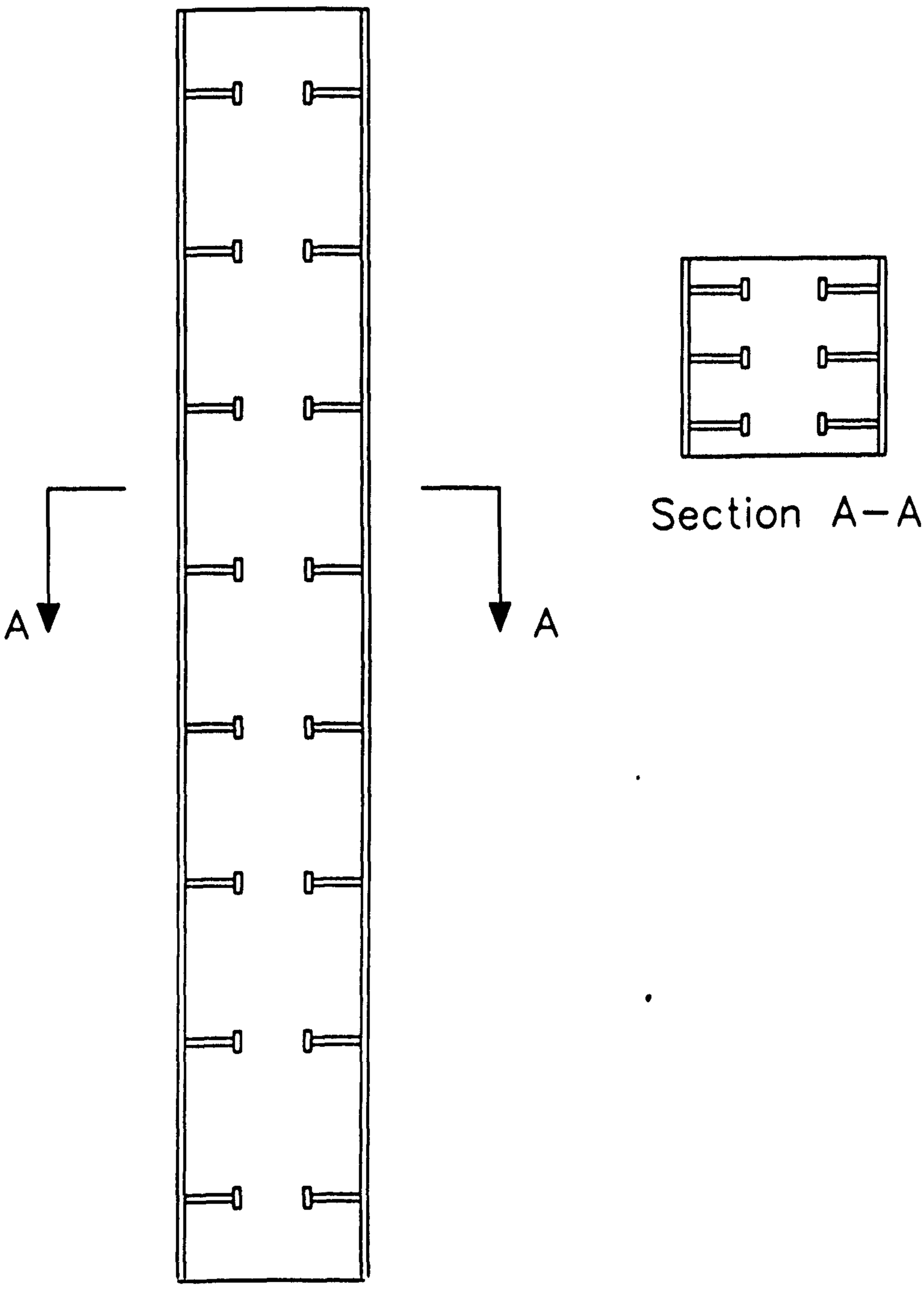

Figure 4.5 Composite Column

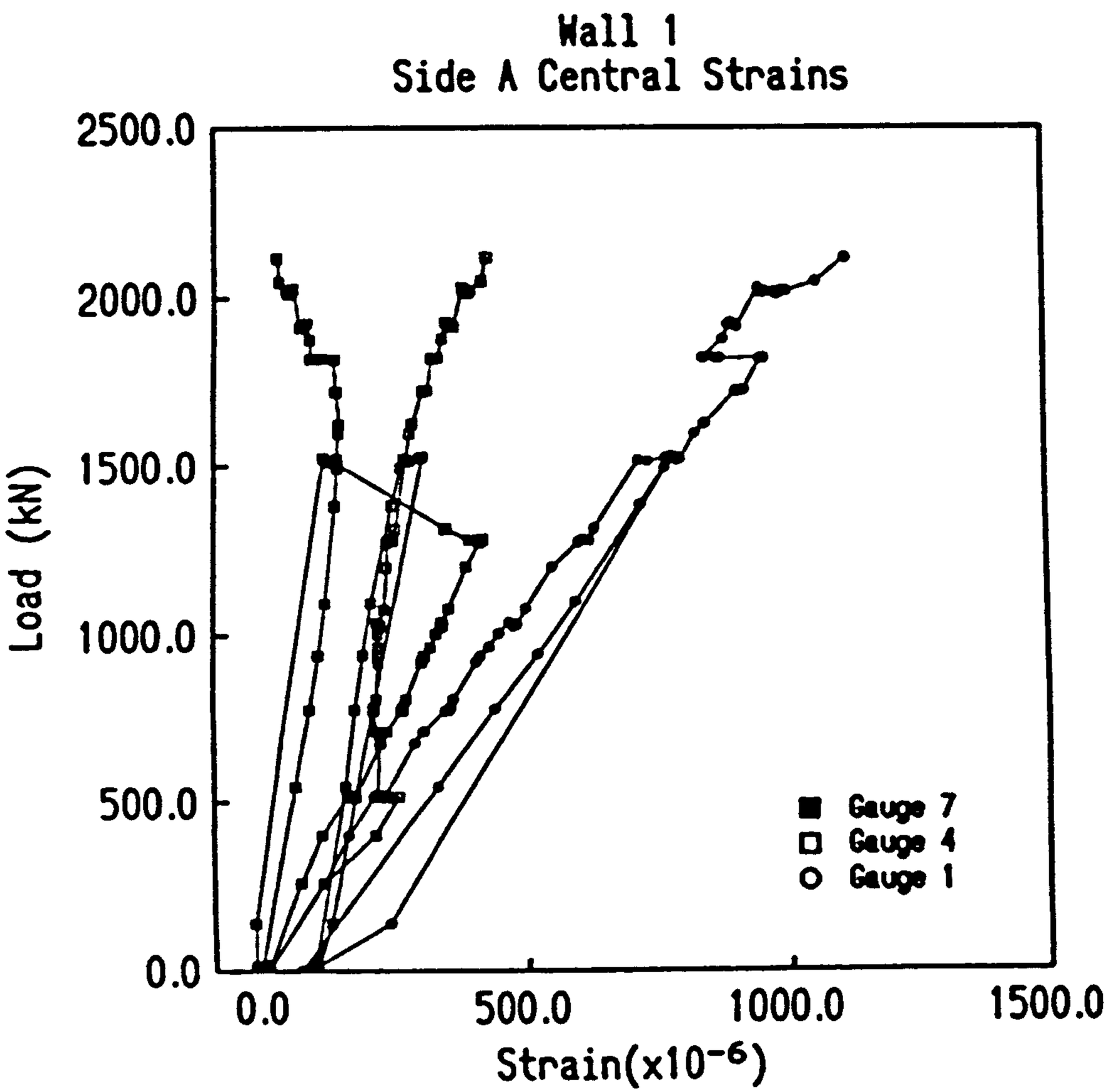

Figure 4.6

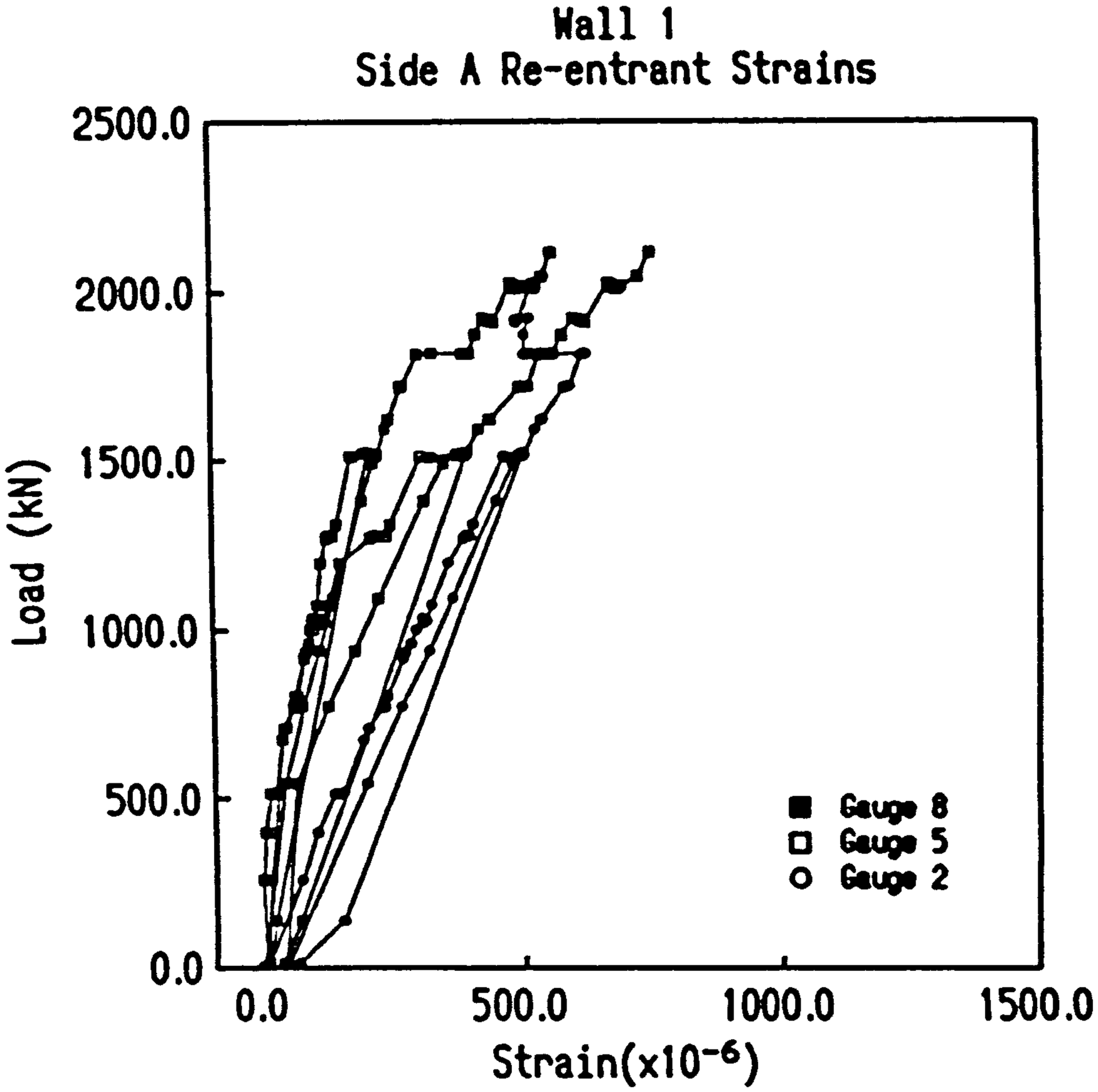

Figure 4.7

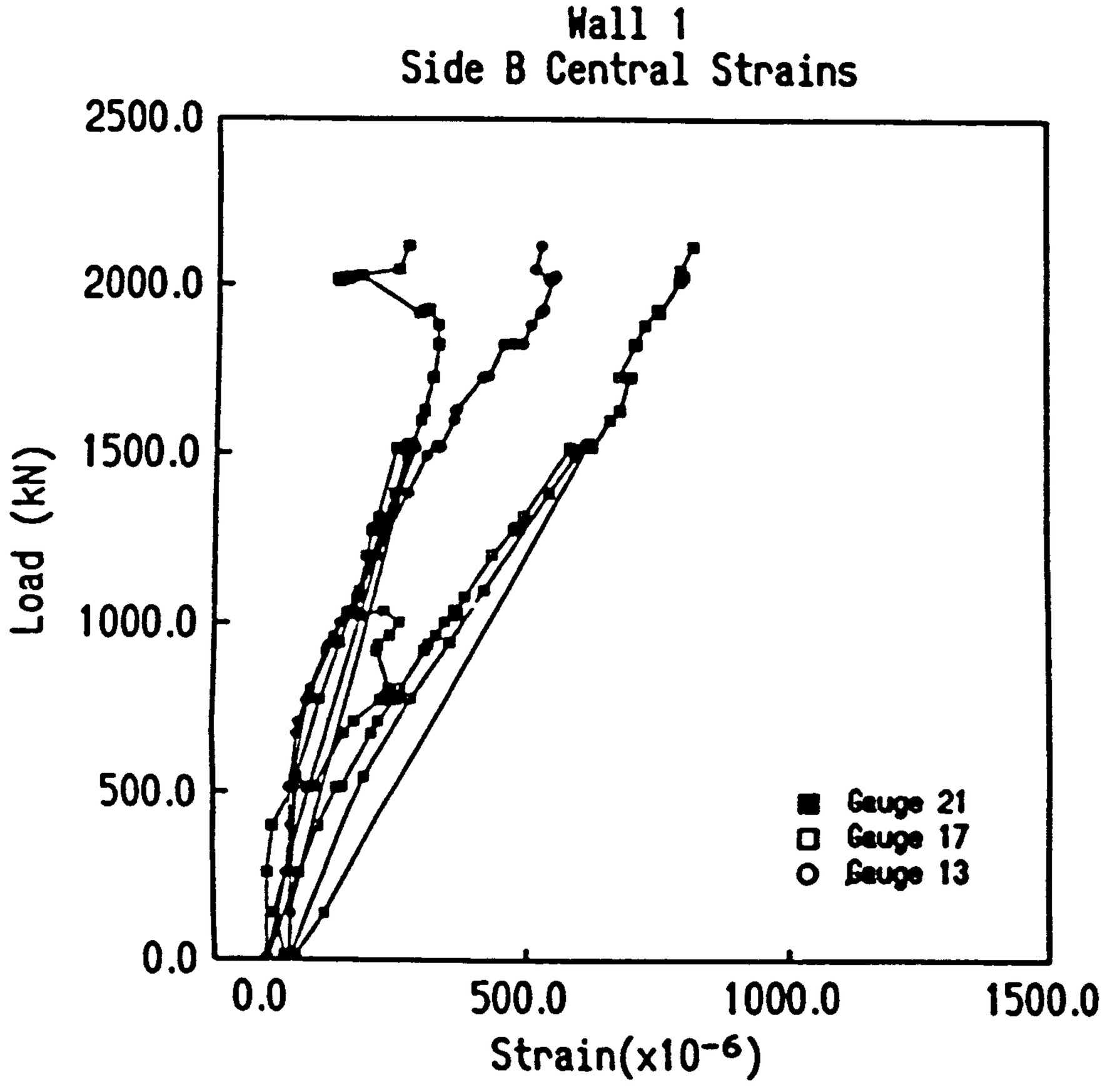

Figure 4.8

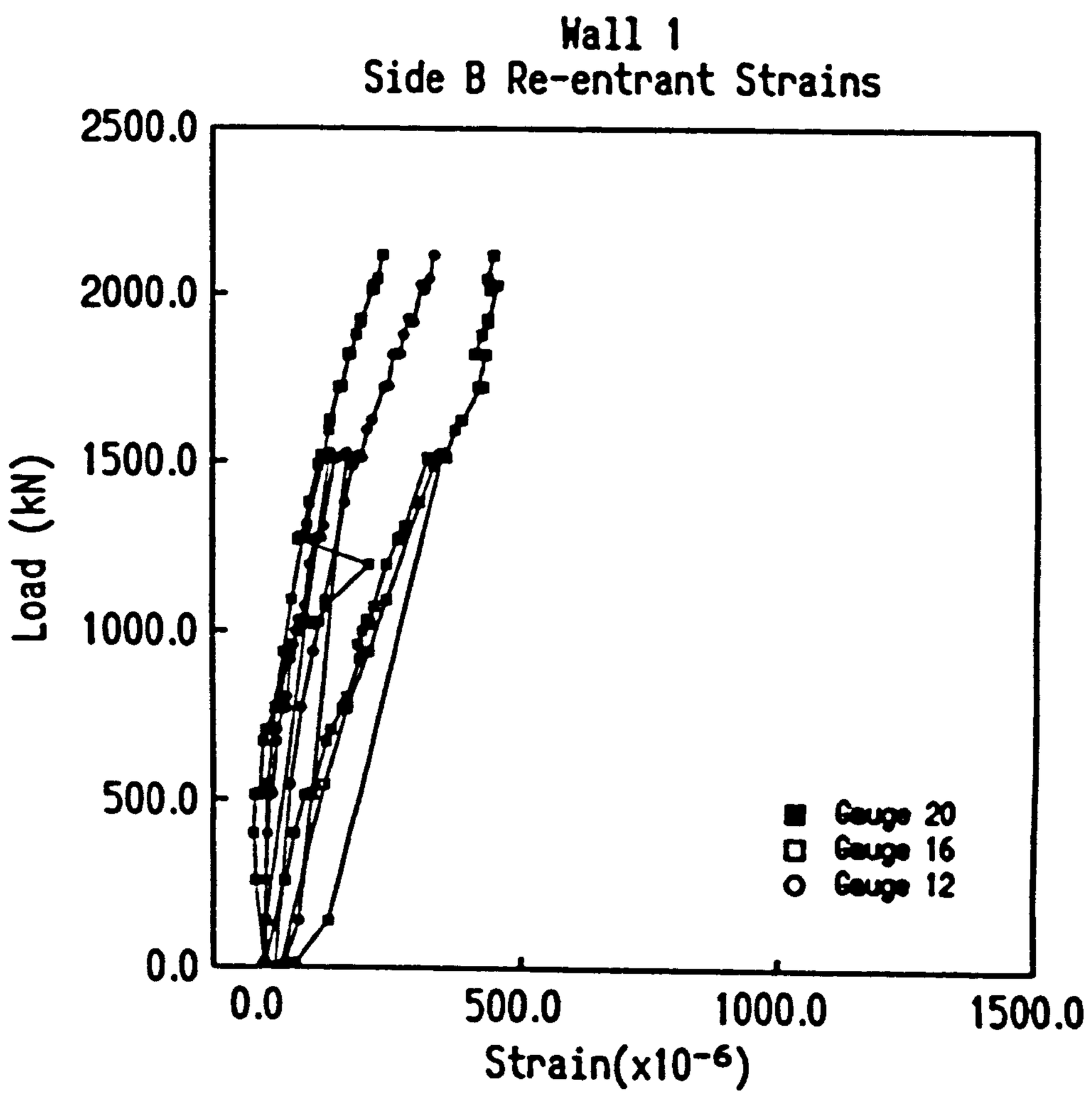

Figure 4.9

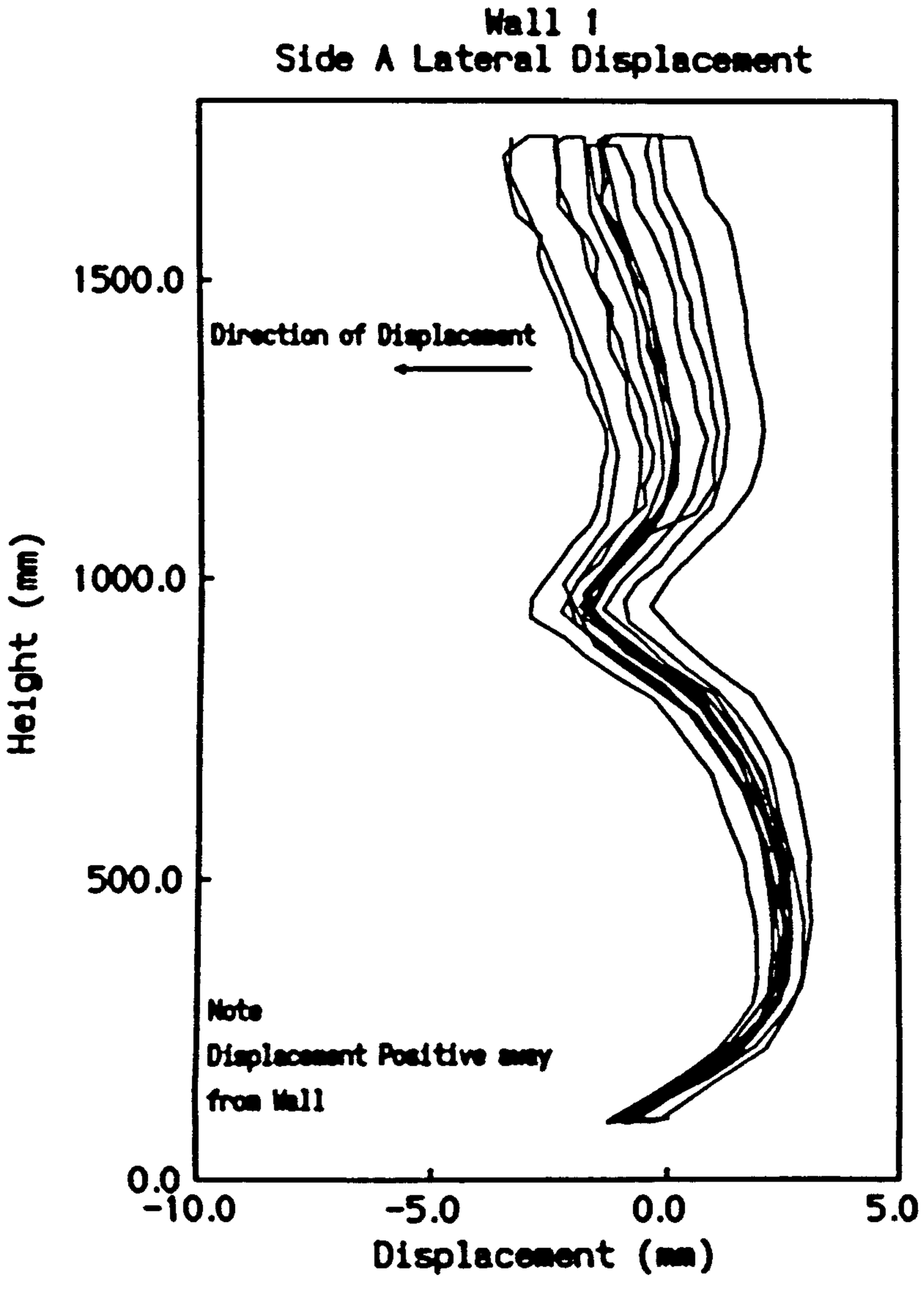

Figure 4.10

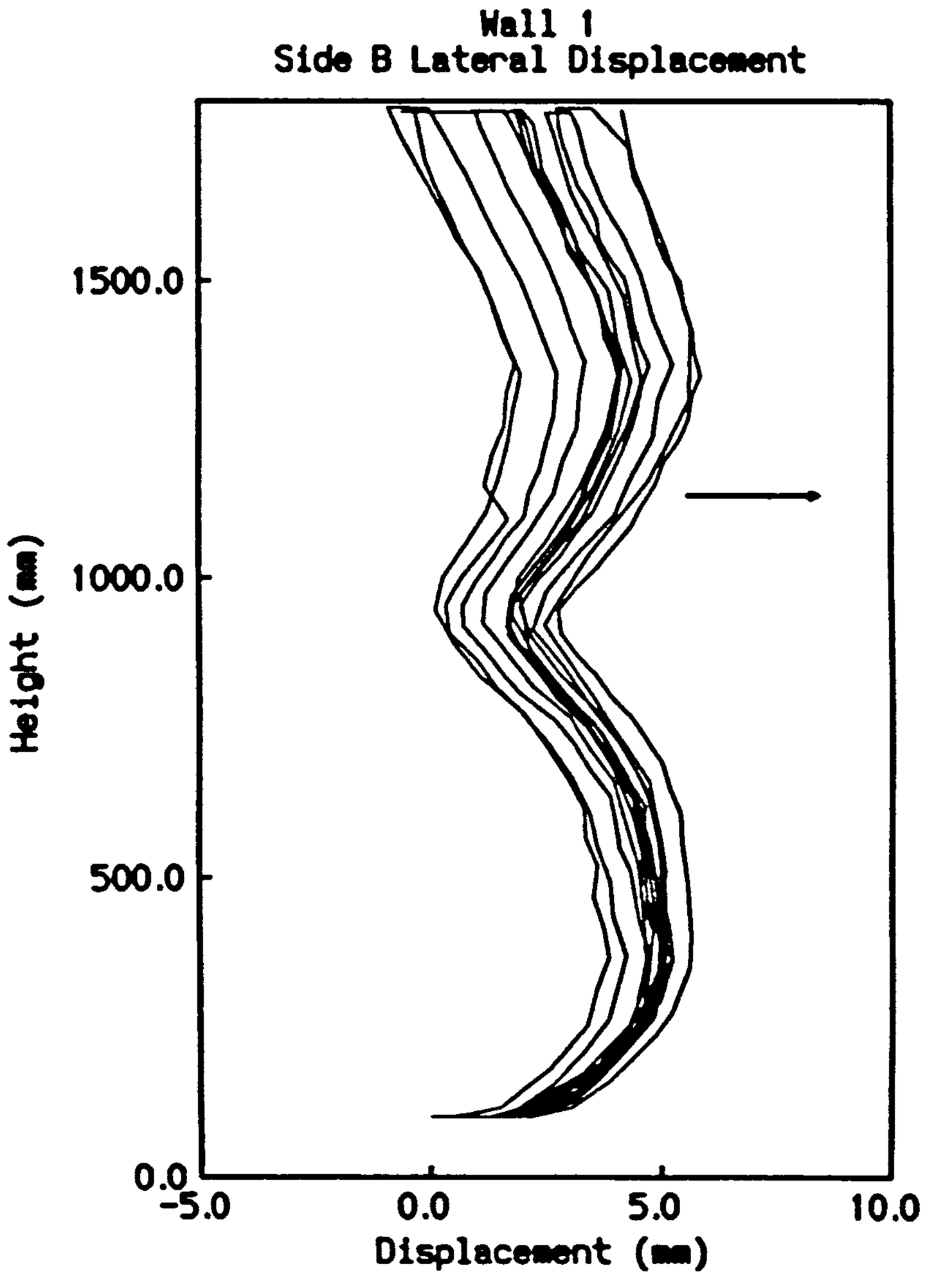

Figure 4.11

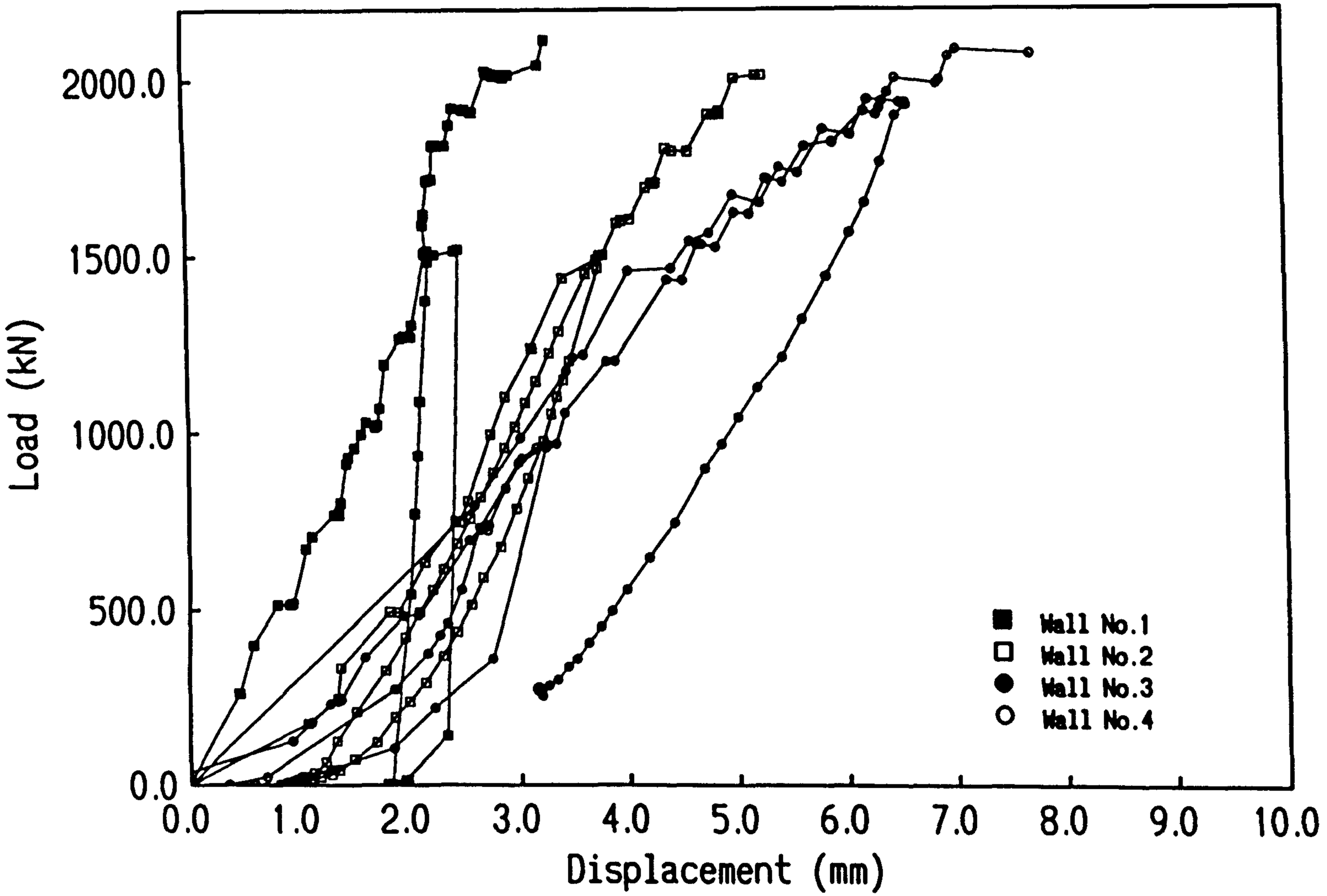
Walls 1-4
Axial Displacement
Load (kN)
2000.0
1500.0
1000.0
500.0
0.0
0.0
1.0
2.0
3.0
4.0
5.0
6.0
7.0
8.0
9.0
10.0
Displacement (mm)
Wall No.1
Wall No.2
Wall No.3
Wall No.4

Figure 4.12

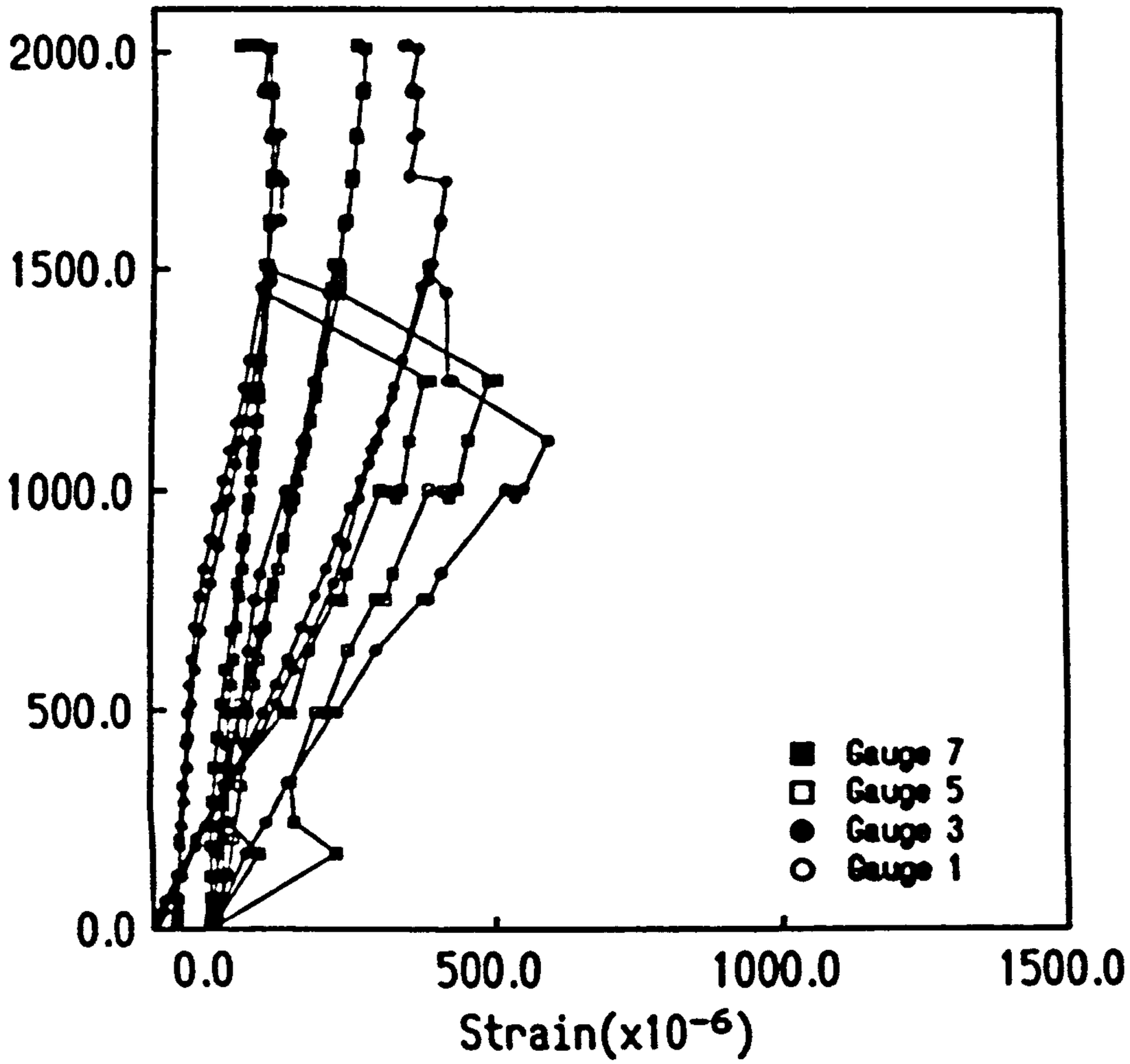

Figure 4.13

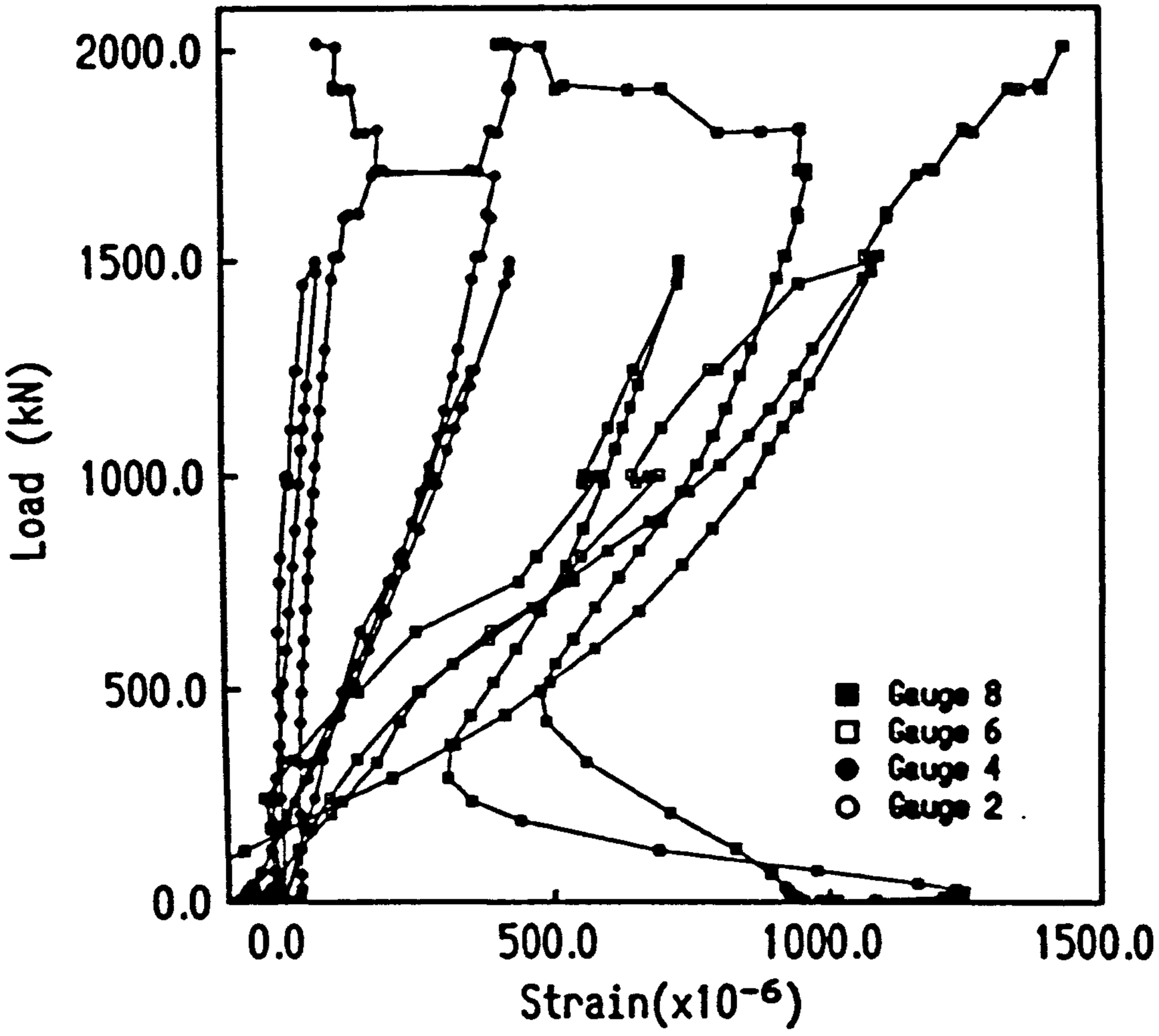

Figure 4.14

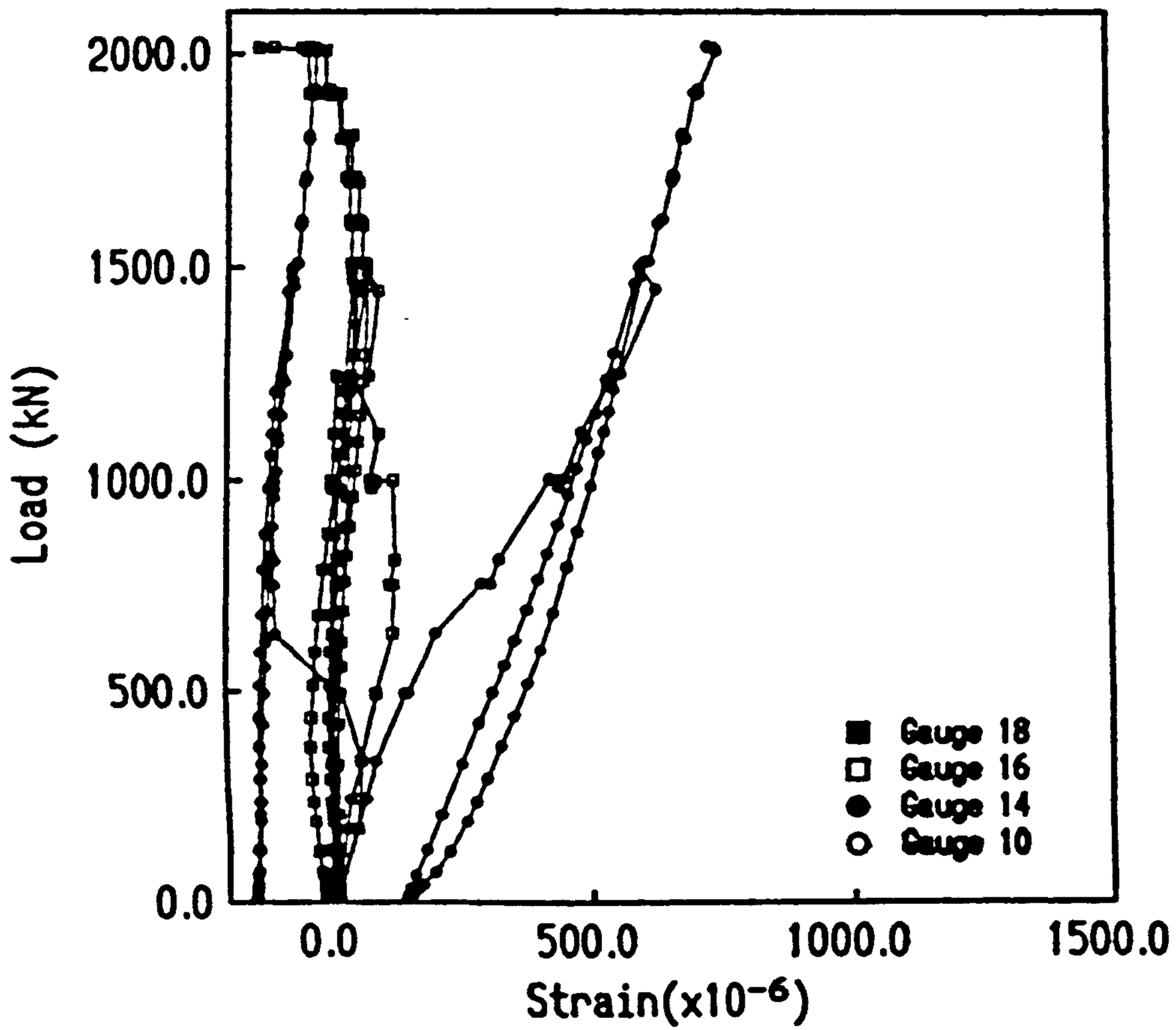

Figure 4.15

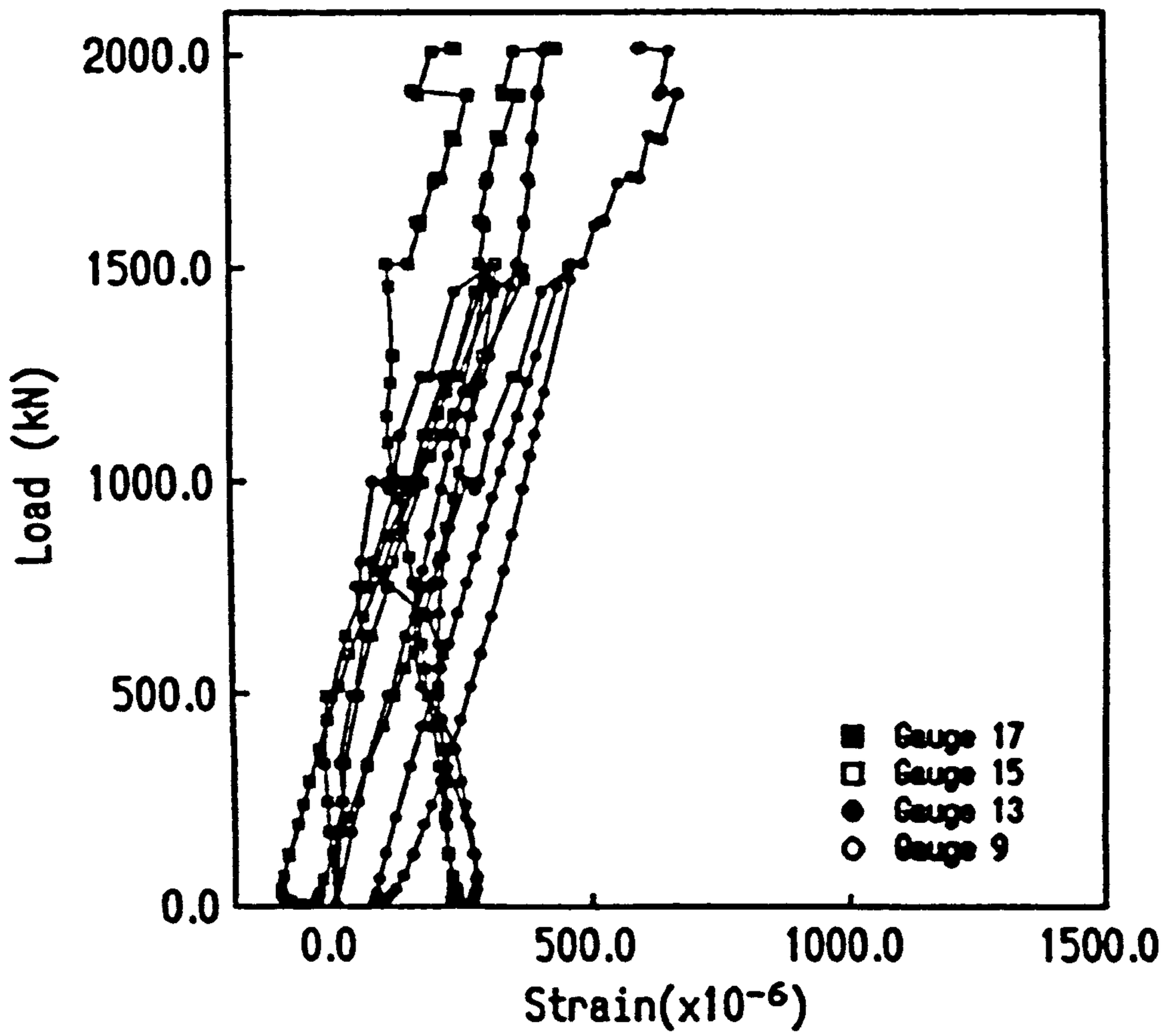

Figure 4.16

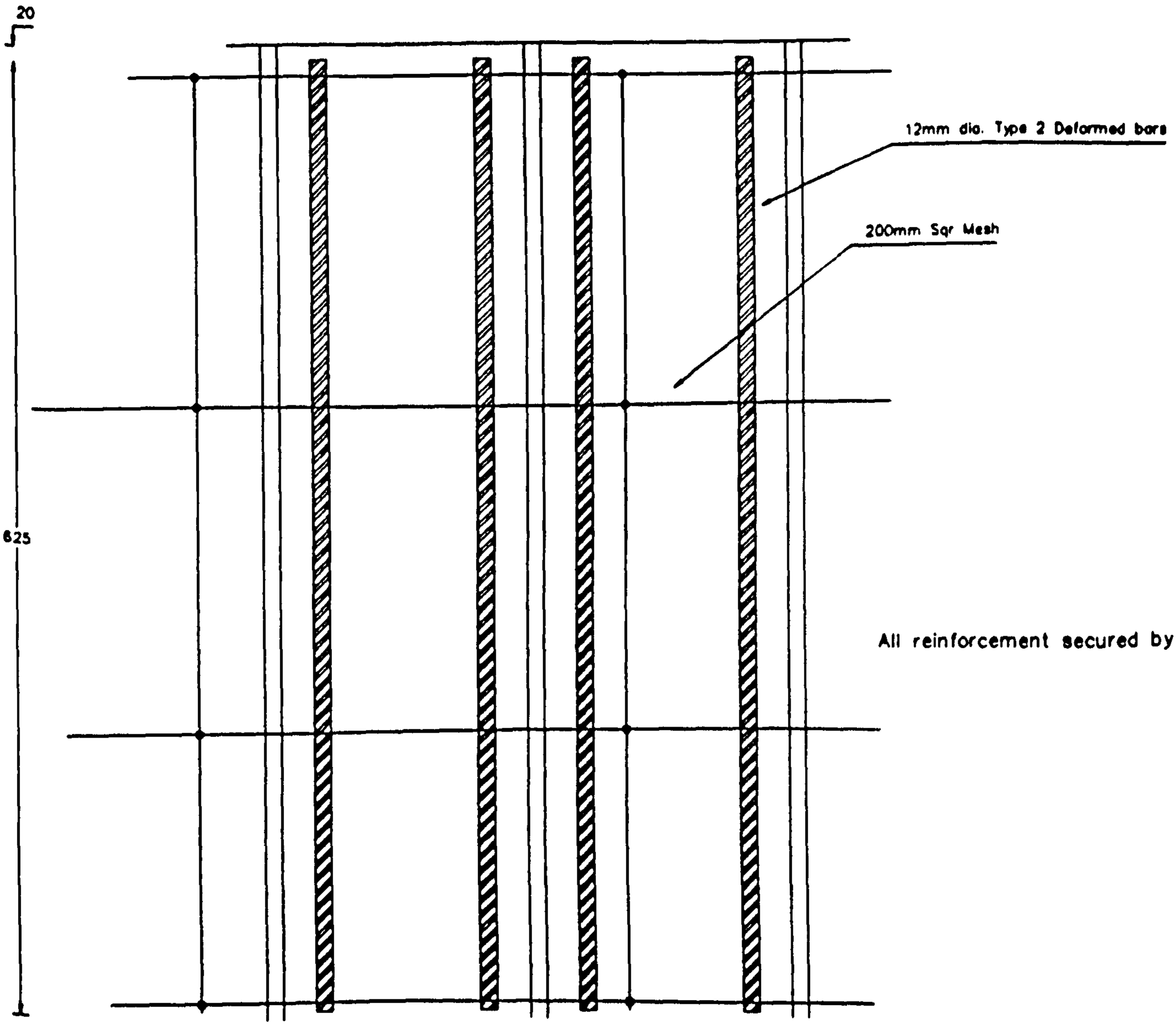

Figure 4.17 Profile Boundary Fixtures

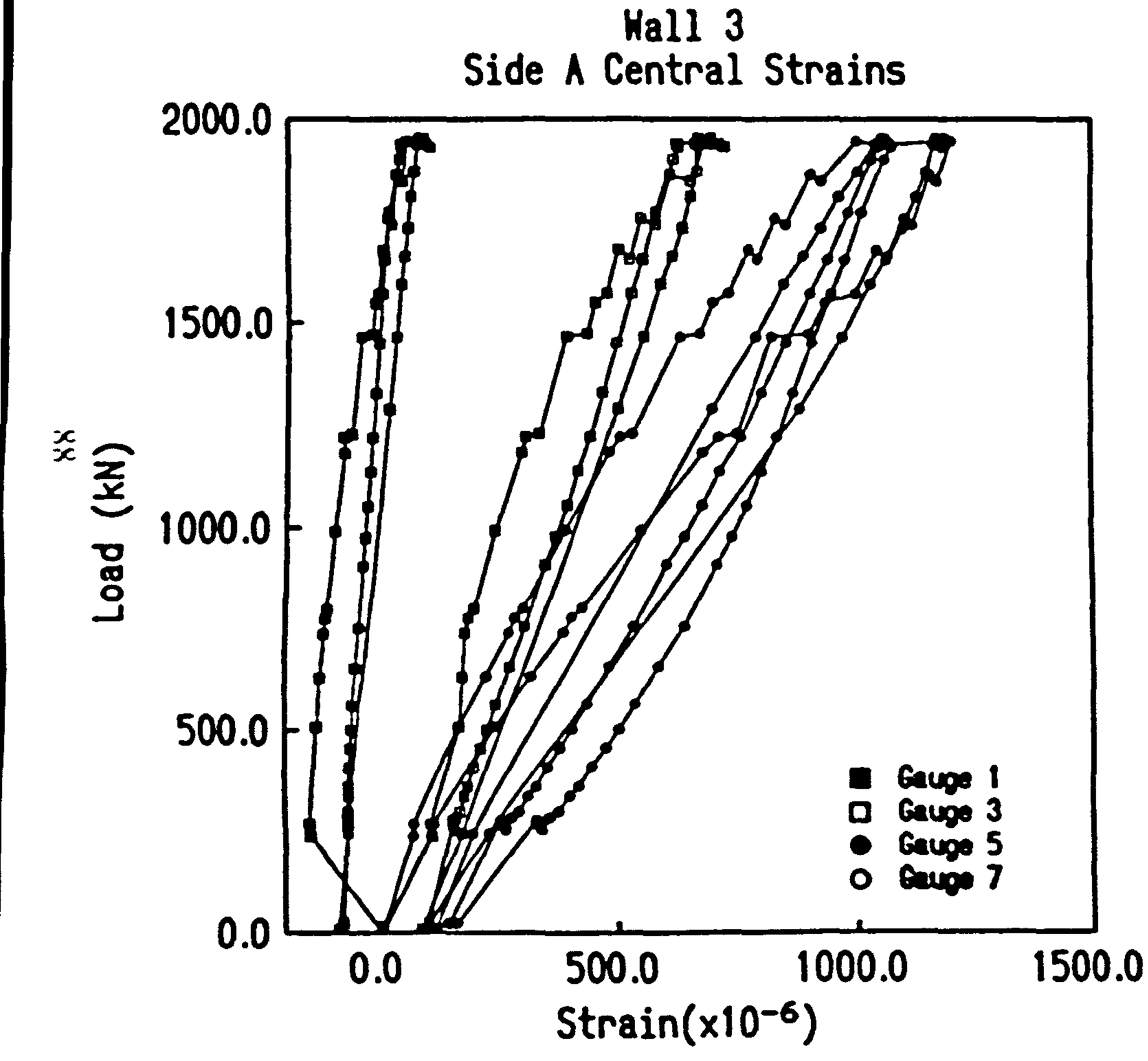

Figure 4.18

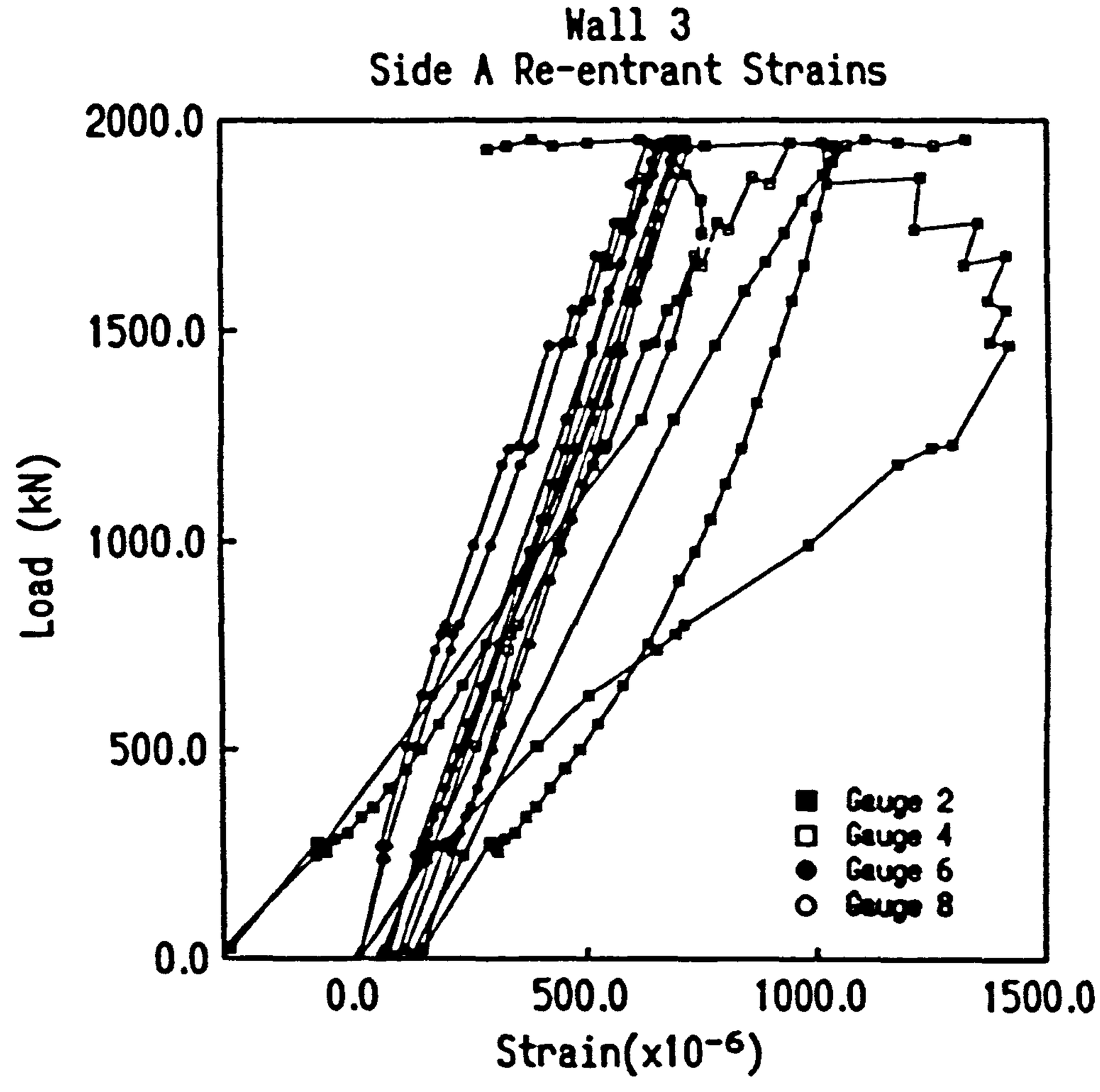

Figure 4.19

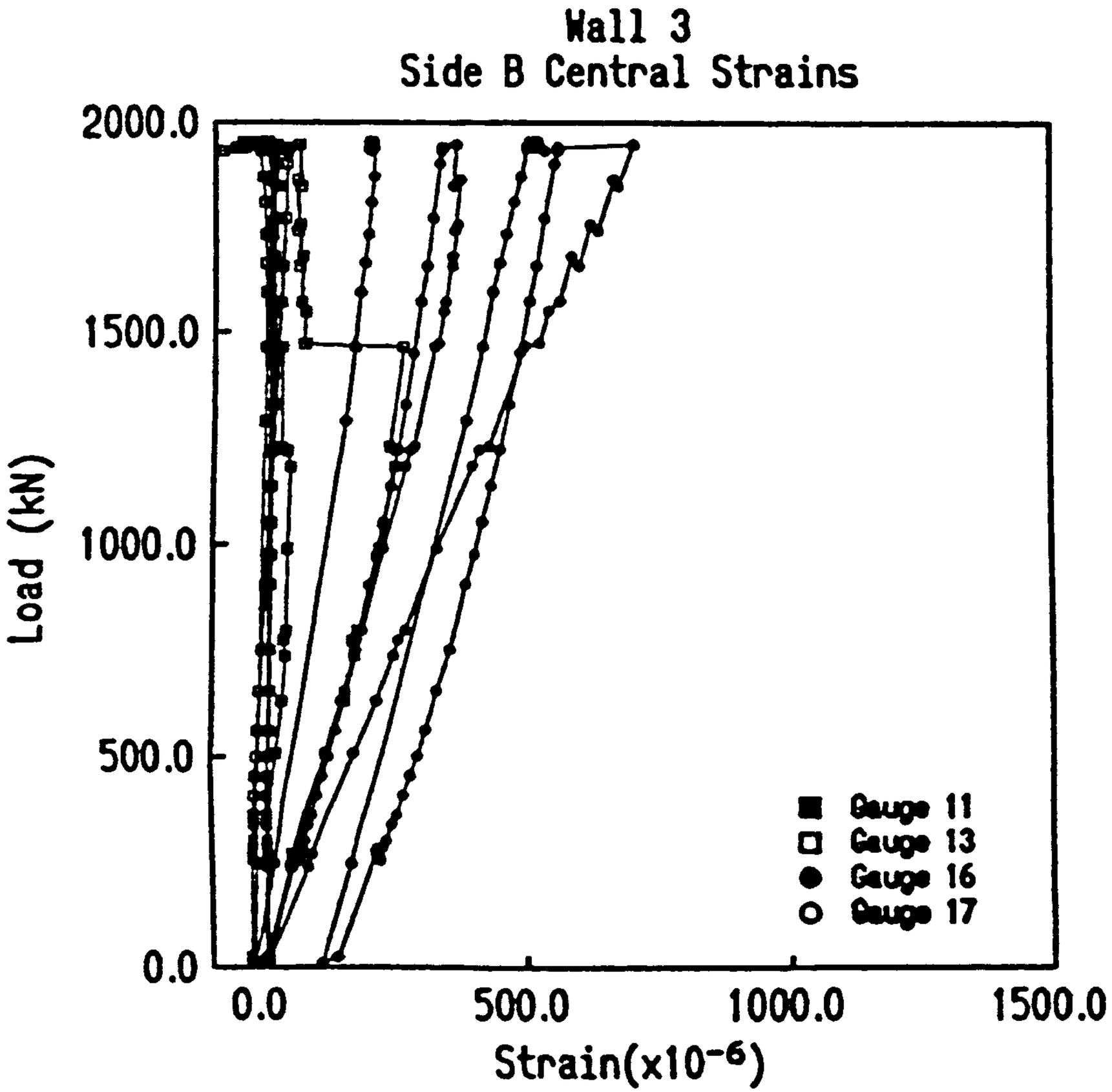

Figure 4.20

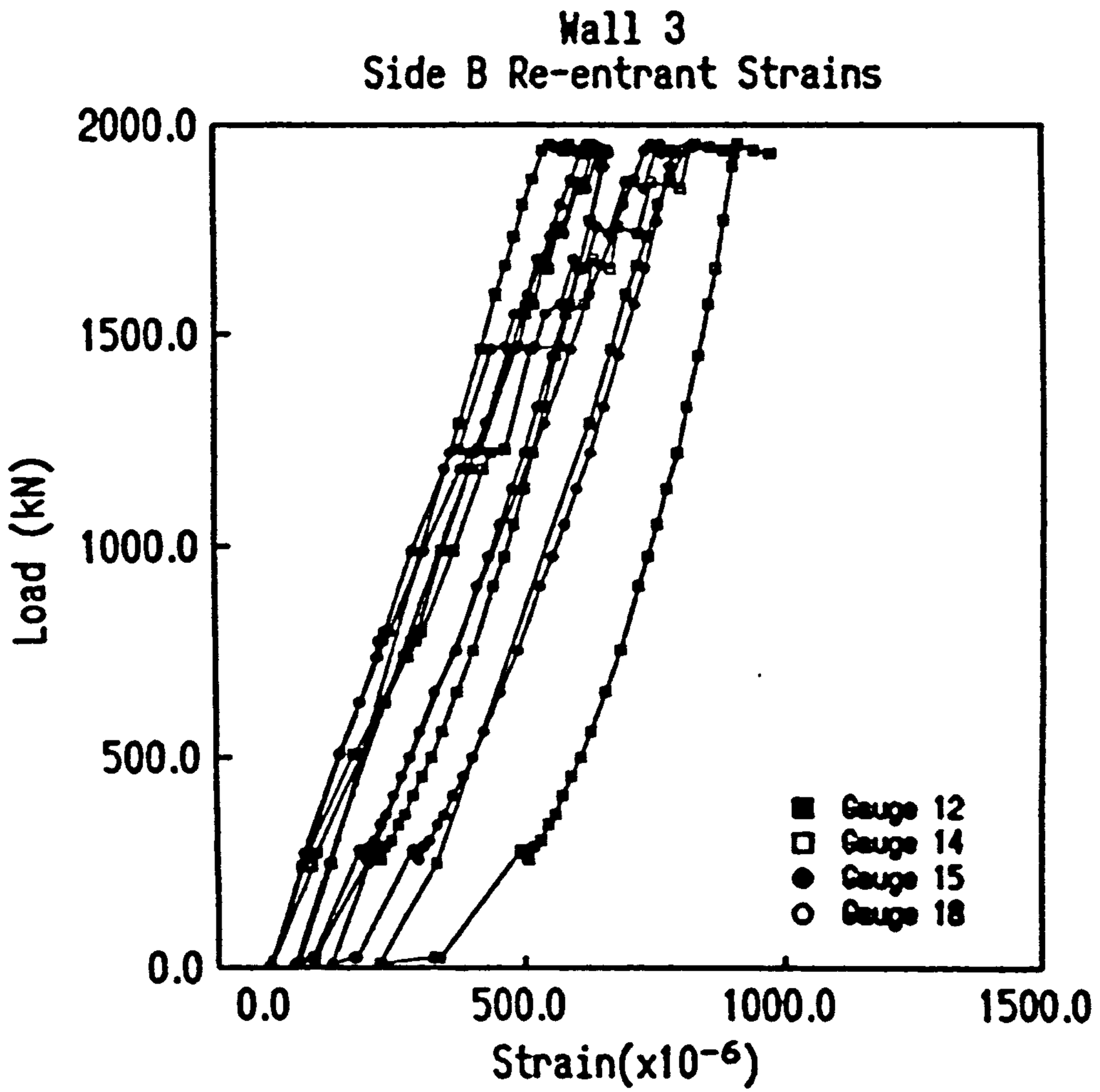

Figure 4.21

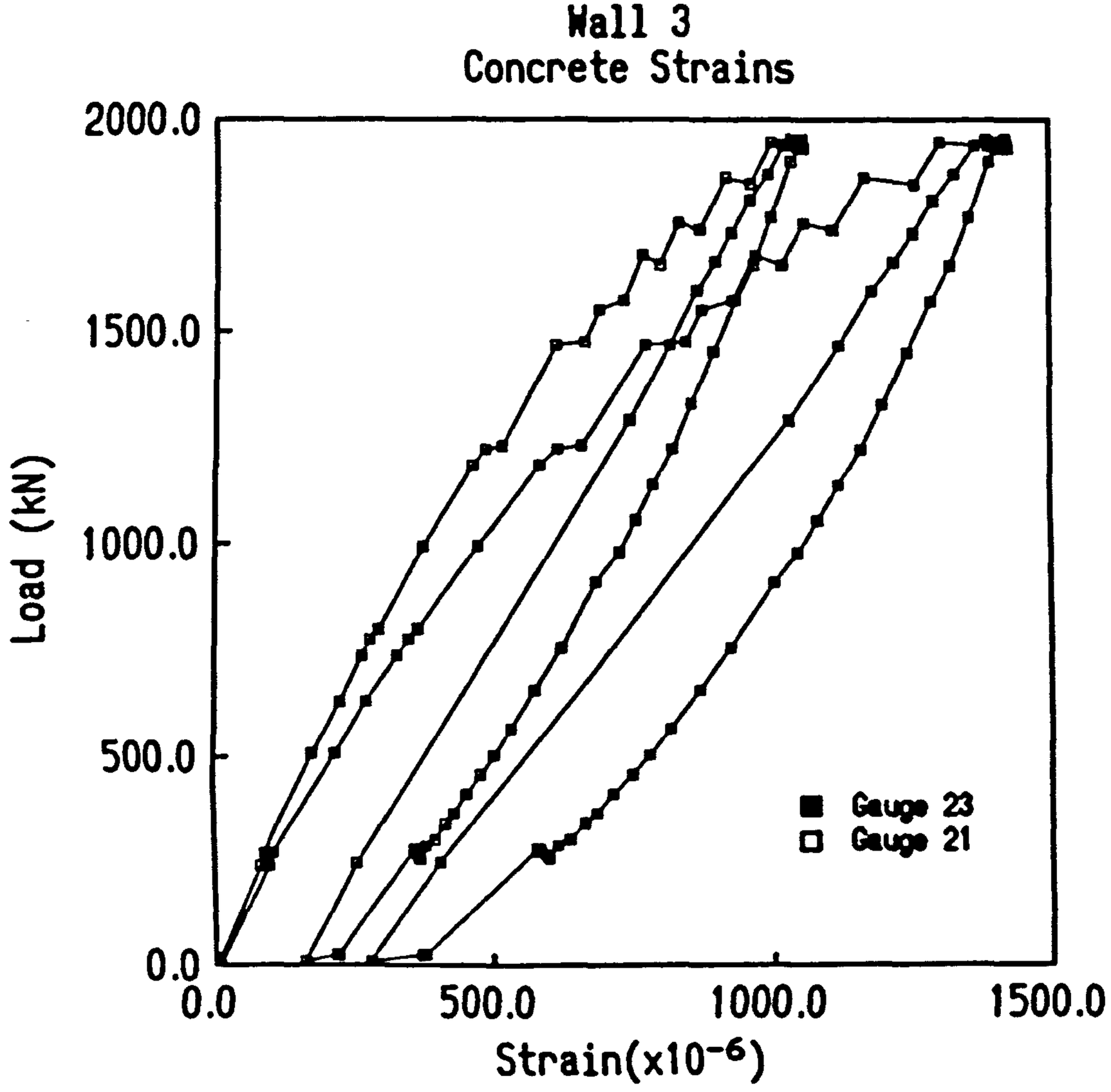

Figure 4.22

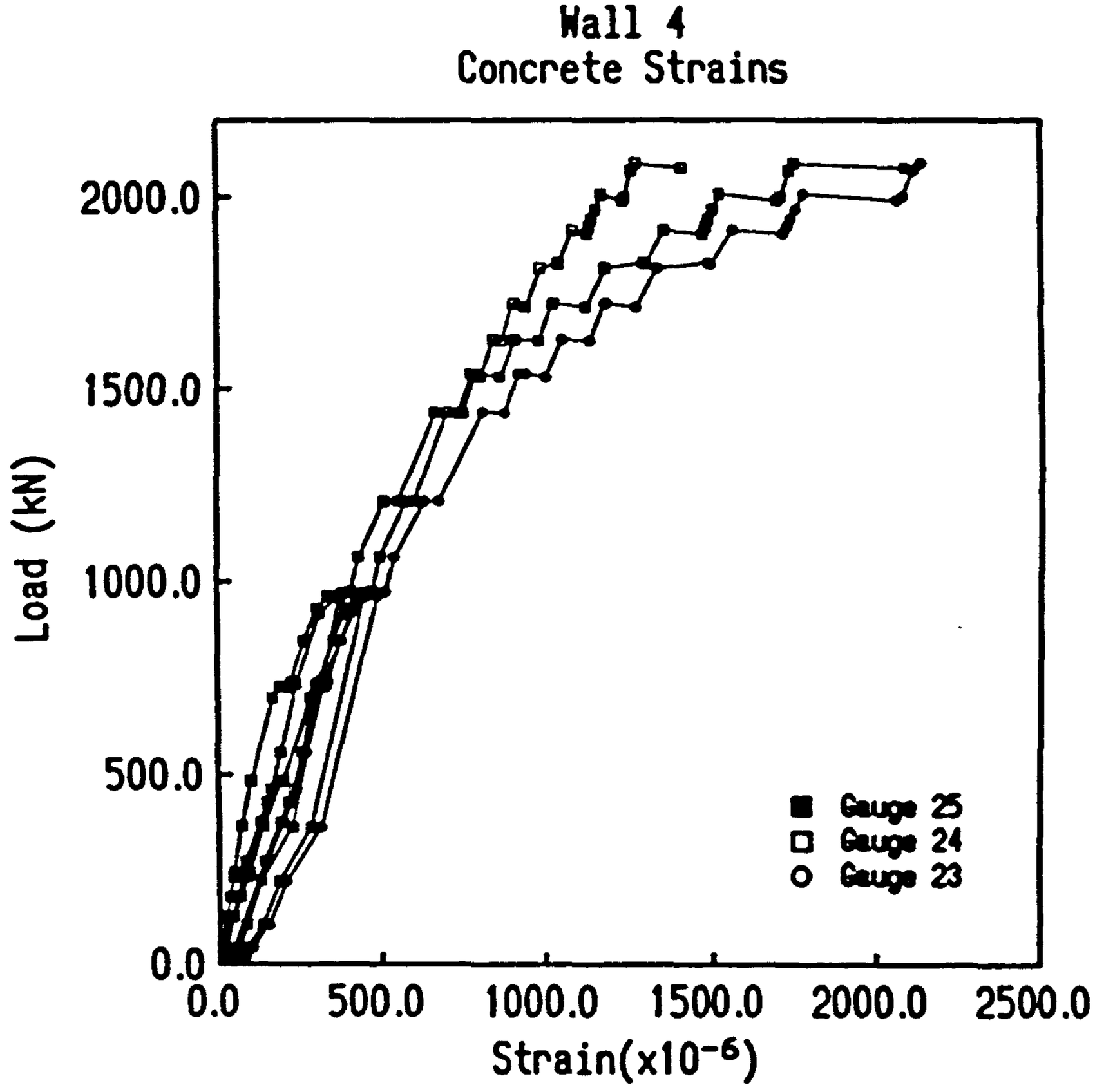

Figure 4.23

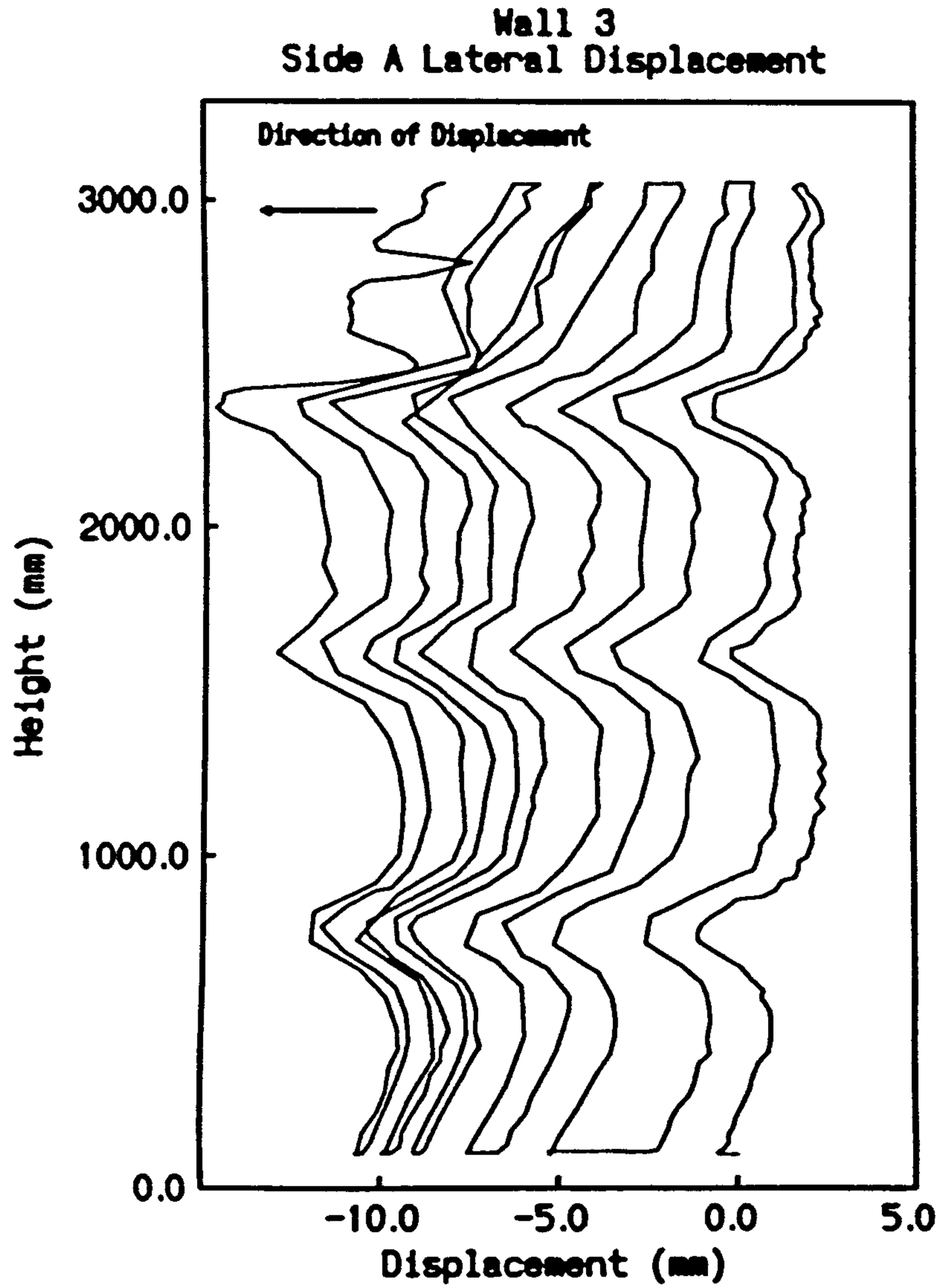
Wall 3
Side A Lateral Displacement
Direction of Displacement
3000.0
2000.0
1000.0
0.0
Height (mm)
-10.0
-5.0
0.0
5.0
Displacement (mm)
Note
Displacement Positive away
from Wall

Figure 4.24

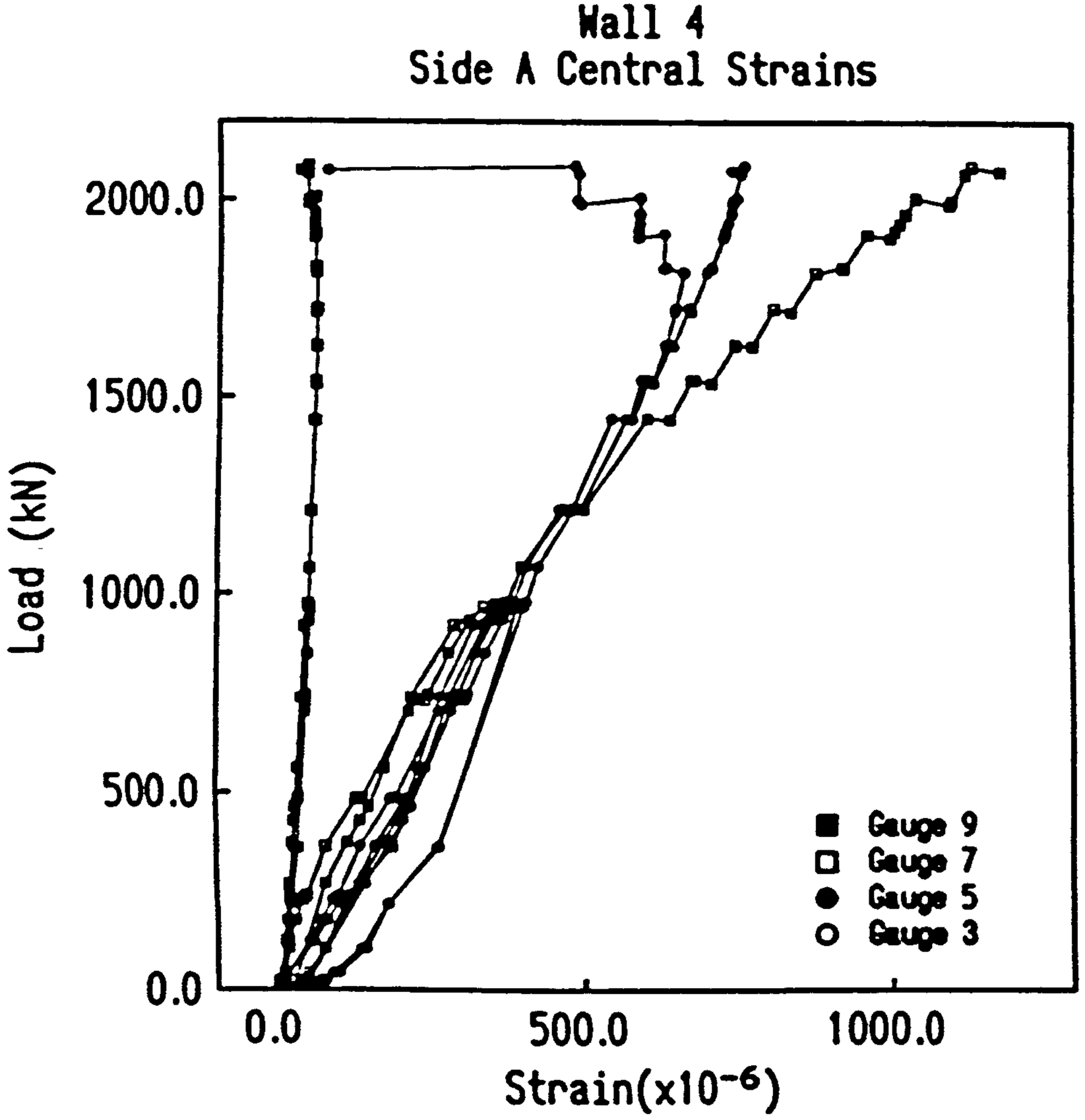

Figure 4.25

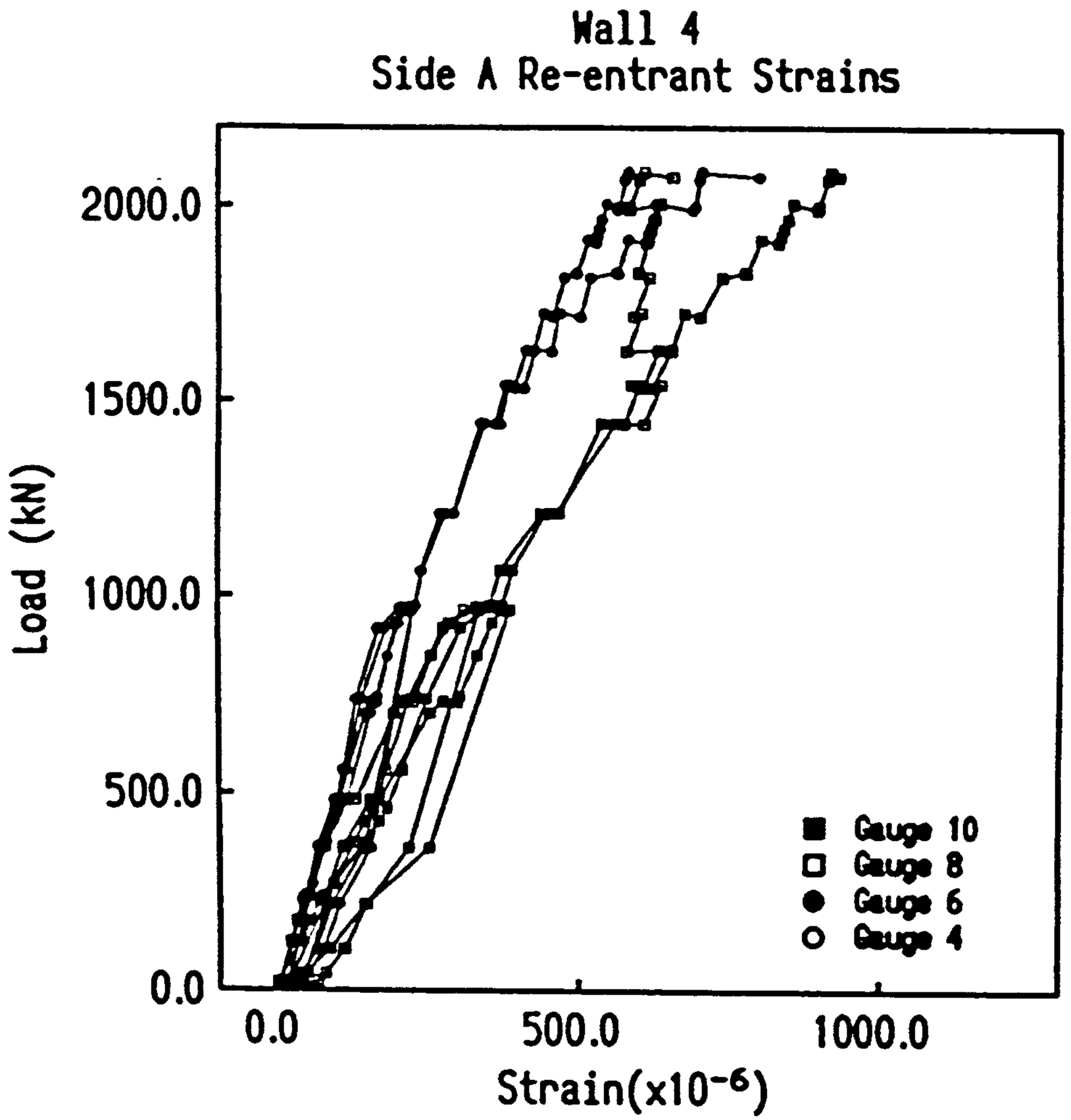

Figure 4.26

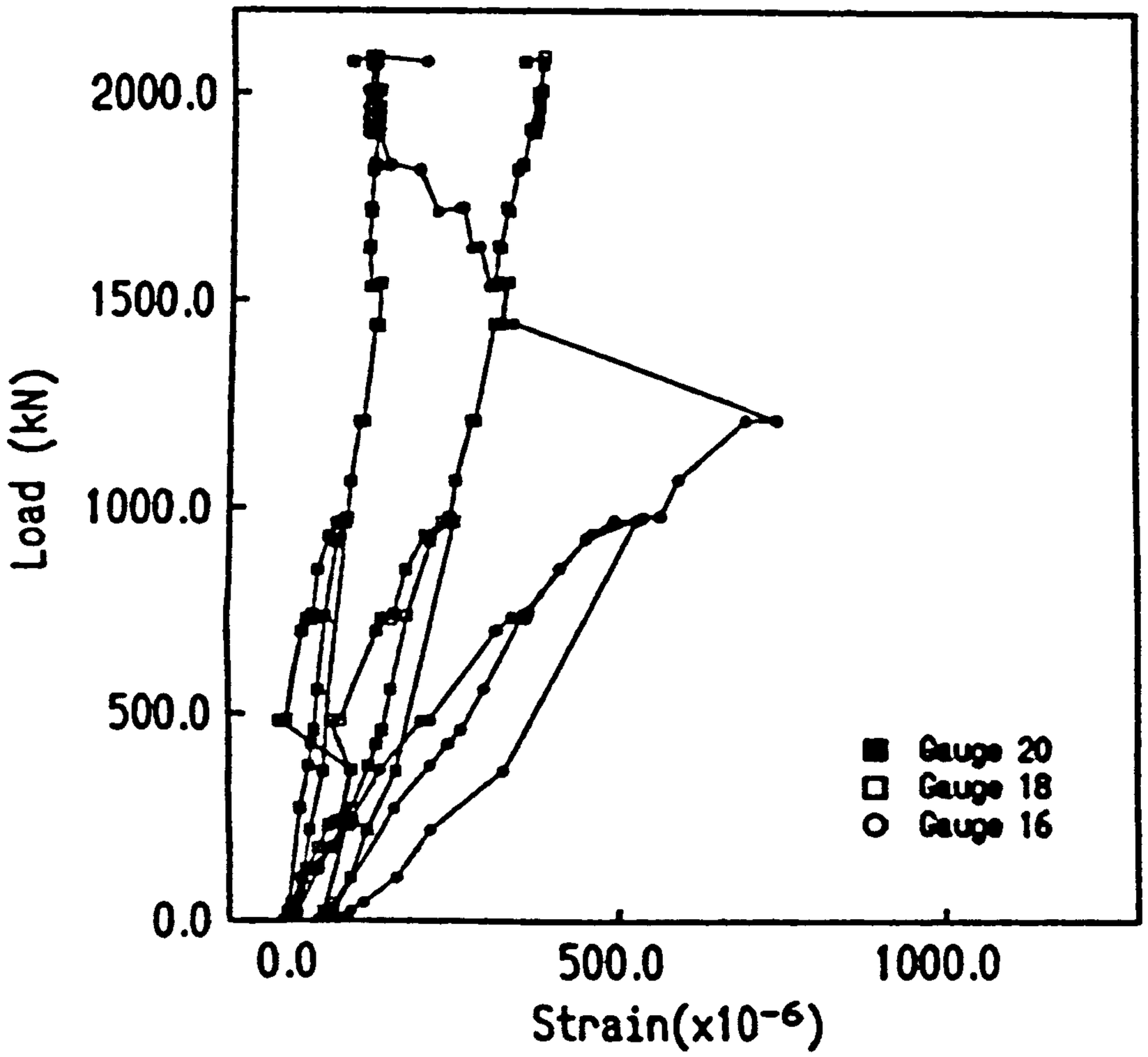

Figure 4.27

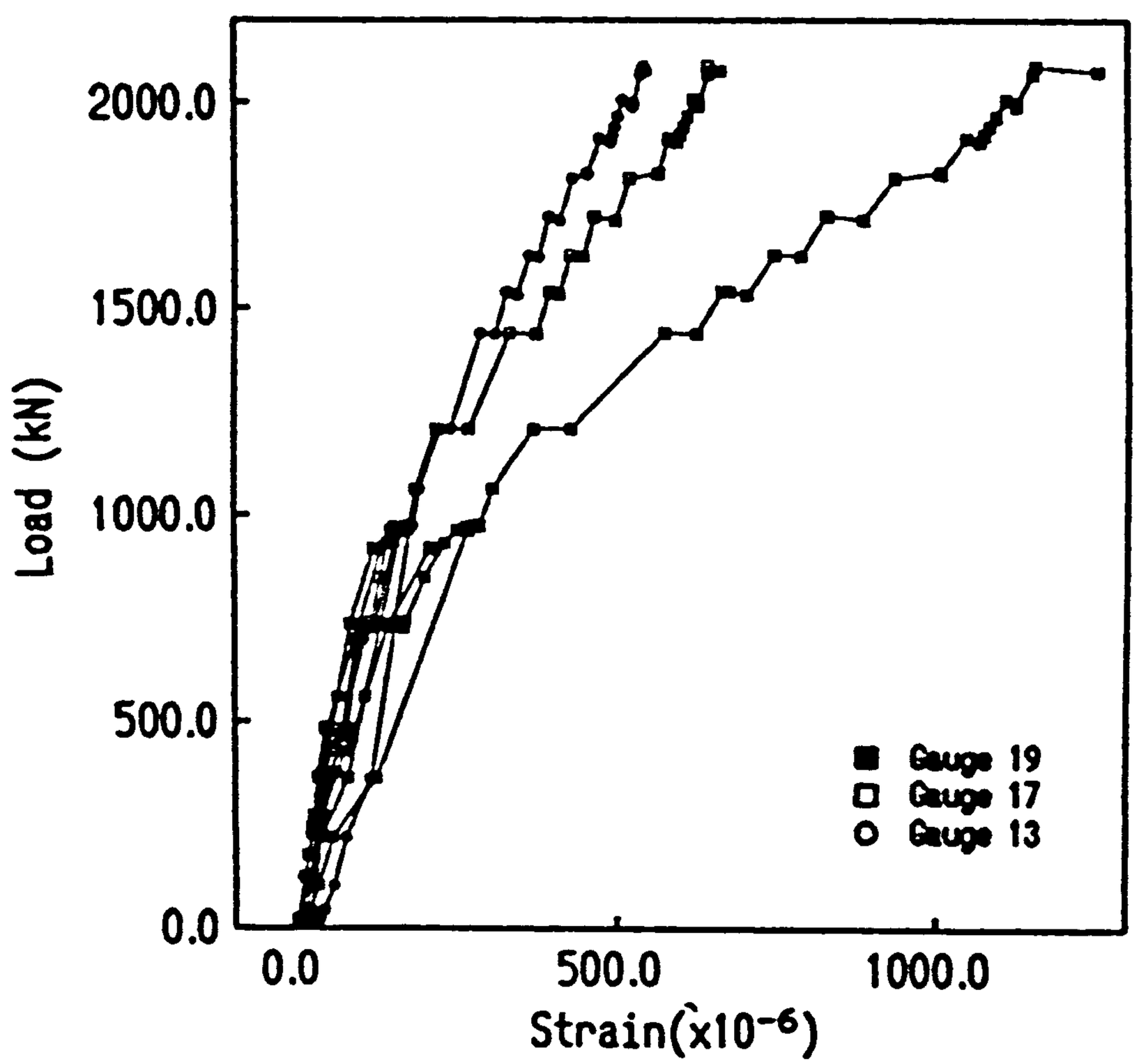

Figure 4.28

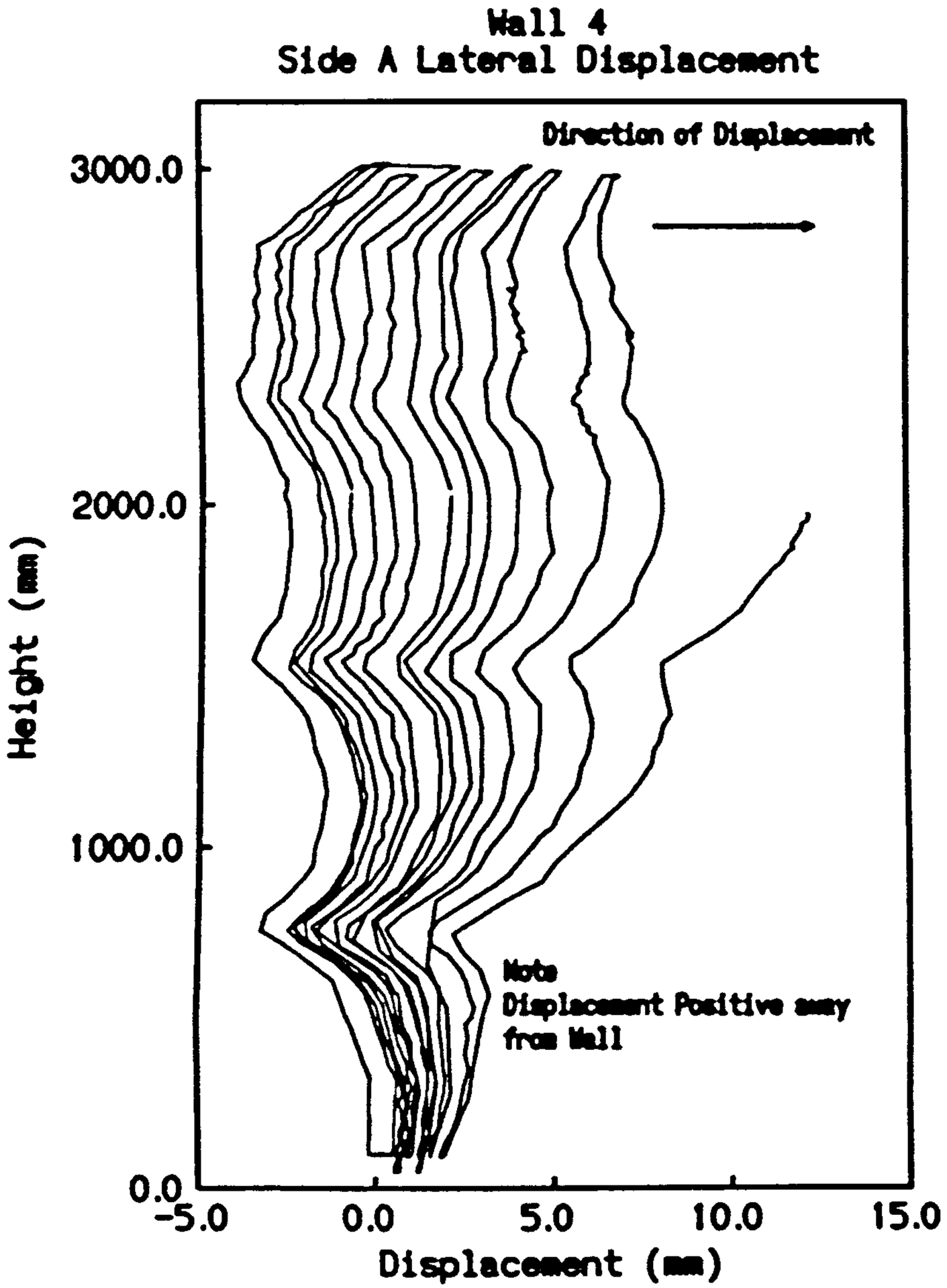

Figure 4.29

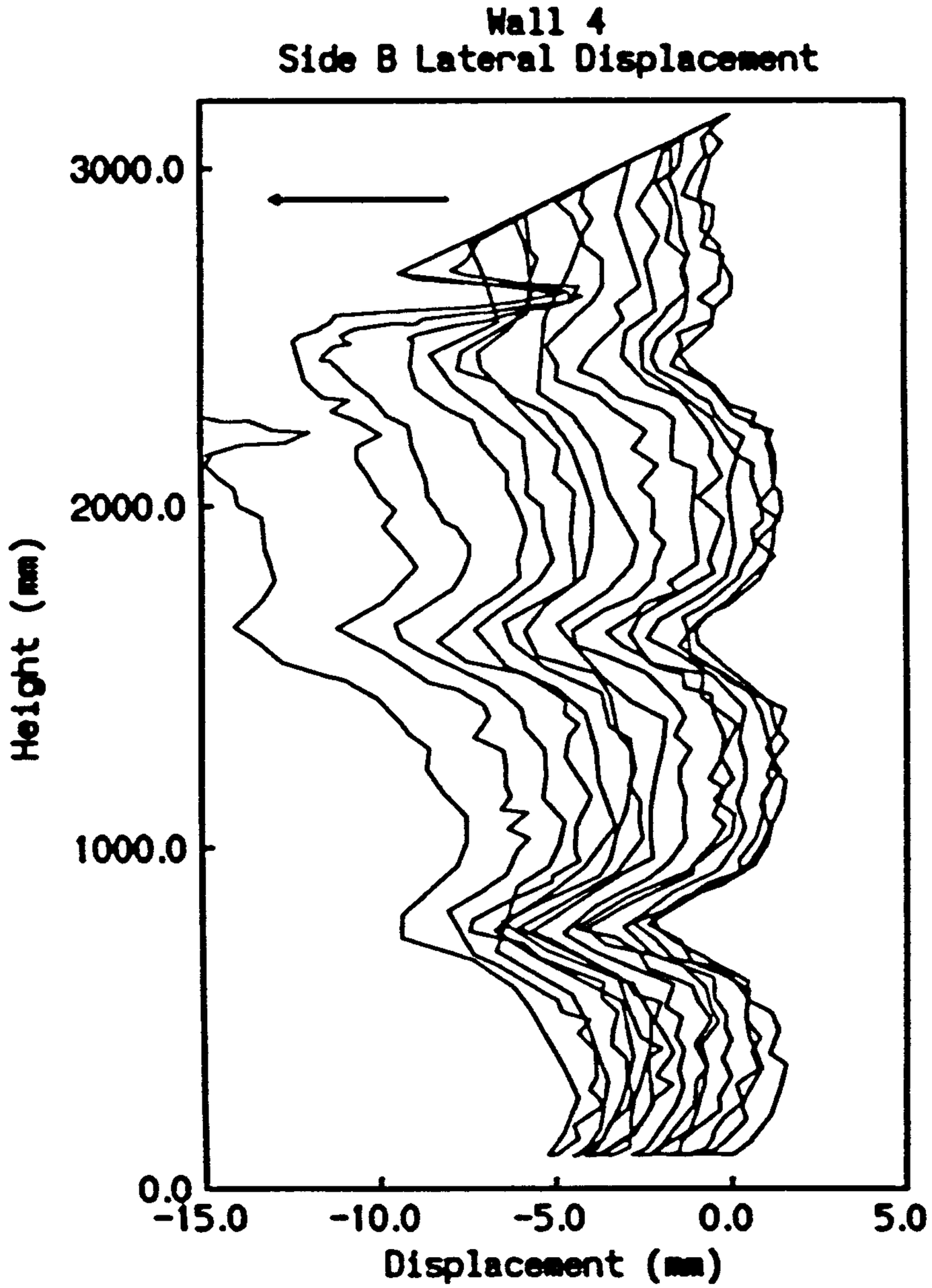

Figure 4.30

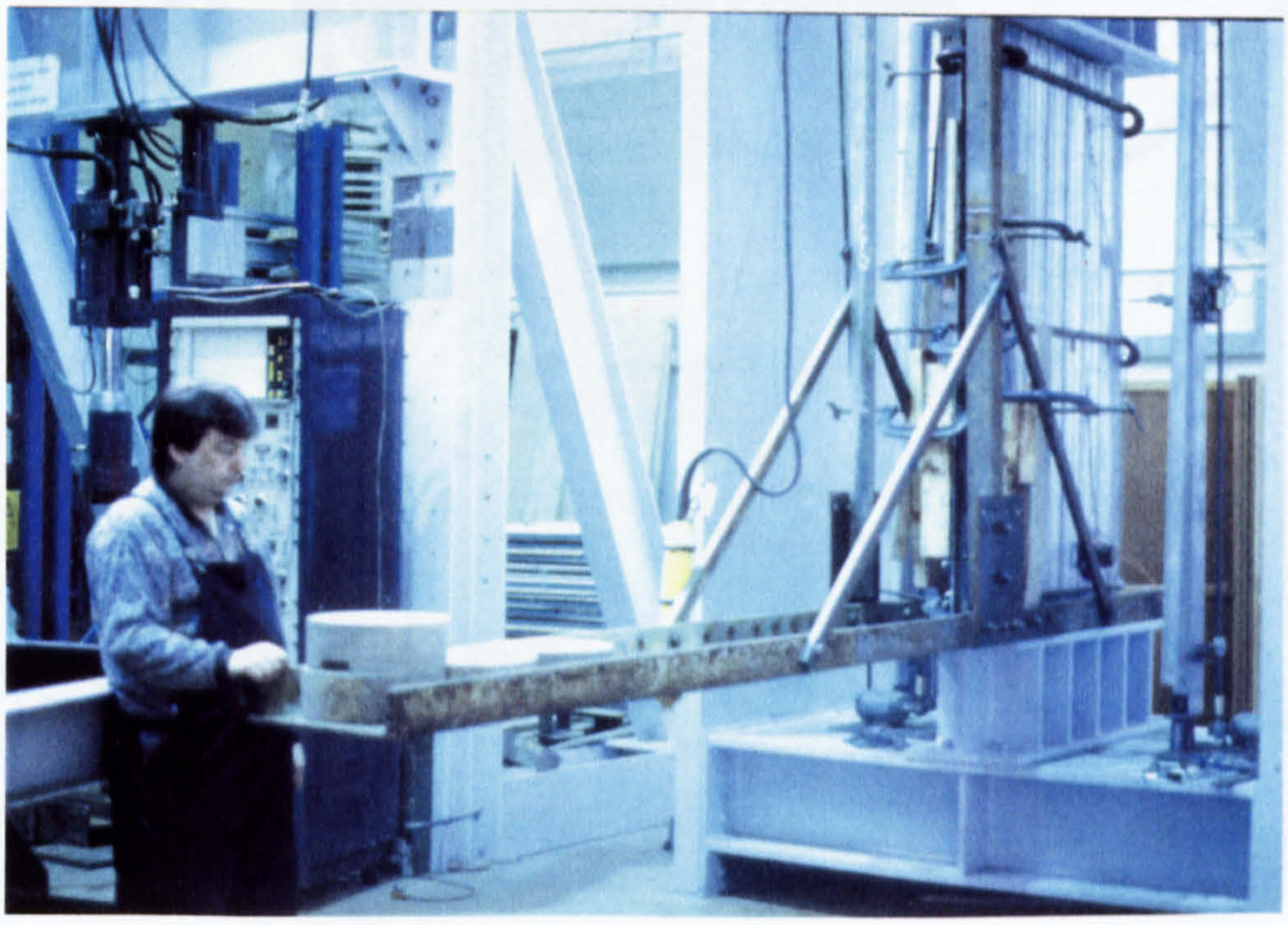

Plate 1 Lifting Rig

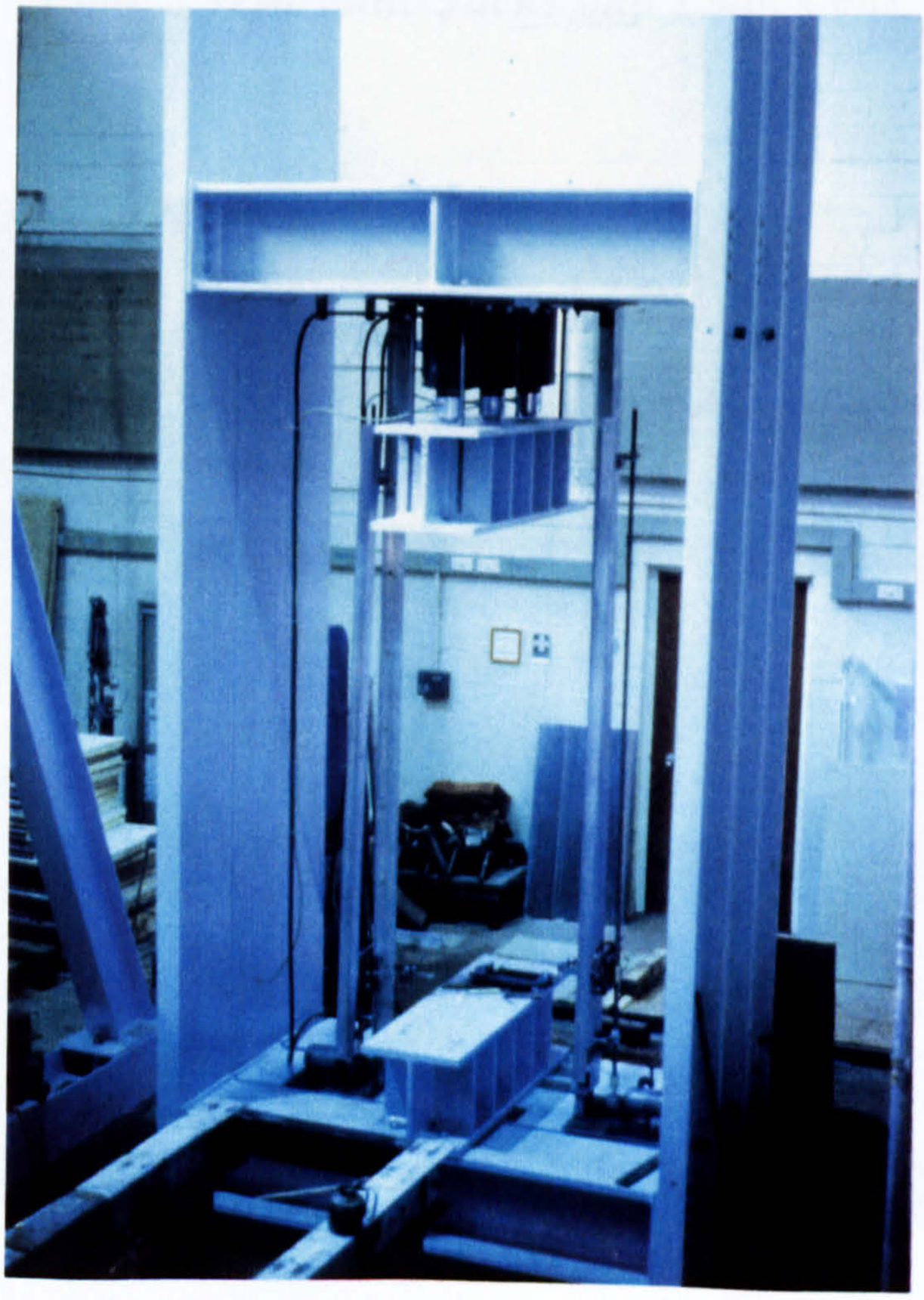

Plate 2 Loading Frame

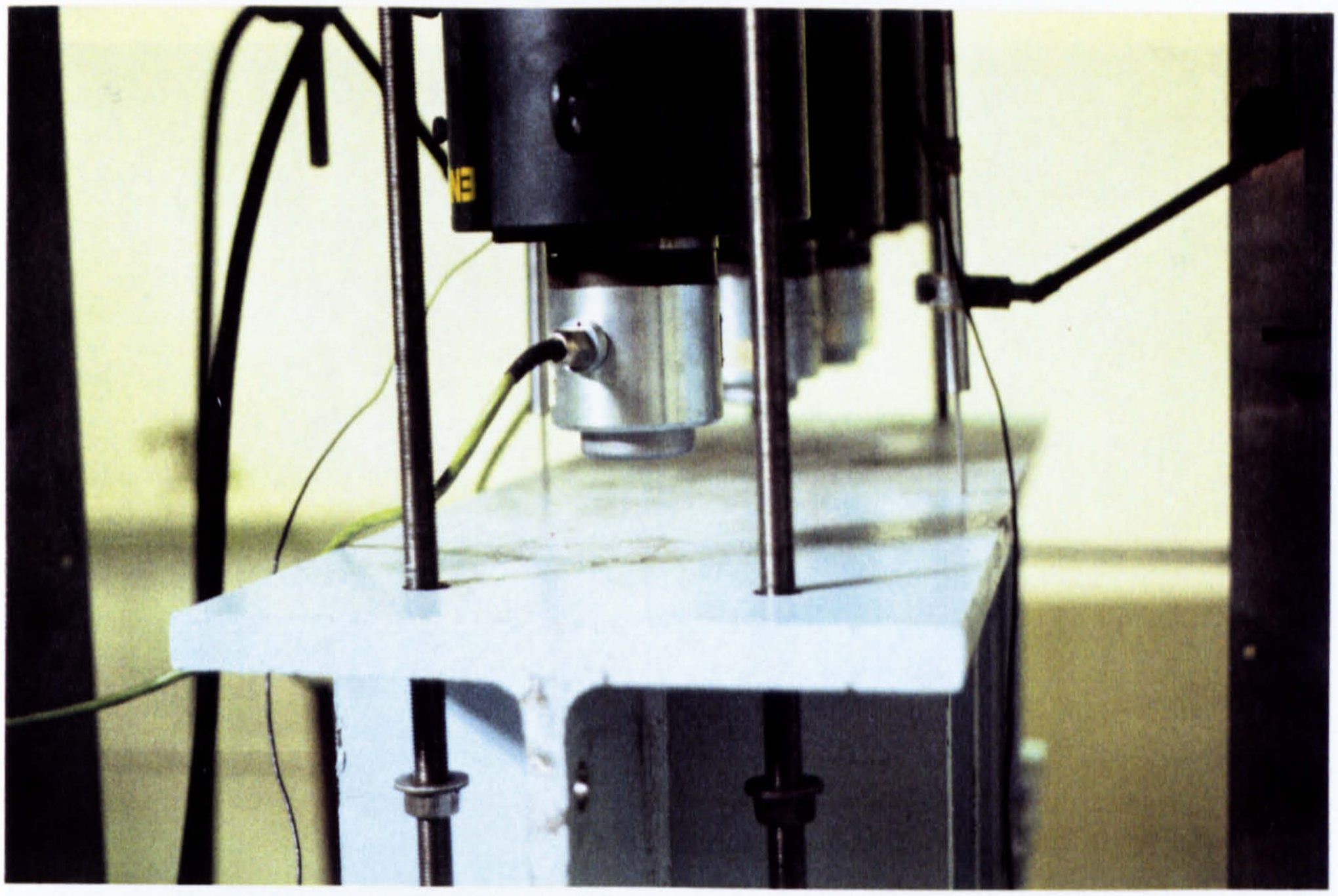

Plate 3 Hydraulic Jacks and Load Cells

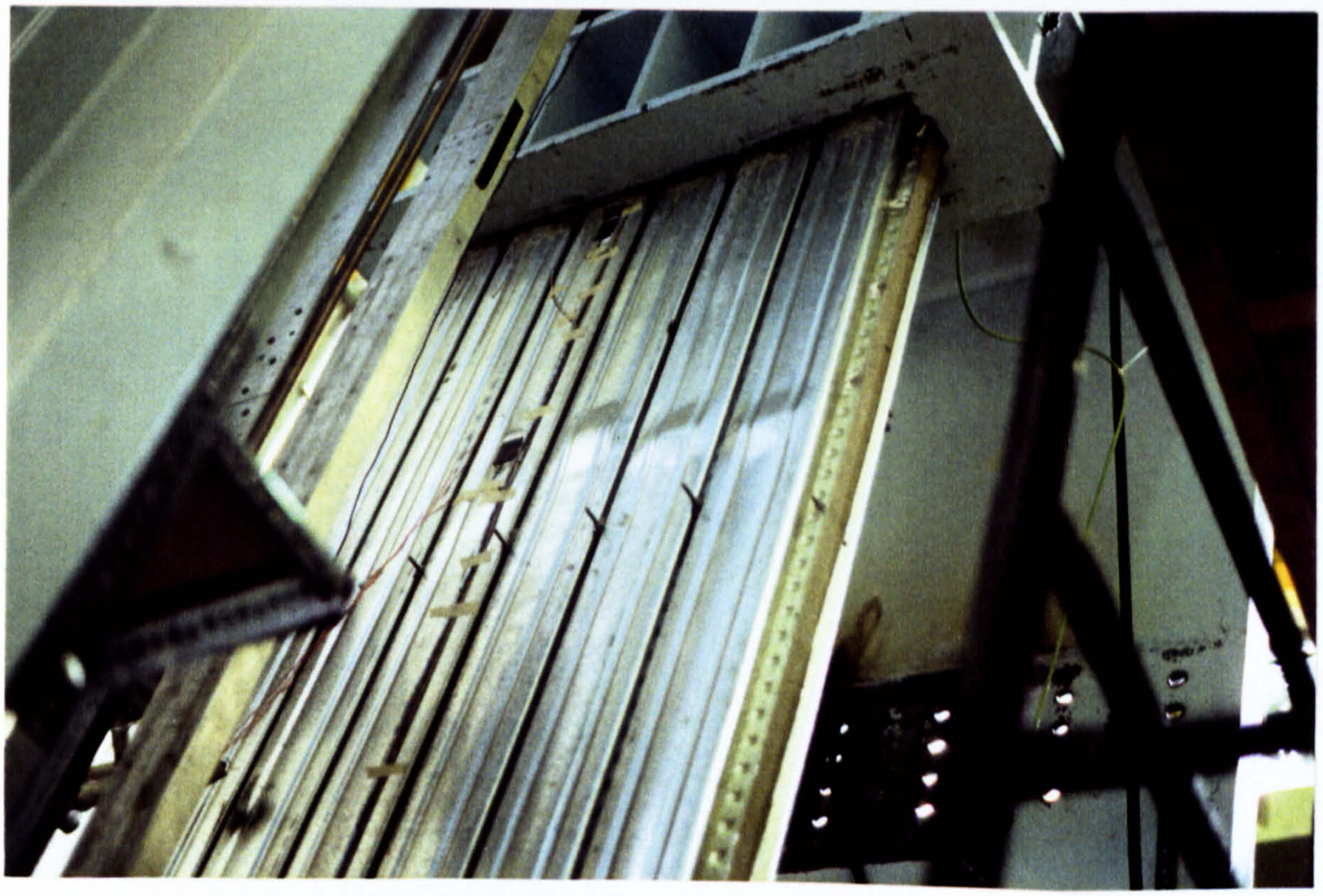

Plate 4 Composite Wall

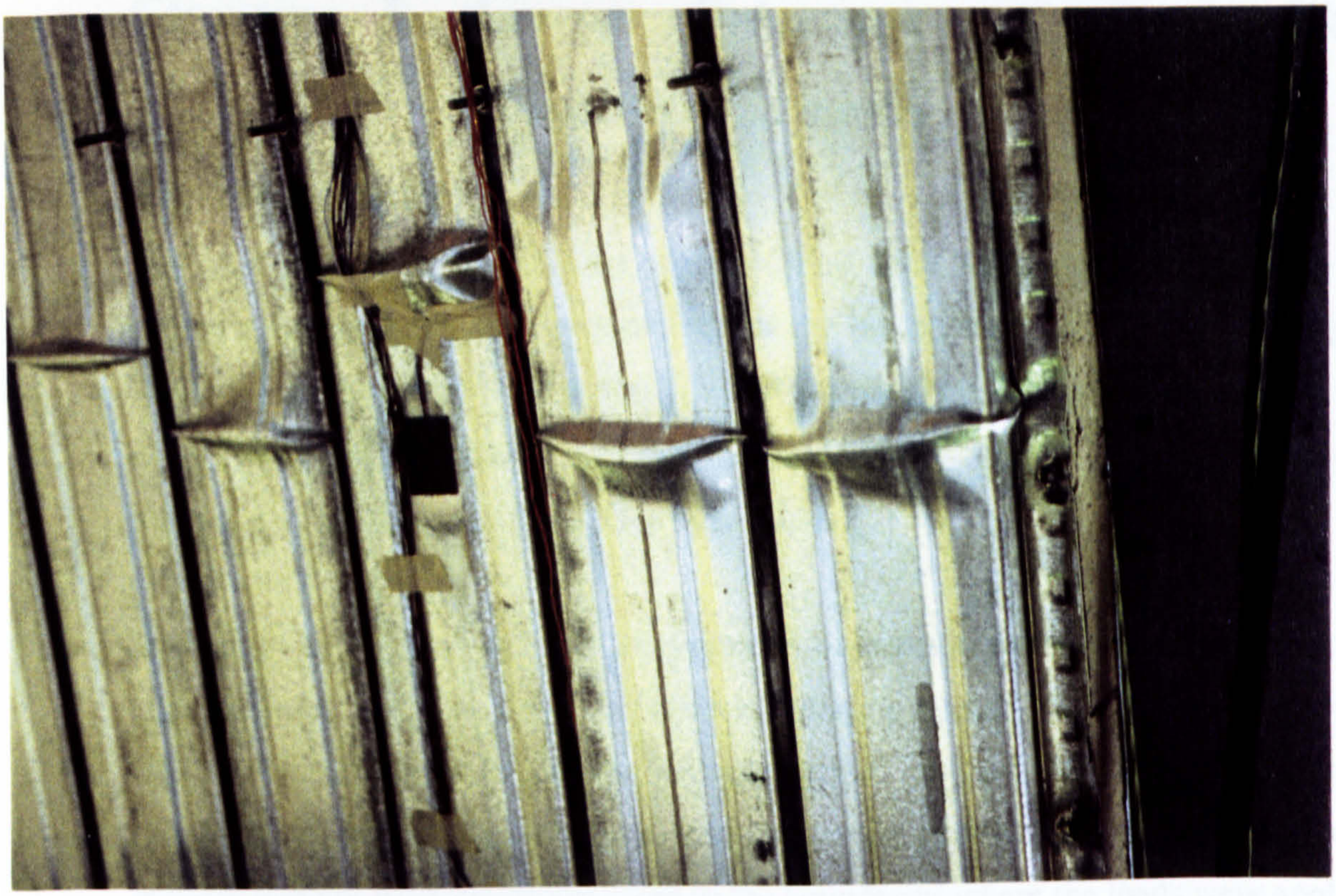

Plate 5 Local Buckling

Chapter 5 Linear Behaviour of Double-Skin Composite Elements

5.1 Introduction

The four pilot tests, studied in Chapter 4, with axial loads applied directly to the concrete surface gave capacities little improved on the respective concrete strengths. This premature loss of bond at loads below the expected ultimate values shows that an understanding of transfer between the concrete and steel is critical if composite walls are to be designed for pratical situations.

The axial behaviour of double skin composite columns has been investigated (Wright and Oduyemi 1992) in order to produce a design method taking account of bond failure and the effect on the element capacity at ultimate conditions. The work primarily considered the structural response in the central portion of the elements without dealing with the effects close to the boundaries where the loads were applied.

There are two areas that this author believes require further attention when considering the behaviour of composite walls and columns :

1. The stability of slender composite elements where interface slip occurs between the concrete and steel layers, and

2. The load transfer behaviour at the point of load application at the boundaries between the steel and concrete layers.

These effects are negligible where the wall or column consists of reinforcement which possesses a high bond strength. Conversely in situations where a fully composite action is not achieved interface slippage will have an adverse effect on the critical buckling load and member strength.

The following chapter investigates the effect of partial interaction on stability of

steel-concrete-steel sandwich elements and load transfer behaviour at the boundaries under various load conditions. The equations are formulated assuming linear stress-strain behaviour which tend to produce analytic solutions.

5.2 Review

5.2.1 Introduction

Although the specific behaviour of composite walling under axial loading has not been considered in previous work, analytic and numerical studies of associated structures, such as beams, do exist.

5.2.2 Review of Associated Work

Newmark et al (1951) were the first to study the effects of incomplete interaction at the steel/concrete interface of composite beams by performing a series of tests on composite beams supplemented by a theoretical analysis.

The experiments examined push-out tests on slabs, to obtain load-slip relationships, and full-scale beams to compare with the theoretical predictions. Although channel shear connectors were primarily investigated several other geometries were considered as comparisons.

The test results suggested that the effect of interface slip was small but a theoretical study was performed for research purposes. The type of structure considered is shown in figure 5.1. The analysis was based on the following assumptions:

1. The shear connection between the slab and beams was assumed continuous along the length despite the location of the shear connectors at discrete intervals.

2. The load-slip relationship was assumed to be linear and directly proportional to the load transmitted across the interface.

3. A linear strain distribution was assumed throughout the concrete and steel elements.

4. The steel and concrete elements were considered to deflect by similar amounts.

The movement at the interface was governed by the linear equation

$$\gamma = \frac{Q}{k} = \frac{qs}{k} \qquad ..5.1$$

where k is the modulus of the connector, Q the load on the connector, q the horizontal shear at the interface per unit length and s the spacing of the connectors.

A differential equation for the force transmitted through the shear connectors was derived and solved for a point loaded beam. Subsequently expressions were given for slip, interface shear, strains and deflections.

A study was performed to investigate the influence of the modulus of the connectors, k, on the strains and the deflections. It was found that an increase of 37% in the value of k decreased the corresponding strain and deflection by 1% and 2% respectively. This insensitivity was more evident when increasing rather than decreasing k.

Theoretical and experimental results showed good agreement but because of the high interface stiffness were not conclusive. It was suggested that the proposed theoretical analysis would be valid for any system where the basic assumptions were satisfied.

Benson and Mayers (1967) considered the buckling of sandwich plates with ideally orthotropic cores (honeycombs) with global and face wrinkling failure modes considered. The equations were developed using potential energy theory with

lagrange multipliers but did not include the effect of partial interaction. For ideal problems exact solutions were formulated with the Rayleigh-Ritz procedure applied for more general problems. Design charts were produced including the effects of global and local buckling.

The inelastic behaviour of composite beams was investigated by Yam and Chapman (1968) who carried out a numerical analysis taking account of non-linearity in the steel, concrete and the connection at the steel-concrete interface. Their analysis considered the effects of cross-section properties, span, type of loading and strain hardening and compared the solutions to experimental results. The load-slip curve (figure 5.2) was modelled by the following equation

$$Q = a(1 - e^{-b\gamma}) \qquad ..5.2$$

where γ is the interface slip and a and b are constants depending on the modelling of the experimental curve.

In the analysis it was assumed that the concrete had no tensile strength with the steel stress/strain curves the same in tension and compression. The resulting non-linear differential equation was established in terms of C, the slab compressive force, and solved by the Predictor-Corrector Method with C=0 boundary conditions.

The results of the analysis showed good agreement with corresponding experimental results and demonstrated that the, then current, recommendations of CP 117 were satisfactory for design purposes.

Plum and Horne (1975) studied the behaviour of continuous composite beams with partial interaction. A general solution was obtained for linear elastic material properties with two additional approximate procedures - hinge rotation and approximate M_o methods. The hinge rotation method reproduced the effect of partial interaction by introducing an additional flexural deformation at the supports and the loading points. The approximate M_o method ignored the effect of partial interaction

on the bending moment distribution therefore reducing the resulting solution from a fourth to a second order differential equation. All beams considered were multi-span with an interface stiffness of 400 N/mm^2 derived from push-out tests.

The results showed deflection, slip and slip strain increasing with decreasing interaction. The accuracy of the approximate methods depended on the function considered. The hinge rotation method was within 2% of the exact value even for poor interaction.

Wegmuller and Amer (1975) investigated the nonlinear response of composite steel-concrete bridges applying a non-linear finite element analysis. A layered beam-plate model was used with the tangent stiffness approach and a Newton-Raphson iterative solution scheme. No attempt was made to model the effect of slip at the interface between the materials.

Ansourian and Roderick (1978) carried out a non-linear analysis of composite beams using a load-slip curve of the following form

$$Q = r\gamma; \quad Q \le \frac{Q_{max}}{5}; \quad \gamma = aQ + bQ^2 + cQ^3 + dQ^4; \quad Q > \frac{Q_{max}}{5} \qquad ..5.3$$

where Q is the force on one connector and r denotes the initial value. The curve, initially linear, was followed by a polynomial section. In order to solve the resulting equations the curvature and extent of yielding were adjusted at every section until equilibrium was achieved. A further iteration was necessary to achieve strain compatibility with the connector forces at the interface.

In order to investigate the predicted results five full-scale tests were carried out with push-out tests to determine the shear connection behaviour. Under most loading conditions the theoretical predictions were within 5% of the experimental results. When complete interaction was assumed errors of up to 50% in the deflection calculations resulted in the elastic-plastic range. The authors concluded that the

effects of incomplete interaction were significant in the nonlinear range even when the shear connection was adequate.

Arizumi et al (1981) applied a finite element method including the effects of material non-linearity and partial interaction at the interface. The proposed element was assembled from beam elements for the concrete slab and steel beam, and spring elements for the partial interaction at the interface.

The method could be applied to simple and continuous composite beams with regularly and irregularly placed shear connectors. The advantages of the method compared to previous work were the reduced number of degrees of freedom and simpler manipulation of the material properties. The numerical results were compared to existing test data and numerical solutions and showed good agreement.

Roberts (1984) established a general formulation for the analysis of composite beams where the equilibrium and compatibility equations were established in terms of displacements. In addition to allowing interface shear slip between the steel and concrete elements normal interface displacements were also permitted.

The effect of shrinkage was considered significant throughout the span producing strains of up to -0.0004. A study of the distribution of shear connectors suggested that concentrating the shear connectors at the ends of the beams had the most beneficial affect on performance.

Johnson and Molenstra (1991) considered the effect of the shear connectors using a non-linear numerical analysis. Their analysis solved the differential equation

$$\frac{\partial^2 F}{\partial x^2} + \frac{1}{p}\frac{\partial p}{\partial x}\frac{\partial F}{\partial x} - \frac{1}{p}\frac{\partial P}{\partial x} f(F,M) = 0 \qquad ..5.4$$

where F is the longitudinal force, p is the spacing of the shear connectors and P is the shear force per connector. The boundary conditions were F=0 at x=0 and x=L.

A Newton-Raphson solution method was used to iterate the values until convergence was achieved.

The stress strain curve for the concrete in compression was the model proposed by Basu and Sommerville (1969) but included a partial safety factor of γ_m=1.5

$$\gamma_m \frac{f_c}{f_{ck}} = 2.41(\frac{\epsilon}{\epsilon_u}) - 1.865(\frac{\epsilon}{\epsilon_u})^2 + 0.5(\frac{\epsilon}{\epsilon_u})^3 - 0.045(\frac{\epsilon}{\epsilon_u})^4 \qquad ..5.5$$

where ϵ is the strain in the concrete resulting in a stress f_c, ϵ_u is the strain at the ultimate stress and f_{ck} is the cylinder strength. The effect of the concrete having a tensile strength was found to be negligible. They concluded that the maximum slips are only slightly influenced by changes in the assumed stress-strain curves for the materials and the shear studs. The modelling of the shear transfer by continuous or discrete means had little effect on the computed results.

Girhammar and Gopu (1991) were the first to consider the buckling of composite columns including the effect of partial interaction. They considered the P-δ effect on single skin concrete/timber beam-columns applying linear elastic theory and assuming

- the interlayer connectors were continuous
- the axial loads were applied at the centre of gravity
- the concrete flange remained uncracked

By applying second order theory a solution was obtained for the critical Euler buckling capacity of the element. The effect of local buckling of the timber away from the concrete was not considered in the analysis as the curvatures of the timber and concrete were constrained to be equal.

It was found that the exact procedures for computing the internal actions were cumbersome and not suited to design purposes. Therefore an approximate procedure

for calculating magnification factors applied to forces and moments calculated in the first-order analysis was proposed. This simplified method showed good agreement with the exact results (less than 2% for the calculated moments) although the application proposed was different from the conventional case.

One drawback of the derived one-dimensional 1st and 2nd order theories was an incorrect result when applying end moments. When the interface stiffness tended to infinity singularities occurred in the solution equations.

Wright and Oduyemi (1992) presented a theoretical solution to a double skin composite beam element with partial interaction. The solution was similar to that of Newmark resulting in two governing differential equations which were solved simultaneously to give a fourth order solution. A step-wise linearization method was proposed allowing the effects of non-linear effects of cracking and shear stud behaviour to be accommodated.

A comparative study was performed comparing experimental tests performed by Narayan et al (1987) to the derived solutions which showed excellent agreement.

5.2.3 Conclusions

Although the work carried out to date has extensively covered the effect of lateral loading on composite beams, only Girhammar and Gopu (1991) have considered the influence of partial interaction on the stability of slender single skin composite elements.

The current work investigating double skin composite walls required a study on the behaviour of slender elements with double skins as the composite walls are likely to show most benefits in situations with large effective heights.

The transfer of load at the boundaries, not previously investigated, may be more critical in determining the behaviour of composite walls and is also considered in the

following analysis.

5.3 Theory

The geometry of the beam/column element is shown in figure 5.3. The section is assembled from a central concrete layer sandwiched between two layers of steel with the same geometric and material properties. At the interfaces between the sections linear shear connections allow relative movement between the layers in the horizontal direction.

In the analysis the following assumptions have been made:

a) Local buckling (face wrinkling) between the steel and concrete elements and the effects of shear deformations are not considered in the analysis.

$$\frac{\partial^2 w}{\partial x^2} = \frac{\partial^2 w_1}{\partial x^2} = \frac{\partial^2 w_2}{\partial x^2} = \frac{\partial^2 w_3}{\partial x^2} \qquad ..5.6$$

This forces the curvatures to be equal in the three sections forming the element and constrains the displacements to have no relative lateral movement between the faces.

b) The axial loads are applied at the centroid of the concrete. This assumption induces no end moments as the upper and lower steel sections have similar material properties and geometry.

c) The concrete is assumed to be uncracked behaving elastically in compression and tension. Although concrete behaves non-linearly under compression and has very little tensile strength this assumption is necessary to obtain solutions by analytic methods. When linear material properties are assumed many of the current codes of pratice suggest approximate values of Young's Modulus.

d) All forces are assumed to be positive in tension.

Consider the differential element shown in figure 5.3. Taking moments about A results in the following second-order equilibrium equation.

$$(\frac{\partial^2 N_1}{\partial x^2} - \frac{\partial^2 N_3}{\partial x^2})r + \frac{\partial^2}{\partial x^2}(M_1 + M_2 + M_3) + (N_1 + N_2 + N_3)\frac{\partial^2 w}{\partial x^2} = p \quad ..5.7$$

The two terms on the left hand side supply the bending contribution of the different layers with the third term reflecting the second order effect produced by the axial load. It is convenient to leave the equation in this form as integration would produce constants dependent on the boundary conditions.

Examining the compatibility at the interfaces between the steel and concrete at the upper and lower boundaries gives

$$\Delta u_2 = u_3 - u_2 - \frac{\partial w}{\partial x}r \quad ..5.8$$

$$\Delta u_1 = u_2 - u_1 - \frac{\partial w}{\partial x}r \quad ..5.9$$

The stresses at each interface are assumed dependent on the interface linear elastic slip constant k (N/mm^2) with the relationships

$$\frac{\partial N_3}{\partial x} = k\Delta u_2 \quad ..5.10$$

$$\frac{\partial N_1}{\partial x} = -k\Delta u_1 \quad ..5.11$$

Combining 5.8 with 5.10 and 5.9 with 5.11 gives

$$\frac{\partial N_1}{\partial x} = -k(u_2 - u_1 - r\frac{\partial w}{\partial x}) \qquad ..5.12$$

$$\frac{\partial N_3}{\partial x} = k(u_3 - u_2 - r\frac{\partial w}{\partial x}) \qquad ..5.13$$

From one-dimensional linear elastic theory, the forces and moments can be expressed in terms of the displacements and curvatures respectively.

$$N_1 = E_1 A_1 \frac{\partial u_1}{\partial x} \qquad ..5.14$$

$$N_2 = E_2 A_2 \frac{\partial u_2}{\partial x} \qquad ..5.15$$

$$N_3 = E_1 A_1 \frac{\partial u_3}{\partial x} \qquad ..5.16$$

$$M_1 = -E_1 I_1 \frac{\partial^2 w}{\partial x^2} \qquad ..5.17$$

$$M_2 = -E_2 I_2 \frac{\partial^2 w}{\partial x^2} \qquad ..5.18$$

$$M_3 = -E_1 I_1 \frac{\partial^2 w}{\partial x^2} \qquad ..5.19$$

Differentiating 5.12 and 5.13 and substituting 5.14 - 5.19 gives

$$-\frac{E_1 A_1}{k}\frac{\partial^3 u_1}{\partial x^3} = \frac{\partial u_2}{\partial x} - \frac{\partial u_1}{\partial x} - r\frac{\partial^2 w}{\partial x^2} \qquad ..5.20$$

and

$$\frac{E_1A_1}{k}\frac{\partial^3 u_3}{\partial x^3} = \frac{\partial u_3}{\partial x} - \frac{\partial u_2}{\partial x} - r\frac{\partial^2 w}{\partial x^2} \qquad ..5.21$$

The applied axial load P is constant across the element and so

$$\begin{aligned} P &= N_1 + N_2 + N_3 \\ &= E_1A_1(\frac{\partial u_1}{\partial x} + \frac{\partial u_3}{\partial x}) + E_2A_2\frac{\partial u_2}{\partial x} \end{aligned} \qquad ..5.22$$

Putting 5.14 - 5.19 and 5.22 into 5.7 gives

$$E_1A_1r\frac{\partial^3}{\partial x^3}(u_1 - u_3) + P\frac{\partial^2 w}{\partial x^2} = \Sigma EI\frac{\partial^4 w}{\partial x^4} + p \qquad ..5.23$$

Subtracting 5.21 from 5.20 and substituting 5.22 gives

$$-\frac{E_1A_1}{k}\frac{\partial^3}{\partial x^3}(u_1 + u_3) = \frac{2P}{E_2A_2} - (1 + \frac{2E_2A_2}{E_2A_2})\frac{\partial}{\partial x}(u_1 + u_3) \qquad ..5.24$$

Adding 5.20 and 5.21 gives

$$\frac{E_1A_1}{k}\frac{\partial^3}{\partial x^3}(u_3 - u_1) = \frac{\partial}{\partial x}(u_3 - u_1) - 2r\frac{\partial^2 w}{\partial x^2} \qquad ..5.25$$

Let

$$\begin{aligned} \gamma_1 &= u_1 + u_3 \\ \gamma_2 &= u_1 - u_3 \end{aligned} \qquad ..5.26$$

Then from 5.24 the axial strain behaviour

$$\frac{E_1A_1}{k}\frac{\partial^3\gamma_1}{\partial x^3} - (\frac{2E_1A_1}{E_2A_2} + 1)\frac{\partial\gamma_1}{\partial x} + \frac{2P}{E_2A_2} = 0 \qquad ..5.27$$

From equation 5.25

$$\frac{\partial^2 w}{\partial x^2} = -\frac{1}{2r}\left(\frac{\partial \gamma_2}{\partial x} - \frac{E_1 A_1}{k}\frac{\partial^3 \gamma_2}{\partial x^3}\right) \qquad ..5.28$$

Putting 5.26 and 5.28 into 5.23 and letting F = -P for a compressive force gives

$$\frac{\Sigma EI\ E_1 A_1}{2rk}\frac{\partial^5 \gamma_2}{\partial x^5} - \left(E_1 A_1 r + \frac{\Sigma EI}{2r} + F E_1 \frac{A_1}{2rk}\right)\frac{\partial^3 \gamma_2}{\partial x^3} + \frac{F}{2r}\frac{\partial \gamma_2}{\partial x} + p = 0 \qquad ..5.29$$

The result of the substitution (equation 5.26) uncouples the differential equations resulting in two differential equations in γ_1 and γ_2, equations 5.27 and 5.29 respectively, allowing simpler solutions than would otherwise be possible. The value of γ_2 has a similar behaviour to the deflection, w, which should allow the buckling capacity of element to be determined.

5.3.1 Critical Buckling Load

The general solution of 5.29 is

$$\gamma_2 = A_1\sinh(\lambda_1 x) + A_2\cosh(\lambda_1 x) + A_3\sin(\lambda_2 x) + A_4\cos(\lambda_2 x) + A_5 + \gamma_2^{ps} \qquad ..5.30$$

with the characteristic equations

$$\lambda_1^4 - \left(\frac{2r^2k - F}{\Sigma EI} + \frac{k}{E_1 A_1}\right)\lambda_1^2 - \frac{Fk}{\Sigma EI E_1 A_1} = 0 \qquad ..5.31$$

$$\lambda_2^4 + \left(\frac{2r^2k - F}{\Sigma EI} + \frac{k}{E_1 A_1}\right)\lambda_2^2 - \frac{Fk}{\Sigma EI E_1 A_1} = 0 \qquad ..5.32$$

Considering the λ_2 solution from the sine and cosine components gives an expression for the critical buckling load of double skin composite beam/columns with partial interaction written as

$$P_{crit} = \frac{(\lambda_2^2 \Sigma EI + 2r^2k)E_1A_1 + k\Sigma EI}{E_1A_1 + \frac{k}{\lambda_2^2}} \qquad ..5.33$$

Assuming that the strut is pin-ended then the sine solution vanishes when

$$\lambda_2 = \frac{i\pi}{L} \quad where\ i = 1,2,3... \qquad ..5.34$$

Then the deflection representative value, γ_2 has the shape

$$\gamma_2 = A_3 \sin\frac{i\pi x}{L} \qquad ..5.35$$

This buckling mode can only be satisfied at the critical values of F, P_{crit}, given by equation 5.33 with $\lambda_2 = i\pi$ /L. Setting λ_2 equal to π/L, the fundamental buckling mode for a pin-ended strut, then the critical buckling load becomes

$$P_{crit} = \frac{(\frac{\pi^2}{L^2}\Sigma EI + 2r^2k)E_1A_1 + k\Sigma EI}{E_1A_1 + \frac{kL^2}{\pi^2}} \qquad ..5.36$$

It should be noted that increasing the lateral loading produces no reduction in the critical Euler loading, as is also the case when considering fully composite situations. As face wrinkling has not been considered the buckling load will not be effected by the point of application of the axial load.

As k tends to infinity, as occurs in a fully composite section equation 5.36 becomes

$$P_{crit} = \frac{(2E_1A_1r^2 + \Sigma EI)\pi^2}{L^2} \qquad ..5.37$$

corresponding to the fundamental buckling load for a fully composite pin-ended section.

As k tends to 0, as in the case where no interaction occurs between the three layers

$$P_{crit} = \frac{\Sigma EI\,\pi^2}{L^2} \qquad ..5.38$$

corresponding to buckling of the three separate columns with the restriction of equal curvatures.

Letting L tend to 0 with a constant k results in equation 5.38. When the length decreases the contribution from partial interaction reduces between the layers and the beam/column behaviour becomes more like that of separate columns.

Letting L tend to infinity then gives equation 5.37 which results in an increased contribution from partial interaction across the interface.

When the boundary conditions are different to that of a pin-ended strut the effective length of the strut can be altered to reflect the changes in the waveform.

5.3.2 Deformation under Axial Loads

Previous authors, Wright and Oeduyemi (1992), have considered the one-dimensional bending effects on double and single skin sandwiches. With the possibility of applying axial loads to the steel and the concrete sections of composite columns/walls it is important to examine this behaviour and the implications for design.

In order to examine the effect of axial loads on the sandwich element the differential equations containing factors γ_1 and γ_2 may be considered separately and solved for the symmetric and skew-symmetric cases respectively.

Applying symmetric loading results in solutions where $u_1 = u_3$ are directly available once γ_1 is calculated as the skew-symmetric equation reduces to zero. In the skew-symmetric case $u_1 = -u_3$ can be calculated by finding γ_2.

5.3.2.1 *Symmetric Axial Loads*

The axial compressive displacements contained in the term γ_1 is governed by equation 5.27. The general solution to this equation is

$$\gamma_1 = A_1 e^{\sqrt{\frac{\beta}{\alpha}}x} - A_2 e^{-\sqrt{\frac{\beta}{\alpha}}x} + A_3 - \frac{2P}{\beta E_2 A_2} x$$

$$\textit{where} \qquad \alpha = \frac{E_1 A_1}{k} \qquad \text{..5.39}$$

$$\beta = \frac{2E_1 A_1}{E_2 A_2} + 1$$

Depending on the boundary conditions this equation can be solved to give values of displacement on the upper and lower steel surfaces.

From symmetry in the axial loading situation the displacements on the upper and lower steel surfaces are equal and therefore

$$u_1 = u_3 = \frac{\gamma_1}{2} \qquad \text{..5.40}$$

Applying load only to the concrete, leaving the steel unloaded at the boundaries, gives the following solution for the axial displacements in the steel.

$$u_1 = u_3 = \frac{P}{E_2 A_2 + 2E_1 A_1}\left[(\xi - \frac{1}{2})L + \frac{1}{\lambda}\left[- e^{\lambda\xi} + \frac{1 - e^{\lambda}}{e^{-\lambda} - e^{\lambda}}(e^{\lambda\xi} + e^{-\lambda\xi})\right]\right]$$

$$\textit{where} \quad \lambda = L\sqrt{\frac{\beta}{\alpha}} = L\sqrt{(\frac{2}{E_2 A_2} + \frac{1}{E_1 A_1})k}$$

$$\xi = \frac{x}{L}$$

..5.41

Differentiating with respect to x gives the steel strains

$$\epsilon_1 = \epsilon_3 = \frac{P}{E_2A_2 + 2E_1A_1}\left[1 - e^{\lambda\xi} + \frac{1 - e^{\lambda}}{e^{-\lambda} - e^{\lambda}}(e^{\lambda\xi} - e^{-\lambda\xi})\right] \quad ..5.42$$

which can be expressed in the form

$$\epsilon_1 = \frac{P}{E_2A_2 + 2E_1A_1}\mu(\lambda,\xi) \quad ..5.43$$

$$\textit{where} \quad \mu = \left[1 - e^{\lambda\xi} + \frac{1 - e^{\lambda}}{e^{-\lambda} - e^{\lambda}}(e^{\lambda\xi} - e^{-\lambda\xi}\right]$$

where μ depends on non-dimensional constants λ and ξ, the proportional distance of point considered along the beam/column. The value of μ may be calculated from equation 5.43 or taken from figure 5.4. The value of μ is plotted against ξ for various values of λ.

If $\mu = 0$, there is no interaction between the steel and concrete layers and no load is transferred between these layers over the whole element length.

If $\mu = 1.0$, there is full interaction between the concrete and steel layers resulting in equal strains across the full length of the element.

It can be seen that below $\lambda = 1$ the composite action is relatively low with little transfer between the concrete and steel layers, while at $\lambda = 32$ a fully composite action ($\mu = 1.0$) is approached. At low values the strain distribution is parabolic but with increasingly higher values μ tends towards a square distribution corresponding to a fully interactive condition.

The concrete strain can also be written in terms of μ from equation 5.22.

$$\epsilon_2 = \frac{P}{E_2A_2 + 2E_1A_1}\left[1 + \frac{2E_1A_1}{E_2A_2}(1 - \mu)\right] \quad ..5.44$$

By applying equations 5.10 and 5.11 the amount of slip can be found at the interface

between the concrete and the upper and lower steel layers

$$\Delta u_2 = -\Delta u_1 = \frac{PL}{E_2 A_2}\frac{1}{\lambda}\left[-e^{\lambda\xi} + \frac{1 - e^{\lambda}}{e^{-\lambda} - e^{\lambda}}(e^{\lambda\xi} - e^{-\lambda\xi})\right] \qquad ..5.45$$

which can be written as

$$\Delta u_2 = \frac{PL}{E_2 A_2}\mu'(\lambda,\xi) \qquad ..5.46$$

$$\textit{where} \quad \mu' = \frac{1}{\lambda}\left[-e^{\lambda\xi} + \frac{1 - e^{\lambda}}{e^{-\lambda} - e^{\lambda}}(e^{\lambda\xi} - e^{-\lambda\xi})\right]$$

with μ' calculated directly or obtained from figure 5.5 where the value is plotted for variations in λ and ξ.

Another important situation that requires consideration is where the steel is loaded at the boundaries without the concrete being directly loaded. This situation may occur when floors are fixed directly to the sheeting at the top of composite walls. In order that the symmetric assumption is satisfied equal loads must be applied to the steel as shown in figure 5.6. The governing equations can be established by superposition using the previously derived formula where only the concrete was loaded and the condition where equal strains are present in the concrete and steel throughout the length of the member. Combining these solutions and forcing the concrete strain at the boundary of the element to be zero, results in the following solutions for the steel and concrete strains.

$$\epsilon_1 = \frac{Q}{2A_1E_1}\left[1 - \mu\frac{E_2A_2}{E_2A_2 + 2E_1A_1}\right] \qquad ..5.47$$

$$\epsilon_2 = \frac{Q\mu}{E_2A_2 + 2A_1E_1} \qquad ..5.48$$

Similarly the interface slips can be written

$$\Delta u_2 = -\Delta u_1 = -QL\left[\frac{1}{2A_1E_1} + \frac{1}{E_cA_c}\right]u'(\lambda,\xi) \qquad ..5.49$$

As with the previous solutions the applied load is assumed to be positive in tension. The situation where one end of the element is restrained preventing interface slip between the surfaces can be analyzed by letting $L = 2L_o$ where L_o is the actual element length and considering only half the section.

5.3.2.2 *Skew-Symmetric and Single Axial Loads*

The condition where a load is placed at the boundary of only one steel section can be modelled by considering the symmetric and skew-symmetric situations and applying superposition (see figure 5.7). The symmetric case has already been considered and so considering equation 5.29, assuming the concrete load is zero and neglecting the second order effect, results in the following differential equation which satisfies the condition $u_1 = u_3$.

$$\frac{\partial^5\gamma_2}{\partial x^5} - \tau^2\frac{\partial^3\gamma_2}{\partial x^3} = 0 \qquad ..5.50$$

$$where \quad \tau = L\sqrt{\frac{EI_{\infty}k}{\Sigma EIE_1A_1}}$$

This equation has the general solution

$$\gamma_2 = Ae^{\tau x} + Be^{-\tau x} + Cx^2 + Dx + E \qquad ..5.51$$

Applying the boundary conditions of an anti-symmetric load where the axial loads have opposite directions at the steel boundaries gives

$$\frac{\partial\gamma_2}{\partial x} = \frac{\partial u_1}{\partial x} - \frac{\partial u_3}{\partial x} = \frac{Q}{2E_1A_1} + \frac{Q}{2E_1A_1} = \frac{Q}{E_1A_1} \; at \; x = 0, \; x = L \qquad ..5.52$$

with no applied end moments

$$\frac{\partial^2 w}{\partial x^2} = 0; \left[\frac{Q}{E_1 A_1} - \frac{E_1 A_1}{k}\frac{\partial^3 \gamma_2}{\partial x^3}\right] = 0 \text{ at } x = 0, x = L \qquad ..5.53$$

and steel displacement zero at the centre

$$\gamma_2 = 0 \text{ at } x = \frac{L}{2} \qquad ..5.54$$

resulting in 5 equations with 5 unknowns allowing a unique solution to the displacement

$$u_1 = \frac{\gamma_2}{2} = \frac{1}{2}\frac{QL\Sigma EI}{E_1 A_1 EI_-}\left[\frac{e^{-\tau}-1}{e^{-\tau}-e^{\tau}}\frac{e^{\tau\xi} - e^{\frac{\tau}{2}}}{\tau} + \frac{e^{\tau}-1}{e^{-\tau}-e^{\tau}}\frac{e^{-\tau\xi} - e^{\frac{\tau}{2}}}{\tau} - (\xi - \frac{1}{2})\right] \qquad ..5.55$$
$$+ \frac{QL}{2E_1 A_1}(\xi - \frac{1}{2})$$

and strain in the steel.

$$\epsilon_1 = \frac{1}{2}\frac{\partial \gamma_2}{\partial x} = \frac{1}{2}\frac{Q\Sigma EI}{E_1 A_1 EI_-}\left[\frac{e^{-\tau}-1}{e^{-\tau}-e^{\tau}}e^{\tau\xi} - \frac{e^{\tau}-1}{e^{-\tau}-e^{\tau}}e^{-\tau\xi} - 1\right] + \frac{Q}{2E_1 A_1} \qquad ..5.56$$

As before these equations are easier to manipulate in non-dimensional form which conveniently leads to terms capable of being expressed by μ and μ'. The steel strain can be written as

$$\epsilon_1 = \frac{-Q\Sigma EI}{2E_1 A_1 EI_-}\mu(\tau,\xi) + \frac{Q}{2E_1 A_1} \qquad ..5.57$$

The value τ replaces λ in the function μ and includes bending terms instead of the previous axial constants.

Applying equations 5.10 and 5.11 gives the interface slip written in terms of μ'

$$\Delta u_1 = -\Delta u_3 = \frac{QL}{2E_1 A_1}\mu'(\tau,\xi) \qquad ..5.58$$

Combining the solutions constructed from the symmetric and skew-symmetric proofs allows a solution using superposition for a single point load at the boundary of one steel layer (figure 5.7). For an axially tensile force on the lower steel then

$$\epsilon_1 = \frac{Q}{E_1 A_1}\left[1 - \frac{1}{2}\mu(\lambda,\xi)\frac{E_2 A_2}{E_2 A_2 + 2E_1 A_1} - \frac{1}{2}\mu(\tau,\xi)\frac{\Sigma EI}{EI_-}\right] \qquad ..5.59$$

and

$$\Delta u_1 = QL\left[\left[\frac{1}{2E_1 A_1} + \frac{1}{E_2 A_2}\right]\mu'(\lambda,\xi) + \frac{1}{2E_1 A_1}\mu'(\tau,\xi)\right] \qquad ..5.60$$

with the corresponding strains and slips on the unloaded upper steel section written as

$$\epsilon_3 = \frac{Q}{E_1 A_1}\left[-\frac{1}{2}\mu(\lambda,\xi)\frac{E_2 A_2}{E_2 A_2 + 2E_1 A_1} + \frac{1}{2}\mu(\tau,\xi)\frac{\Sigma EI}{EI_-}\right] \qquad ..5.61$$

and

$$\Delta u_2 = QL\left[\left[\frac{1}{2E_1 A_1} + \frac{1}{E_2 A_2}\right]\mu'(\lambda,\xi) - \frac{1}{2E_1 A_1}\mu'(\tau,\xi)\right] \qquad ..5.62$$

5.4 Error in One-Dimensional Approximation

Applying one-dimensional elasticity to double skin composite elements creates an error in the solution relating to this approximation. As no shear loads are applied vertically at the ends of the double skin element, the shear stresses should satisfy

$$\tau_{xy} = \tau_{yx} = 0 \qquad ..5.63$$

at the boundary on the interface between the layers (see figure 5.8). The previous derivation does not reflect this condition and therefore is slightly inaccurate. Despite this effect, the solutions are still applicable in most cases given that previous authors had the same error present in their solutions without noticable effects. Also, connections tend to be discrete rather than continuous provided either by stud connectors or embossments.

5.5 *Application of Derived Equations*

The equations established offer some guidance in the design of walls and columns with external reinforcement. A comparison between the theorectical, numerical and test results will be performed in chapter 6. In general the brittle interface failures occuring in the pilot tests may limit the applicability to situations where linear elastic interface models are more suitable, such as occur when shear studs are used.

5.6 *Summary*

The previous theoretical work analyzed the behaviour of the important effects of buckling and load transfer between the layers the wall. The equations developed include an elastic analysis of the critical bucking load for double skin composite sections and the slips, displacements and strains produced under various forms of point loading at the boundaries. Although these equations are useful they do not reflect the non-linear material and slip relationships occurring under ultimate conditions. In the following chapter a numerical model will be developed with non-linear material and interface models capable of supplying variations in the stiffness throughout the length.

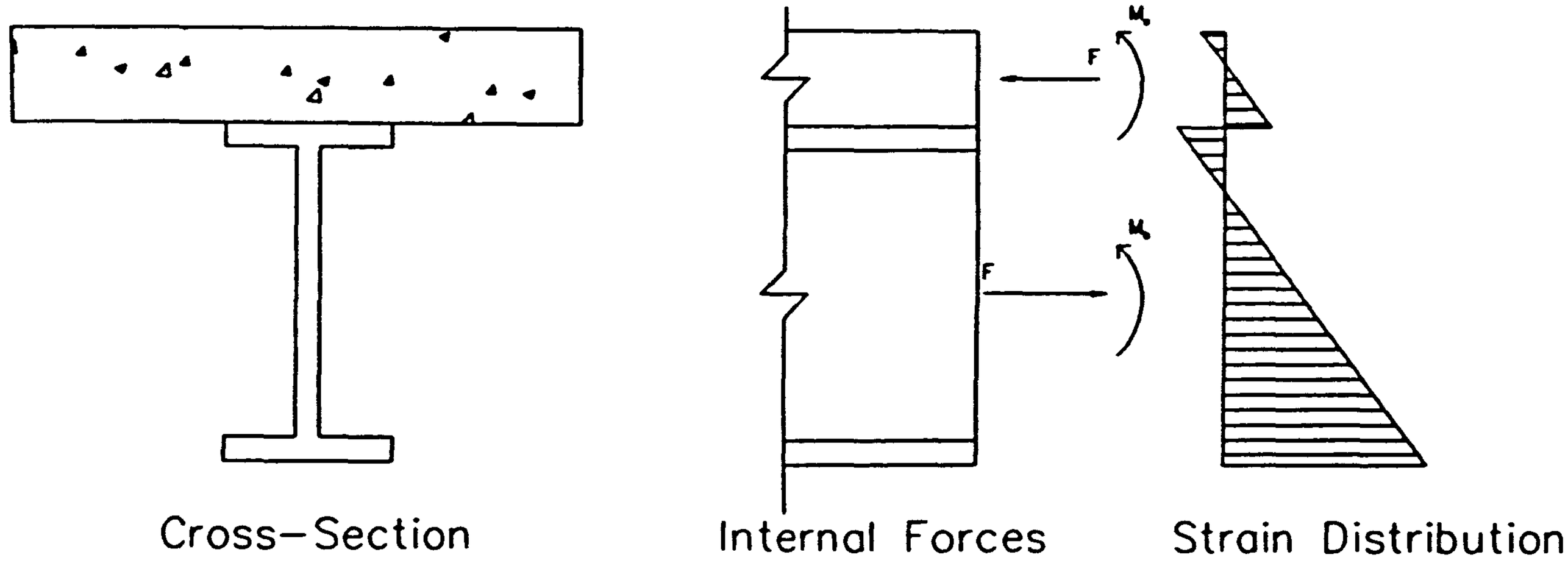

Figure 5.1 Newmark Model

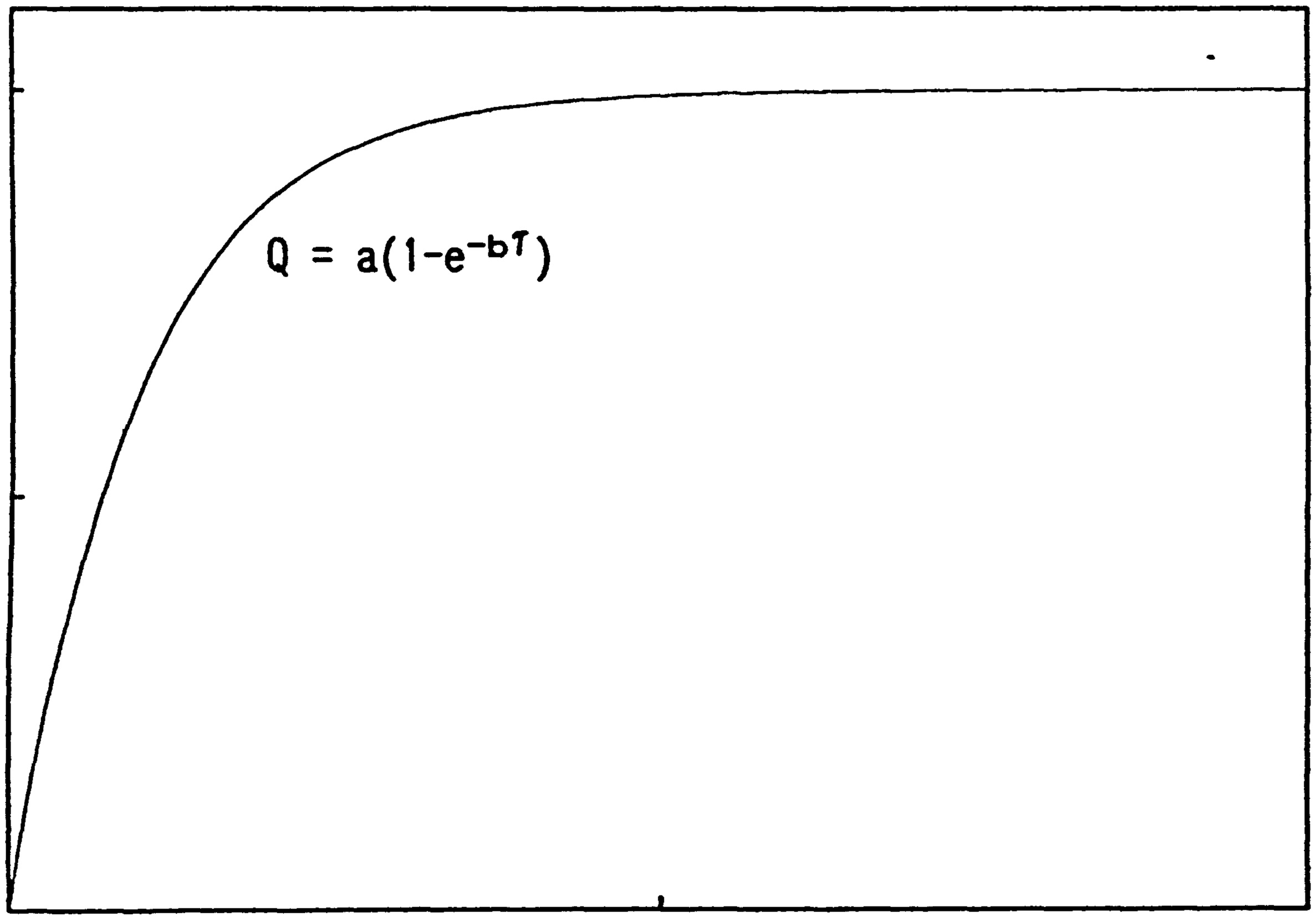

Figure 5.2

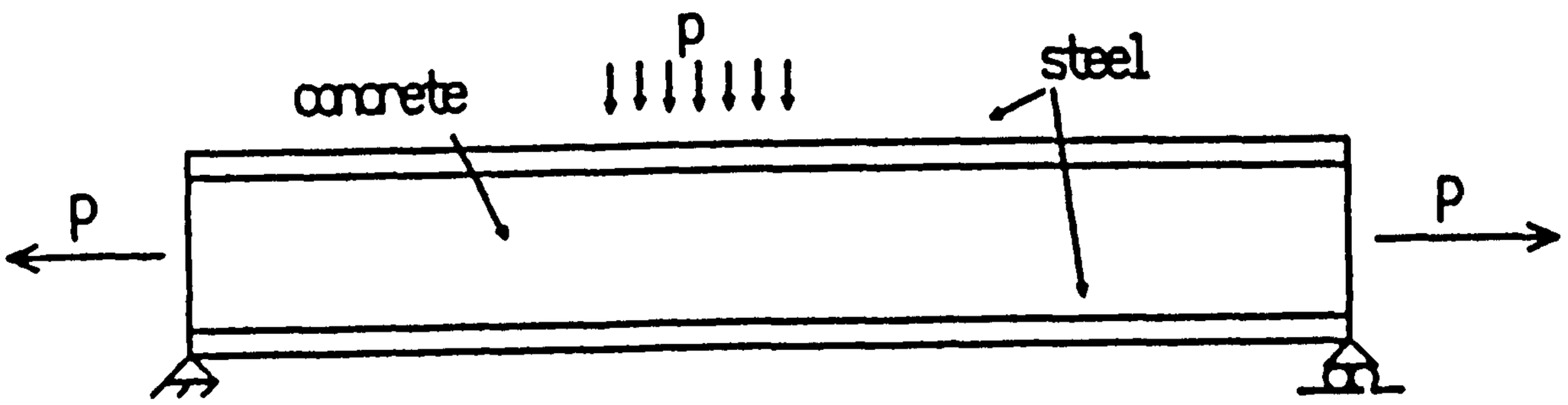

Double Skin Composite Element

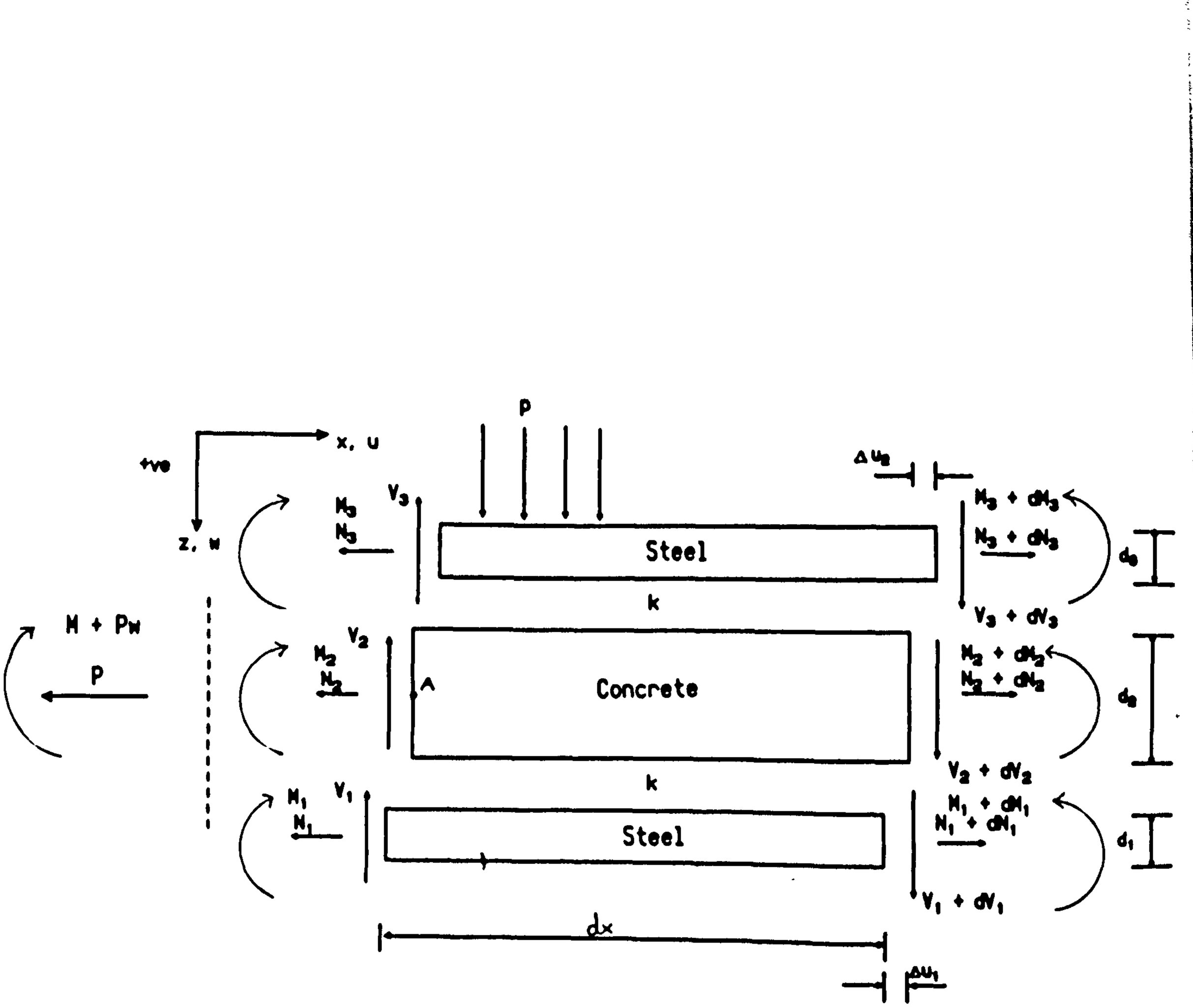

Figure 5.3 Differential Element

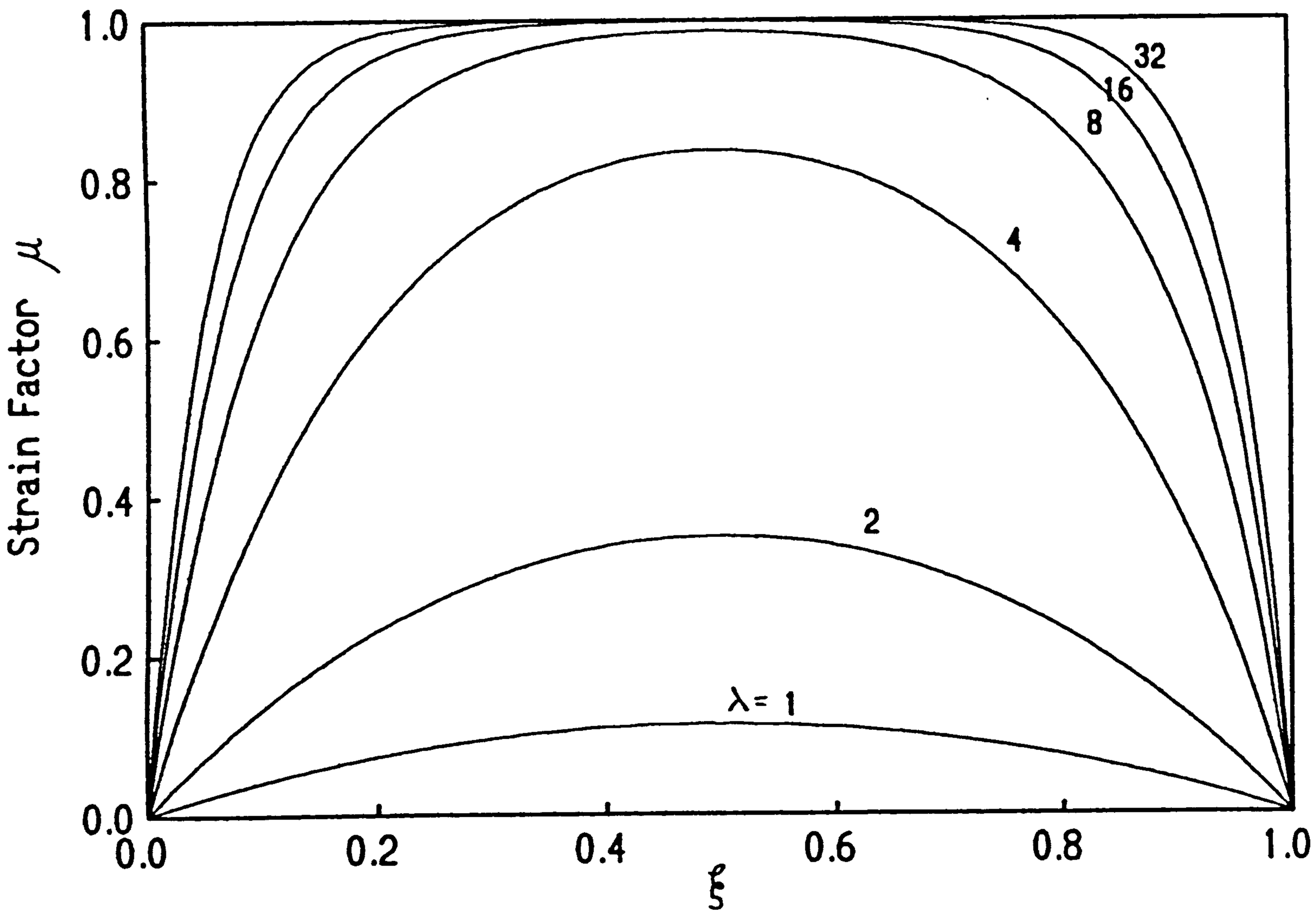
Axial Steel Strain
Strain Factor vs ξ
Strain Factor μ
1.0
0.8
0.6
0.4
0.2
0.0
0.0
0.2
0.4
0.6
0.8
1.0
ξ
32
16
8
4
2
λ= 1

Figure 5.4

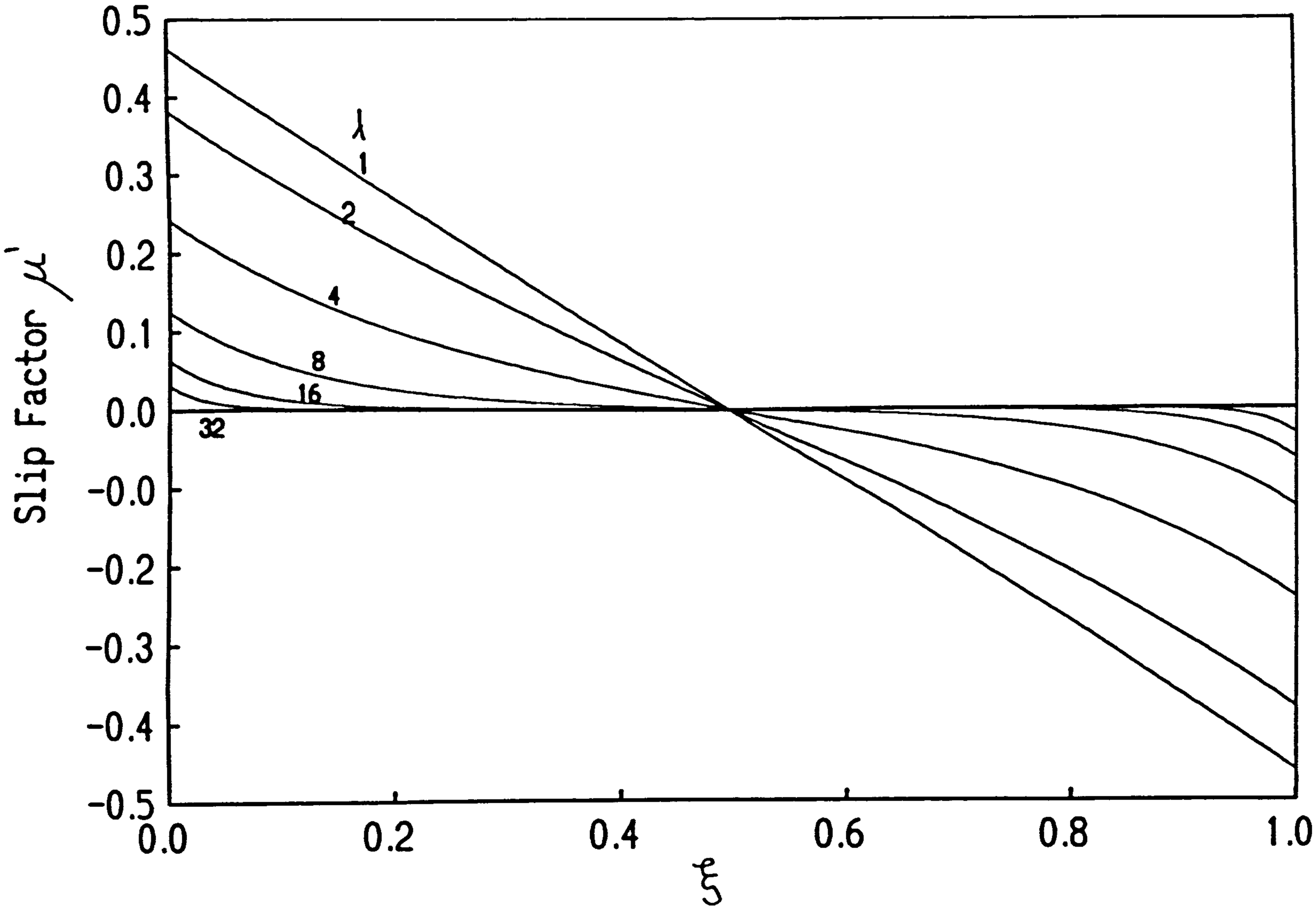
Axial Steel Slip
Slip Factor vs ξ
Slip Factor μ'
0.5
0.4
0.3
0.2
0.1
0.0
-0.0
-0.2
-0.3
-0.4
-0.5
λ
1
2
4
8
16
32
0.0
0.2
0.4
0.6
0.8
1.0
ξ

Figure 5.5

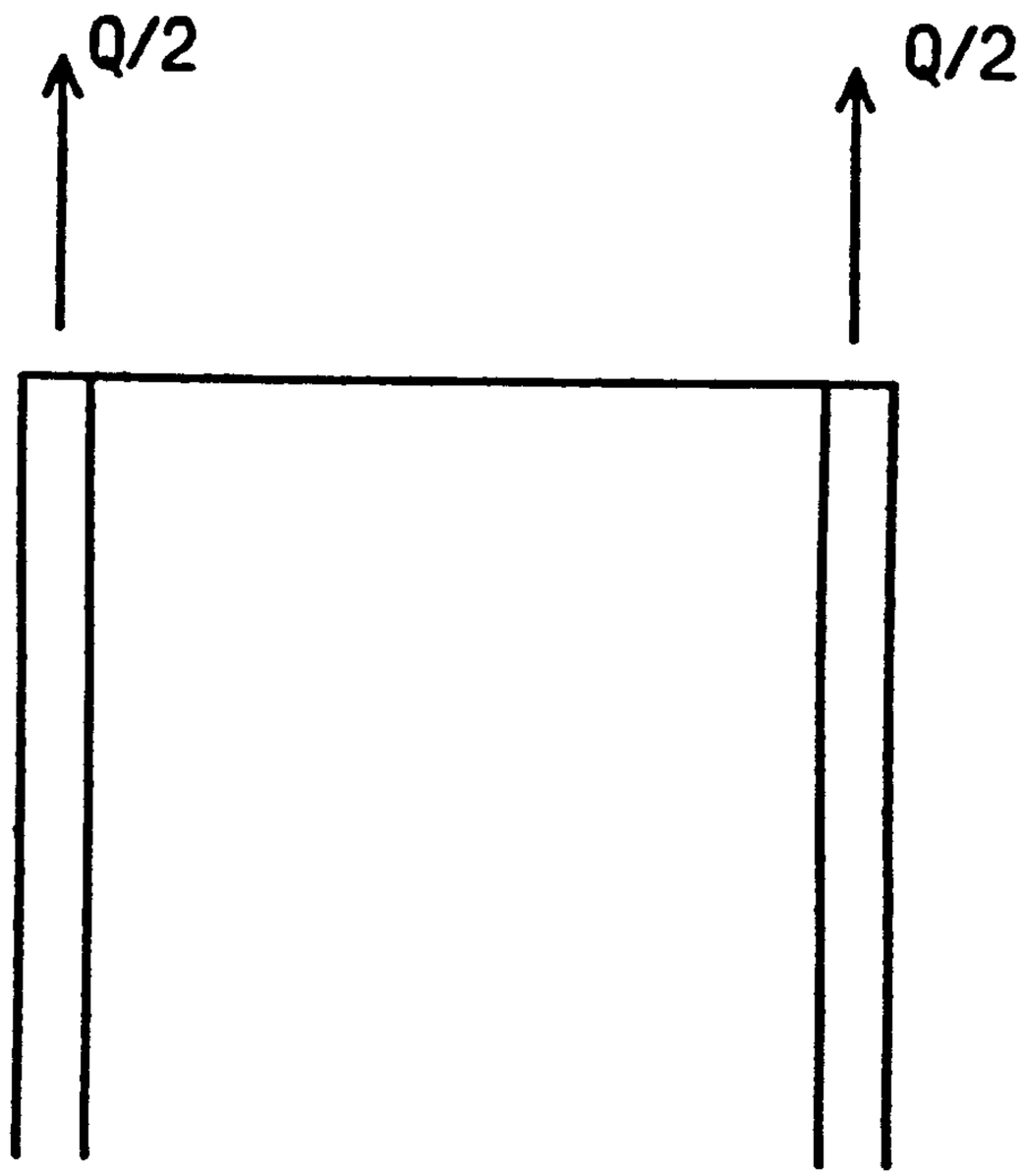

Figure 5.6 Boundary Conditions

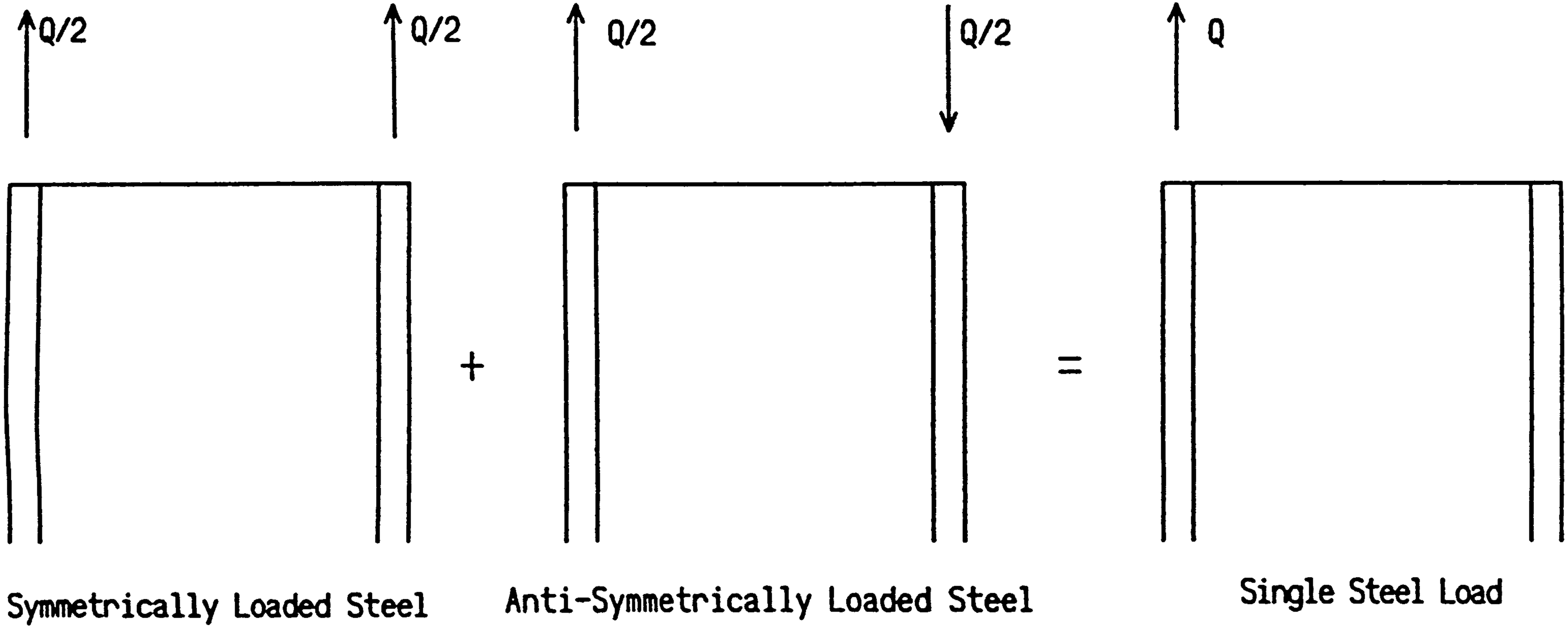

Figure 5.7 Superposition of Load Cases

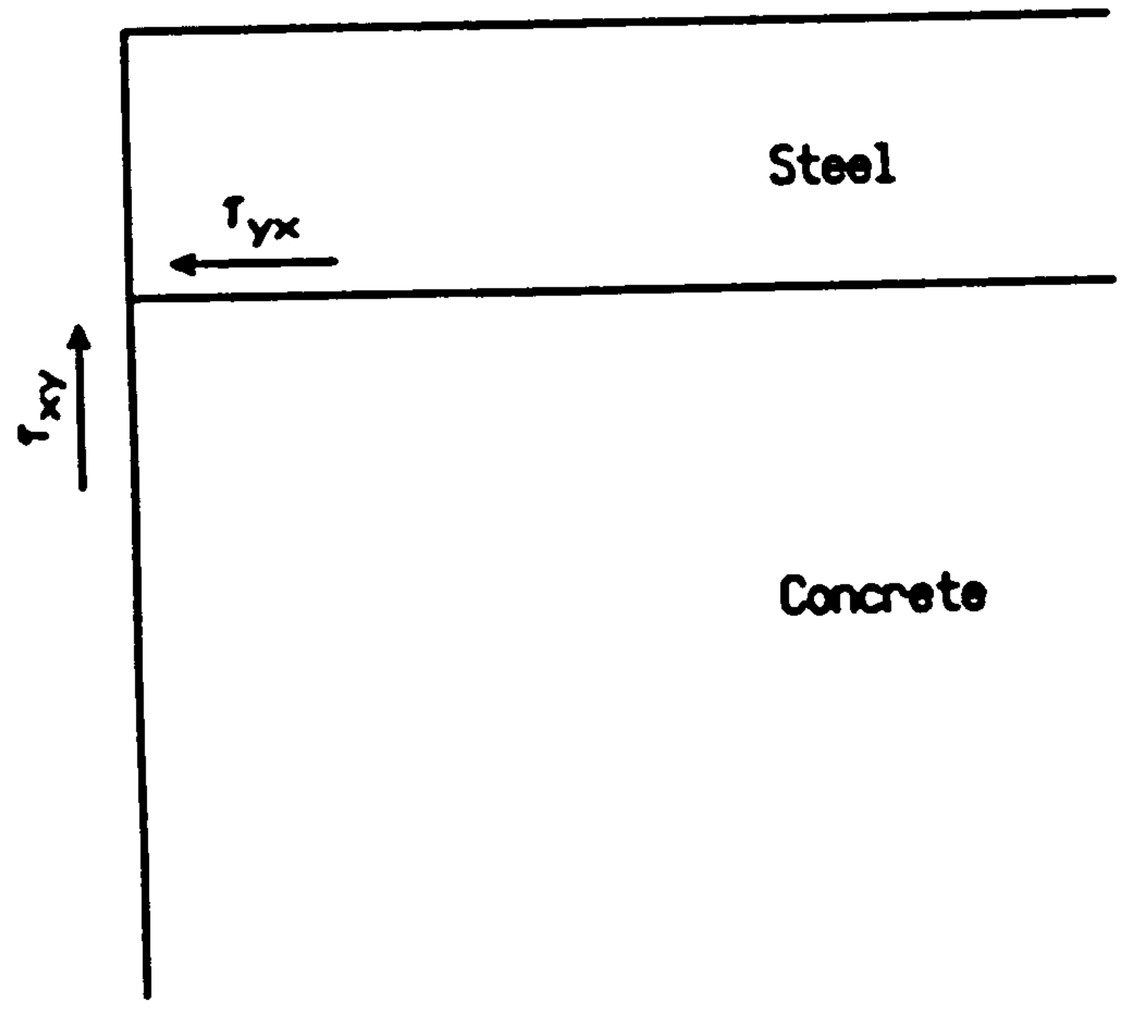

Figure 5.8 Two-Dimensional Boundary Condition

Chapter 6 Non-Linear Analysis of Double Skin Composite Elements

6.1 Introduction

The previous chapter considered the performance of double skin composite elements by assuming a linear material behaviour in the steel and concrete layers and also at the interfaces between the layers. Although these assumptions enabled a direct analytic solution of the problems associated with interface slip to be obtained they tend to be limited in scope and application especially under ultimate conditions. In this chapter a finite difference model is developed with the following features :

1. Material non-linearity is included for the steel and concrete behaviour.

2. Slip behaviour at the interface between the steel and concrete is controlled by a non-linear relationship. This behaviour can vary across the element to account for variations in stiffness resulting from changes in the spacing of connection devices.

3. The second order P-Δ effect is included for the behaviour in slender situations.

4. Uniformly distributed and point loads can be laterally applied to the element.

5. Axial loads may be applied at the boundaries of the top steel, concrete and bottom steel.

6. Internal reinforcing bars may be applied at the concrete boundaries.

The purpose of the model was to obtain a better understanding of the behaviour of composite elements under axial loading conditions and also assist in forming a design method covered in Chapter 8.

Two methods were considered for the analysis of the composite wall/column - the Finite Element Method and the Finite Difference Methods.

The finite element method (FEM) offered an easier implementation of boundary conditions when dealing with shapes with complex geometries than the finite difference method. High order equations modelled by the finite difference method (FDM) are also more difficult to deal with because of greater complexity in the application of boundary conditions as the 'molecule' size increases. The reduction in the order of convergence occurring in the FDM in using difference expressions does not occur in the FEM.

Despite these advantages the FDM has the advantage of being a direct method replacing the differential equation by a difference expression and avoiding the necessity to cast the equations in integral form. As the geometry was one-dimensional the problems associated with boundary conditions were manageable with only the ends of the composite wall/column requiring consideration. These features allowed an easier implementation of the FDM with less computer coding than that required for the FEM.

6.2 Finite-Difference Method

Having found the relevant governing differential equations the finite-difference method was applied to obtain solutions. This method replaces the differential expression by the difference expression reducing differential equations to algebraic ones.

If there exists a function $y = f(x)$ for which the derivative $f'(x)$ is required at a point x_1, then for a small distance along the x-axis the curve can approximated by a straight line.

$$y'|_{x_1} = \lim_{\delta x_1 \to 0} \frac{f(x_1 + \delta x_1) - f(x_1 - \delta x_1)}{2\delta x_1} \qquad ..6.1$$

$$\approx \frac{f(x_1 + \delta x_1) - f(x_1 - \delta x_1)}{2\delta x_1}$$

This finite-difference approximation can also be applied to higher derivatives. To implement the method the domain in question must be discretized into a grid with segments δx apart.

6.3 Non-Linear Iteration and Solution Schemes

In applying the finite difference scheme to the problem of double-skin composite elements various numerical schemes were implemented to obtain a convergent and reliable solution method.

The three major techniques applied were :

1. LU Decomposition
2. Newton Raphson Method, and
3. Newmark's Method

which are discussed below.

6.3.1 LU Decomposition

The LU decomposition is necessary in the solution scheme for solving the Newton-Raphson and Newmark double integration schemes and therefore should be explained.

If a matrix A can be written as the product of two matrices

$$\boldsymbol{L.U = A} \qquad ..6.2$$

where L is a lower triangular and U is an upper triangular then to solve a set of

linear equations, the decomposition given in 6.2 can be performed

$$\boldsymbol{A.x} = (\boldsymbol{L.U}).\boldsymbol{x} = \boldsymbol{L}.(\boldsymbol{U}.\boldsymbol{x}) = \boldsymbol{b} \qquad ..6.3$$

by first solving for a vector y so that

$$\boldsymbol{L.y} = \boldsymbol{b} \qquad ..6.4$$

and then solving

$$\boldsymbol{U.x} = \boldsymbol{y} \qquad ..6.5$$

The advantages of this form of solution is that the solution of a triangular set of equations is relatively simple and once the LU decomposition of A is performed then as many right-hand side b matrices as required can be solved at a later stage.

6.3.2 Newton-Raphson Scheme

To solve certain non-linear equations the solution scheme adopted was the Newton-Raphson iteration which is the most frequently used iterative method. Although there are in general no full proof solution schemes for the solution of non-linear partial differential equations in multi-dimensions Newton's scheme which is not restricted to one dimension offers rapid convergence near a root where the derivative of the function can be evaluated efficiently and whose derivative is continuous and non-zero in the neighbourhood of a root.

To explain the method only the multi-dimensional case will be considered but frequent reference will be made to the one-dimensional case as it provides a ready base for graphical representation of the solution scheme.

Consider the case of N functions involving the variables $x_i, i = 1,2...,N$:

$$f_i(x_1,x_2,...,X_N) = 0 \qquad i = 1,2,...,N \qquad ..6.6$$

If $\boldsymbol{X}$ denotes the entire vector of values x_i, then, in the neighbourhood of $\boldsymbol{X}$, each of the functions f_i can be expanded in Taylor series

$$f_i(X + \delta X) = f_i(X) + \sum_{j=1}^{N} \frac{\partial f_i}{\partial x_j}\delta x_j + O(\delta x^2) \qquad ..6.7$$

By neglecting the terms of order δX^2 a set of linear equations is obtained for the corrections δX that move each function closer to zero simultaneously.

This can be represented in the following matrix form

$$\sum_{j=1}^{N} \alpha_{ij}\delta x_j = \beta_i \qquad ..6.8$$

where

$$\alpha_{ij} \equiv \frac{\partial f_i}{\partial x_j} \qquad \beta_i \equiv -f_i \qquad ..6.9$$

Having solved the above matrix equation using a LU decomposition the corrections can then be added to the previous solution vector to give a new estimate

$$X_i^{new} = x_i^{old} + \delta x_i \qquad i = 1,...,N \qquad ..6.10$$

The iterations are repeated until the solution has converged to an appropriate degree which is governed by the required accuracy of the task and the machine.

In order to explain the solution method and associated problems a function with one independent variable can be used. In this case the Taylor expansion of 6.7 reduces to

$$f(x + \delta x) \approx f(x) + \frac{\partial f}{\partial x}\delta x \qquad ..6.11$$

The solution proceeds by first calculating the error at x_1 (x at increment 1) and $f'(x_1)$ normally referred to as the tangent stiffness in solid mechanics, and calculating δx_1, the first approximation from the equation

$$\delta x_1 = -\frac{f(x_1)}{f'(x_1)} \qquad ..6.12$$

This is repeated as shown graphically in figure 6.1 until the error is acceptably small. If the first guess of the solution is grossly inaccurate the Newton-Raphson Method can give meaningless results. If the trial values are near a local extremum then the method will send the solution off to infinity as can be seen in figure 6.3. Another common problem is non convergent cycles, as shown in figure 6.2, where the iterative values never converge but oscillate around the solution.

The Newton-Raphson formula can also be applied using a numerical in the place of an analytic derivative.

$$f'(x) \approx \frac{f(x + dx) - f(x)}{dx} \qquad ..6.13$$

This was applied to the composite beam-column problem as finding an analytic differential solutions would have been restrictive, as some of the constitutive models were not smooth functions, and probably impossible when considering the multi-dimensional nature of the problem. The disadvantages of using numerical derivatives are :

1. If the value of dx is taken too small then the value of f'(x) will be affected by roundoff, but if too large then the order of convergence will only be linear.

2. The value of the function is calculated twice instead of the once as occurs with the analytic method.

Where the scheme is operating in zones where the changes in gradient are large (ie close to the failure load of a structure) then iterations tend to be slow. A lack of convergence usually denotes failure of the structure under the applied load. This problem may be overcome by stepping the load level up gradually, until close to the

point of failure, and observing the solution values.

6.3.3 Newmark's Method

This method was described by Newmark (1942) and is a form of double integration which can applied in calculating the buckling loads of struts with non-linear material properties.

The first step is to generate the moment-curvature relationship of the element for a beam/column which can then be solved by applying Newmark's Method to obtain a value for the critical load of the section.

Consider the strut shown in figure 6.4. The equations for a strut under an axial load, P, and moment, M_0 + Pw can be written

$$P = \int_0^d \sigma(\epsilon_b - \psi h)b(h - r_0)dh \qquad ..6.14$$

$$M_0 + Pw = \int_0^d \sigma(\epsilon_b - \psi h)b(h - r_0)(h - r_0)dh \qquad ..6.15$$

with two independent variables ε_b, the strain at the base of the section and ψ, the curvature, which remains constant over the depth, d. In situations where only first-order loading is considered then for known values of axial load and bending moment a Newton-Raphson Iteration can be performed on equations 6.14 and 6.15 directly, to obtain a solution. When the second-order moment, Pw, is significant then the solution is more complicated as the moment at each section is dependant on the curvature. In order to overcome this problem Newmark's method can be applied.

The strut is divided into a specified number of sections with an initial displacement w_0 and corresponding curvature ψ_0, Newmark's method is then applied to obtain a solution as follows;

1. An estimate is made of the total displacement ω

2. This estimate of the total displacement implies a bending moment $P\omega$ which in turn implies a change of curvature ψ calculated by the Newton-Raphson technique from equations 6.14 and 6.15.

3. The total curvature is then calculated by adding this change to the initial curvature, ψ_o.

4. The total curvature is then integrated twice by the FDM with appropriate boundary conditions for a new estimate of the displacement at each section.

5. Steps 2-4 are repeated until the values of displacement and curvature at each section are sufficiently accurate.

The integration can be carried out by any standard method but in this case the LU decomposition was chosen with a standard FDM as the most efficient way of integrating the equations. Where a distributed load or series of point loads are included then these are easily handled by adding the resultant moments on to the buckling moment Pw produced in the section. The omission of an initial displacement at the sections leads to solutions which 'blow up' where the load is greater than the critical buckling load and converge to zero where the load is less than this value.

This method is extremely useful in situations where a direct solution by the FDM is not possible as is the case for non-linear material properties.

6.4 Non-Linear Theory

In the analysis that follows a double skin composite wall/column with non-linear material properties is analyzed, including the effect of partial interaction at the upper and lower steel/concrete interfaces together with the second-order P-Δ effect. A

numerical analysis using previously discussed numerical techniques is implemented using a one-dimensional finite difference approximation.

The following assumptions have been made in the analysis:

a) The load is applied at the centroid of the concrete or steel layers.

b) The load-slip relationship at the steel-concrete interface has a non-linear relationship.

c) Shear deformations across the element are assumed negligible. As the greatest proportion of the applied load is normally axial this approximation should not have a significant effect.

d) The curvatures of the concrete and steel sections are assumed equal in each of the three layers. The effect of local buckling as a result is not reflected explicitly in the solution.

e) The internal reinforcement is assumed to have full bond with the concrete section.

From Figure 6.5 and considering overall equilibrium of the section

$$M + P\omega = M_1 + M_2 + M_3 + M_r + N_3(r_3 - r_2) + N_1(r_1 - r_2) \quad ..6.16$$

$$P = N_1 + N_2 + N_3 + N_r \quad ..6.17$$

The contribution from the bar reinforcement internally located inside the concrete is included separately from the M_2 and N_2 terms for the moment and force respectively. From assumption c) the strain at any point in the concrete and internal reinforcement can be written as a function of the strain at the lower edge, the curvature and the distance from the lower edge, h.

$$\epsilon_2 = \epsilon_b - \psi h \quad where \quad \psi = \frac{\partial^2 \omega}{\partial x^2} \qquad ..6.18$$

Similarly by including interface slip, the strains in the external layers can be similarly expressed

$$\epsilon_3 = \epsilon_b - \psi h + \Delta \epsilon_2 \qquad ..6.19$$

$$\epsilon_1 = \epsilon_b - \psi h + \Delta \epsilon_1 \qquad ..6.20$$

The forces and moments can now be expressed as functions of ϵ_b, ψ, $\Delta\epsilon_1$, and $\Delta\epsilon_2$.

$$N_2 = \int_0^{d_2} \sigma_2(\epsilon_b - \psi h) b(h) dh \qquad ..6.21$$

$$N_r = \sum_{i=1}^{i=n_r} A_r^i \sigma_r(\epsilon_b - \psi h_i) \qquad ..6.22$$

$$N_3 = \int_0^{d_3} \sigma_1(\epsilon_b - \psi h + \Delta \epsilon_2) b(h) dh \qquad ..6.23$$

$$N_1 = \int_0^{d_1} \sigma_1(\epsilon_b - \psi h + \Delta \epsilon_1) b(h) dh \qquad ..6.24$$

$$M_2 = \int_0^{d_2} (h - r_2) \sigma_2(\epsilon_b - \psi h) b(h) dh \qquad ..6.25$$

$$M_3 = \int_0^{d_3} (h - r_3)\sigma_1(\epsilon_b - \psi h - \Delta\epsilon_2) b(h)\,dh \qquad ..6.26$$

$$M_1 = \int_0^{d_1} (h - r_1)\sigma_1(\epsilon_b - \psi h + \Delta\epsilon_1) b(h)\,dh \qquad ..6.27$$

$$M_r = \sum_{i=1}^{i=n_r} h_i A_r^i \sigma_r(\epsilon_b - \psi h_i) \qquad ..6.28$$

Substituting equations 6.21-6.28 into 6.16 and 6.17 gives

$$\begin{aligned} M + P\omega = {} & \int_0^{d_2} (h - r_2)\sigma_2(\epsilon_b - \psi h) b(h)dh + \sum_{i=1}^{i=n_r} h_i A_r^i \sigma_r(\epsilon_b - \psi h_i) \\ & + \int_0^{d_3} (h - r_3)\,\sigma_1(\epsilon_b - \psi h + \Delta\epsilon_2) b(h)dh \\ & + \int_0^{d_1} (h - r_1)\,\sigma_1(\epsilon_b - \psi h + \Delta\epsilon_1) b(h)dh \\ & + (r_3 - r_2)\int_0^{d_3} \sigma_1(\epsilon_b - \psi h + \Delta\epsilon_2) b(h)dh \\ & + (r_1 - r_2)\int_0^{d_1} \sigma_1(\epsilon_b - \psi h + \Delta\epsilon_1) b(h)dh \end{aligned} \qquad ..6.29$$

$$\begin{aligned} P = {} & \int_0^{d_2} \sigma_2(\epsilon_b - \psi h) b(h)dh + \sum_{i=1}^{i=n_r} A_r^i \sigma_r(\epsilon_b - \psi h_i) \\ & + \int_0^{d_3} \sigma_1(\epsilon_b - \psi h + \Delta\epsilon_2) b(h)\,dh \\ & + \int_0^{d_1} \sigma_1(\epsilon_b - \psi h + \Delta\epsilon_1) b(h)\,dh \end{aligned} \qquad ..6.30$$

At the upper interface the rate of change in force can be expressed in terms of a stress/slip relationship $\sigma_i(\Delta u_2)$

$$\frac{\partial N_3}{\partial x} = -b\,\sigma_i(\Delta u_2) \qquad ..6.31$$

where b is the breadth of the interface between the steel and concrete. The strain discontinuity is associated with the rate of change of the slip

$$\frac{\partial \Delta u_2}{\partial x} = -\Delta \epsilon_2 \qquad ..6.32$$

Similar expressions exist for the lower steel/concrete interface

$$\frac{\partial N_1}{\partial x} = -b\,\sigma_i(\Delta u_1) \qquad ..6.33$$

$$\frac{\partial \Delta u_1}{\partial x} = -\Delta \epsilon_1 \qquad ..6.34$$

At this stage 4 equations of equilibrium including compatibility (6.29, 6.30, 6.31 and 6.33) have been produced with 4 unknowns that require solving. Without the inclusion of the P-Δ effect and assuming linear material relationships then these equations are solvable by analytic methods. Including the P-Δ effect would produce solutions equivalent to those obtained in chapter 5 but would still not account for non-linear material behaviour. In general these equations must be solved numerically if the material non-linearities are to be included.

6.5 Numerical Analysis

To solve these non-linear differential equations which control the response of the structure involves applying the finite-difference method with the other previously discussed solution schemes - LU decomposition, Newton Raphson method, Newmark's Method.

The first step is to divide the column/wall into a series of n grid points equally spaced along the length in order to implement the finite difference method (see figure 6.8). It should be pointed out that there are no nodes at the ends of the column although the values at these points are sometimes required for the boundary conditions. Where these points are referred to the subscripts 0 or n+1 are used.

At each node there are four equations (6.29, 6.30, 6.31, and 6.33) and four unknowns (ε_b,Δu_1, Δu_2 and Ψ). To solve for these variables the solution is divided into two parts.

In the inner loop the interface displacements Δu_1 and Δu_2 are held constant with only the curvature ψ and the lower concrete strain ε_b free. This leaves only Equations 6.29 and 6.30 at each node which can be simplified and integrated using a form of Simpson's Rule (the extended midpoint rule). At each section the three layers are divided into a number of sublayers each having a unique width Δb_i, depth Δh_i and position above the concrete base h_i (see figure 6.9). The integral over the depths of the sections can therefore be replaced by these approximate summations over the cross-section as a whole. . This numerical integration is better at coping with discontinuities in the stress functions - ie moving from compression to tension in the concrete - although there is some loss in accuracy depending on the amount of discretisation. This gives

$$M + Pw = \sum_{i=1}^{i=n_2} (h_i - r_2)\sigma_2(\epsilon_b - \psi h_i)\Delta b_i \Delta h_i + \sum_{i=1}^{i=n_r} h_r A_r' \sigma_r(\epsilon_b - \psi h_i)$$
$$+ \sum_{i=1}^{i=n_3} (h_i - r_2)\sigma_1(\epsilon_b - \psi h_i + \Delta\epsilon_2)\Delta b_i \Delta h_i \qquad ..6.35$$
$$+ \sum_{i=1}^{i=n_1} (h_i - r_2)\sigma_1(\epsilon_b - \psi h_i + \Delta\epsilon_1)\Delta b_i \Delta h_i$$

and

$$P = \sum_{i=1}^{i=n_2} \sigma_2(\epsilon_b - \psi h_i)\Delta b_i \Delta h_i + \sum_{i=1}^{i=n_r} A_r^i \sigma_r(\epsilon_b - \psi h_i)$$

$$+ \sum_{i=1}^{i=n_3} \sigma_1(\epsilon_b - \psi h_i + \Delta\epsilon_2)\Delta b_i \Delta h_i \qquad ..6.36$$

$$+ \sum_{i=1}^{i=n_1} \sigma_1(\epsilon_b - \psi h_i + \Delta\epsilon_1)\Delta b_i \Delta h_i$$

Before carrying out the Newmark iteration an initial displacement of the form

$$\omega_o = A_o \sin\frac{\Pi x}{L} \qquad ..6.37$$

with the corresponding curvature

$$\psi_o = \frac{\partial^2 \omega_o}{\partial x^2} = -\frac{\Pi^2}{L^2} A_o \sin\frac{\Pi x}{L} \qquad ..6.38$$

is calculated for each node to prevent numerical difficulties in case where there is no applied lateral load acting to produce a deflection. During the Newmark integration equations 6.35 and 6.36 are solved using a two-dimensional Newton-Raphson technique for ε_b and ψ at each node. The curvature at each node is represented by the finite difference approximation

$$\psi_i \approx \frac{\omega_{i+1} - 2\omega_i + \omega_{i-1}}{\Delta x^2} \qquad ..6.39$$

By knowing the curvature ψ, the values of deflection ω can be calculated at each stage in the integration with respect to the boundary conditions which, for simple supports are $\omega_o = 0$ and $\omega_{n+1} = 0$. The matrix produced can be easily solved by using

the LU decomposition previously mentioned as only back-substitutions are required after the initial forward reduction.

To include the effect of variations in the interface slip a further iteration is performed which has the previous Newmark scheme nested in the loop. The outer loop releases Δu_1 and Δu_2 and uses equations 6.31 and 6.33 in a multi-dimensional Newton-Raphson scheme until convergence is achieved. The equations solved are of the form

$$\sum_{j=1}^{2n} \alpha_{ij}\delta u_i = \beta_i$$

$$\text{where} \quad \alpha_{ij} \equiv \frac{\partial}{\partial u_j}\left[\frac{\partial N_i}{\partial x} + b\sigma_i(\Delta u)\right] \qquad ..6.40$$

$$\beta_i \equiv -\left[\frac{\partial N_i}{\partial x} + b\sigma_i(\Delta u)\right]$$

The main problem in the outer loop is determining the slip strain distribution at the ends of the column at nodes 1 and n from equations 6.32 and 6.34. The value of Δu_o and Δu_{n+1} are unknown but if the steel and concrete end loads are known the interface strains can be calculated from

$$-\Delta\epsilon_1 \approx \frac{\Delta u_2 - \Delta u_0}{2\Delta x} = \frac{\Delta u_2 - \Delta u_1}{2\Delta x} + \frac{\Delta u_1 - \Delta u_0}{2\Delta x}$$

$$= \frac{\Delta u_2 - \Delta u_1}{2\Delta x} + \frac{-\Delta\epsilon_0 + -\Delta\epsilon_1}{4} \qquad ..6.41a$$

$$= \frac{2}{3}\frac{\Delta u_2 - \Delta u_1}{\Delta x} - \frac{\Delta\epsilon_0}{3}$$

The ability to determine the value of $\Delta\epsilon_o$ at each interface allows different amounts of load to be carried on each layer. The end loads on each of the three layers are known, therefore the value of $\Delta\epsilon_o$ at each interface can be found by subtracting the strain in the concrete from the upper and lower steel strains.

6.6 One-Dimensional Material and Interface Models

6.6.1 Introduction

Before a solution to the non-linear equations is formed the stress-strain relationships in the steel and concrete sections and the load-slip relationship at the top and bottom interfaces must be chosen. It was decided to incorporate linear relationships in the equations to allow comparison with exact solutions and also non-linear models more suited to modelling experiments.

6.6.2 Concrete Models

In the present form it is possible to include any material relationship where a 1 to 1 relationship exists between stress and strain ie. the material behaviour is not dependent on the loading history. The behaviour of the concrete can either represented by a simple linear model where

$$\sigma_c = E_c \epsilon \qquad ..6.41b$$

or by a more complicated non-linear model such as that proposed by Basu and Sommerville (1969) (see figure 6.6).

$$\sigma_c = f_{ck}\left[2.41\left(\frac{\epsilon}{\epsilon_u}\right) - 1.865\left(\frac{\epsilon}{\epsilon_u}\right)^2 + 0.5\left(\frac{\epsilon}{\epsilon_u}\right)^3 - 0.045\left(\frac{\epsilon}{\epsilon_u}\right)^4\right]$$

where f_{ck} is the ultimate concrete stress, ϵ the concrete strain and ϵ_u the strain at the ultimate stress. The ϵ_u was taken as 0.002 with an ultimate strain of 0.0035. The effect of concrete tensile strength was assumed to be negligible.

In the analysis of experimental results from the composite walls, the Basu and Sommerville model was applied whereas to validate the numerical analysis the linear material model based on Equation 6.41b was compared with the analytic results of chapter 5.

6.6.3 Steel Models

The steel behaviour may be represented by a linear model

$$\sigma_s = E_s \epsilon$$

and by a stepped linear model made up from straight lines as shown in figure 6.7. A slight gradient is accomodated after yield to prevent numerical instabilities developing when stepping out the soltuion. To include the effects of local buckling of the outer skins the steel areas can be reduced to effective areas dependent on the geometry and thickness of the plate.

6.6.4 Interface Shear

6.6.4.1 Review

The initial interface model proposed by Newmark et al (1951) was necessarily linear in order that an analytic solution be obtained. With the development of computers non-linear interface models such as that proposed by Yam and Chapman (1971) were possible which gave more accurate predictions of the behaviour at ultimate conditions. This model and another non-linear relationship proposed by Ansourian and Roderick (1978) have been discussed in chapter 5.2. Hirst and Yeo (1978) proposed a linear interface model based on simple beam theory with

$$K \equiv \frac{E}{2\left[\frac{2.4h(1+\mu)}{bt} + \frac{h^3}{tb^3}\right]}$$

where k is the interface stiffness, h, the height, b, the breadth and t, the width of the connecting element. Within the range of design loads this linear assumption was assumed valid and was justified by a comparison with a non-linear analysis.

It should be noted that previous authors (Newmark, Yam and Chapman, Hirst and Yeo) have primarily considered only interface connections with shear studs or other ductile connectors. Studs possess a ductile behaviour which is relatively easy to model in comparison with the sometimes brittle behaviour of composite slabs with profiled steel sheeting.

Experiments similar to stud push-out tests have been carried out on various profiled

steel sheets by Daniels (1988) who investigated the load-slip behaviour and ultimate perfomance. Daniels used three critical load levels to define the behaviour of the sheeting. These were

- average load at which slip was first recorded (P_s)
- maximum load recored (P_{max})
- maximum load after slip on both sides (P_f)

Daniels noted that the applied shear at which slip occured was highly variable, even between the sides of the same test, because of the nature of the chemical bond.
The tests showed two types of behaviour present, ductile and brittle. Ductile behaviour occurred where the embossments provided a greater resistance than the chemical bond between the steel and the concrete Brittle behaviour occurred when the chemical bond was stronger than the embossement strength.

The tests on Cofastra 40/0.75 with a similar geometry to the Superholorib profile, used in the composite wall tests, gave an average load-slip plot as shown in figure 6.10. The behaviour is ductile with an initial strength from the chemical bond followed by, under larger slips, strong ductile resistance provided by the embossements.

In the current work three interface models have been incorporated allowing a variety of walls, beams and columns with different interface conditions to be analysed.

6.6.4.2 Linear Interface Model

The interface behaviour between the steel and concrete may be represented by a linear model

$$\sigma_i = k\Delta u$$

where k is the interface stiffness (N/mm^3). This model was only applied for numerical accuracy comparisons with exact solutions.

6.6.4.3 Non-linear Interface Model

For a more accurate representation of shear stud behaviour the non-linear model proposed by Yam and Chapman may be used (see section 5.2). This model allows the plastic behaviour of the studs to be taken into account once yielding has occurred.

6.6.4.4 Profile Interface Model

In order to take account of the complicated response occuring with the Superholorib profile in the composite wall experiments, a model based on the pull-out test results carried out by Daniels (1988) was devised. The model proposed, shown in figure 6.11, consists of 4 straight line sections with an initially high peak obtained from the brittle chemical bond followed by a slight decline and then a steady rise as the ductile bond from the embossements is mobilised.

Although this model is likely to be only an approximation of the Superholorib behaviour it should allow a better understanding of the nature of the interface to be devloped.

6.7 Program DSCW

The numerical analysis carried was incorporated in a computer program written in Turbo Pascal [(c)] called DSCW.

Difficulties encountered during the writing of the code were primarily caused by convergence of the numerical routines to the required accuracy at each iteration. In situations where the numerical derivatives were calculated with too small a value of increment, problems occurred with machine accuracy.

6.8 Program Validation

In order to verify the performance of the DSCW program 4 separate comparisons were made:

1. Convergence to the analytic Newmark solution for Linear Case.

2. Convergence to Euler Buckling Equation for Linear fully composite condition.

3. Convergence to Euler-type Buckling Solution based on linear equation of Chapter 5.

4. Convergence to axial strains and slips based on linear equations of Chapter

5.

6.8.1 Convergence to Newmark Solution

To verify the correct solution under a uniformly distributed load a comparison was made with the theoretical solution derived by Newmark *et al* (1952). The composite beam analyzed had an a upper cross-section 1000mm wide x 100mm deep and a lower layer of 1000mm wide by 1mm deep. The beam was 10m in length with the material properties of E_t=20kN/mm^2 and E_b=200kN/mm^2 for the upper and lower layers respectively and k=10,000N/mm^2 at the interface. The length was divided into 12 and 24 elements with the upper layer into 20 and 50 sections to investigate the speed of convergence. A central point load of 1000N was applied for all cases.

The results given in table 6.1 show that the code converges towards the exact Newmark solution as the number of elements increases from 12 to 24. The advantage in going from 20 sections to 50 sections in the top layer would appear to be negligible in comparison with the disadvantage of a 20% increase in computational time.

Perhaps the most interesting feature is the variation in accuracy from the end of the beam towards the centre. As the exact solution results in a zero value at the centre, any computation will produce an infinite error at this point unless a central boundary condition is used. This has the effect of reducing the accuracy substantially in the neighbourhood of the centre although increasing the number of elements reduces the

effect of this problem.

6.8.2 Convergence to Euler Buckling Solution

The previous example showed the convergence of the finite difference solution to the exact solution for a composite beam but did not investigate the performance of the Newmark's Method for obtaining the Critical buckling load of a column.

To investigate the behaviour of the code in obtaining critical buckling loads a fully composite 10m column was considered with cross-section 1000m wide x 100mm deep and E=200kN/mm^2. Although the critical value of the column can be calculated using the Euler Buckling Equation this is not convenient as the displacements 'blow up' close to this value. It is easier to apply an initial curvature to the column and examine the resulting displacements with increasing load. For the linear elastic condition the displacements are given by

$$\omega = \frac{a_1}{\left[1 - \left(\frac{P}{P_{crit}}\right)\right]} \sin\frac{\pi x}{L} \qquad ..6.42$$

where a_1 is the amplitude of the initial displacement at the midpoint of the column, P, the applied load, P_{crit}, the buckling load and L, the length of the column. The results are given in table 6.2 for increasing loads for 8 and 16 elements.

The table shows a gradual convergence to the Euler Buckling load for the column. As can be seen from the results the accuracy increases, as expected, as the number of elements is increased. Unfortunately as the load is increased the errors increase because of the greater curvatures produced at higher loads. This suggests that some care may be necessary when interpreting results where large displacements have occurred.

6.8.3 Convergence to Theoretical Solution of Chapter 5

In order to check the performance of the code where the effects of partial interaction

were included a 10m column with a cross-section consisting of 1mm deep x 1000mm wide top and bottom layers with a 100mm deep x 1000mm wide central layer was investigated. The Young's Modulus of the outer and central sections were 200kN/mm^2 and 20kN/mm^2 respectively with varying interface stiffnesses of 1N/mm^2, 1000N/mm^2, and 100000 N/mm^2 applied. As with the previous example an initial sinusoidal displacement was assumed with the exact solution given by equation 6.42 with P_{crit} established from eqaution 5.36.

The results given in table 6.3 show that

- as interface stiffness increases the errors resulting from the approximations reduce. ie. for a stiffness of 1N/mm^2 and a load of 20kN with 8 elements the resulting error was 7.56% compared with 1.46% with a stiffness of 10,000N/mm^2.

- as the applied load is increased the errors increase because the curvature of the column is increasing. ie for a stiffness of 1N/mm^2 and a load of 20kN with 8 elements the resulting error was 7.56% compared with 10.53% under a 80kN load.

- increasing the number of elements from 8 to 16 more than doubles the accuracy of the results

6.8.4 Convergence to Theoretical Axial Strain and Slip Solutions

Setting the initial nodal displacement to zero and considering the axial strain in the steel and the concrete slip under concrete loading at the boundaries, allowed a comparison between the theoretical exact solutions produced in chapter 5 to be compared with numerical values.

The column from the previous example was considered under a 10kN point load, on the concrete end surface, with an interface stiffness of 200N/mm^2. The theoretical

values given in tables 6.4 and 6.5 below are calculated from equations 5.42 and 5.45 for the steel strains and interface slip respectively.

The convergence of the strains to the exact solution is more rapid than for the slips produced at the interfaces due to higher order of the difference expression for the slips. As expected, increasing the discretisation increases the accuracy of the results obtained. The equations tend to overestimate the slips occurring in the composite walls/columns.

The output file for the 8 element analysis is given in Appendix A. It should be noted that the slips and strains stated in part 4 were taken as the average of the upper and the lower slips and strains.

6.9 Summary

A materially non-linear model including a global P-Δ effect has been developed capable of modelling combined axial and bending moments. The finite difference method was implemented to solve the resulting equations.

Convergence has been shown for numerical linear steel and concrete material models and compared with the analytic solutions of chapter 5.

In the next chapter the theoretical and numerical solutions produced will be compared with experimental results from composite walls and columns.

Table 6.1 Convergence to Newmark Solution - Slip

Distance from LHS (mm)	Newmark Slip (mm)	12 Elements 20 Layers (mm)	Error (%)	12 Elements 50 Layers (mm)	Error (%)	24 Element 20 Layers (mm)	Error (%)
833.33	2.6869e-2	2.6883e-2	0.05	2.6841e-2	-0.10	2.6871e-2	0.01
1666.66	2.5895e-2	2.5657e-2	-0.92	2.5616e-2	-1.08	2.5856e-2	-0.15
2500	2.38699e-2	2.4171e-2	1.27	2.4133e-2	1.11	2.3789e-2	-0.34
3333.33	2.00368e-2	1.9527e-2	-2.54	1.9495e-2	-2.70	1.9922e-2	-0.57
4166.67	1.29622e-2	1.4808e-2	14.24	1.4782e-2	14.04	1.2848e-2	-0.88
5000	0	2.012e-21	infinity	-	infinity	-	infinity

Table 6.2 Convergence to Euler Buckling Load - Dispalcement

Applied Load (kN)	Theoretical Central Defl. (mm)	8 elements Central Defl. (mm)	Error (%)	16 elements Central Defl. (mm)	Error (%)
2.0e4	6.8305e-2	6.9406e-2	1.61	6.865e-2	0.51
4.0e4	7.9278e-2	8.089e-2	2.03	7.986e-2	0.73
6.0e4	9.4452e-2	9.693e-2	2.62	9.545e-2	1.06
8.0e4	11.6809e-2	12.090e-2	3.50	11.862e-2	1.55
10.0e4	15.3033e-2	16.063e-2	4.96	15.662e-2	2.34
12.0e4	22.1823e-2	23.925e-2	7.86	23.045e-2	3.89
14.0e4	40.295e-2	46.86e-2	16.29	43.599e-2	8.20
16.0e4	216.66e-2	-	-	-	-

Table 6.3 Convergence to Buckling Solution of Chapter 5 - Displacement

\ Load \ k (N/mm2) \	20 (kN)	Error (%)	40 (kN)	Error (%)	80 (kN)	Error (%)
1 Exact	0.6803		0.7855		1.1372	
8 Element	0.6289	7.56	0.7205	8.28	1.0175	10.53
16 Element	0.6733	1.03	0.7760	1.21	1.1201	1.50
1000 Exact	0.6493		0.7075		0.8620	
8 Element	0.6589	-1.48	0.7191	-1.64	0.8804	-2.13
16 Element	0.6519	-0.38	0.7110	-0.49	0.8683	-0.73
1e5 Exact	0.6489		0.7066		0.8592	
8 Element	0.6584	-1.46	0.7182	-1.64	0.8777	-2.15
16 Element	0.6515	-0.40	0.7101	-0.50	0.8655	-0.73

Table 6.4 Convergence to Axial Strains Solution of Chapter 5

Distance from LHS (mm)	Theoretical Strain ($x10^{-6}$)	8 Elements Strain($x10^{-6}$)	Error (%)	16 Elements Strain ($x10^{-6}$)	Error (%)	32 Element Strain ($x10^{-6}$)	Error (%)
625	2.066			1.835	11.18	2.038	1.36
1250	3.107	2.394	22.95	3.008	3.19	3.079	0.90
1875	3.632			3.518	3.14	3.611	0.58
2500	3.896	3.718	4.57	3.843	1.36	3.882	0.36
3125	4.029			3.983	1.14	4.020	0.22
3750	4.094	3.958	3.32	4.070	0.59	4.088	0.15
4375	4.123			4.102	0.51	4.119	0.10
5000	4.132	4.072	1.45	4.117	0.36	4.128	0.10

Table 6.5 Convergence to Axial Slips Solution of Chapter 5

Distance from LHS (mm)	Theoretical Slip ($x10^{-5}$ mm)	8 Elements Slip ($x10^{-5}$ mm)	Error (%)	16 Elements Slip ($x10^{-5}$ mm)	Error (%)	32 Element Slip ($x10^{-5}$mm)	Error (%)
625	230.1			240.6	-4.56	235.24	-2.23
1250	116.0	148.7	-28.19	134.6	-16.03	120.11	-3.54
1875	58.46			66.79	-14.25	61.289	-4.84
2500	29.39	62.25	-111.81	37.21	-26.61	31.194	-6.14
3125	14.64			18.20	-24.32	15.722	-7.39
3750	7.019	14.16	-101.74	9.602	-36.80	7.6812	-9.43
4375	2.822			3.733	-32.28	3.0859	-9.35
5000	0	0	-	0	-	0	-

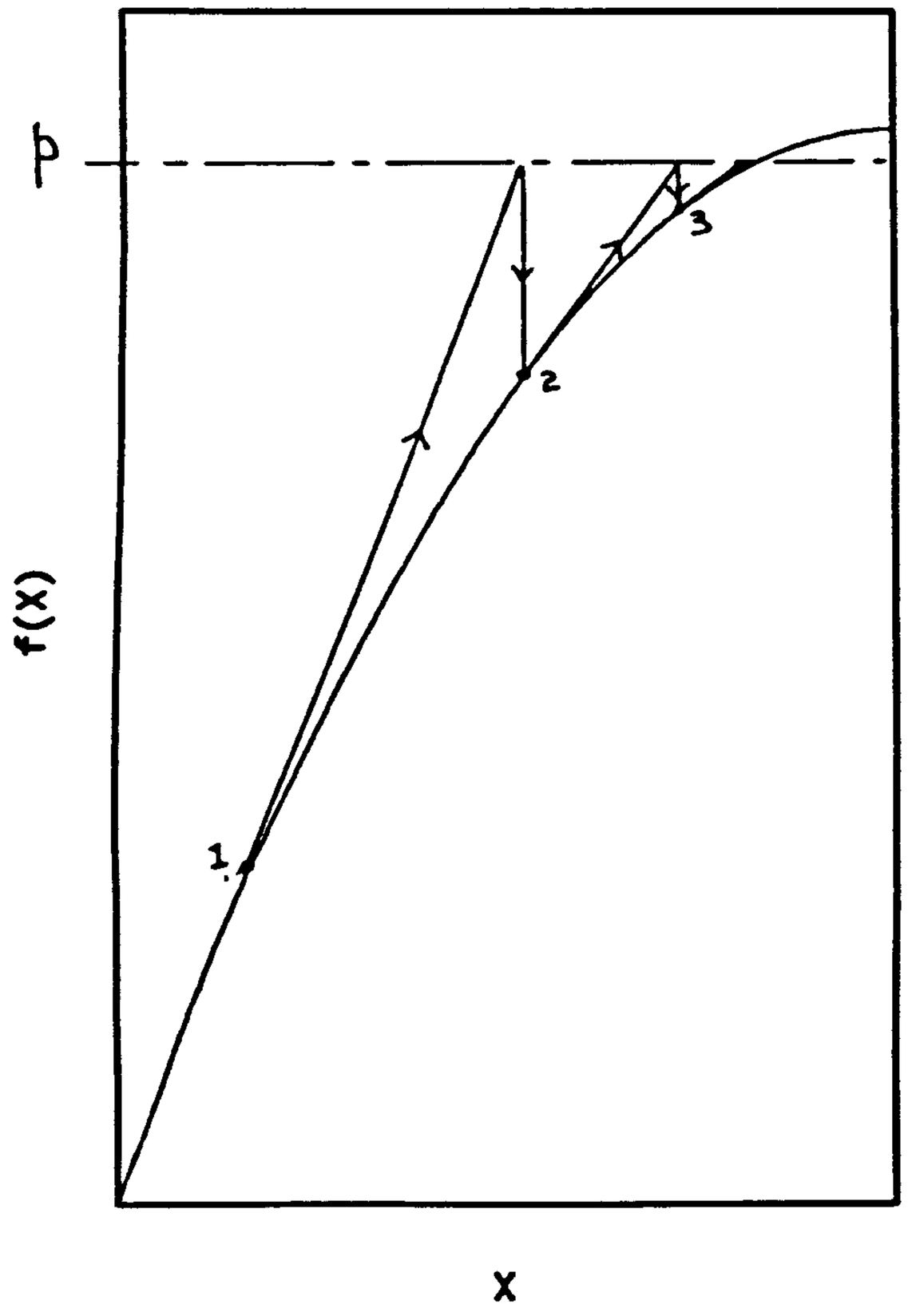

Figure 6.1 Convergent Cycles

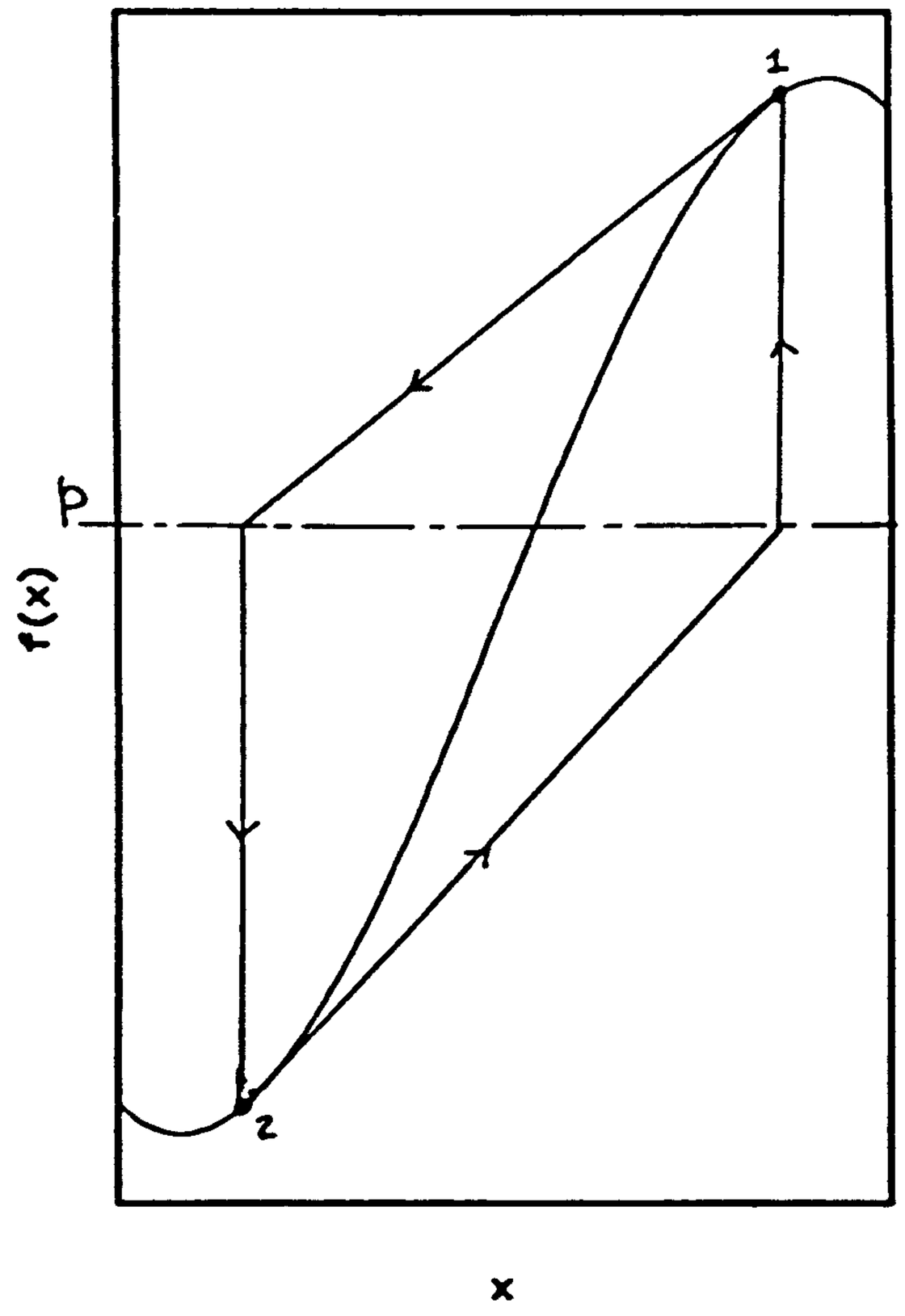

Figure 6.2 Non-Convergent Cycles

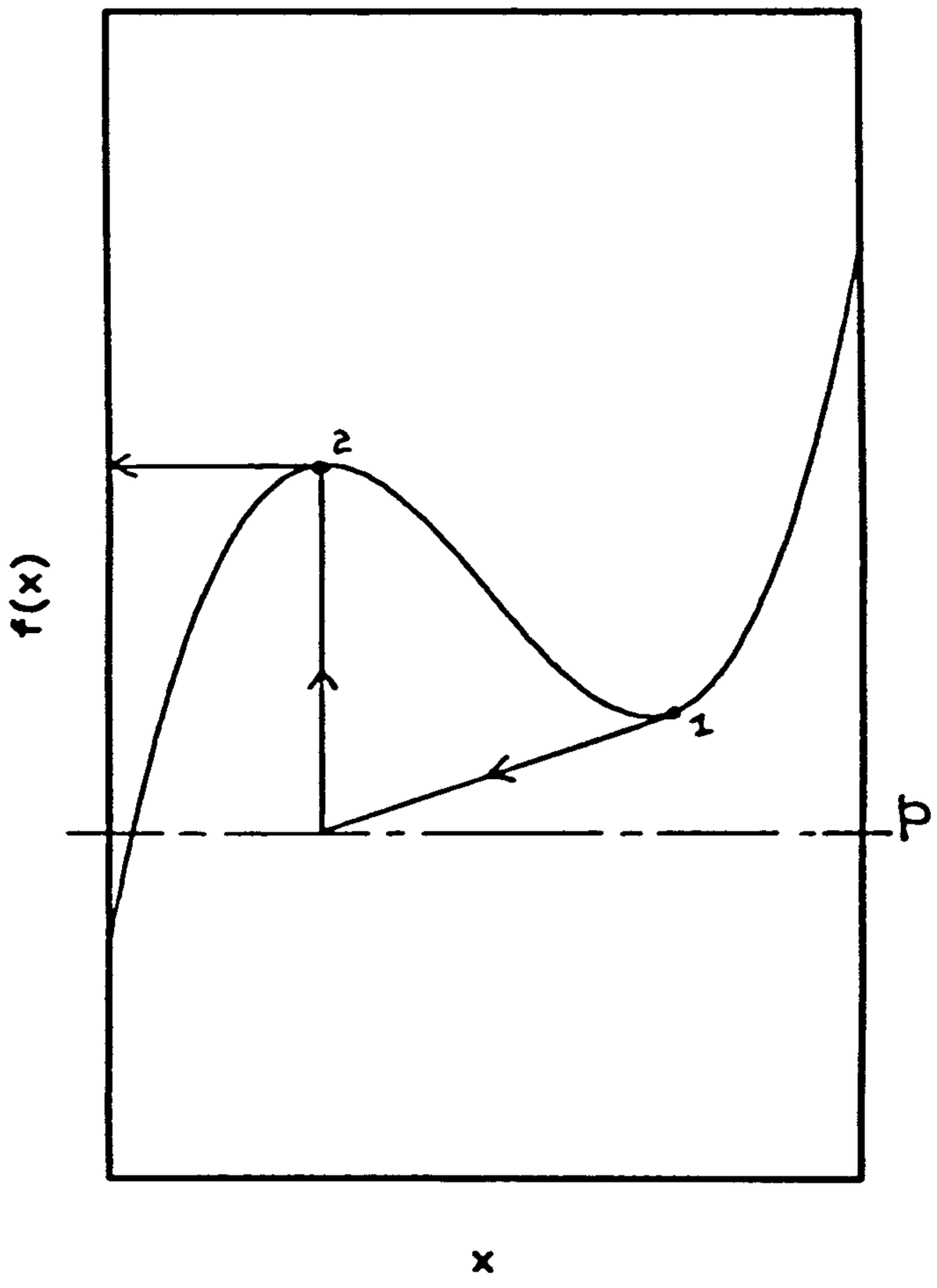

Figure 6.3 Local Extremum

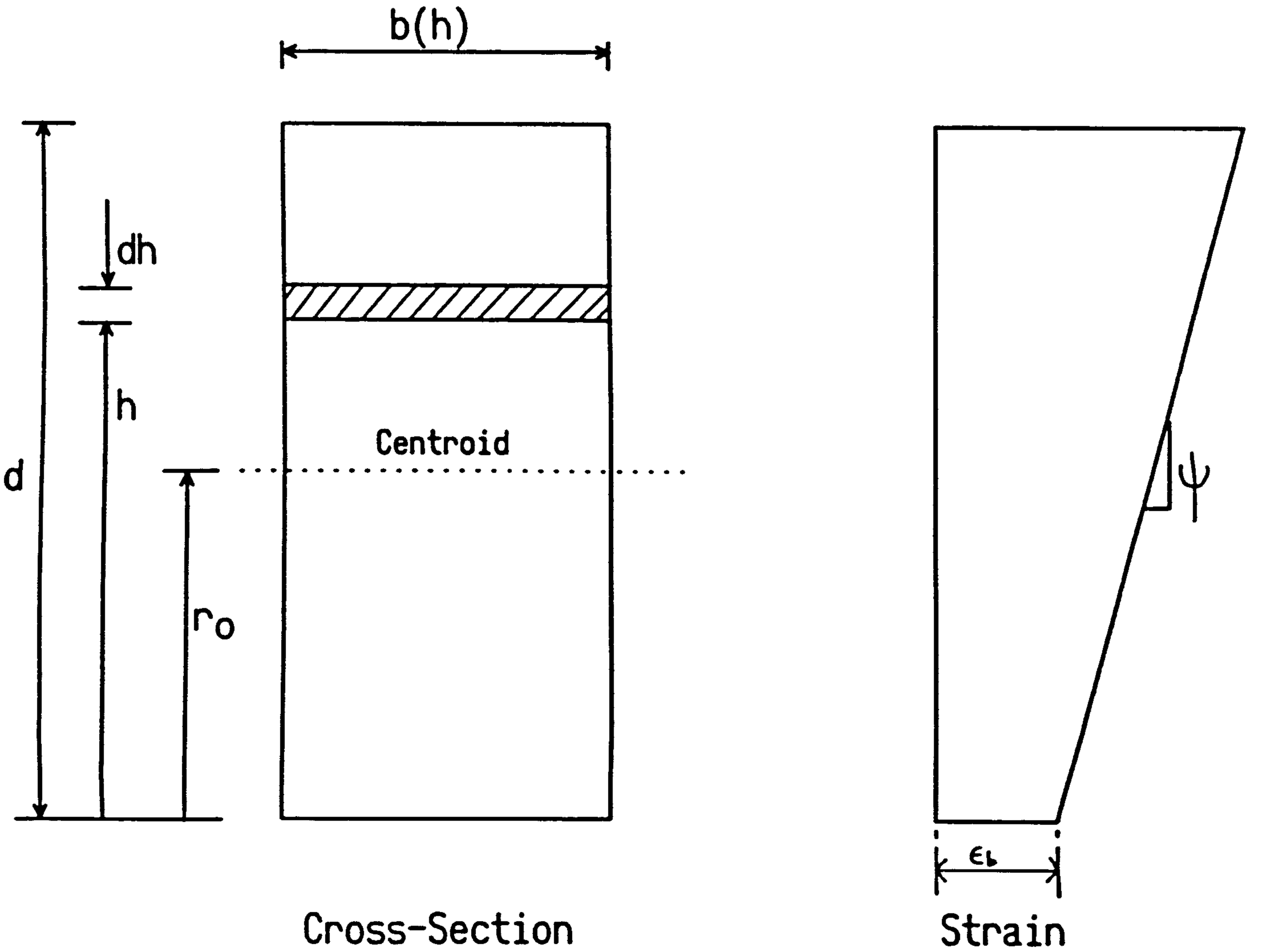

Figure 6.4

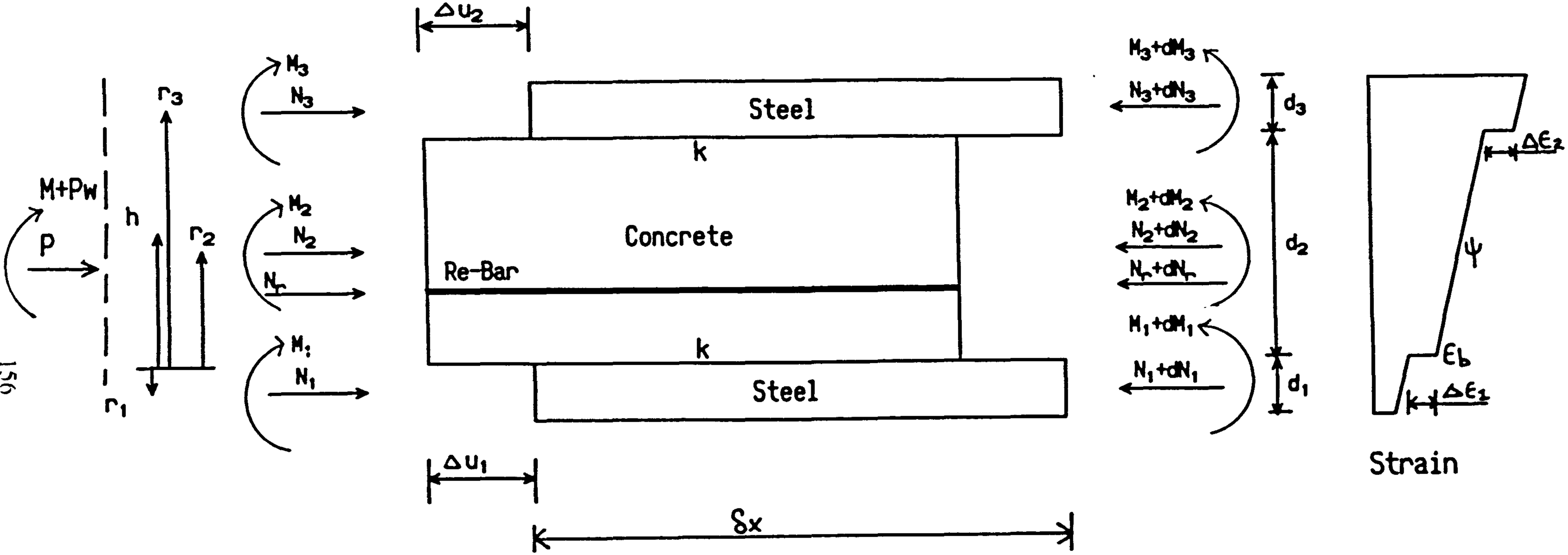

Figure 6.5 Double Skin Differential Element

Basu and Summerville
Concrete Model

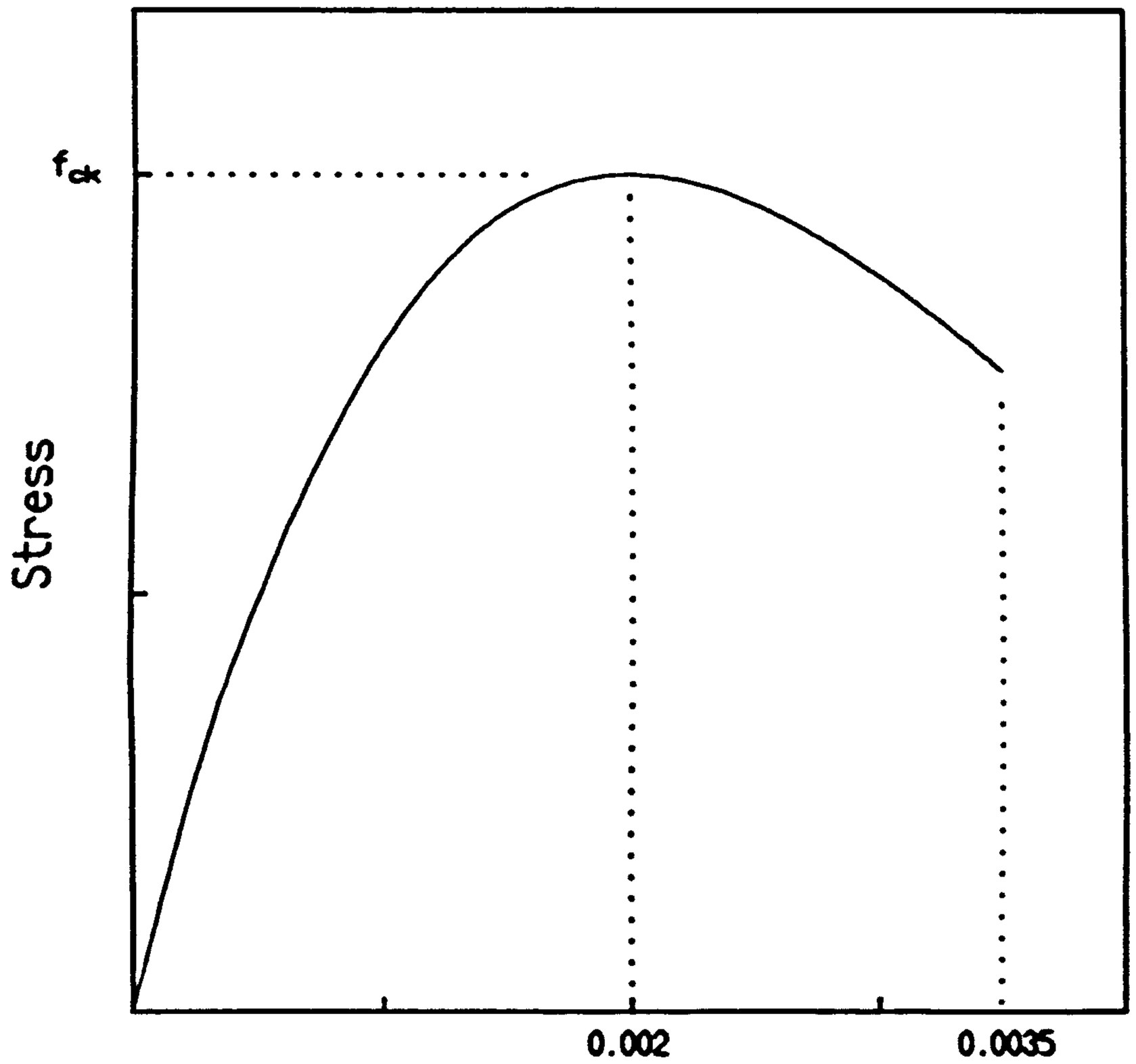

Figure 6.6

Steel Model
Stress vs Strain

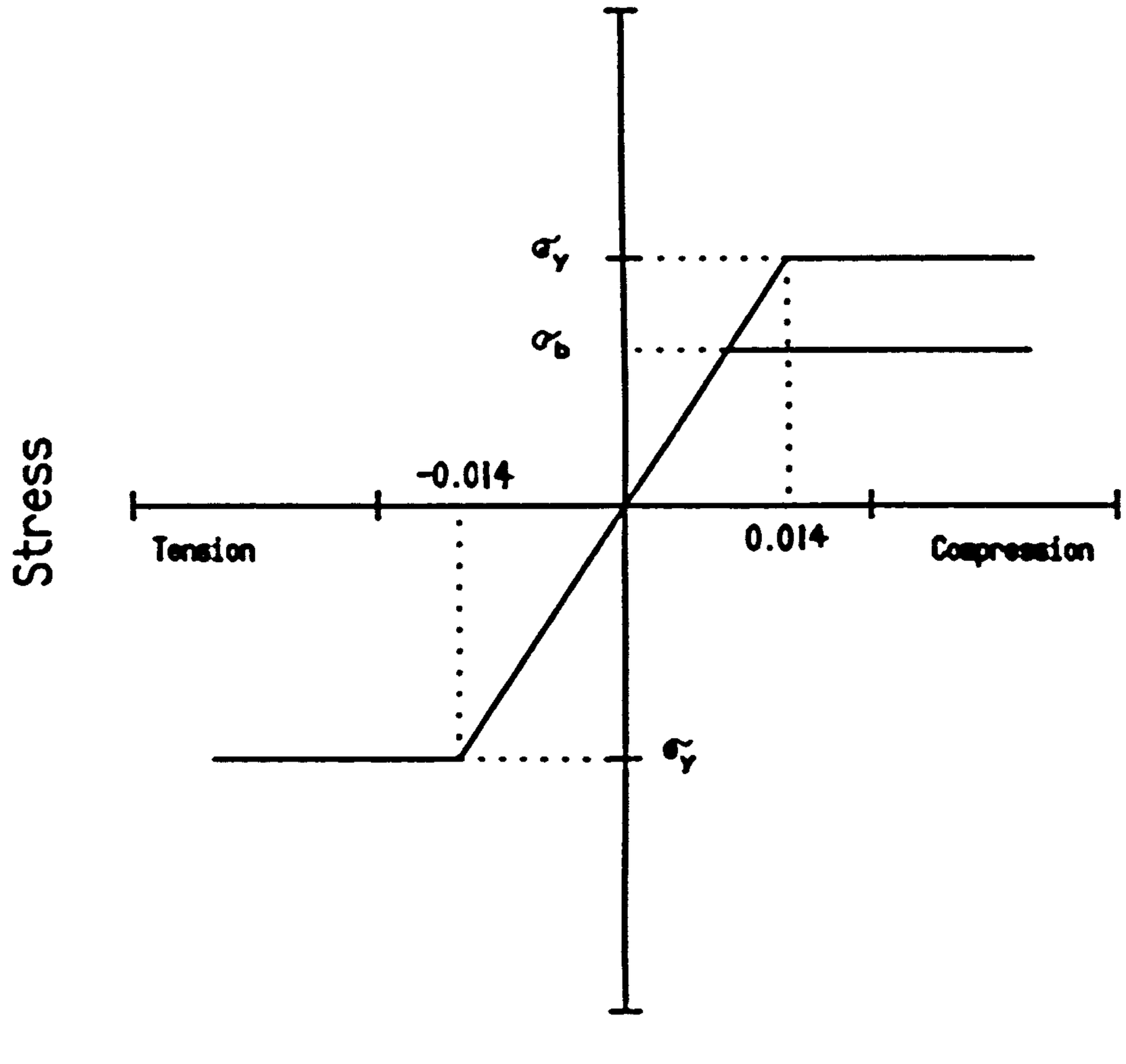

Figure 6.7

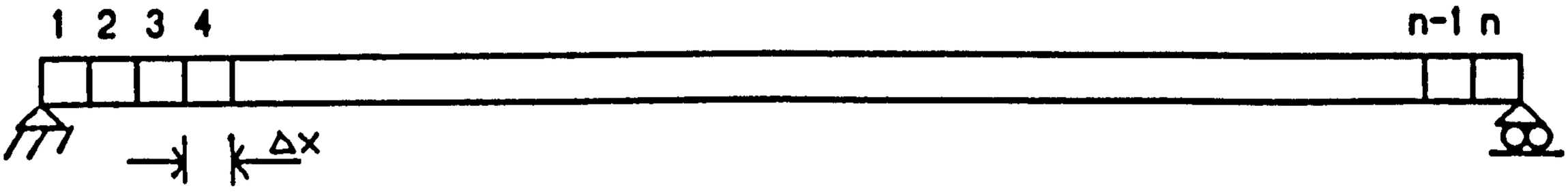

Figure 6.8 Finite Difference Grid Spacing

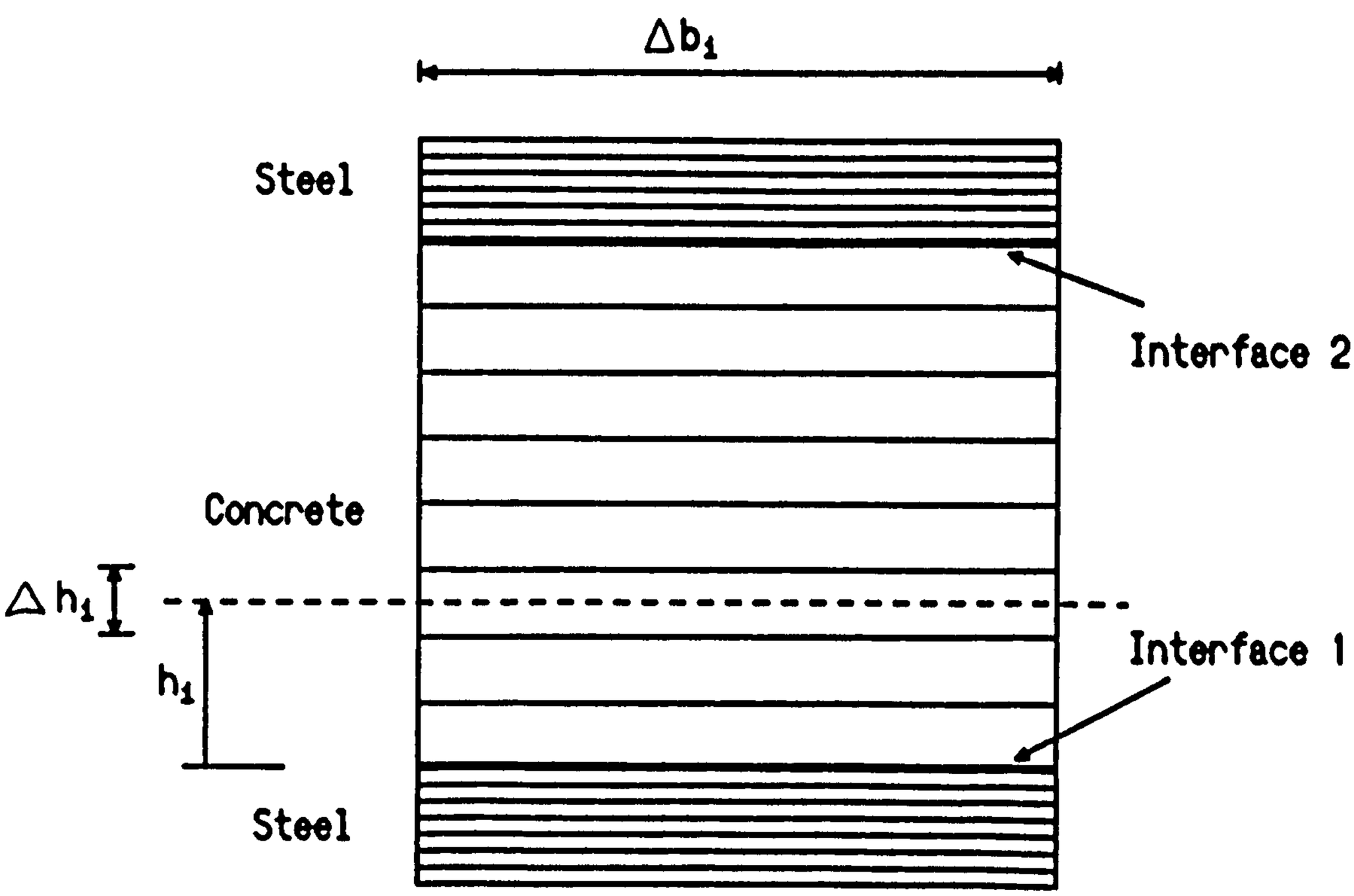

Figure 6.9 Sub-Division of Layers

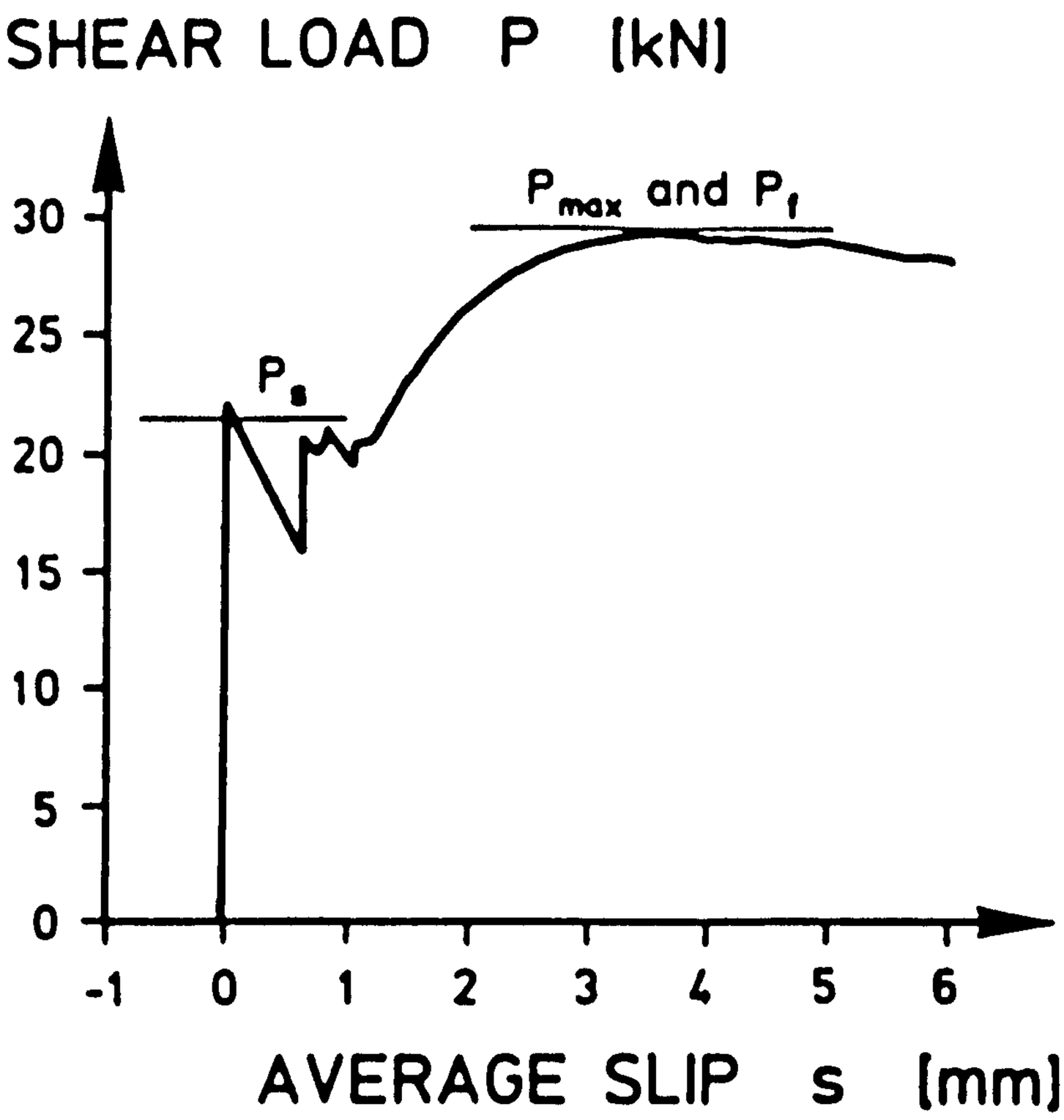

Figure 6.10 Cofrastra 40/0.75 Load-Slip (Daniels 1988)

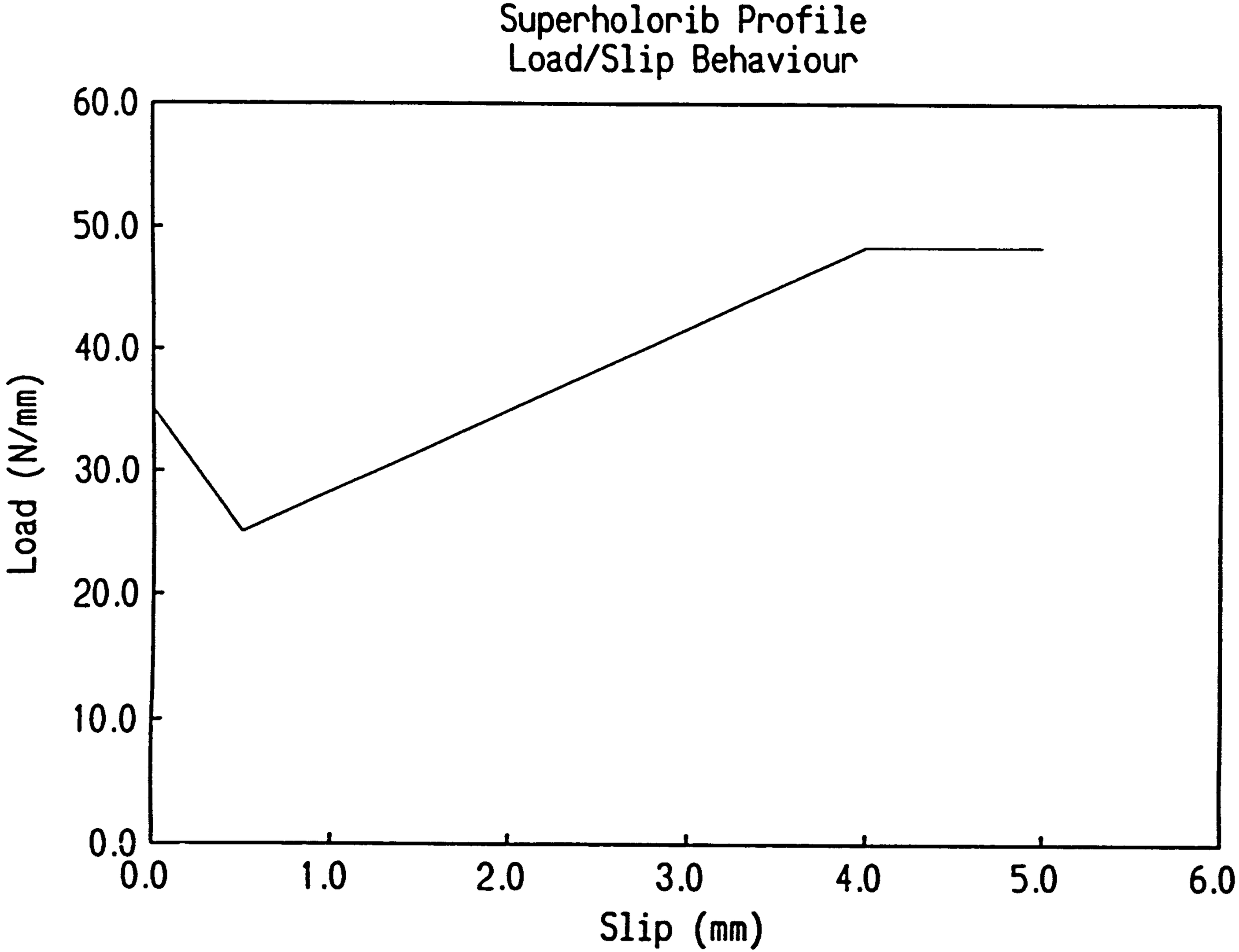
Superholorib Profile
Load/Slip Behaviour
Load (N/mm)
60.0
50.0
40.0
30.0
20.0
10.0
0.0
0.0
1.0
2.0
3.0
4.0
5.0
6.0
Slip (mm)

Figure 6.11

Chapter 7 Analytical and Numerical Analysis of Composite Elements

7.1 Introduction

The previous two chapters developed theoretical and numerical solutions to the problem of composite elements subject to axial and lateral loads. Analytic equations and computer program DSCW were developed allowing the calculation of steel and concrete strains and slips at the top and bottom interfaces under different loading arrangements.

In the following chapter the behaviour of experimental composite beams, beam/columns and walls is analyzed in order to verify the accuracy of the non-linear modelling and obtain a better understanding of the behaviour of composite elements. The analysis is performed on two series of experimental results.

The first series of experimental results examined is work carried out by Oduyemi and Wright (1988, 1989 and 1990) who performed three series of tests on double skin composite elements investigating beam, column behaviour and beam/column behaviour. Their work, previously described in section 4.2, considered the behaviour of composite elements constructed using external steel plates fixed to the concrete by shear studs.

The second series of tests analyzed are those performed in the current study on composite walls. Although the analysis is complicated, particularly in wall 2, by the brittle load-slip relationship at the steel concrete interface it should be possible to obtain a qualitative understanding of the response to axial loading by applying an interface model based on the work by Daniels (1988).

7.2 Double Skin Composite Beam with Ductile Connectors

7.2.1 Background

The beam tests performed at Cardiff by Oduyemi and Wright (1988) investigated the effect of various parameters on the failure mechanism.

To verify the performance of DSCW, Beam B2 was analyzed with the one-dimensional Basu and Summerville concrete model, the stepped steel model and the Yam and Chapman (1968) non-linear interface model and compared with the corresponding experimental results. The maximum concrete stress was found from the cube test results on the micro-concrete infill taken at the time of testing with the steel yield strength and Young's Modulus taken from coupon tensile tests.

The push-out test results were used to obtain the constants in the Yam and Chapman load-slip curve. A reduction was included for the ultimate stud strength in the tension side equivalent to that applied in the experimental work. This reduction proposed by Johnson *et al* (1969) recommends that the strength of connectors be reduced to account for the effects of tensile cracking of the concrete. In the tension side the stud strength was reduced by 29% although the original recommendations by Johnson *et al* only suggested a 20% reduction in capacity. This reduction was found in the original test to give reasonable results when compared to the Finite Element Composite Model devised by Jefferson (1990).

The test considered shown in figure 7.1 consisted of a concrete centre with 2 steel plates, each 3mm thick, fixed to the top and bottom of the core by 6mm diameter shear studs. The studs were spaced in two rows at 100mm spacing with 135mm long studs on the bottom layer to prevent the vertical shear failure which had occurred in previous tests. The loading of the beams consisted of two loads located 175mm from the centre-line applied by a hand-operated jack via a calibrated load cell. Instrumentation consisted of dial gauges to measure deflections at the loading points

and mid-span of the beam, electric resistance strain gauges on the external steel plates, Demec studs to measure the extreme fibre concrete strains and dial gauges to measure the end slips between the steel and the concrete.

7.2.2 Comparison between DSCW and Experimental Results

A comparison between the results obtained by applying the DSCW program and the experimental results was carried out by examining the resulting central deflections, steel strains and end slips by applying loads in 10kN increments. The program correctly predicted flexural failure by yielding of the bottom steel.

7.2.2.1 Central Deflections

A graph showing the results of the experimental deflections against those predicted by program DSCW is given in figure 7.2. It can be seen that the stiffness of beam BS2 is initially greater than the values obtained numerically. This is probably due to the end slips being less than predicted from DSCW and therefore increasing the value of bending moment for a given deflection. The divergence after the 30kN load level may be a result of vertical shear cracking increasing the deflection of the beam as shear deflections were not included in the formulation of DSCW.

7.2.2.2 End Slips

The results of the end slips given in figure 7.3 show good agreement between the experimental and numerical results particularly on the top compression face. On both sides the end slip is initially small as the chemical bond between the steel sheet and concrete prevents large relative slips. The behaviour on the bottom tension face shows a initial greater variation than the compression face as the reduction imposed on the shear stud strength may not be uniform for increasing load.

7.2.2.3 Steel Strain

The results of the steel strains, figure 7.4, show a similar pattern to the end slips with good agreement on the top compression face. The main differences occur on the bottom tension face for reasons similar to the previous discrepancies in the end slips.

7.2.3 Discussion

In general, the values of displacement, end slip and steel strain found from the computer analysis show good agreement with the experimental results. Although the computer program assumes a continuous rather than discrete connection, this assumption appears reasonable in this case where adequate connection was provided. The main discrepancies were thought to be due to vertical shear displacemets and the existence of some chemical bond strength at the steel/concrete interface. As long as the beams under consideration fail by flexure or slip then reasonably accurate predictions of the ultimate load can be achieved. The program should therefore provide an upper bound to the possible failure modes.

No account of local buckling was considered necessary as the spacing of the shear connectors was adequate to prevent any instability failure before steel yield.

7.3 Double Skin Composite Beam/Columns with Ductile Connectors

7.3.1 Background

These tests, also performed by Oduyemi and Wright (1990), considered the combined action of axial loads and lateral loads on the behaviour of beam/composite columns. The problem in applying the axial load to the steel and the concrete at the boundaries had a significant effect on the results, particularly the end slip.

The comparison between the experimental and numerically calculated results was performed on Beam A2 shown in figure 7.5. which consisted of 2 external top and bottom mild steel plates, 4mm and 3mm thick respectively, fixed to a 150mm concrete core by 6mm diameter shear studs. The studs were placed in two rows at 100mm spacing with the bottom studs 135mm long to prevent vertical shear failure. The beam/column was 2300mm in length with a concrete strength of 44N/mm^2 and an elastic modulus of 27.2kN/mm^2.

After an axial compressive load of 100kN was applied at the boundaries a 2 point lateral load symmetrically placed 550mm about the centre was applied until failure was achieved.

7.3.2 Comparison between DSCW and Experimental Results

A comparison of the results obtained from the experiment and those predicted by the program was performed investigating the central deflections, steel strains and end slips by applying loads in the 10kN loading stages. The program correctly predicted flexural failure of the steel on the tension side. The computer model consisted of 15 concrete divisions with single steel elements on the external faces. As before, the Basu and Summerville concrete and Yam and Chapman interface models were used with no loads assumed acting on the steel end cross-sections.

7.3.2.1 Central Deflections

A graph showing the results of the experimental central deflections plotted with those predicted by the program DSCW is given in figure 7.6.

The results show good agreement between the predicted and experimental results with the only divergence occurring in the initial stages of loading.

7.3.2.2 Steel Strain

The results of the experimental top and bottom steel strains compared to those predicted by DSCW are given in figure 7.7.

The results shows an initial error in agreement between the values obtained from the experiments and DSCW with the program overpredicting the compressive strains on the steel. The trend is for an increasing divergence between the values with increasing load. It should be noted that the bottom strains are plotted negatively for convenience in showing the results.

7.3.2.3 End slips

The end slips plotted in figure 7.8 show the poorest agreement between the experimental and numerical results. This is a result of the measurement of slip being taken at the end of the beam where the assumed boundary conditions do not agree with those actually occurring in the experiment. In the numerical study the steel boundaries were assumed unloaded with the axial load passing directly from the load point to the concrete boundary. Although this has little effect on the lateral displacements which depend primarily on the magnitude of the lateral load this obviously has a great effect on the values of steel end slip and to a lesser extent strain.

In the experiments the amount of axial load passed to the external steel varied with the amount of lateral loading applied. As the lateral loading increased the bottom steel on the tensile face slipped towards the centre, gradually unloading at the ends, with the steel on the compressive face slipping away from the centre, gradually becoming more heavily loaded at the ends.

Even when no lateral loading is applied a uniform strain distribution cannot be assumed across the steel and concrete sections. For a uniform value of axial strain across the ends the steel sections require a greater stress than the concrete section. If a compressible load spreading plate is used to apply the axial load then the amount of load applied to the steel at the ends will depend on the compressibility of the spreading plate.

7.3.2.4 Conclusions

The interaction at the ends of the beam/column created complicated boundary conditions with the steel strain and end slips affected by changes in the boundary conditions as well as by the applied lateral load. Although DSCW produced results approximately similar to the experiments, the errors, as expected, were greater than in the previous beam analysis.

7.3.3 Steel Strain Distribution

The level of interaction between the steel and concrete influences the axial capacity of beam/columns. In the design of conventional composite columns the existence of low bond strength means direct bearing must be applied at the ends of the member. An assessment of the interface behaviour may be performed by assuming axial loading is applied on the concrete boundary with the steel boundaries remaining unloaded.

A comparison between the numerical results and theoretical results of the steel strain distribution across the element is given in figure 7.9. Particular care must be taken in choosing a value of Young's Modulus to be used in Equation 5.36 and also in choosing a value for k, the interface stiffness. The values of Young's Modulus and initial tangent modulus were obtained from the test results giving $E_c = 27.2 kN/mm^2$ and $k = 0.28\ kN/mm^2$. These values would be more conservative for design purposes to account for tension cracking and non-linear stress-strain behaviour in the concrete. Applying Equation 5.43 with these values of E_c and k gives $\lambda = 11.9$. This level of interaction produces some composite performance without achieving full interaction (see figure 5.4) which require higher values of λ. The linear and non-linear plots are of a similar shape but give significantly different values. It should be noted that

$$\lambda = C\sqrt{k} \qquad ..7.1$$

where C is a constant dependant on the geometry and material properties. This implies that in order to double λ it is necessary to increase the value of k by four times its current value.

It can be seen from both the linear and non-linear plots that the steel strain rises sharply away from the ends with a maximum reached at approximately 600mm along the length. After 600mm the strain remains approximately constant with symmetry about the centre-line. These observations suggest that :

a. Strengthening the length of the element up to a distance of 600mm, in this

case, by equivalent bar reinforcement will allow a fully composite action to be achieved across the element.

b. Shear studs in the intermediate zone where the strain is constant are unnecessary and need not be provided for load transfer from the concrete to the steel layers (Although they may be required to prevent buckling or to resist lateral loading). Therefore, concentrating the studs at the ends of the element will be more effective than spreading them evenly over the length.

If the value of λ is too low, equivalent strains in the steel and concrete may never be achieved ie. only a small number of shear studs are located at the interface. In this case direct bearing at the ends of the column will be required.

7.3.4 Critical Buckling Load of Beam/Column

So far the analysis of partial interaction has only considered first-order displacements, slips and strains. The effect of partial interaction on the critical buckling may reduce the axial capacity of the beam/column and therefore should be considered.

Applying the previous values of E_c and k reduced the critical buckling load from 2377kN, calculated from the Euler buckling equation, to 2361kN from Equation 5.36. For this case the reduction in capacity is small with an adequate connection provided by locating the 6mm diameter shear studs in 2 rows at 100mm spacing. In situations where the beam/column possessed a poorer bond the reduction in critical load would be greater.

In this case the critical load is much greater than the ultimate axial load of approximately 950kN. If the column length is increased to provide greater slenderness the difference between the full and partial interaction buckling loads will be less.

By increasing the length of the column from 2.3m to 4.6m the critical load reduced

to 594kN and 593kN for full and partial interaction respectively. As the concrete capacity was greater than the critical buckling load, no concrete crushing occurred. Therefore DSCW was applied giving a critical load of 588kN which compares reasonably well with the numerical analytic results. It should be noted that no initial displacement or lateral loading were introduced in the analysis.

7.3.5 Discussion

The values of central displacement predicted by the DSCW were close to the experimental results as lateral movement is not greatly affected by the axial boundary conditions. The central steel strains were similar to the experimental results with the main discrepancies between the values appearing before the application of the lateral loads.

The end slips as expected showed the greatest errors due to their proximity to the loading point and difficulty in assessing the value of steel end load to be applied. In this case to ensure no concrete crushing at the ends, internal reinforcement bars to a distance of 600mm from each end may be required or the boundaries must be subjected to direct bearing.

The calculations of critical buckling load suggested that no reduction in capacity is required to take account of partial interaction for slender elements of similar construction.

7.4 Composite Walling with Profiled Steel Sheeting

7.4.1 Introduction

Research into the performance of composite walls utilising profiled steel sheeting is described in chapters 3 and 4 of this thesis with various heights and design details investigated. The modelling of these walls by analytical and numerical methods was performed in similar manner to the previous cases by applying the chapter 5 analytic

results and the non-linear program DSCW. Only three of the four composite walls tested were considered in the analysis as the first wall was unsuitable despite obtaining the greatest failure load. This was a result of the steel sheeting bearing against the loading beam directly and changing the loading conditions at the steel boundaries.

The analytic and numerical models considered global buckling of the composite walls with local buckling of the external steel sheeting not explicitly included in the analysis. Although no local buckling was observed in the first two experiments where concrete failure and slip were the controlling factors, the following two tests, with increased bond, showed local buckling of the profiled steel sheeting before failure. The analytical and numerical equations derived in chapters 5 and 6 respectively were unable to take account of this effect as the curvature was constrained to be equal across the steel-concrete-steel layers.

It should be noted that the experimental values are not plotted on the graphs as the analysis is focused on the qualitative rather than quantitative reponse. Other reasons for omitting the experimental results from the graphs are the variations between the different sides and sections of the walls and the difficulty of modelling the brittle behaviour.

7.4.2 Buckling Strain and Computer Modelling

The identification of the critical strain of the Superholorib profiled steel sheeting was performed by examining the strain gauge results for evidence of a slow fall in the strain. This is shown clearly in Gauge 5 of Figure 4.25 where the strain increases with load up to a maximum value of 600 microstrain before decreasing slowly up to failure. Although the re-entrant portions of the profile also carry a proportion of the axial load this requires a higher failure strain because of the reduced buckling lengths.

Adjusting either the effective steel area, or the maximum strain carried by the

external reinforcement, to account for local buckling was not incorporated in DSCW. This allowed particular attention to be focussed on the interface behaviour. In situations where the external steel strain exceeded 600 microstrain the results noted the likely appearance of local buckling at this particular load level.

7.5 Composite Wall 2

7.5.1 Introduction

The main problem in modelling this experiment was the apparent brittle interface existing between the steel and the concrete faces, despite the ductile behaviour normally expected with this profile. In order to obtain a better understanding of this behaviour, the interface load-slip relationship was modelled with the numerical model developed from the work by Daniels (1988) (see section 6.7.3).

In the experiment no mesh was welded to the surface of the steel sheeting with the only interface bond developed by the sheeting acting against the surface of the concrete. The numerical concrete strength was based on the cube strength results taken at the time of the original test.

Similar boundary conditions to those of the experiment were employed with the concrete boundaries taking the full axial load and the steel ends remaining unloaded.

7.5.2 DSCW Model Details

Only a 152.5mm width of the total cross-section of the wall was considered necessary to represent the behaviour. Figure 7.10 shows the representative element which consisted of 30 concrete sections sandwiched between 4 steel sections on the top and bottom surfaces. The concrete behaviour was modelled with the Basu and Summerville (1968) concrete model with the maximum sustainable concrete stress taken from the test results. The Cofrastra 40/0.75 interface model previously developed from the work by Daniels (1990) was applied to obtain a realistic

indication of the performance of the geometrically similar SuperHolorib 51/0.9 profile. As with all the experiments, except Composite Wall 1, the axial load was only applied at the concrete boundaries. The length of 1.9m was divided into 16 divisions for sufficient accuracy in the numerical results. Although some shrinkage strains were recorded in the experiments no account was taken of this effect in the analysis which considered only the strains developed under the applied load.

7.5.3 Results of DSCW Analysis of Wall 2

The composite wall failed by concrete crushing at the boundaries under an axial load of 2019kN. The resulting steel and concrete strain distribution are shown in figures 7.11 and 7.12 with the interface slips in figure 7.13. The plots are given for various values of axial load up to failure.

7.5.4 Discussion of Results

The results agree with the experimental values with a similar failure load and mechanism. An interesting result of having an initially brittle failure followed by a ductile response at the interface is the transfer of strain to the steel sheeting from the concrete core.

7.5.4.1 Steel Strains

Figure 7.11 shows that under low axial loads (336kN) the initially high bond produced at the interface rapidly transfers load into the steel, resulting in equal strains in the steel and concrete a short distance from the boundaries. As the axial load is gradually increased some slip occurs with a fall in bond stress which increases the distance taken for the concrete and steel strains to become uniform. At an axial load of 1766kN the level of slip prevents the steel achieving the concrete strain at any point in the length. The maximum strain of approximately 550 microstrain compared reasonably with the experimental results (figures 4.13 - 4.16) where strains of between 550 and 650 microstrain were recorded before bond failure at the interface.

7.5.4.2 Concrete Strains

Figure 7.12 again shows that under low axial loads the strain is distributed uniformly between the steel and the concrete. As the axial load increases a higher proportion of load is carried by the concrete particularly close to the boundaries.

7.5.4.3 Interface Slip

Initially under low axial loads the highest levels of slip (figure 7.13) occur at the boundaries where the majority of the load is transferred. As a result, in the central portion of the wall the interface stresses are low. Under higher levels of axial load the interface slip becomes significant away from the boundaries producing interface stresses near the centre of the element.

7.5.5 Conclusions

Perhaps the most interesting result of the numerical study on the second test is the level of the slips at the steel/concrete interface.

Assuming the model behaves similarly to the Superholorib profile used in the experiments, the large drop in steel sheeting stress prior to failure may be a result of loss of chemical bond at the interface. Although the drop in steel stress is small when modelled with a gradual decline in bond stress after chemical bond failure, the actual interface behaviour may be more brittle with a rapid fall in bond stress before any build up in the ductile response.

Also significant is the level of interface slip when concrete crushing occurs. In composite beam behaviour where the element is subjected to bending stresses the levels of slip occurring are large (approx. 2-5mm) allowing a full ductile interface bond stress to develop. In this case under axial strains the end slip at failure is less than 1mm (figure 7.13) and the high ductile sheeting stresses are never developed. This suggests that unless a high bond can be rapidly developed under increasing slip the effect of the steel sheeting as external reinforcement may be limited as the chemical bond strength is lost before ultimate failure.

7.5.6 Performance of Interface Model

The values of strains produced in this analysis are close to numerical results up to the brittle interface failure. After this failure the experiments show a larger reduction in strain than those from DSCW because the interface model had too shallow a decline in the load-slip relationship. Unfortuantely, if this gradient is increased, substancial numerical problems arise with the strain at brittle failure affected by the number of nodes. This is a result of the averaging of the interface slips close to the ends of the wall. The greater the number of nodes the higher the value of interface shear developed at the final node, and threfore the lower the axial load required to produce fracture between the steel and concrete layers. Consequently this type of numerical analysis is generally unsuitable in these situations with a large reduction in strain after brittle failure.

7.6 Composite Wall 3

7.6.1 Introduction

The third composite walling test performed on a 3.4m section had A98 mesh welded across the ribs up to a distance of 600mm from the boundaries. The loading system was similar to the previous test with only the concrete loaded at the boundaries. The alteration applied to the sheeting was a modification to the interface relationship, replacing the brittle superholorib model by the ductile Yam and Chapman interface model. In order to model the effect of the steel mesh the constants a and b, required to define the load-slip relationship, were calculated for the surfaces of the steel sheeting with and without the mesh.

7.6.2 DSCW Model Details

The only changes in the input file were to increase the height of the element from 1.9m to 3.4m and to change the relationship at the interface to the Yam and Chapman model. The two constants were set :

1. a = 90.30 N/mm and b = 4.31 from 0 to 600mm
2. a = 48.37 N/mm and b = 0.69 from 600mm to 2800mm
3. a = 90.30 N/mm and b = 4.31 from 2800mm to 3400mm

The value of **a** represents the maximum sustainable load per unit length at the interface while **b** models the rate of increase of the load towards **a**. As the value of **a** is increased the relative amount of load transferred at the interface increases and vice-versa.

Particular attention was given to the effect of numerical stability when modelling the large change in the interface stiffness across the element. It was noticed that instabilities in the finite difference solution appeared in the transition to the poorer bond (600mm and 2800mm from the base) especially when the level of discretisation was low. Applying the Lax Equivalence Theorem which states that 'convergence is necessary and sufficient for stability' suggests that although the instabilites never completely vanish, their effect may be minimised by increasing the discretisation. Sufficient accuracy was provided by 16 element divisions over the height of the composite wall.

In the central section no mesh was applied with the response based on an approximation of the Superholorib model without the initial brittle behaviour.

Although some buckling of the sheeting was observed during the laboratory experiments no modifications were made to program DSCW to account for this effect.

7.6.3 Results of DSCW Analysis of Wall 3

The program again predicted concrete crushing failure at the ends of the composite wall under an axial load of 2019kN. The steel and concrete strains are given in figures 7.14 and 7.15 respectively with the interface slips shown in figure 7.16. The plots are shown for similar values of axial load to the results of Composite Wall 2.

7.6.3.1 Steel Strain

The steel shows a generally similar response to the previous results with the load gradually transferring from concrete into the steel until the strains become uniform between the two materials. There are two main differences in the response resulting from the change in the interface model between the steel and concrete surfaces :-

- By removing the initial brittle response, the distance from the ends required to obtain a uniform strain distribution becomes greater, especially under low load levels.

- The increased wall height and bond strength at the interface allow higher levels of strain to be achieved in the steel. The analysis suggests that full bond transfer was achieved at approximately 900mm from the ends of the element.

The values of steel strain obtained from the analysis are greater than the 600 microstrain necessary for local buckles to develop. This agrees with the experimental observations at the time of testing. In the experiments local buckling between the re-entrant ribs was observed close to point where the mesh terminated.

7.6.3.2 Concrete Strain

The concrete strains shown in figure 7.15 again show the decline in concrete strain away from the boundaries of the wall. As expected, the reduction in strain is greater than the previous results near the centre of the wall, for equal concrete loads at the boundaries.

7.6.3.3 Interface Slip

The interface slip behaviour in figure 7.16 shows significant slips over the length of the composite wall for all values of axial load as no account was taken of the brittle response at the interface. The interface end slips at failure were approximately 0.5mm.

7.6.4 Conclusions

The advantage of having a ductile response with a high stiffness is evident from the test results. In the previous test the bond stress reduced significantly after brittle failure at the interface without the ductile behaviour being mobilised. In this analysis the ductile response developed rapidly for smaller values of interface slip, so that a short distance down the composite wall full interaction between the steel and concrete sections was achieved. It is evident that the value of **b** in the Yam and Chapman relationship has a significant effect on the development of bond between the steel and concrete layers.

7.7 Composite Wall 4

7.7.1 Introduction

The final composite wall tested was similar to the third wall except for the addition of reinforcing bars located up to a distance of 600mm from each boundary.

7.7.2 DSCW Model Details

The input file was altered to allow reinforcing to be included in the concrete layer. As in the experiments, four 12mm diameter high tensile bars were added to the representative section up to a distance of 600mm from the each end.

7.7.3 Results of DSCW Analysis of Wall 4

The internal reinforcing of the concrete at the boundaries prevented the concrete crushing previously resulting in failure of composite walls 2 and 3. As a result concrete crushing occurred below the level of the reinforcement at a load of 2104kN. The steel and concrete strains are given in figure 7.17 and 7.18 respectively with the interface slips shown figure 7.19.

7.7.3.1 Steel Strains

The results are similar to those from Composite Wall 3 as the interface models were

identical. The proportion of load carried on the steel is slightly reduced for equivalent axial loads as the addition of the reinforcing increased the effective concrete stiffness near the ends. As in the experiments the steels strains were above those necessary for local buckling to develop.

7.7.3.2 Concrete Strains

The primary effect of the reinforcement on the concrete strains was to reduce the strains near the ends of the walls preventing crushing failure. By comparing figures 7.15 and 7.18 for Composite Walls 3 and 4 respectively a large reduction in the concrete strain can be seen between 0 and 600mm from the ends of the wall.

The only drawback of reducing the concrete strains was to lower the amount of load transferred into the steel in the initial 600mm distance. As a result, at 600mm along the wall where the internal reinforcement terminated, less load was transferred into the steel than previously giving higher values of concrete strain.

7.7.3.3 Interface Slip

The interface slips (figure 7.19) showed approximately similar end slips as Composite Wall 3 but with greater variations along the length. The slips show a gradual decline away from the ends until 600mm distance where a sharp increase appears. As before this is due to the fall in the concrete stiffness resulting in greater concrete strains and therefore larger transfers of load at this point.

7.7.4 Conclusions

The effect of adding reinforcement to the ends of the wall prevented concrete crushing and increased the load capacity of the walls. Unfortunately the effective concrete stiffness over this reinforced length was increased, slightly reducing the level of strain present in the steel.

7.8 Analytical Studies

The investigation of the effect of partial interaction on the critical buckling load of materially linear members derived in Chapter 5 produced solutions that are capable of giving reasonable results, if the value of interface stiffness can be estimated effectively. If conditions, such as those present with composite walls, exist with an initial brittle bond followed by a ductile behaviour, then the chosen value of stiffness should ignore the unreliable brittle bond. In the case of the composite walls the calculated value of interface stiffness was based on a secant modulus at 1mm slip. This produced a conservative estimate of the composite wall performance. The value of Young's Modulus was based on measured values taken at the time of testing.

Table 7.1 gives the values of buckling load for full and partial interaction and the value of λ. The values of critical buckling loads are lower than those obtained from the Euler calculation which assumes full interaction between the three layers. The magnitude of difference between these values suggests that there may be a significant reduction in axial capacity when the composite walls are slender. It should be noted that the calculated values were greater than the concrete crushing loads.

The low values of λ also suggest that the level of interaction in axial situations is poor with little contribution from the external steel sheeting.

7.9 Conclusions

The main result of the numerical analysis of the composite walls was to show that the ductile strength of the profile embossments are not mobilised before concrete crushing failure occurs. Although these tests were only performed on the Superholorib profile there is no reason to believe that a similar response would not be observed with others currently used in practise. This problem may be avoided by welding mesh or similar connectors to the profile surface but this will increase the overall construction costs.

Although the loss of bond will affect the capacity of walls in slender situations, crushing failures will occur for greater values of slenderness than equivalent reinforced concrete walls, as the steel has no influence on the axial capacity.

7.10 Summary

This work in this chapter initially verified the performance of DSCW by examining the behaviour of a composite beam and beam/column under increasing levels of lateral loading.

The results obtained showed good agreement with the experimental values particularly in the case of the composite beams where no axial loads were applied. The composite beam/column analysis showed good agreements between the displacements but poorer results when considering the end slips and steel strains which were dependent on the type of load application at the boundaries.

The analytic studies based on the equations of chapter 5 suggested that when analyzing slender beam/columns the effect of partial interaction on stability would be small.

Three previously tested composite walls were then analyzed with DSCW in order to investigate the load transfer behaviour in axial loading situations. The results suggested that after brittle failure of the chemical bond the level of strain produced were not sufficient to mobilise the high strength ductile behaviour of the embossments.

The analysis of stability suggested that the effect of partial interaction on the ultimate strength of slender columns was likely to be significant and therefore should be included in any recommendations on the design of slender walls.

Table 7.1 Buckling Loads and interaction parameter λ

Composite Wall No.	Ch. 5 Buckling Load (kN)	Euler Buckling Load (kN)	λ
2	11035	19302	0.89
3	4392	6340	2.24
4	4509	6457	2.24

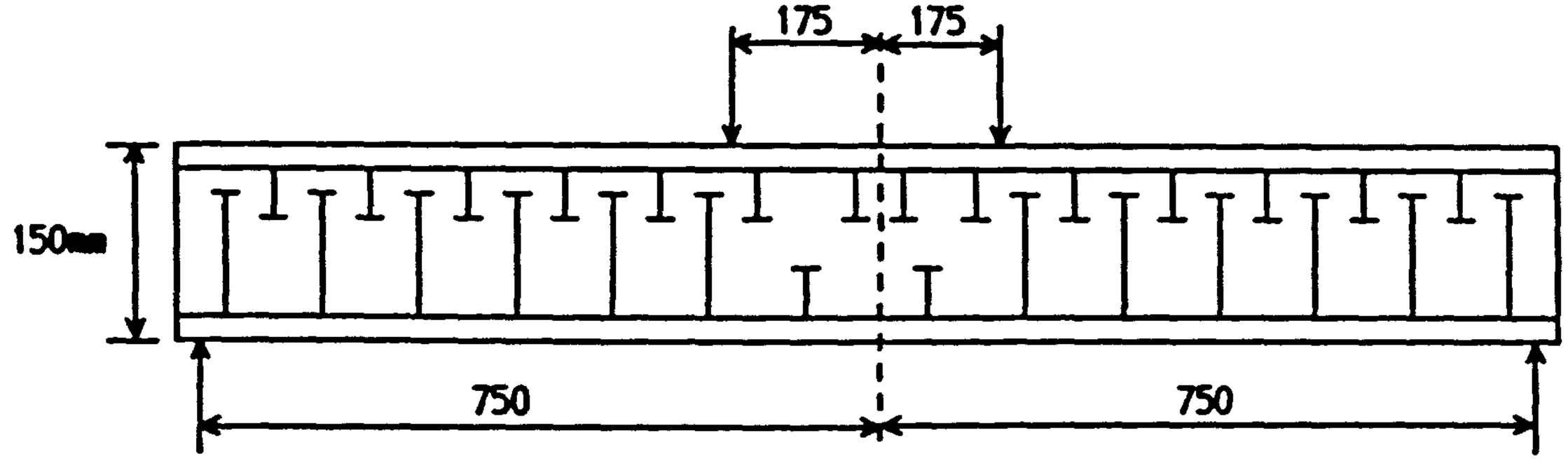

Figure 7.1 Composite Beam B2 - Oduyemi and Wright (1988)

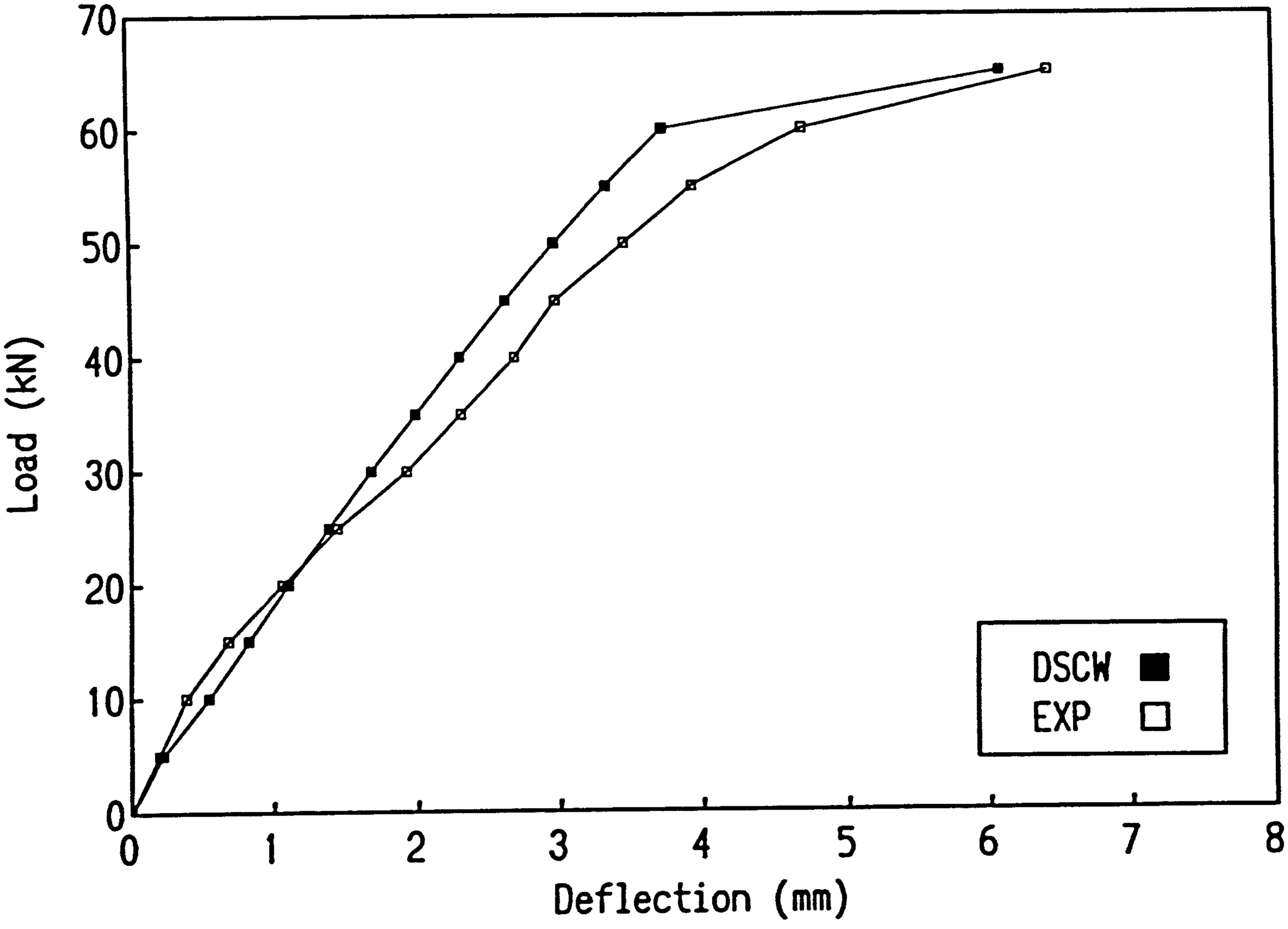
Beam B2 - DS1
Load vs Deflection
Load (kN)
70
60
50
40
30
20
10
0
0
1
2
3
4
5
6
7
8
Deflection (mm)
DSCW
EXP

Figure 7.2

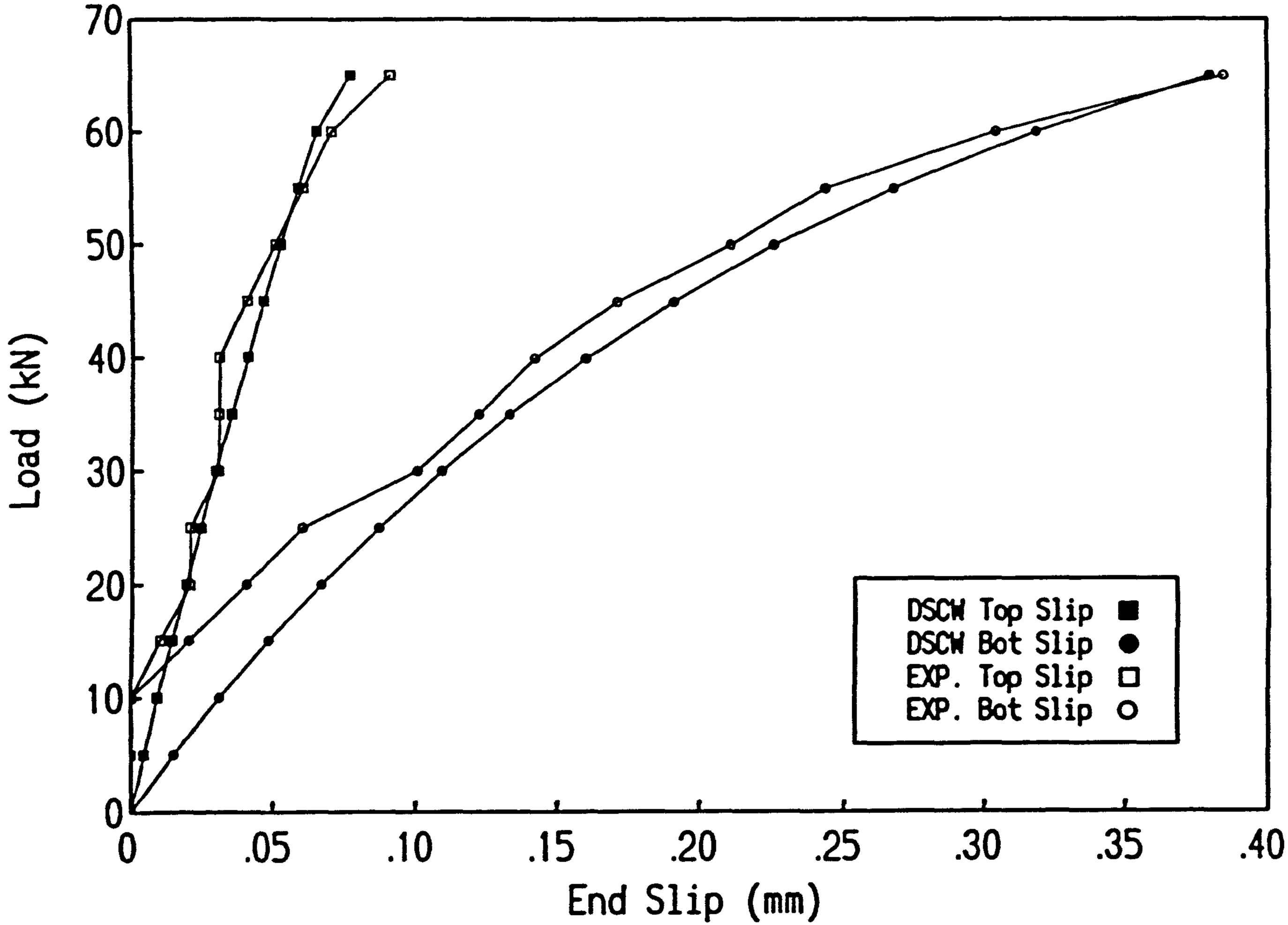
Beam B2 - DS1
Load vs Slip
Load (kN)
End Slip (mm)
0
10
20
30
40
50
60
70
0
.05
.10
.15
.20
.25
.30
.35
.40
DSCW Top Slip
DSCW Bot Slip
EXP. Top Slip
EXP. Bot Slip

Figure 7.3

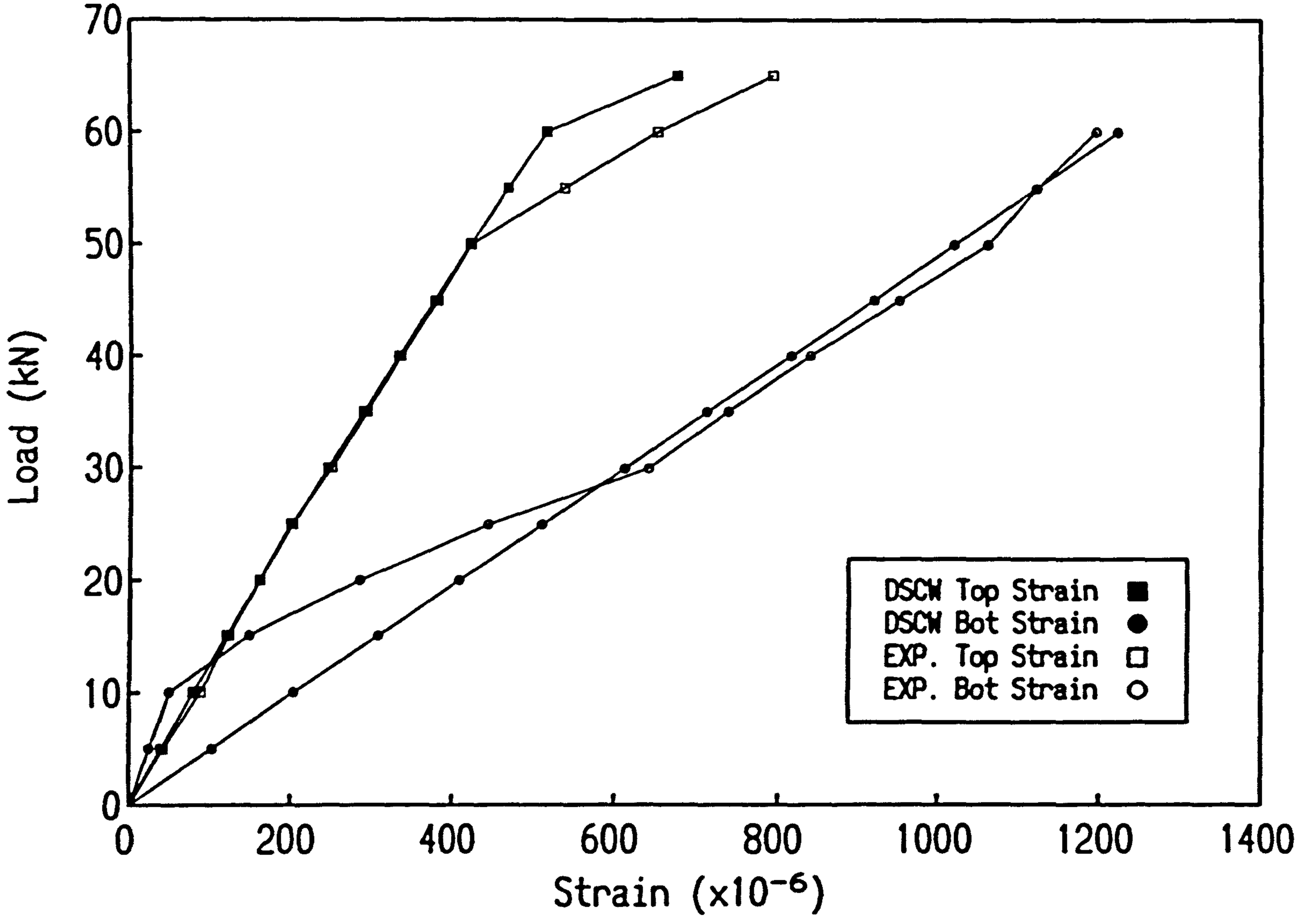
Beam B2 - DS1
Load vs Strain
Load (kN)
70
60
50
40
30
20
10
0
0
200
400
600
800
1000
1200
1400
Strain (x10⁻⁶)
DSCM Top Strain
DSCM Bot Strain
EXP. Top Strain
EXP. Bot Strain

Figure 7.4

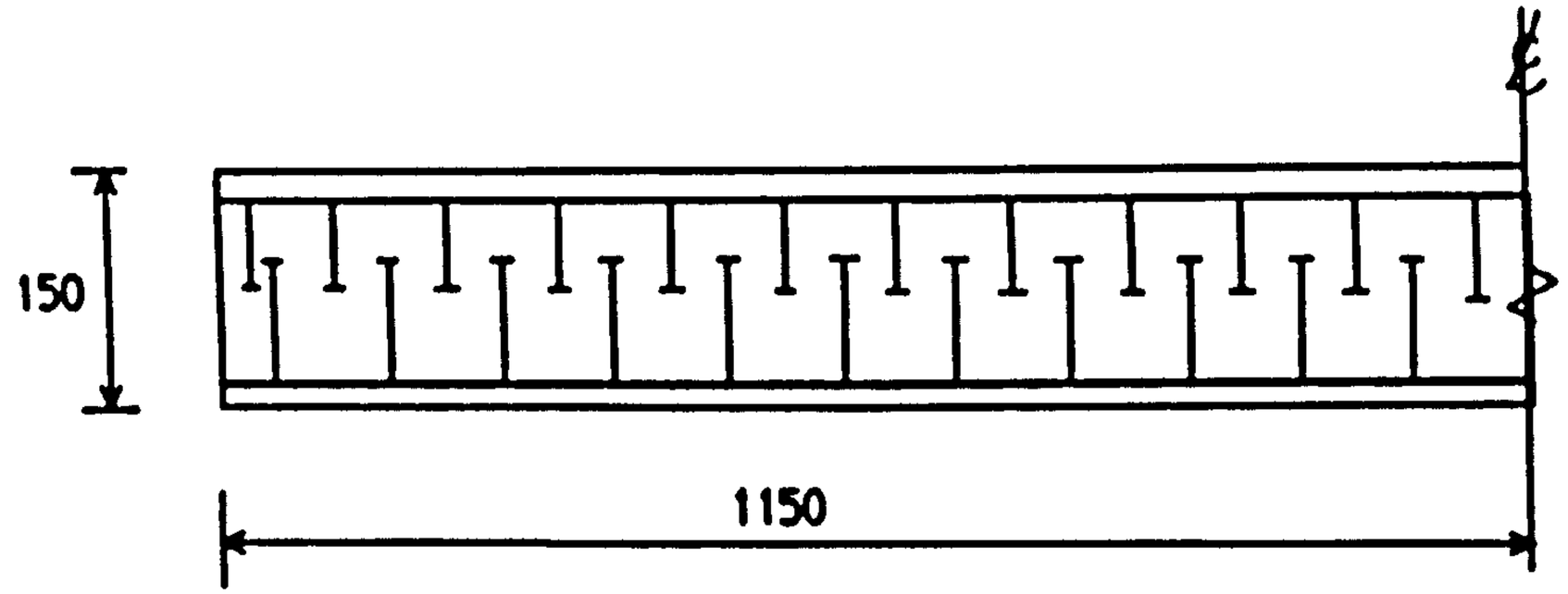

Short Studs : 6mm by 35mm
Long Studs : 6mm by 135mm

Figure 7.5 Composite Beam/Column - Oduyemi and Wright (1990)

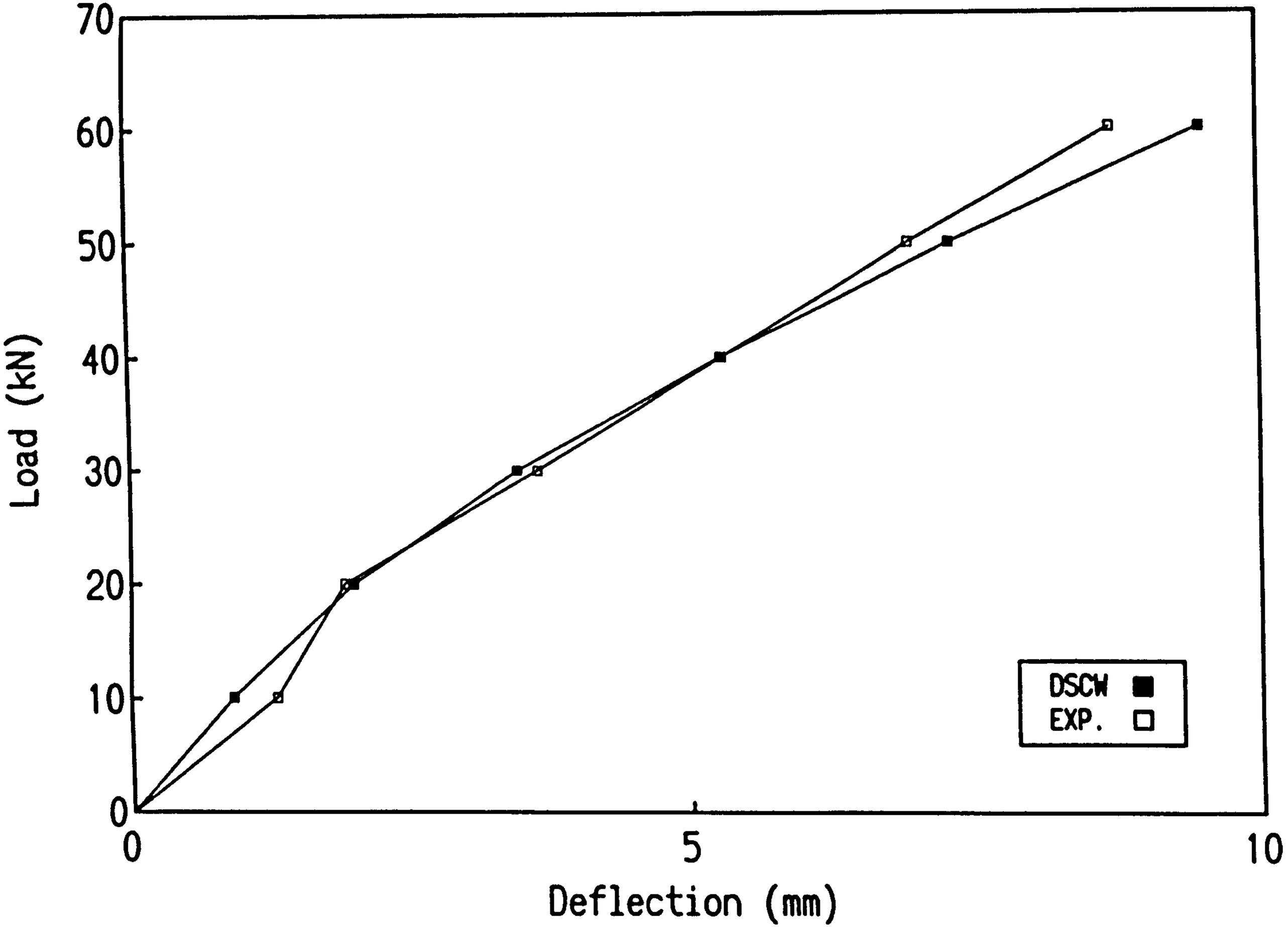
Beam A2 - DS3
Load vs Deflection
Load (kN)
70
60
50
40
30
20
10
0
0
5
10
Deflection (mm)
DSCW
EXP.

Figure 7.6

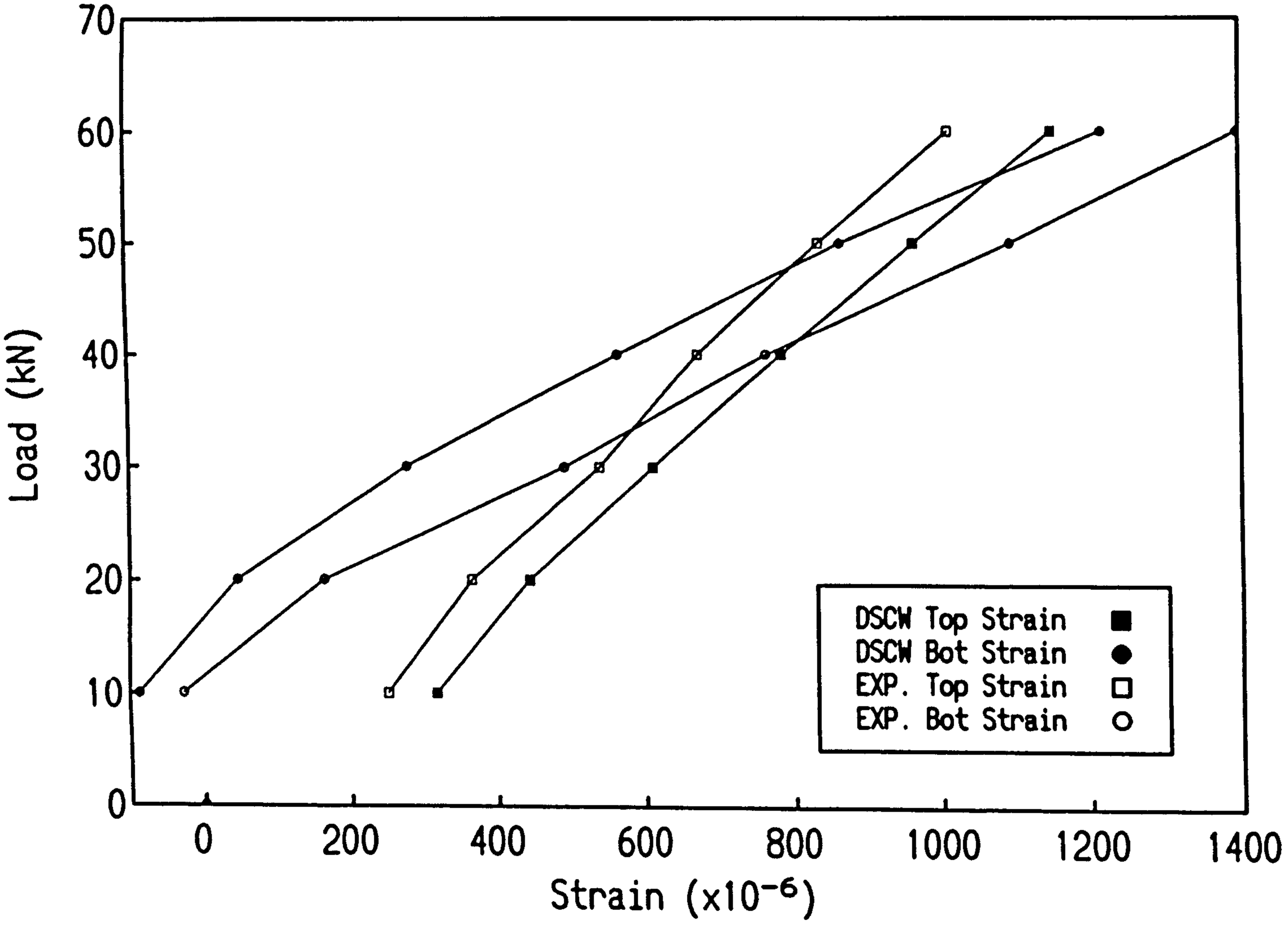
Beam A2 - DS3
Load vs Strain
Load (kN)
70
60
50
40
30
20
10
0
0
200
400
600
800
1000
1200
1400
Strain (x10⁻⁶)
DSCW Top Strain
DSCW Bot Strain
EXP. Top Strain
EXP. Bot Strain

Figure 7.7

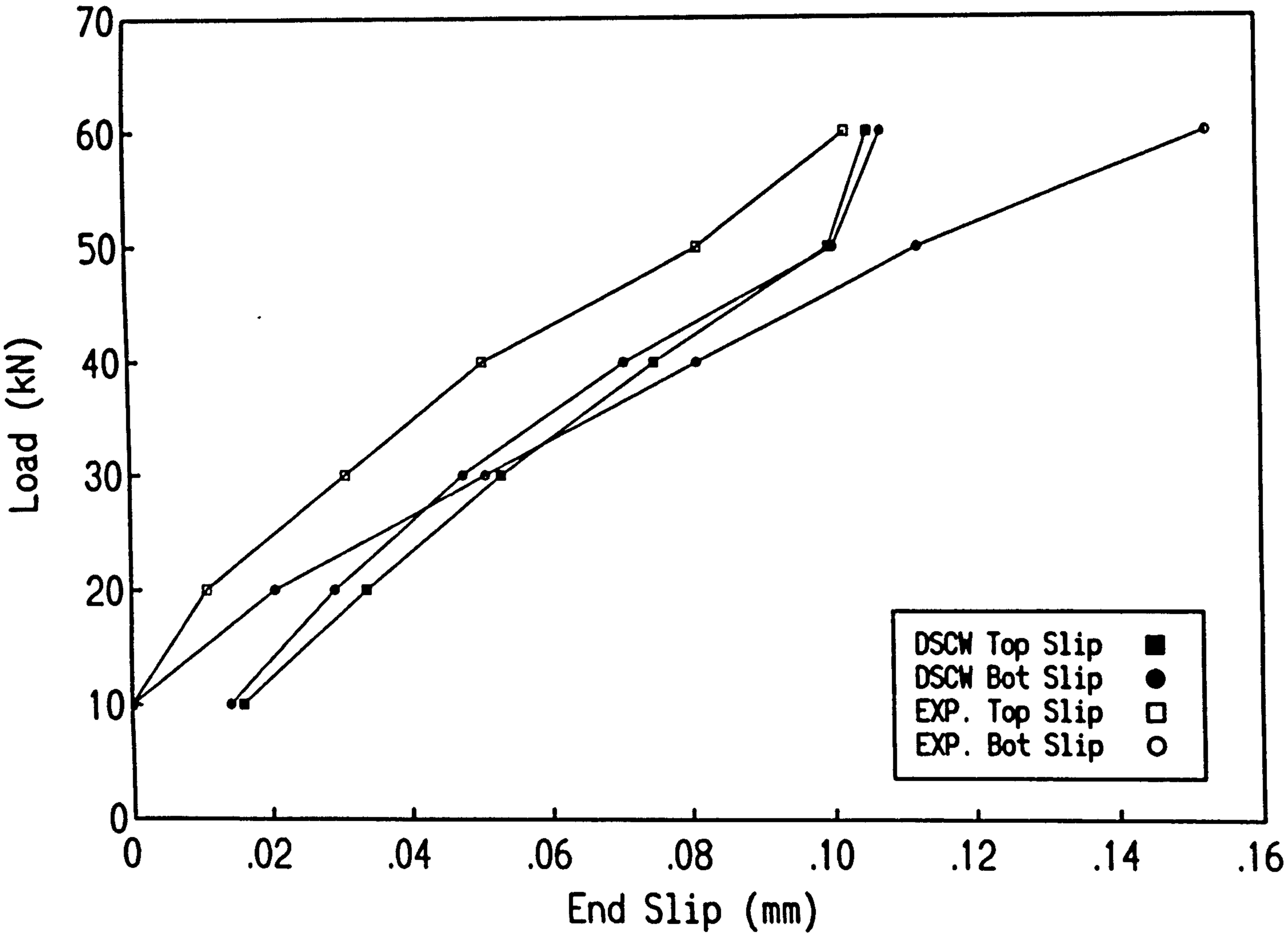
Beam A2 - DS3
Load vs Slip
Load (kN)
70
60
50
40
30
20
10
0
0
.02
.04
.06
.08
.10
.12
.14
.16
End Slip (mm)
DSCW Top Slip
DSCW Bot Slip
EXP. Top Slip
EXP. Bot Slip

Figure 7.8

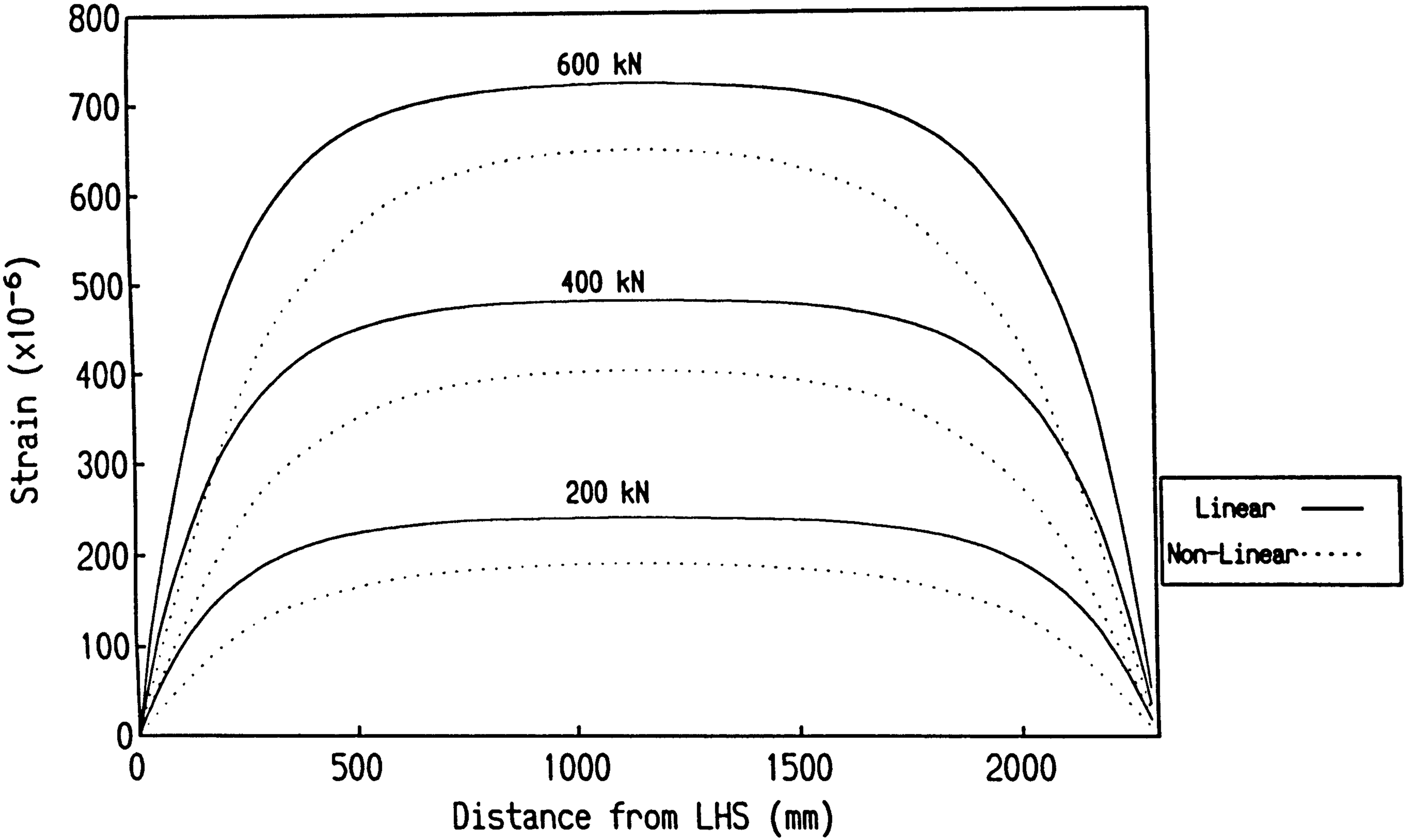
DSCW Steel Strains
Strain vs Position
800
700
600
500
400
300
200
100
0
Strain (x10-6)
600 kN
400 kN
200 kN
0
500
1000
1500
2000
Distance from LHS (mm)
Linear
Non-Linear

Figure 7.9

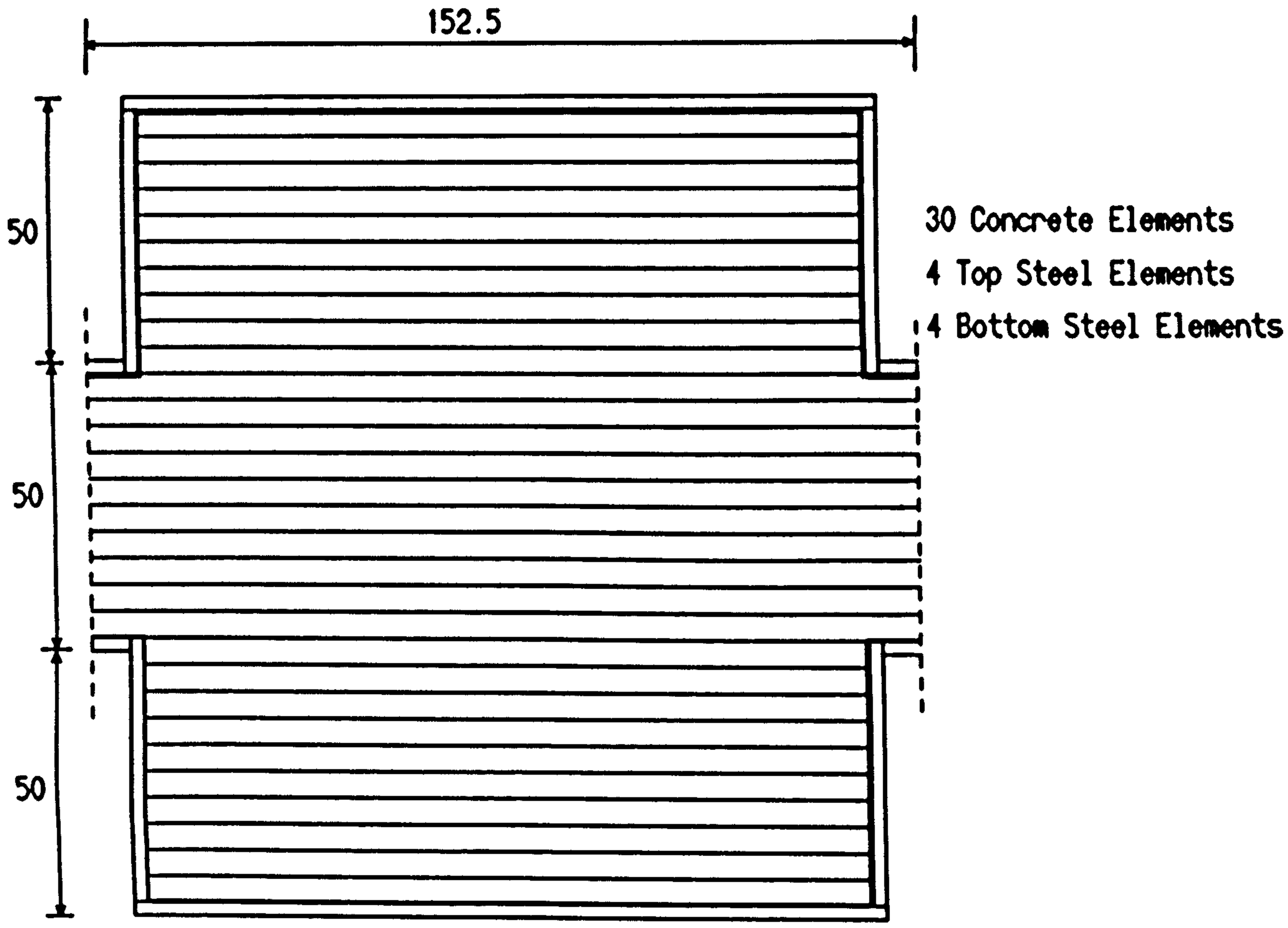

Figure 7.10 DSCW - Numerical Composite Wall Section

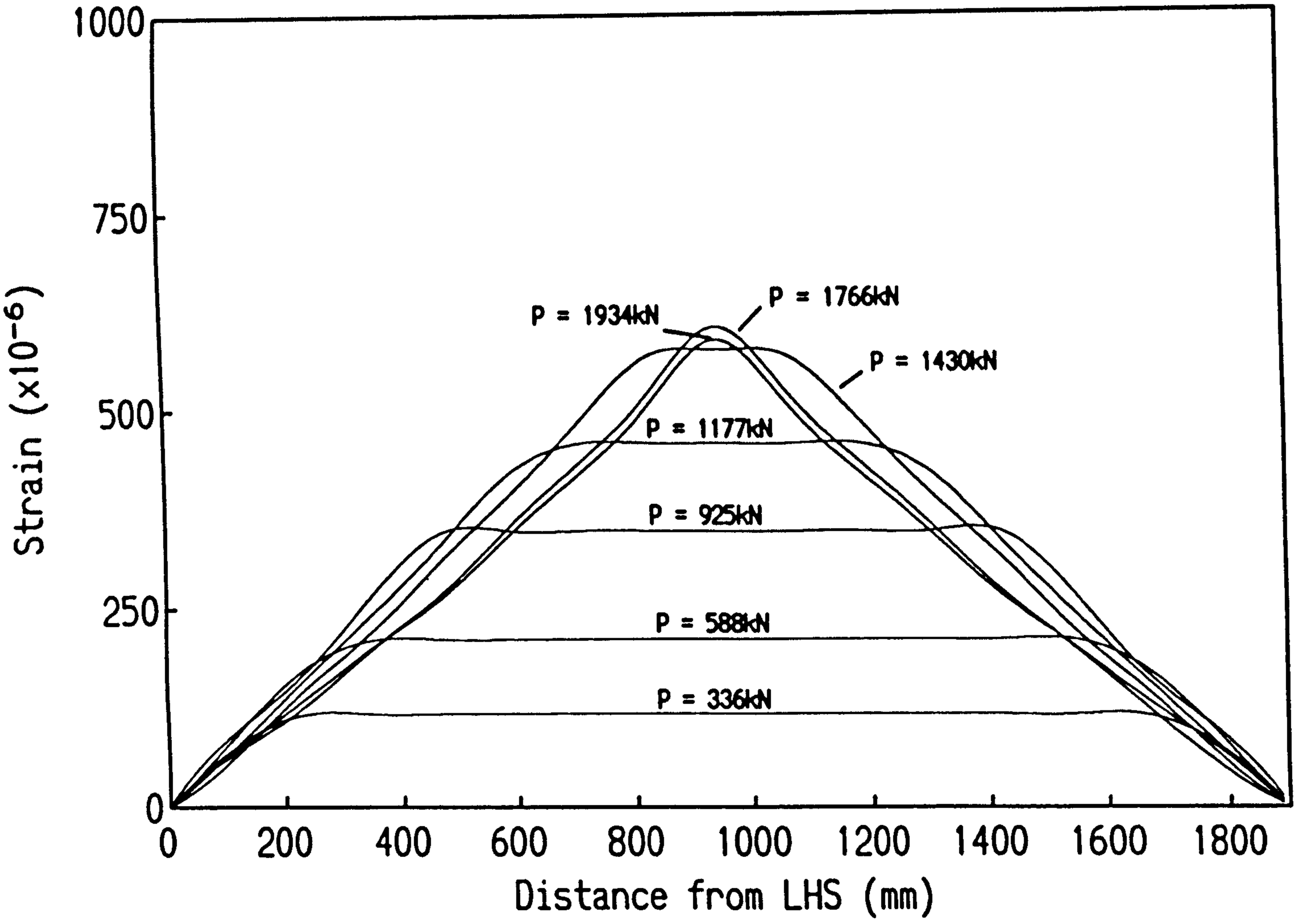
Composite Wall 2
Steel Strain vs Position
Strain (x10⁻⁶)
1000
750
500
250
0
P = 1934kN
P = 1766kN
P = 1430kN
P = 1177kN
P = 925kN
P = 588kN
P = 336kN
0
200
400
600
800
1000
1200
1400
1600
1800
Distance from LHS (mm)

Figure 7.11

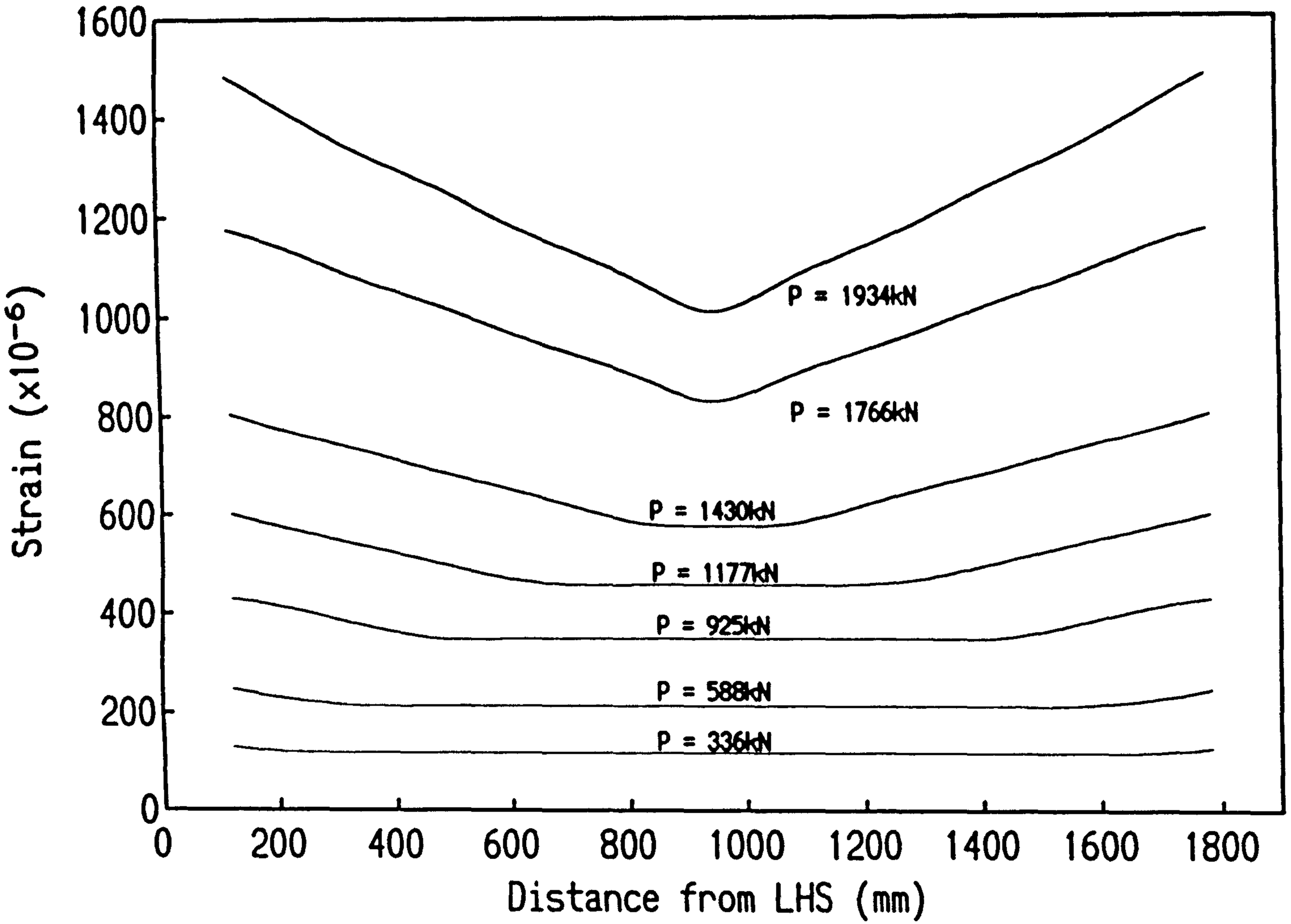
Composite Wall 2
Concrete Strain vs Position
Strain (x10⁻⁶)
Distance from LHS (mm)
P = 1934kN
P = 1766kN
P = 1430kN
P = 1177kN
P = 925kN
P = 588kN
P = 336kN
0
200
400
600
800
1000
1200
1400
1600
1800

Figure 7.12

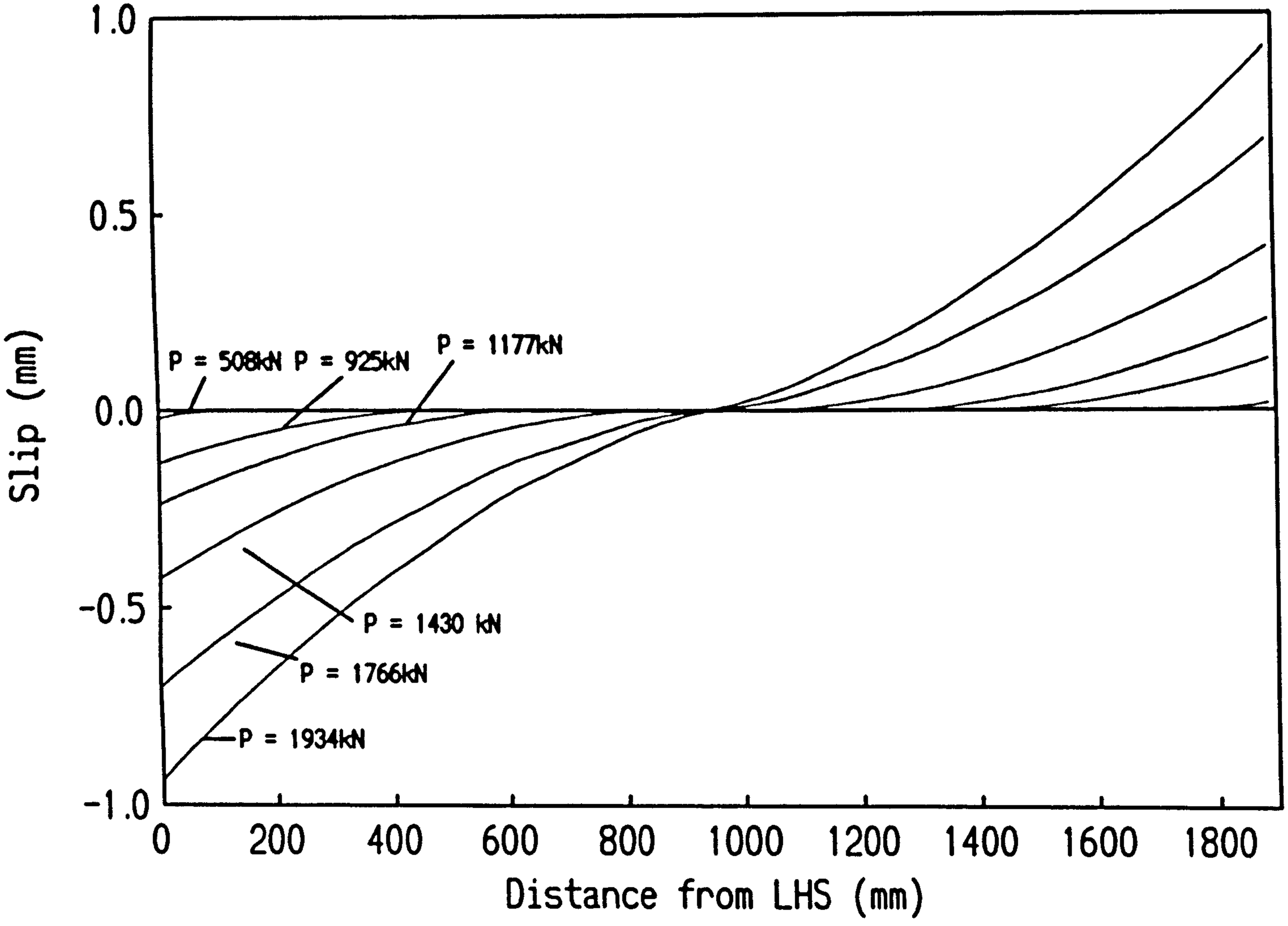
Composite Wall 2
Steel Slip vs Position
Slip (mm)
1.0
0.5
0.0
-0.5
-1.0
P = 508kN
P = 925kN
P = 1177kN
P = 1430 kN
P = 1766kN
P = 1934kN
0
200
400
600
800
1000
1200
1400
1600
1800
Distance from LHS (mm)

Figure 7.13

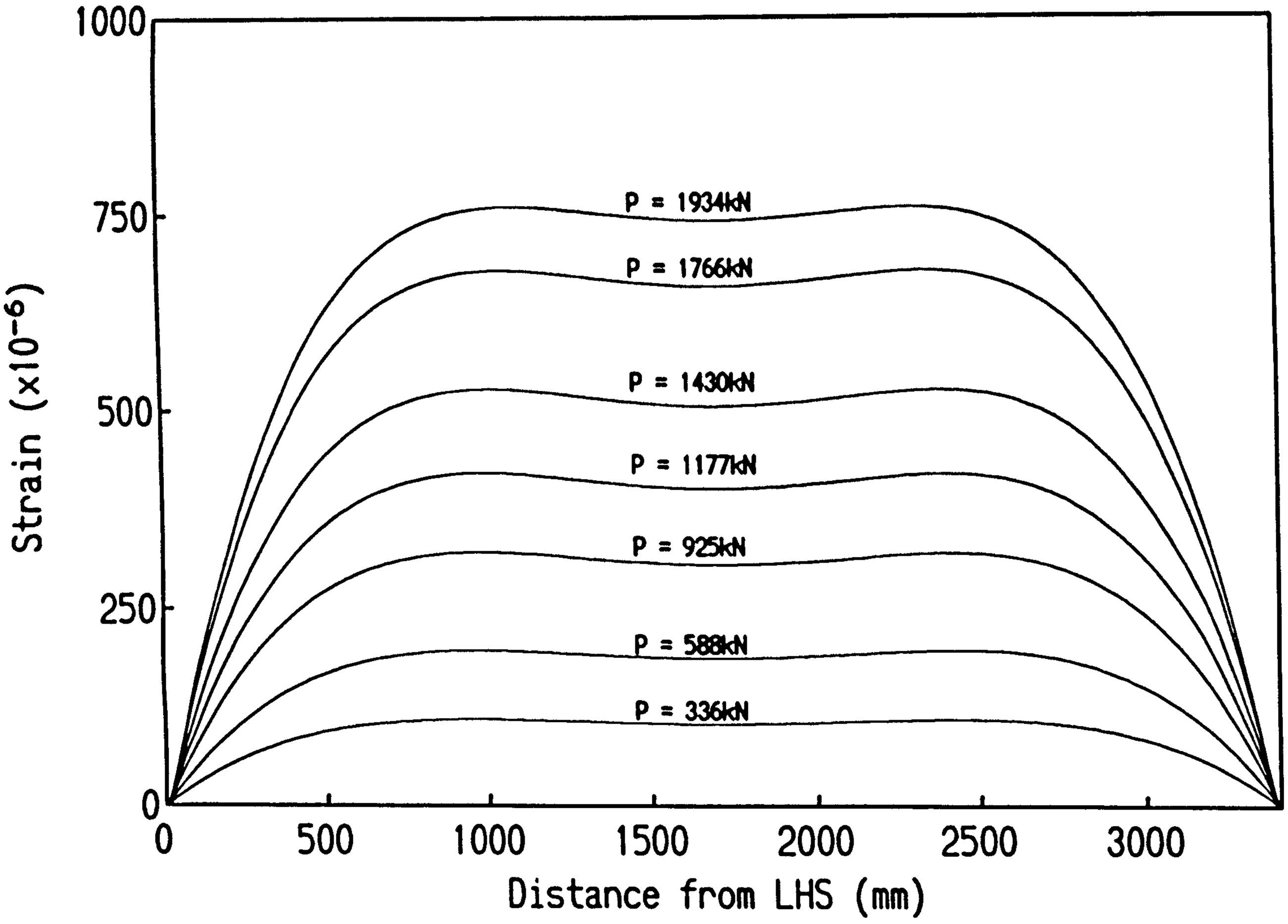
Composite Wall 3
Steel Strain vs Position
Strain (x10-6)
1000
750
500
250
0
P = 1934kN
P = 1766kN
P = 1430kN
P = 1177kN
P = 925kN
P = 588kN
P = 336kN
0
500
1000
1500
2000
2500
3000
Distance from LHS (mm)

Figure 7.14

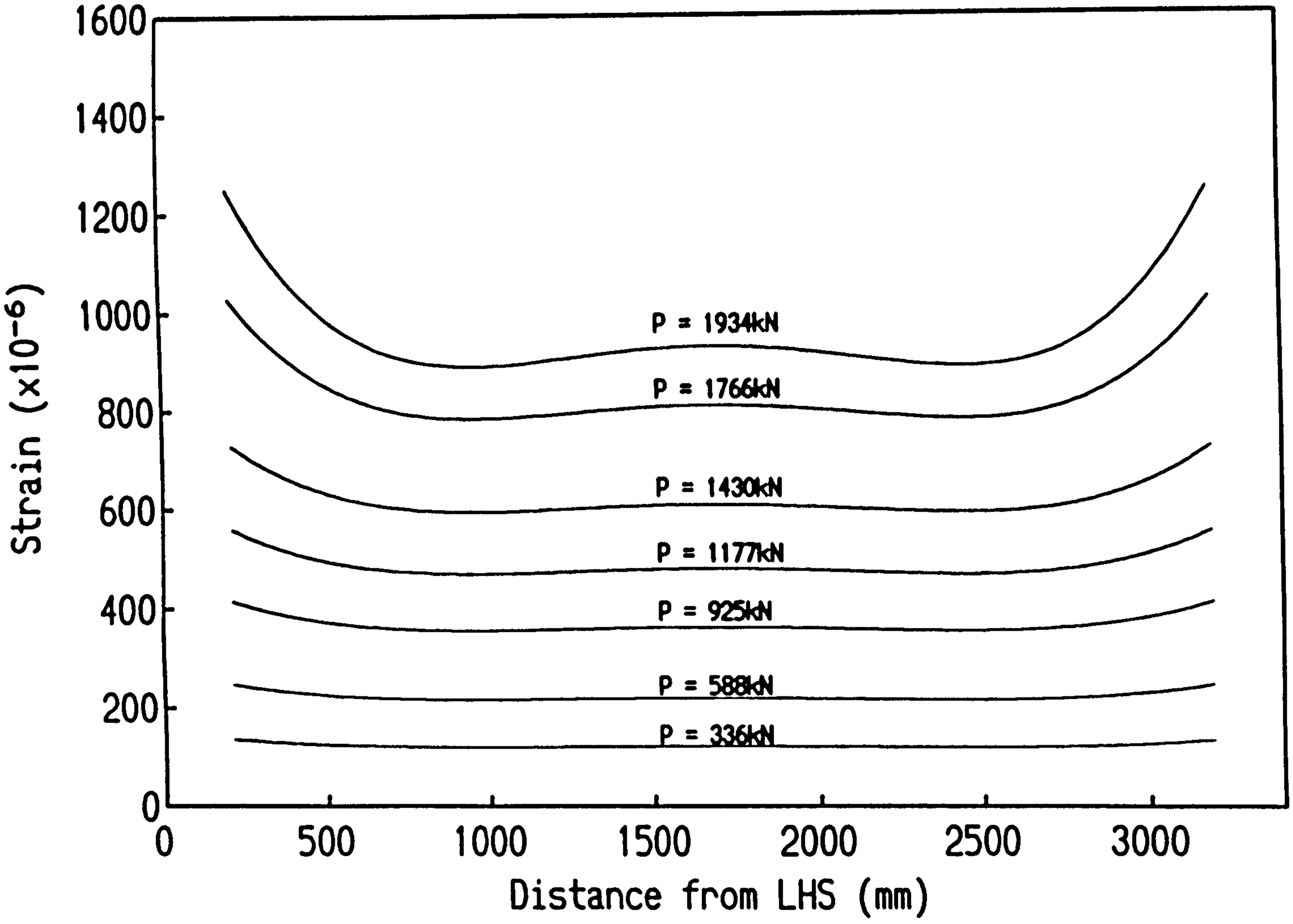
Composite Wall 3
Concrete Strain vs Position
Strain (x10⁻⁶)
1600
1400
1200
1000
800
600
400
200
0
P = 1934kN
P = 1766kN
P = 1430kN
P = 1177kN
P = 925kN
P = 588kN
P = 336kN
0
500
1000
1500
2000
2500
3000
Distance from LHS (mm)

Figure 7.15

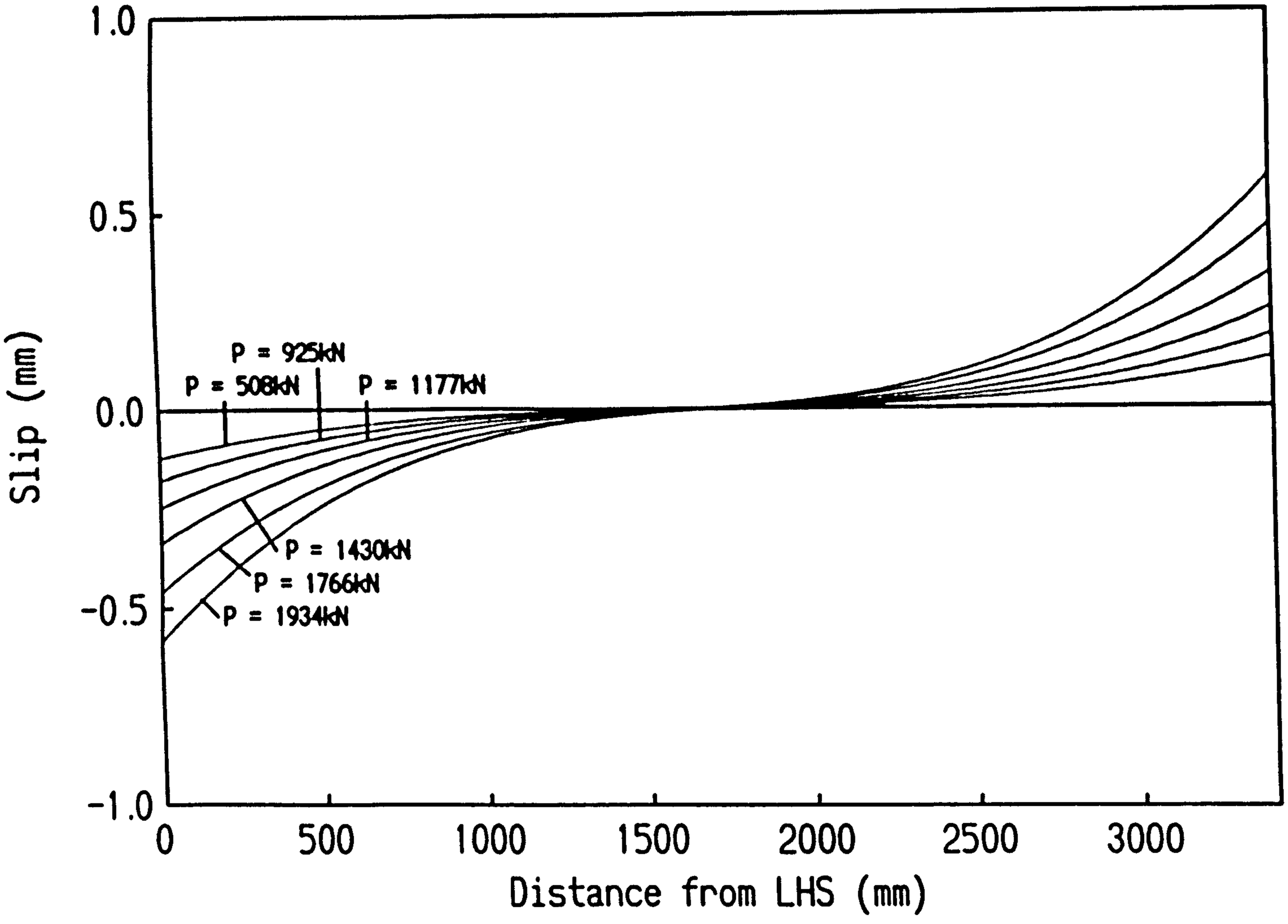
Composite Wall 3
Steel Slip vs Position
Slip (mm)
1.0
0.5
0.0
-0.5
-1.0
P = 925kN
P = 508kN
P = 1177kN
P = 1430kN
P = 1766kN
P = 1934kN
0
500
1000
1500
2000
2500
3000
Distance from LHS (mm)

Figure 7.16

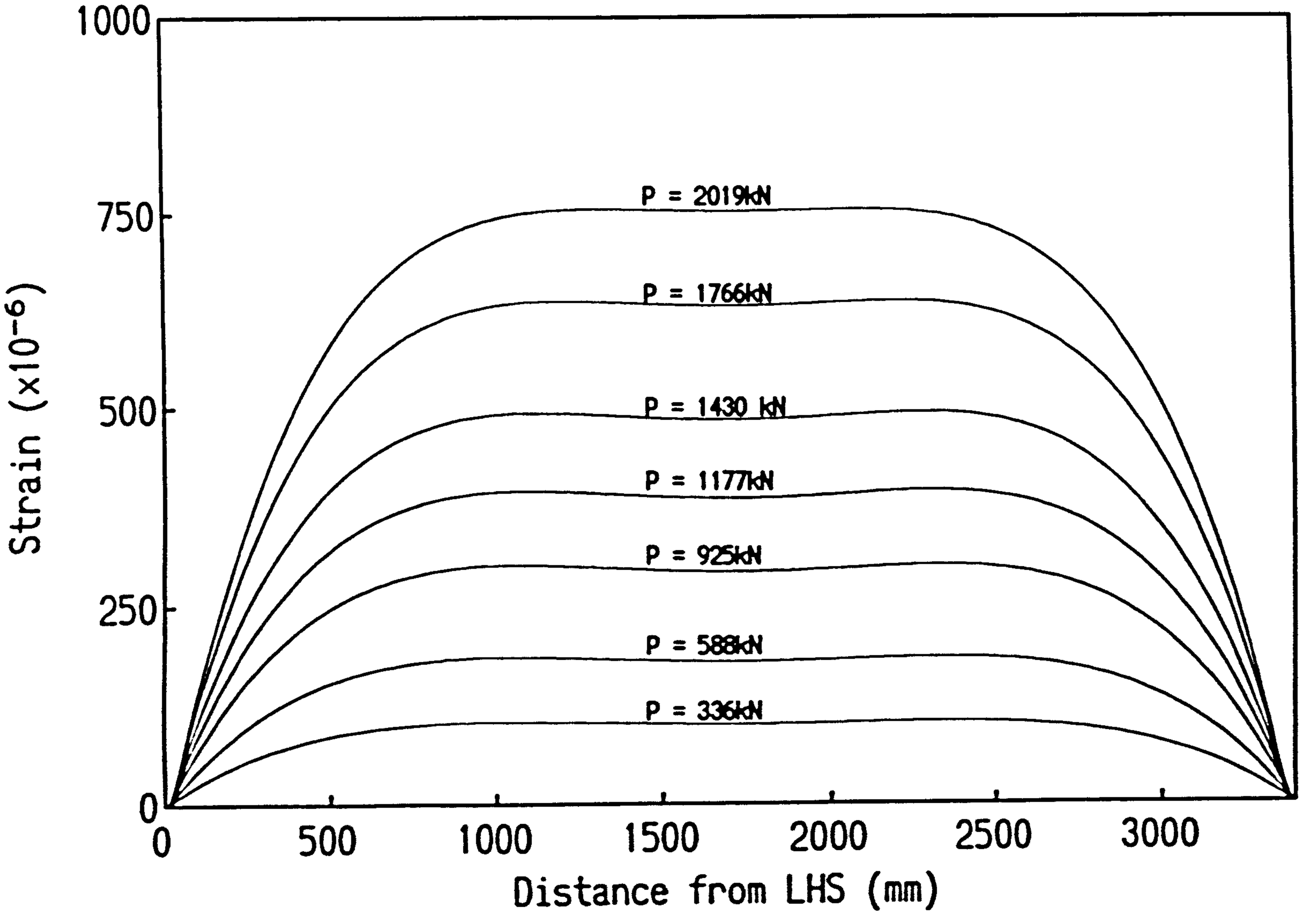
Composite Wall 4
Steel Strain vs Position
Strain (x10-6)
1000
750
500
250
0
P = 2019kN
P = 1766kN
P = 1430 kN
P = 1177kN
P = 925kN
P = 588kN
P = 336kN
0
500
1000
1500
2000
2500
3000
Distance from LHS (mm)

Figure 7.17

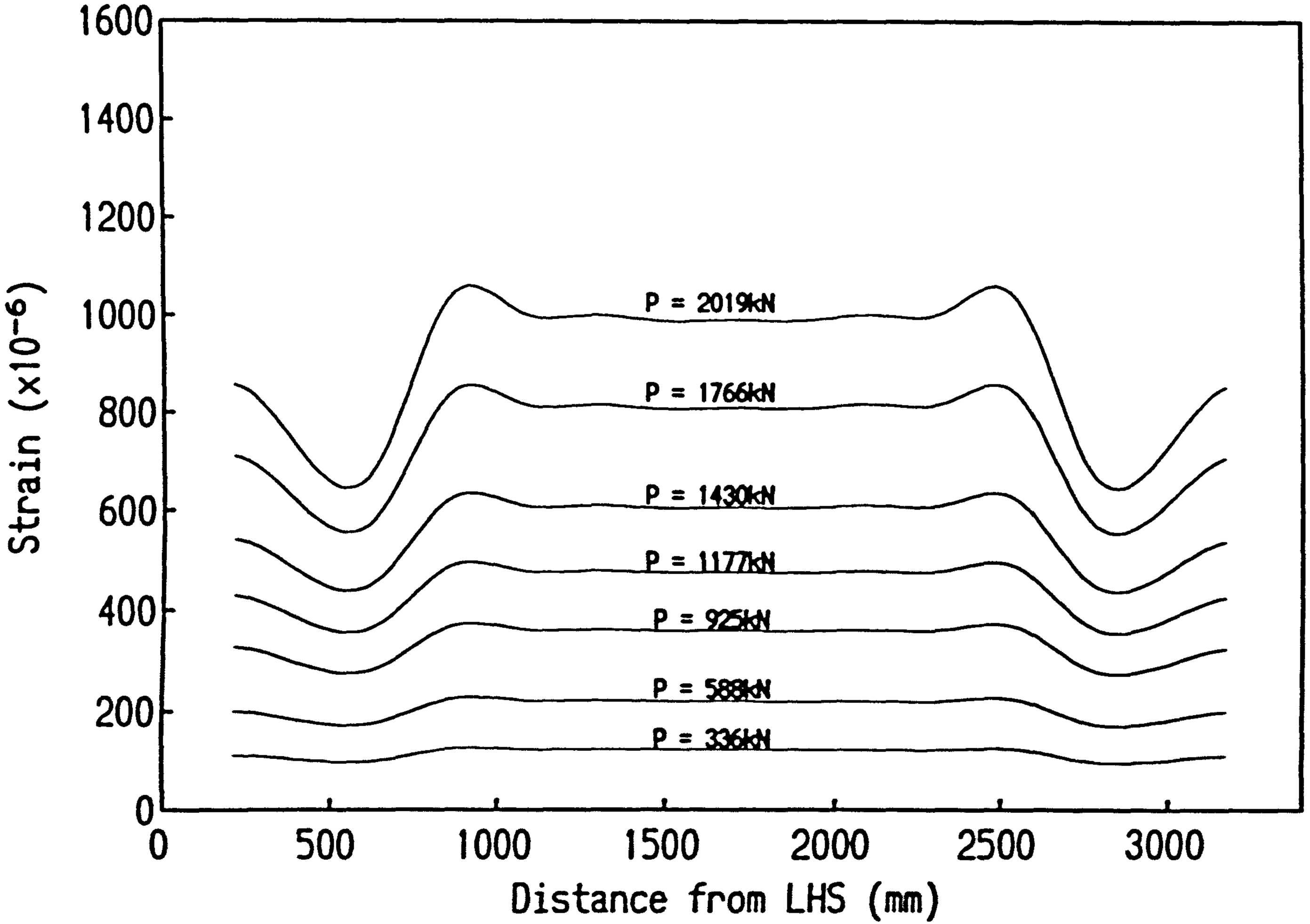
Composite Wall 4
Concrete Strain vs Position
Strain (x10^-6)
Distance from LHS (mm)
P = 2019kN
P = 1766kN
P = 1430kN
P = 1177kN
P = 925kN
P = 588kN
P = 336kN
0
200
400
600
800
1000
1200
1400
1600
0
500
1000
1500
2000
2500
3000

Figure 7.18

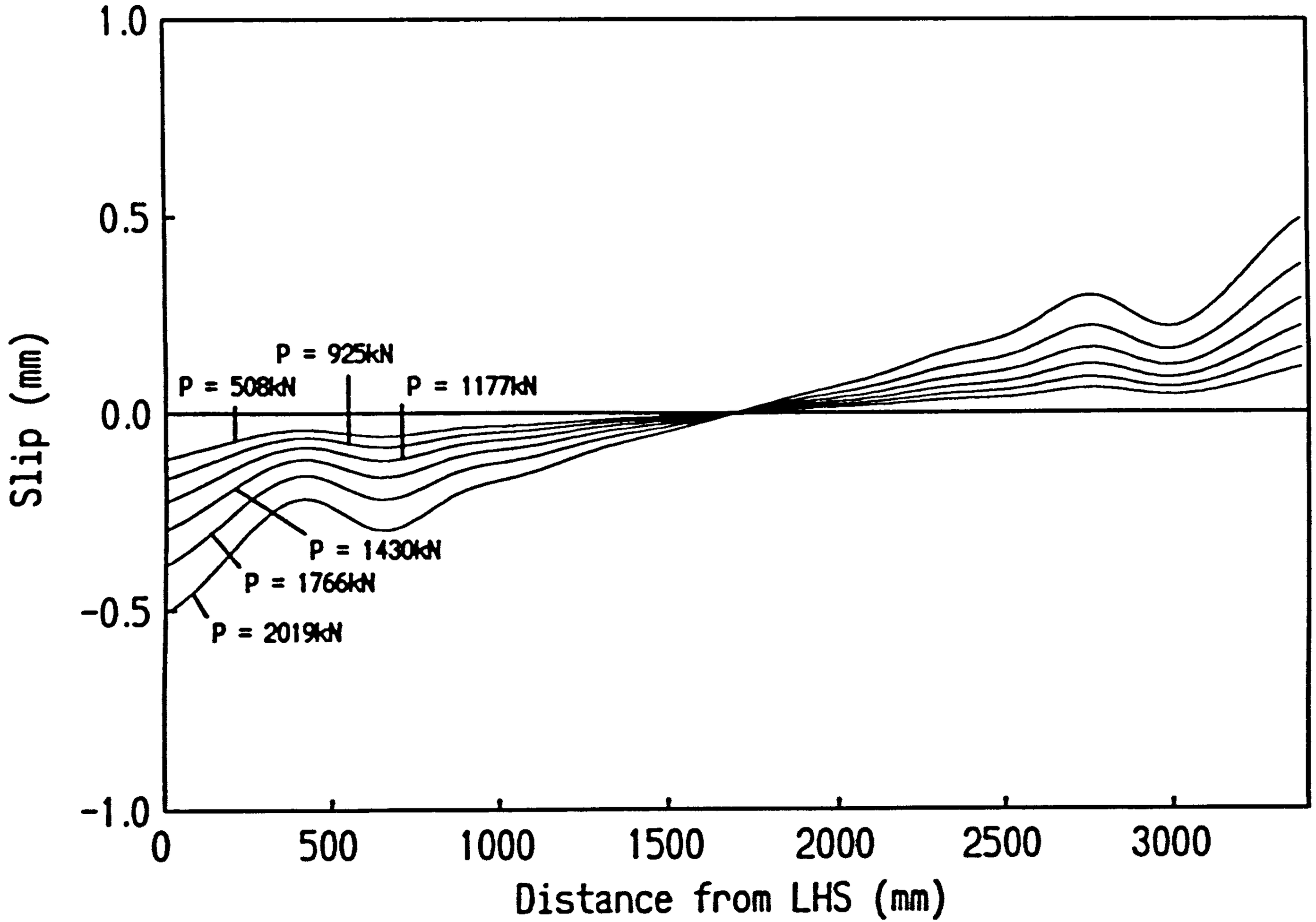
Composite Wall 4
Steel Slip vs Position
1.0
0.5
0.0
-0.5
-1.0
Slip (mm)
P = 508kN
P = 925kN
P = 1177kN
P = 1430kN
P = 1766kN
P = 2019kN
0
500
1000
1500
2000
2500
3000
Distance from LHS (mm)

Figure 7.19

Chapter 8 Design of Double Skin Composite Columns

8.1 Introduction

A possible design method for double skin composite columns, reviewed in Chapter 4, has been proposed by Wright, Oduyemi and Evans (1991) with some supplementary work by Kountoris (1990). They suggested a design method based on the BS 8110 approach but noted that the effect of partial interaction in slender section was unclear with some additional work required.

At present, the design methods for composite columns in the codes of practice are only applicable to concrete filled hollow sections or steel sections encased in concrete. The codes of practice provide design methods accounting for local and global buckling of steel columns and shear failure for concrete columns. The design approach varies between the different codes with the sections are either analyzed as steel sections strengthened by concrete or concrete sections with a special type of reinforcement.

The design of double skin composite columns where interface slip and bond strength are important aspects of design will complicate the estimation of the ultimate strength and buckling capacity.

The purpose of this chapter is to provide some additional design guidance in these slender situations and to suggest possible stud details in axially compressive situations. Also included is a review of the current design methods applied worldwide to composite columns.

8.2 Composite Column Design

The current recommendations for the design of composite columns are contained in the codes of practice for Great Britain, Western Europe, North America, Japan and Australia. The following is a brief review of the approach to design with particular

reference to bond strength and buckling capacity.

8.2.1 Japan (AIJ) Architectural Institute of Japan

The superior performance of composite columns under dynamic earthquake conditions has led to extensive studies by Japanese researchers. Concrete-encased steel columns are normally used in high-rise buildings whereas concrete-filled steel hollow sections are used in underground stations and some buildings. The basis of design is the allowable stress method although the ultimate strength must be evaluated for earthquake resistance. The strength of a cross-section is calculated by superimposing the steel and reinforced concrete contributions with a reduction factor to account for the strain limit in the concrete.

In general, concrete columns in buildings tend to be stocky because of the large lateral forces produced in earthquakes. This has resulted in less consideration of slenderness in design where the Euler buckling load produces a strength reduction factor, R, used with factors of safety on the materials.

$$R = \left(1 - \nu \frac{P}{P_E}\right) \qquad ..8.1$$

where ν is a safety factor.

The width/thickness ratios of steel sections are also limited to specified values. If insufficient bond is present between the steel and concrete in concrete filled sections, direct bearing must be provided at the boundaries.

8.2.2 BS 5400 Part 5 British Standards Institution

The code provisions of BS 5400 are based on limit state design with loading factors and partial safety factors for materials. The ultimate moment is calculated from a plastic stress distribution with an approximation for combined axial load and moment.

In order to take account of slenderness effects the European buckling curves for steel

columns and a dimensionless slenderness parameter are applied in the design. Different curves are used depending on the geometry of the cross-section. The equivalent stiffness of the section E_c is taken as

$$E_c = 450 f_{cu} \qquad ..8.2$$

which accounts for the assumption of an uncracked section and creep.

Where the connection between the steel and concrete is insufficient ($\tau > 0.6N/mm^2$ for encased sections and $\tau > 0.4N/mm^2$ for filled sections) connectors must be provided.

8.2.3 ACI-318-83 American Concrete Institute

The American Concrete Institute applies limit state design with loading factors and capacity reduction factors.

Slenderness is considered by applying moment magnifiers and a reduced Euler load.

$$\delta = \frac{C_m}{(1 - \frac{P}{\phi P_E})} \qquad ..8.3$$

where C_m is the ratio of the equivalent uniform end moment to the numerically larger end moment and ϕ, a strength reduction factor accounting for the variability in the critical load taken as 0.7 for axially loaded tied columns. The equivalent stiffness is found from

$$E_c = 57000 (F_{cyl})^{0.5} \ (lb/inch^2) \qquad ..8.4$$

which gives a higher value than the previous equations as a cracked section is used. Direct bearing must be provided at the connections.

8.2.4 AISC-LRFD-1986 American Institute of Steel Construction

The design method uses the limit state approach with loading factors and capacity

reduction factors. The design of composite columns is based on the design equations for steel columns.

However, when considering slenderness the design equations for composite columns are modified to account for the presence of concrete. Although moment magnifiers are applied, in the case of uniaxial bending the steel buckling curves are used as no minimum eccentricities are specified. The value of equivalent stiffness is calculated from a value of E_c based on a cracked sectional analysis.

$$E_c = w^{1.5}(f_{cyl})^{0.5} \qquad ..8.5$$

where w = unit weight of concrete in lb/ft^3 and F_{cyl} in ksi.

Direct bearing must be provided at the connections.

8.2.5 Eurocode 4

The limit state method is applied with partial safety factors on the materials and covered in section 4.8 of the document. A strength reduction is derived using the European Buckling curves in conjunction with the cross-section interaction curve.

The relative slenderness is calculated from

$$\lambda = \sqrt{\frac{N_{pl.R}}{N_{cr}}} \qquad ..8.6$$

where N_{cr} is the Euler buckling load and $N_{pl.R}$ is the plastic resistance of the section to compression with the partial safety factors for the material properties taken as 1.0. It should be noted that the equation for $N_{pl.R}$ contains values based on the relative slenderness which requires an initial estimate. The value of E_c is based on the secant modulus of the concrete taken from tabulated values.

8.2.6 ECCS Recommendations

The ECCS recommendations are similar to EC4 with the load carrying capacity based on a fully composite action between the steel and concrete sections up to failure. The ultimate load carrying capacity of the column is given by

$$N_k = KN_u \qquad ..8.7$$

where K is a reduction factor dependent on the equivalent slenderness ratio λ and the effective buckling curves for bare steel columns according to the ECCS European Recommendations for Steel Construction. The value of E_c is found from

$$E_c = 600 f_{ck} \qquad ..8.8$$

8.2.7 Conclusions

In the design of composite columns the effect of slenderness is accounted for by either strength reduction (BS 5400 and EC4) or moment magnification (ACI and AISC). Where the interface bond strength is considered insufficient for full interaction direct bearing at the connections must be established. There is no attempt to estimate the effect of partial interaction when a full interface bond is not achieved. This requirement, although necessary for short columns, appears less relevant to slender columns where interface load transfer through bending is more important.

In the following sections the design of double skin composite columns with ductile connectors is considered. Attention is focused on the effect on the buckling capacity of partial interaction under slender conditions, and detailing to provide sufficient bond at the end boundaries.

8.3 Design for Axial Load

In conditions where ductile interface bond is present, ie. where shear studs attach the steel sheeting to the concrete core, the effect of partial interaction requires close attention when dealing with load transfer at the boundaries and the global buckling of the member. The current codes of practice do not consider the effect of a ductile connection at the steel/concrete interface and therefore some possible modifications must be considered.

The work of Chapter 5,6 and 7 suggests that premature failure at the ends of

composite columns is possible particularly when the steel plates are directly loaded with inadequate interface connection to distribute axial load. In design practice the loading arrangments are likely to either transfer load uniformly over the ends, or load the steel surfaces through some intermediate connection.

To overcome this load transfer problem there are two possible options.

In a similar manner to the codes of practice the load may be applied to the column by direct bearing on the steel and concrete boundaries. In this situation only a nominal connection between the steel and concrete faces, preventing local buckling of the steel plate, is required. This allows mobilisation of the full plastic capacity of the section as the steel and concrete strains are approximately uniform throughout. The main disadvantage of direct bearing is that continuous columns are more structurally efficient and cost effective.

Alternatively the axial load directly to the steel surface, as shown in figure 8.1, requires a greater bond capacity for the reasons previously stated. To design this connection one possible method may be to apply the analytic equations derived in Chapter 5 in which linear solutions were derived for various boundary conditions.

One criterion for the design of this connection is to limit the stess at the A (see figure 8.2) to less than the design strength p_y, or buckling stress p_b. For a symmetric loading arrangement, the value of stress may be calculated by manipulating Equation 5.47 so that

$$\sigma_1 = \frac{P}{A_1}\left[1 - \mu \frac{E_2 A_2}{E_2 A_2 + E_1 A_1}\right] \qquad ..8.9$$

From Figure 5.4 the value of μ may be calculated by knowing the value of d_A, the distance from the centroid of the connection to point A. Applying Equation 8.9 gives the value of stress at A which should be less than the p_y or p_b. A check on the concrete stress is not required as the strain in the concrete is always less that in the

steel, for these boundary conditions.

In situation where the connection is located away from the column boundaries then the load should be divided equally between the top and bottom segments (see figure 8.3). Where only a single load acts on the steel surface, Equation 5.59 should be applied as this includes the effects of the eccentricity. The Chapter 5 equations have some drawbacks that should be considered.

Firstly, these equations are based on a linear elastic analysis whereas the stess-strain curve for concrete is non-linear with limit state conditions consistent with BS 8110 normally applied.

Secondly, equations require an estimation of the value of E_c, which varies considerably between different codes of practice.

Finally, the equations assume a continuous connection at the interface although the connection provided by shear studs is discrete. Although this does not have a significant effect on the deflection of beams behaviour at a connection may be different.

Example

Calculate the steel stress produced at d_A = 300mm from the centroid by 2 symmetric axial loads of 270kN acting on a composite column 3000mm in length with cross-section 300mm wide x 600mm deep with 3mm steel plates. The column has a concrete cube strength of 40N/mm^2 and an interface stiffness of 0.2kN/mm^2.

Solution

Taking $E_2 = 450f_{cu}$ gives E_2 = 18kN/mm^2.

If the column is secured at the base then $L_e = 2L_o$ which from Equation 5.41 gives

$$\lambda = 6000\sqrt{\left[\frac{2}{18x1.8x10^5} + \frac{1}{200x900}\right]0.2} \qquad ..8.10$$

$$= 6.67$$

Then, applying figure 5.4 with $\xi = x/L = 300 / 6000 = 0.05$ and $\lambda = 6.67$ gives $\mu = 0.65$.

Therefore, from Equation 8.9

$$\sigma_1 = \frac{270x10^3}{900}(1 - 0.65x0.9) \qquad ..8.11$$

$$= 124.5\ N/mm^2$$

This provides a significant reduction from the stress of 300 N/mm² if no interface bond stength was present.

8.4 Critical Buckling Capacity

8.4.1 Introduction

The choice of design method was between the moment magnification method, used in the American Codes, and those of BS 5400 part 5, also used in the European Codes of Practice.

8.4.2 BS 5400 part 5 Method

Previous work by Oduyemi and Wright (1989) has noted the problem of applying the European Buckling Curves to these Composite Columns, since the steel plates act compositely and by themselves are not axial load carrying. It was therefore suggested that the method of BS8110 was more appropriate with the plates considered as external reinforcment.

The problem of applying the European buckling curves to these composite columns may be overcome by applying Equation 5.36 instead of the Euler Equation, which includes the effect of partial interaction at the interface. The buckling curve b may then be used to calculate k_l and therefore the critical load. If the value of interface

stiffness is large then the steel plates essentially behaves as a welded box section without web plates. If the value of interface stiffness is small then they behave as independently with bending about their own centroids.

8.4.3 Moment Magnification

The application of partial interaction in the calculation of moment magnification is a more convenient and direct method than applying European buckling curve approach. In these recommendations composite columns are considered as externally reinforced concrete columns in contrast to the steel sections supported by concrete approach of the European recommendations.

In the design equations proposed by ACI, the Euler Buckling load, P_1, can be replaced by equation 5.36 thus increasing the value of the additional moment considered in the design especially where poor interaction is present. In the case of concentric axial loads an initial eccentricity of $e_{min} = 0.6 + 0.03H$ (inches) according to the ACI standard may be applied.

8.4.4 Design Example

a) Calculate the applied moment from slenderness considerations imposed on a 300mm x 300mm double skin composite column 7.5m in length with 6mm steel plates, subject to an axial load and initial moment of 2000kN and 100kNm respectively, and

b) Calculate the type of load application required.

The section has properties : f_{cu} = 40N/mm^2, p_y = 270N/mm^2 with an interface stiffness of 0.1kN/mm^2. Taking $E_c = 450f_{cu}$ gives Ec = 18kN/mm^2

Applying equation 5.36 gives the critical load of 3858kN compared to the Euler load for the fully composite section of 4974kN.

Minimum eccentricity = 15.2 + 0.03 * 300 = 24.2mm

Minimum Moment = 24.2×10^{-3} * 2000 = 48.4 kNm < 100kNm

Applying the moment magnifier design method gives

$$M_{max} = \frac{C_m M_o}{1 - (\frac{P}{P_{crit}})}$$

$$= \frac{1 x 100}{1 - (\frac{2000}{0.7 x 3858})}$$

$$= 385.5 kNm$$

The value of λ calculated from equation 5.41 gives

$$\lambda = 15 x 10^3 \sqrt{(\frac{2}{18 x 9 x 10^4} + \frac{1}{200 x 1.8 x 10^3}) 0.1}$$

$$= 9.50$$

which from figure 5.4 at no position achieves full interaction.

In this case where the interaction is very low, the steel and concrete at the boundaries of the column should be subject to direct bearing from adjacent elements.

8.5 Summary

The methods developed from the analytical analysis of double skin composite columns provide an estimation of the effects of partial interaction on the load transfer at connections and the global buckling of double skin composite columns. Although these equations are suggested further experimental work is required to verify their effect particularly in the case of the load transfer problem at the interface.

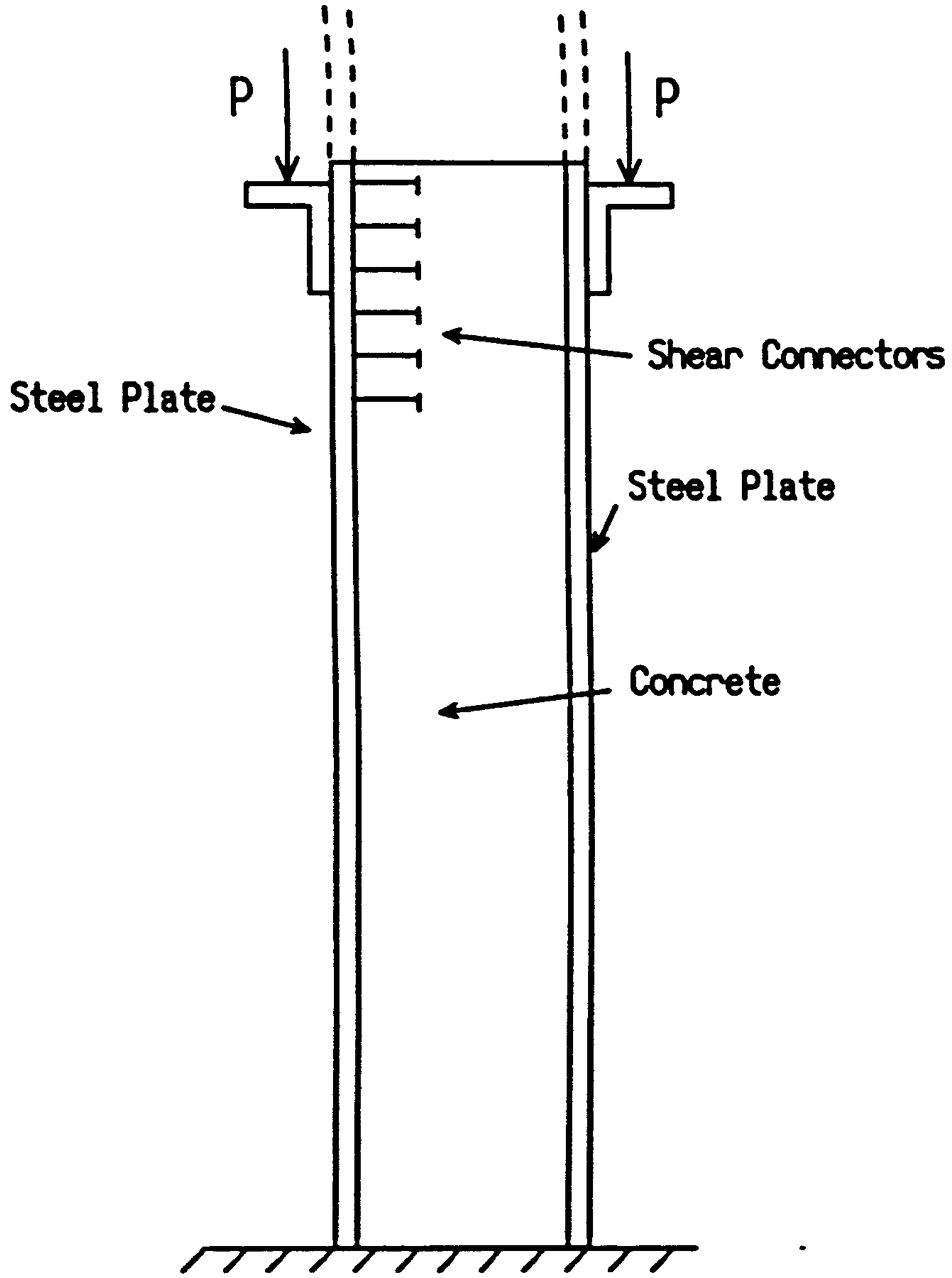

Loading Position (high bond)

Figure 8.1

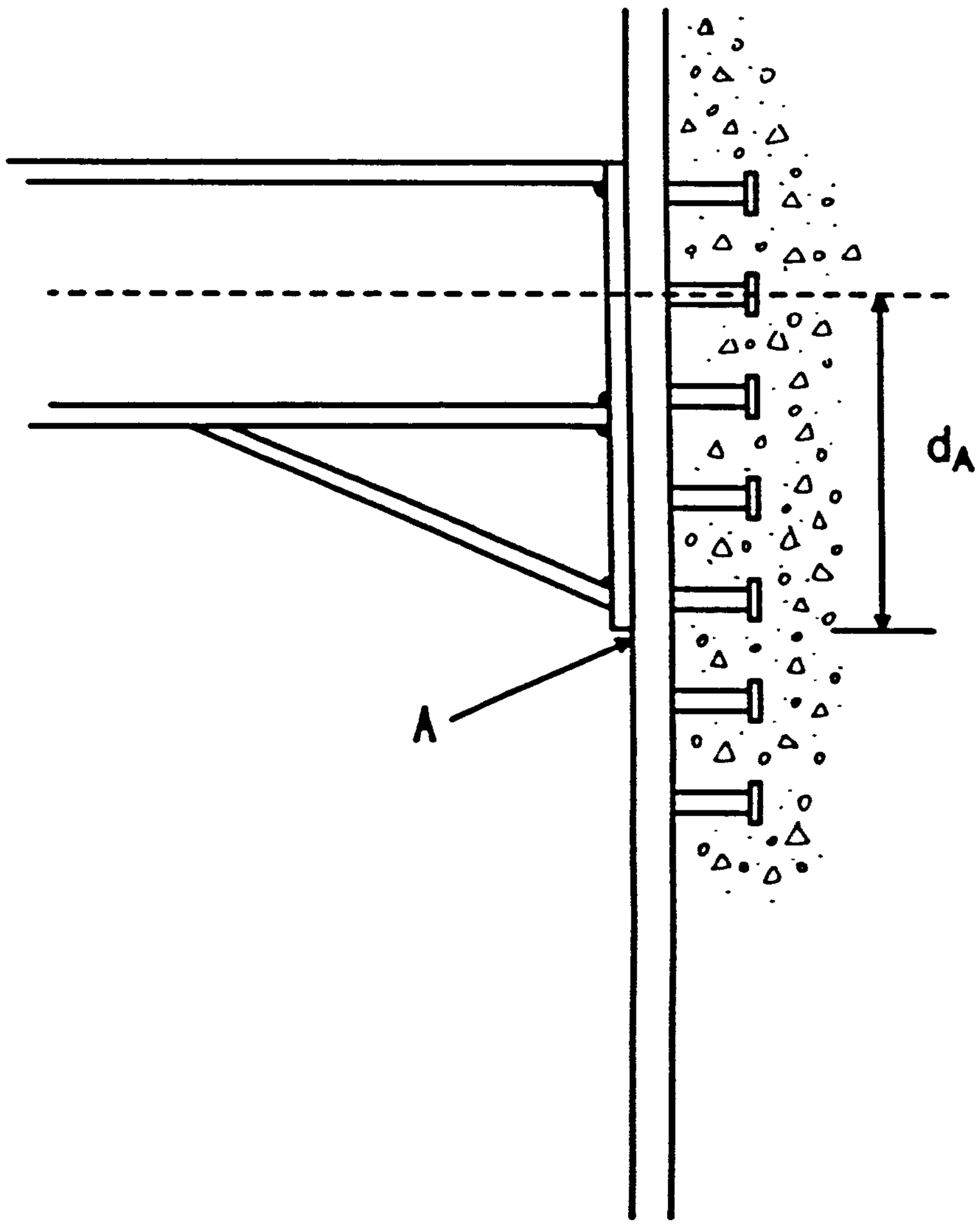

Connection Detail

Figure 8.2

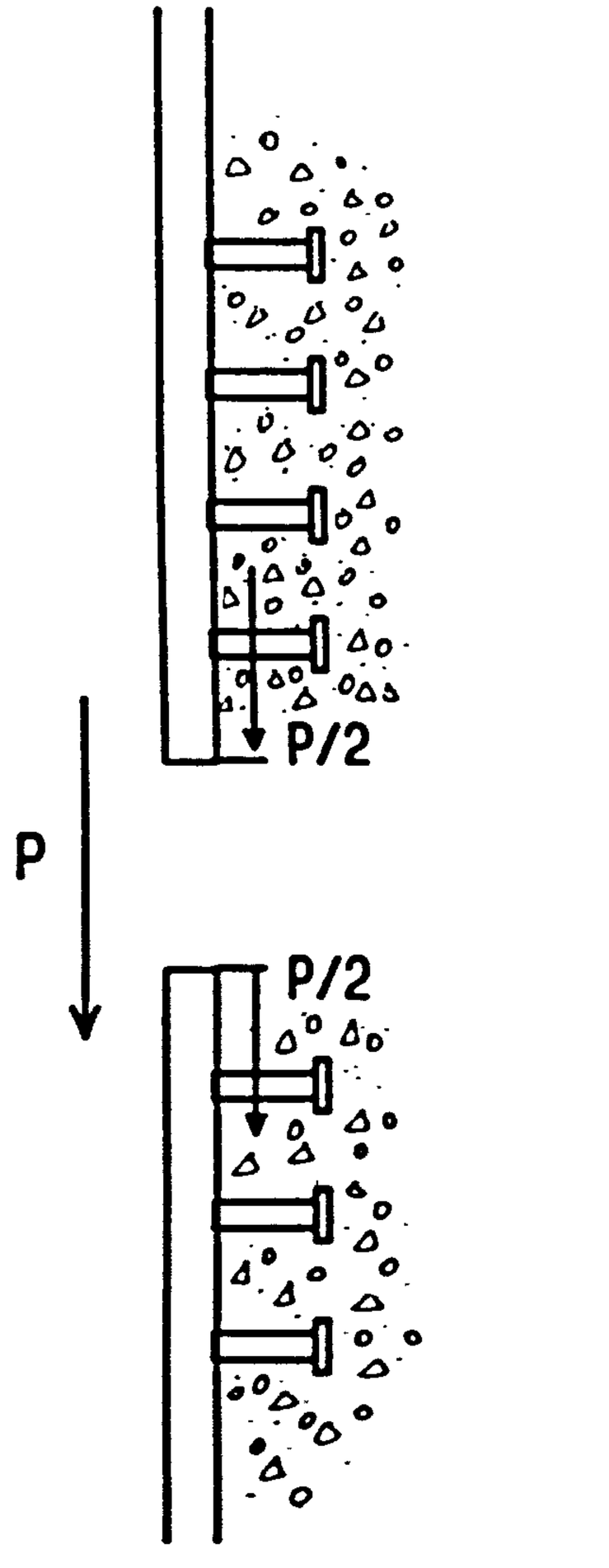

Intermediate Connection

Figure 8.3

Chapter 9 Design of Composite Wall with Profiled Steel Sheeting

9.1 Introduction

The experimental full-scale tests, numerical and analytic studies investigating the behaviour of composite walls revealed several complications that must be accounted for if design recommendations are to be formed.

For design purposes the strength of these walls will have an upper bound on performance similar to reinforced concrete walls and a lower bound similar to plain concrete walls.

There would appear to be no reason at present for the walls not to be designed as plain walls ignoring the beneficial effect of the sheeting as external reinforcement. Ideally, the steel sheeting should be taken into account to achieve a higher level of performance. In this case any appropriate design method must consider the additional effects of local buckling and interface slip of such an element.

In the following section a design method is proposed, modified from the current requirements of BS 8110 allowing the external steel reinforcement to be considered structurally, resisting loads at the ultimate limit state. The design ultimate resistance of the walls is also compared to results from DSCW with the relevant material and load factors.

9.2 Experimental and Theoretical Investigations

9.2.1 Introduction

The current experimental work investigating the ultimate failure loads of the walls was described in Chapter 4. Axial loads were generally applied directly to the surface of the concrete without direct bearing on the steel boundaries. In traditional reinforced concrete columns and walls the reinforcement bars normally terminate

below the top of element which allows for sufficient tolerances in the cutting of the bars. Applying the same method to the design of walls with profiled steel sheeting prevents discontinuities in the steel boundary with loaded and unloaded sections.

The results of these tests suggested that the two main areas affecting the structural performance of the composite walls are the interface bond behaviour and local buckling of the steel sheeting between the ribs.

9.2.2 Interface Bond Behaviour

The interface behaviour between the steel and concrete surfaces appeared on the evidence of the experimental investigation to be extremely brittle with a complete loss of bond occurring between the surfaces at loads below ultimate failure. The implications of this behaviour would have prevented the sheeting from consideration in the ultimate strength design. Once the bond was broken the steel strains reduced to zero and would therefore give no subsequent strength contribution to the section in compression or tension. It therefore appeared that the walls could only be safely designed as plain concrete walls with the profiled steel sheeting only acting as permanent formwork after the casting of the walls.

The subsequent numerical studies performed using a ductile interface model based on the Cofrastra Decking, possessing a similar performance to the Superholorib decking, suggested that the initial conclusions drawn for the experimental investigation may have been wrong. The numerical investigation carried out in chapter 7 suggested that the interface strains produced in axially loading the walls were not sufficient to produce the much stronger ductile bond observed in situations with higher strains, such as in flooring applications.

In composite floors the average strain at the lower concrete surface is likely to be approximately -0.01 compared to the maximum strain in the upper surface of 0.0035 at failure. The general behaviour under the loading of composite slabs is different to composite walls. In slabs the only resistance to the tensile forces produced under

bending is from the composite decking. When the slabs are loaded and chemical bond failure results, this produces further slippage until the ductile mechanical interlock bond re-establishes equilibrium. In walls, the concrete and steel together resist the axial loading. When chemical bond failure occurs the new equilibrium point is determined by the combined response of the concrete and the decking. In the current investigation the concrete supported the greatest proportion of the axial load as the additional strains produced were not sufficient to mobilise the mechanical interlock bond.

The analytic studies of double skin composite elements performed in Chapter 5 investigated the transfer of load between the steel and concrete elements where an axial load is only applied at the concrete boundary. These studies suggested that at a specific distance from the boundary, dependent on the interface stiffness, the strains between the steel and concrete were equivalent. It was suggested that by increasing the bond and bar reinforcing the concrete over this length, a full interaction could be achieved for the section as a whole.

In the third and fourth experiments into wall behaviour mesh welded to the decking surface and reinforcing bars were applied in order to obtain a better bond with the concrete surface. The reinforcement at the top of the wall permitted the load to be shed into the steel decking without failure over this transfer distance. The numerical studies considered the effect of reinforcing the ends of the walls and showed that at the point where the reinforcing ends there was a large increase in the interface slip. This was due to the increased effective stiffness of the reinforced concrete section over a plain section.

9.2.3 Local Buckling

Local buckling of the steel sections between the re-entrant ribs was observed in the experimental investigation particularly where additional bond was provided at the top and bottom of the walls. The effect of the local buckling was to reduce the load carrying capacity of the steel decking and therefore the failure load of the composite

section.

Neither the analytic studies of chapter 5 or the numerical investigation of chapter 6 included local buckling explicitly in the formulation of the problem.

9.2.4 Discussion

The experimental investigation, analytic and numerical studies have revealed a number of factors that any proposed design method must deal with for a satisfactory and safe design.

The design method must consider the brittle interface behaviour under low strains primarily at the compression face and the tendency for concrete failure to occur close to the element boundaries before strains are equivalent across the sections. Local buckling of the steel sheeting although dependant on the efficiency of the bond is likely to effect the performance of the sheeting in the majority of situations and must be considered. The following sections details a possible design method suitable for engineering practice.

9.3 Design Methodology

Ideally, in circumstances where local buckling and bond failure were prevented, the walls could be designed according to the method of BS 8110 for combined axial and bending moments. This would produce a response as shown in figure 9.1 with the concrete and steel strengths fully mobilised over the full length. This interaction diagram was constructed applying the following equations

$$N = 0.45 f_{cu} b d_c + f_{st} A_{st} - f_{sb} A_{sb} \qquad ..9.1$$

$$M = 0.45 f_{cu} b d_c \left[\frac{h}{2} - \frac{d_c}{2}\right] + f_{st} A_{st} \left[\frac{h}{2} - d_t\right] + f_{sb} A_{sb} \left[\frac{h}{2} - d_b\right] \qquad 9.2$$

with the procedure

1. A value of x/h was assumed.
2. d_c was calculated from $d_c = 0.9x$.
3. The values of strain for the top and bottom reinforcement were calculated based on a concrete strain of 0.0035 on the compression face.
4. The steel stress were calculated from the strains under the condition that

$$f_{st} = E_s f_{st} \leq 0.87 f_y$$
$$f_{sb} = E_s f_{sb} \leq 0.87 f_y \qquad ..9.3$$

5. N and M were calculated using the values of x, fst and fsb to produce a point on the interaction diagram
6. Steps 1 to 5 were then repeated with a different value of x/h until the interaction diagram was completed.

In normal designs a minimum eccentricity of the axial load such that

$$e_{min} = 0.05h \qquad ..9.4$$

is normally shown on the design charts diagrams. The area of the diagram between the load axis and this line is void for design purposes.

In circumstances where the interface bond was insufficient to be considered in design, the overall element behaviour would be similar to that of plain concrete, a large reduction from the reinforced concrete envelope. A similar interaction curve was calculated for an unreinforced concrete section by the previous method excluding the reinforcement bars.

The interaction curve for a composite wall will be located in the region between the plain concrete and reinforced concrete interaction curves. The greater the level of interaction achieved at the interface the closer the interaction curve will come to that of reinforced concrete whilst the poorer the interaction, the closer the curve will come to that of a plain concrete section. This assumes that the effect of local buckling is negligible and implies that the stress in the steel can achieve the yield

stress and greater. In general, the closer the behaviour of composite to internally reinforced wall the greater the performance and benefit in utilising the idea in engineering practice. If an engineer is given the choice between a system that gives both permanent formwork and the reinforcement and one that only provides the reinforcement, in normal circumstances the former will be chosen from a cost basis. Unfortunately, the full-scale tests have shown that the composite walls are not equivalent to similar reinforced walls as interface bond failure and local buckling are further restrictions on the capacity.

9.3.1 Interface Bond

The current investigation has shown that the steel concrete interface bond cannot be relied upon in compressive situation as the interface strains are not sufficient to mobilise the strong ductile response. As a result, it is this authors opinion that until further studies are performed with other profiles, the strength of the steel decking in compressive situation must be assumed negligible and not included in the design equations.

This condition implies that under a concentric axial load the capacity of the walls is determined by the compressive strength of the concrete with no contribution from the external steel sheeting. The other result is to make unnecessary any local buckling check on the profiled steel sheet at the ultimate state. The condition has not been applied to the steel decking when in tension as the average strains on the tension face are greater than on the compressive face allowing a full bond to be developed.

9.3.2 Local Buckling

As mentioned previously, the effect of allowing no compressive forces in the steel decking makes unnecessary any local buckling check on the steel sheeting. In situations where sufficient bond is mobilised, the axial resistance of the steel sheeting may be calculated using the BS 5950 Pt 4 : 1982 recommendations reducing the effective cross-sectional area of the sheeting depending on the width and thickness

across the flat portions.

9.3.3 Connection Details

In composite slabs with profiled steel sheeting the problem of end moments is not encountered with the slab or beam designed to resist uniformly distributed loads imposed between the supports. Unless the composite walls are considered to only carry simply supported loads then some method of allowing end moments must be devised.

The proposed detail, shown in figure 9.2, is to reinforce the ends of the element with internal reinforcement capable of resisting this end moment and design for the bar reinforcement to carry the moment at the end of the element and the profiled steel decking to carry the moment at the point where the reinforcement terminates. In order that shear bond failure does not occur at this point a check should be applied to determine the maximum stress that the steel decking can carry based on the shear bond capacity of the decking over the length l_b. Normally the bond capacity ranges from $0.05N/mm^2$ for brittle decking to $0.3N/mm^2$ for more ductile decking geometries. In the case of the Superholorib profile a shear bond strength of approximately $0.2N/mm^2$ can be expected.

The possibility of fixing the reinforcement bars to the steel decking has been considered. This would provide a full bond between the steel and the concrete and perhaps allow full mobilisation of the steel decking but would create construction problems and be costly. The main difficulties would be in assembling the steel decking around the starter bars from the pad foundation with sufficient tolerances in the welds to attach additional sections.

9.4 Design Details

9.4.1 Introduction

The proposed design is similar to that of BS 8110 with a moment-axial load

interaction curve formed based on the particular profile used in the design instead of various levels of reinforcement. Additional consideration modifies the interaction diagram by considering the bond length, l_b, and the effect of this failure mode on the design bond stress, p_b, at the ultimate limit state.

9.4.2 Design Bond Stress

The experimental investigation by Daniels suggests that the average bond stress at failure of the Superholorib profiled steel decking is approximately 0.2N/mm^2. Considering the length from the point at which the internal reinforcement terminates to the end of the element, L_b, leads to an expression for the design strength of the sheeting

$$p_b = \frac{L_b f_b b_s}{A_s \gamma_m} \leq 0.93 p_y \quad (N/mm^2) \qquad ..9.5$$

where L_b = shear bond length (mm)

f_b = ultimate bond capacity (N/mm^2)

b_s = total width of sheeting (mm/m width)

A_s = area of sheeting (mm^2/m width)

γ_m = partial safety factor for this type of failure

p_b = design bond strength (N/mm^2)

p_y = design yield strength (N/mm^2)

This equation provides an additional constraint on the design strength of the walling similar to the anchorage length requirements for reinforcement bars. The critical section for bond failure will be where the reinforcing bars terminate excluding the anchorage length.

9.4.3 Modification to Axial Capacity

The effect of neglecting the compressive resistance of the steel decking is to reduce the maximum strength of the cross-section to the concrete capacity such that

$$N_{max} = 0.45 f_{cu} A_c \qquad ..9.6$$

applicable for a concentric axial load without the minimum eccentricity condition.

9.4.4 Modifications to Interaction Diagram

The modified interaction diagram taking account of interface bond strength is given in figure 9.3. Each curve is based on a different value of p_b/f_{cu}. The curve is formed in a similar way to 9.1 with some additional conditions.

1. A value of x/h was assumed.
2. d_c was calculated from $d_c = 0.9x$.
3. The value of strain for the top and bottom external reinforcement should be calculated based on a concrete strain of 0.0035 on the top compression face.
4. The steel stresses were calculated from the strains under the condition that

$$f_{st} = E_s \epsilon_{st} \leq p_b \leq 0.93 p_y \leq 0 \qquad ..9.7$$

$$f_{sb} = E_s \epsilon_{sb} \leq p_b \leq 0.93 p_y \leq 0 \qquad ..9.8$$

with p_b calculated from equation 9.5.

5. N and M were calculated using the values of x, f_{st} and f_{sb} to produce a point on the interaction diagram
6. Steps 1 to 5 were repeated for various values of x/h until the interaction diagram was completed.
7. The value of L_b is varied and steps 1 to 6 are repeated.

The resulting curves show that with the condition $p_b/f_{cu} = 0$ the response of the section to combined axial loads and moments is equivalent to that of plain concrete.

As this value increases a condition is reached where the steel achieves yield before bond failure occurs. At this point any further increase in p_b will have no effect on

the load carrying capacity.

9.4.5 Single Element Design Method

The design of the composite walling element can be divided into a series of checks performed at critical sections on the element. These critical sections are likely to be positioned, as shown in figure 9.4, at

A. the boundary of the section where concrete with bar reinforcement transfer the axial load and moments into adjacent sections.

B. the level at which the bar reinforcement terminates and the strength depends on the concrete and steel decking

C. the position of maximum moment in the central portion of the element.

The design method may be split into a series of stages:

1. The thickness of the wall element is estimated.

2. Section A is designed and based on the standard column interaction charts. The bond length required to carry the applied loads is calculated from the BS 8110 code provisions.

3. Section B is checked using the interaction diagram for the particular thickness. The bond length of the anchorage for the bar reinforcement is equivalent to the bond length for the steel decking.

4. Section C is checked using the interaction diagram and a new bond length.

9.5 Design Example

In order to illustrate the design method in a typical application the following

example was produced.

Design a braced composite wall to resist the a factored moments and axial loads shown in figure 9.5. The element is to be designed with fcu = 40 N/mm^2 and a nominal cover of 25mm. The wall has a cross-section 3000mm by 200mm thick with a height of 3500mm. The external reinforcement will be Superholorib decking 0.9mm thick with a cross-sectional area 1550mm2 /m width.

Solution

BS 8110 Cl.3.8.1.3

Effective height of element = 3500 x 0.75 / 200 = 13.12 < 15

Therefore, design as short column

Section A - Column Design Chart BS8110

$N/bh = (1600x10^3)/(1000 \times 200) = 8.0$

$M/bh^2 = (96x10^6)/(1000 \times 200^2) = 2.4$

Minimum Steel Reinforcement 0.4% required

Use T10 diameter bars at 150mm^2 c/c

Bond length required 32 x dia. = 320 mm

Section B - Composite Wall Design Chart Fig 9.3

Calculate Strength at a distance of 1000mm from end.

$N/bhf_{cu} = (1600x10^3)/(1000 \times 200 \times 40) = 0.2$

$M/bh^2f_{cu} = (120x10^6)/(1000 \times 200^2 \times 40) = 0.075$

So, $p_b/f_{cu} = 4.3 \rightarrow p_b = 172$ N/mm^2 < $0.93p_y = 260.2$N/mm^2

The end reinforcement length required L_b can be calculated from

$L_b = p_bA_s\gamma_m/f_bb_s = (172 \times 1550 \times 1.25) / (0.2 \times 1722) = 968$mm

Therefore, the bond length is satisfactory

Section C - Composite Wall Design Chart Fig 9.3

Calculate Strength at a distance of 2000mm from end.

$N/bhf_{cu} = (1600x10^3)/(1000 \times 200 \times 40) = 0.2$

$M/bh^2f_{cu} = (130x10^6)/(1000 \times 200^2 \times 40) = 0.0812$

So, $p_b/f_{cu} = 6.0 \rightarrow p_b = 240\ N/mm^2 < 0.93p_y = 260.2N/mm^2$

The end reinforcement length required L_b can be calculated from

$L_b = p_bA_s\gamma_m/f_bb_s = (240 \times 1550 \times 1.25) / (0.2 \times 1722) = 1350mm$

Therefore, the bond length is satisfactory and within the ultimate limit.

Similarily design reinforcement at the base of the wall.

9.6 Slenderness Considerations

The current recommendations dealing with slender reinforced concrete elements are based on work by Cranston at the Cement and Concrete Association. He showed that the curvature at the critical section could be assumed to depend on the effective height/depth ratio giving

$$\frac{1}{r_m} = \frac{1}{175h}\left[1 - 0.0035\frac{l_e}{h}\right] \qquad ..9.9$$

where l_e is the effective length of the element and h the depth in the direction of bending. Cranston suggested that the additional moment for different loading conditions could be approximated by

$$e_{add} = \frac{1}{10}l_e^2\left(\frac{1}{r_m}\right) \qquad ..9.10$$

Combining equations 9.9 and 9.10 gives

$$e_{add} = \frac{h}{1750}\left[\frac{l_e}{h}\right]^2\left[1 - 0.0035\frac{l_e}{h}\right] \qquad ..9.11$$

BS 8110 simplifies this equation to

$$a_u = \frac{1}{2000}\left[\frac{l_e}{b'}\right]^2 h \qquad ..9.12$$
$$= \beta_a h$$

The additional moment added to the initial moment is then taken as

$$M_{add} = N\beta_a kh \qquad ..9.13$$

where k is a reduction factor taken conservatively as 1 or found from

$$k = \frac{N_{uz} - N}{N_{uz} - N_{bal}} \qquad ..9.14$$

where N is the ultimate axial load, N_{bal}, the axial load for balanced failure and N_{uz}, the capacity of the element under a pure axial load.

The original formulation of the curvature was based on balanced failure with the concrete and steel failing at 0.0035 and 0.002 strain respectively. The value of k takes into account the fact that as the value of axial load increases the curvature at failure and the steel tensile strain decrease until at $N = N_{uz}$ the additional moment is theoretically zero.

In order to apply the BS 8110 slenderness recommendation to the design of composite walls some adjustments to the reinforced concrete equations are required to account for greater curvatures at failure due to interface slip and the reduction in axial capacity.

9.7 Slender Composite Walls Recommendations

For a wall to be considered slender the span/depth ration must be greater than 15 for braced, and 10 for unbraced columns. In normal circumstances the composite walls will not be less than 200mm thick giving a height of 3000mm before slenderness is considered.

In order to take account of slenderness it is proposed that the additional eccentricity be taken as

$$a_u = \frac{1}{1500}\left[\frac{l_e}{b'}\right]^2 h \qquad ..9.15$$

resulting in 33.3% increase in M_{add} compared to an equivalent reinforced concrete element. The addition allows for the greater curvatures present in composite elements at the ultimate failure load.

As the ultimate axial load is based on the concrete strength it is likely that crushing failure of the element will occur at greater values of slenderness than the equivalent reinforced concrete element because of the reduced axial compressive strength.

9.8 Local Buckling of Profiled Steel Sheeting

Although the decking has been neglected in compressive situations by welding mesh or otherwise increasing the bond it may be possible to permit some compressive resistance. In situations where adequate bond is developed at the interface, the steel strain may be sufficient to locally buckle the steel decking between the re-entrant ribs.

There are currently two codes of practice that are relevant in determining the capacity of the profiled steel sheets in axial compression - BS 5950 Pt 4 : 1982 on the design of composite floors with profiled steel sheeting and BS 5950 Pt 5 : 1979 on design in cold formed sections.

The local buckling encountered in profiled steel floors is a result of loads applied when the profile acts as permanent formwork. Although the code gives effective flange and web areas for application in design it also states that 'it may be more appropriate to determine section properties by testing' (BS 5950 Pt 4 Cl 15).

In the case of an compression flange that extends between the webs of adjacent troughs, the effective width to be considered in design is given by

$$b_{es} = \frac{828\,t}{\sqrt{p_y}}\left[1 - \frac{181\,t}{b\sqrt{p_y}}\right] \qquad ..9.16$$

where b is the section width, p_y, the yield strength, and t, the thickness of the plate. Other equations exist where intermediate stiffeners are positions over the width and at free edges.

Although welding mesh increased the bond strength at the interface resulting in local buckling of the steel sheeting it increased the construction time of the sheeting and so may be an unsatisfactory solution for design practice.

9.9 Summary

A basic design method based on the requirements of BS 8110 has been proposed with some modifications based on the experimental, analytic and numerical investigations of composite walls. The major drawback of this method is the significant reduction in the axial capacity of the walls by neglecting the resistance of the steel decking in compression although, in tension the steel decking is assumed to be fully mobilised. Further tests are obviously required to obtain further information on the interface behaviour especially in combined axial and bending situations. It should be noted that a yield strength of 280 N/mm^2 is specified for the Superholorib decking which compared to the yield strengths of Type 2 deformed bars at 460N/mm^2 is a significant reduction.

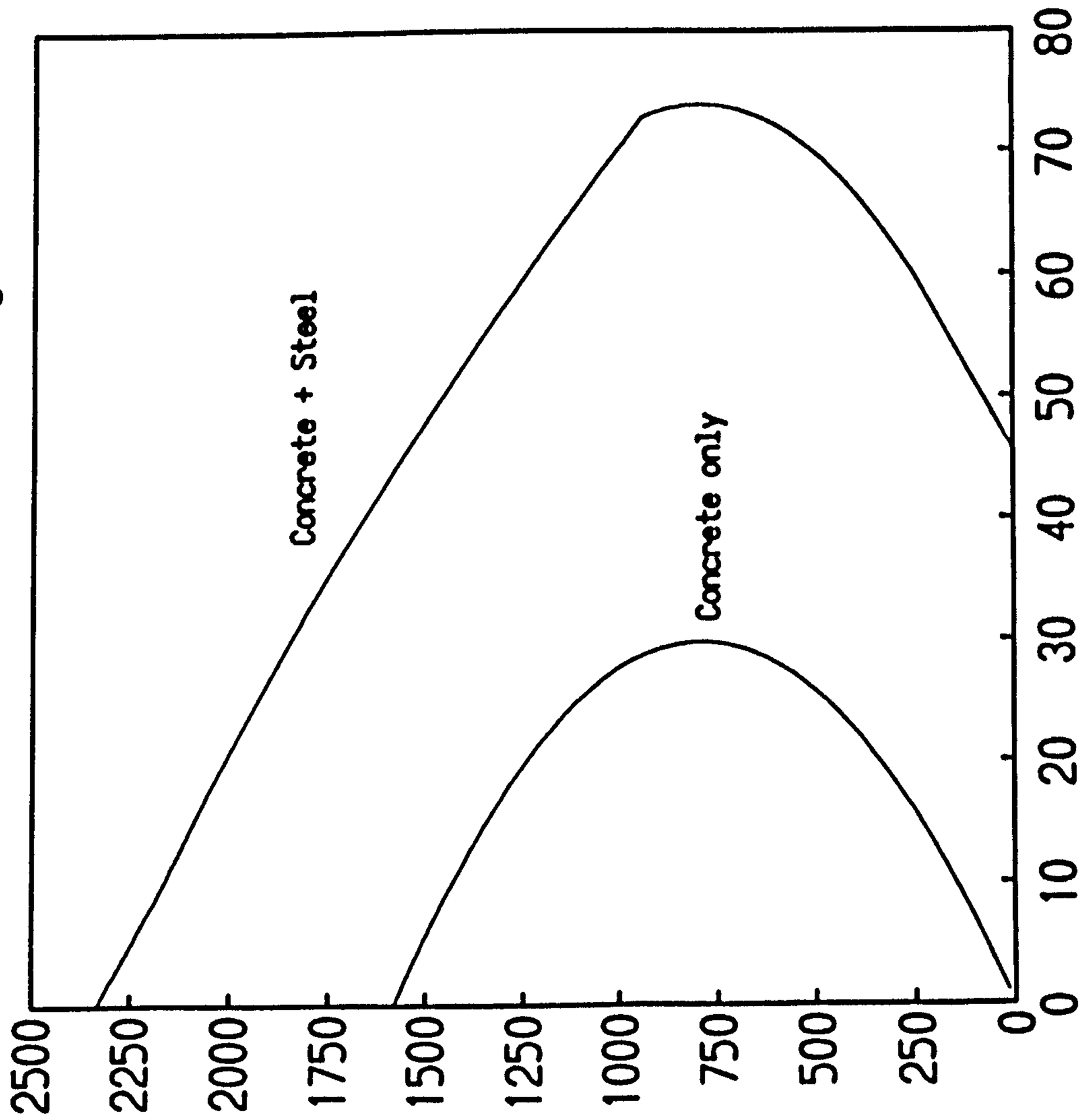
Column Interaction Diagram
Axial Load (kN)
2500
2250
2000
1750
1500
1250
1000
750
500
250
0
Concrete + Steel
Concrete only
0
10
20
30
40
50
60
70
80
Bending Moment (kNm)

Figure 9.1

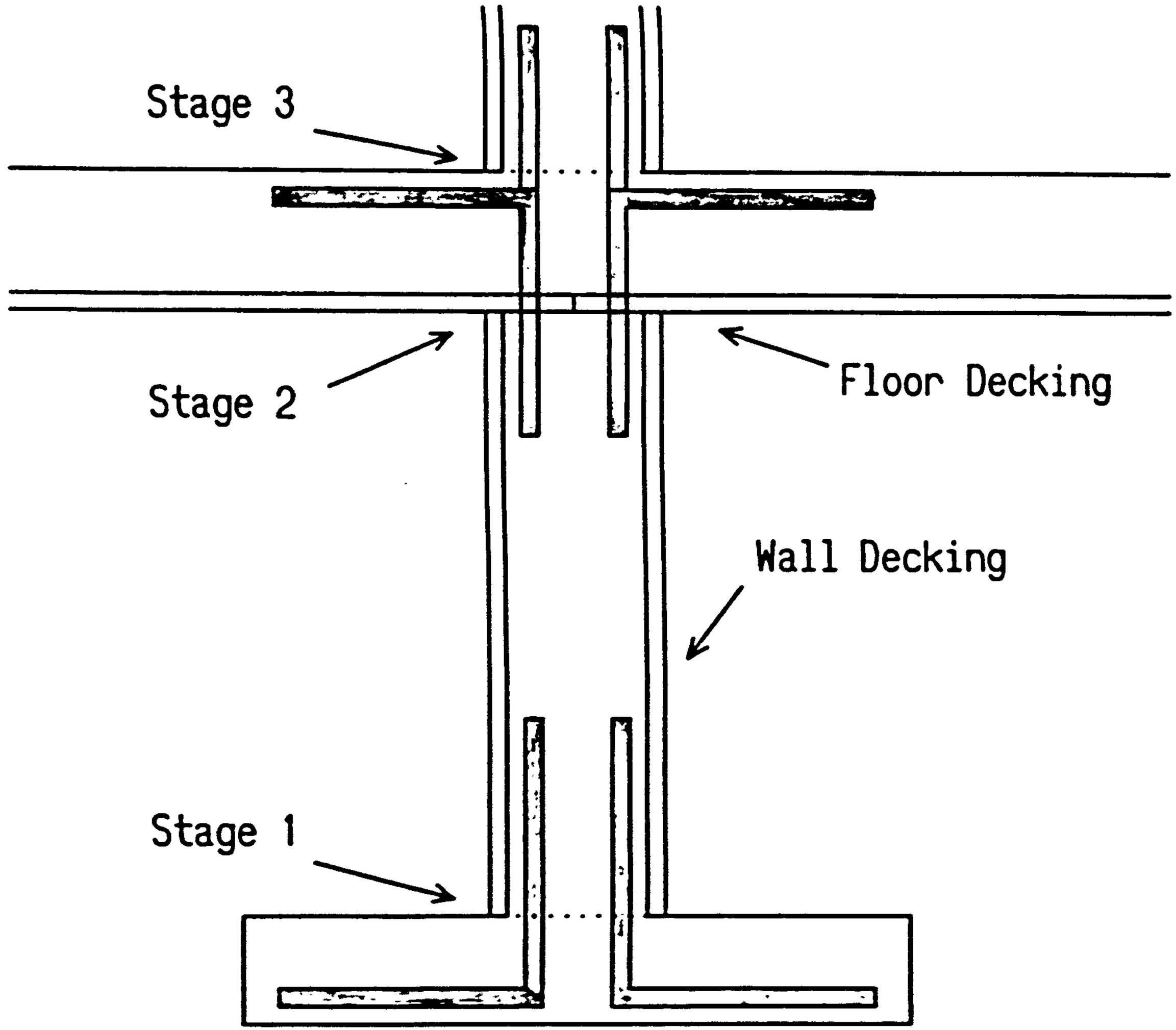

Single Bay Reinforcement Details

Figure 9.2

Column Design Chart
Superholorib Decking

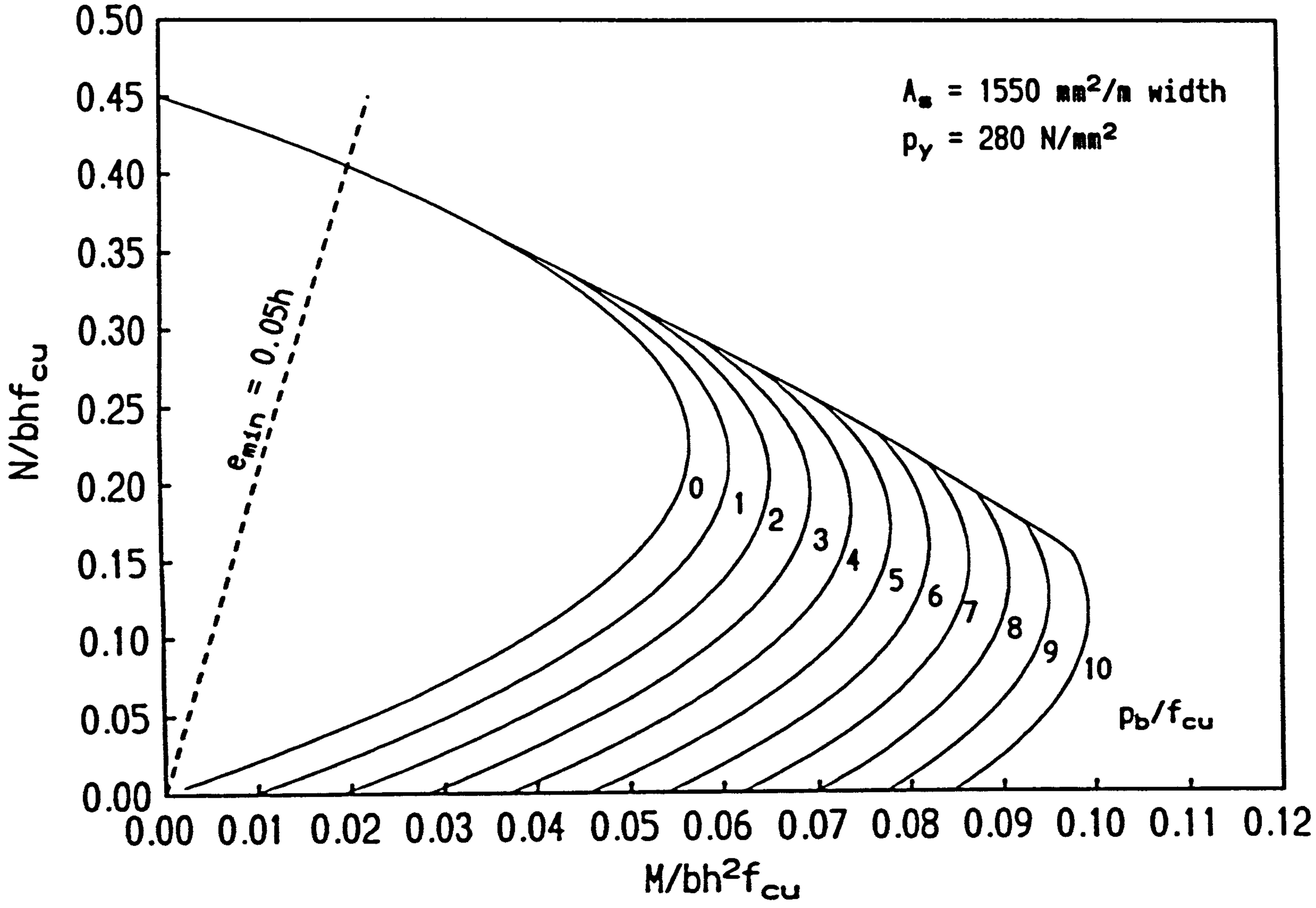

Figure 9.3

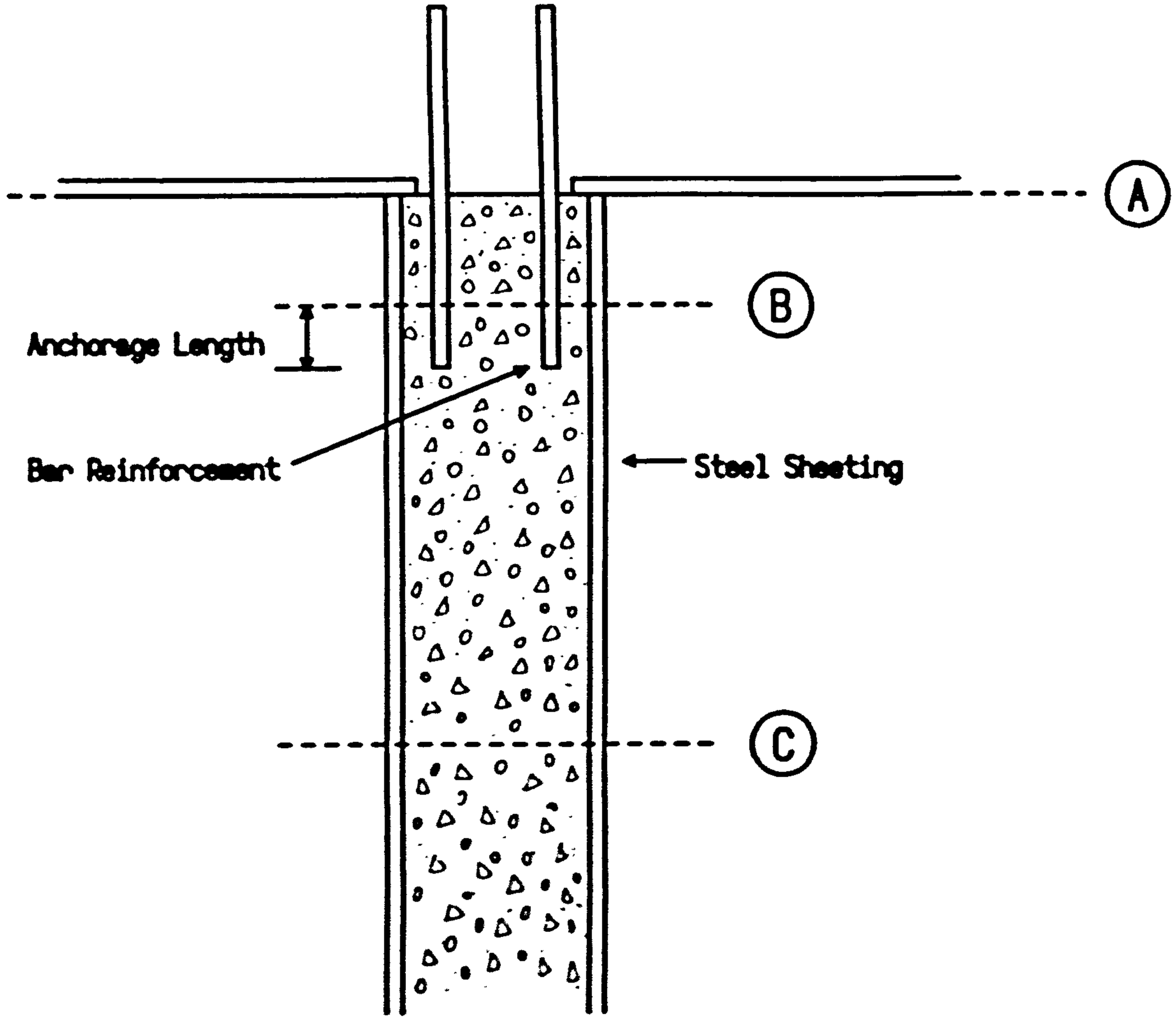

Critical Sections for Design

Figure 9.4

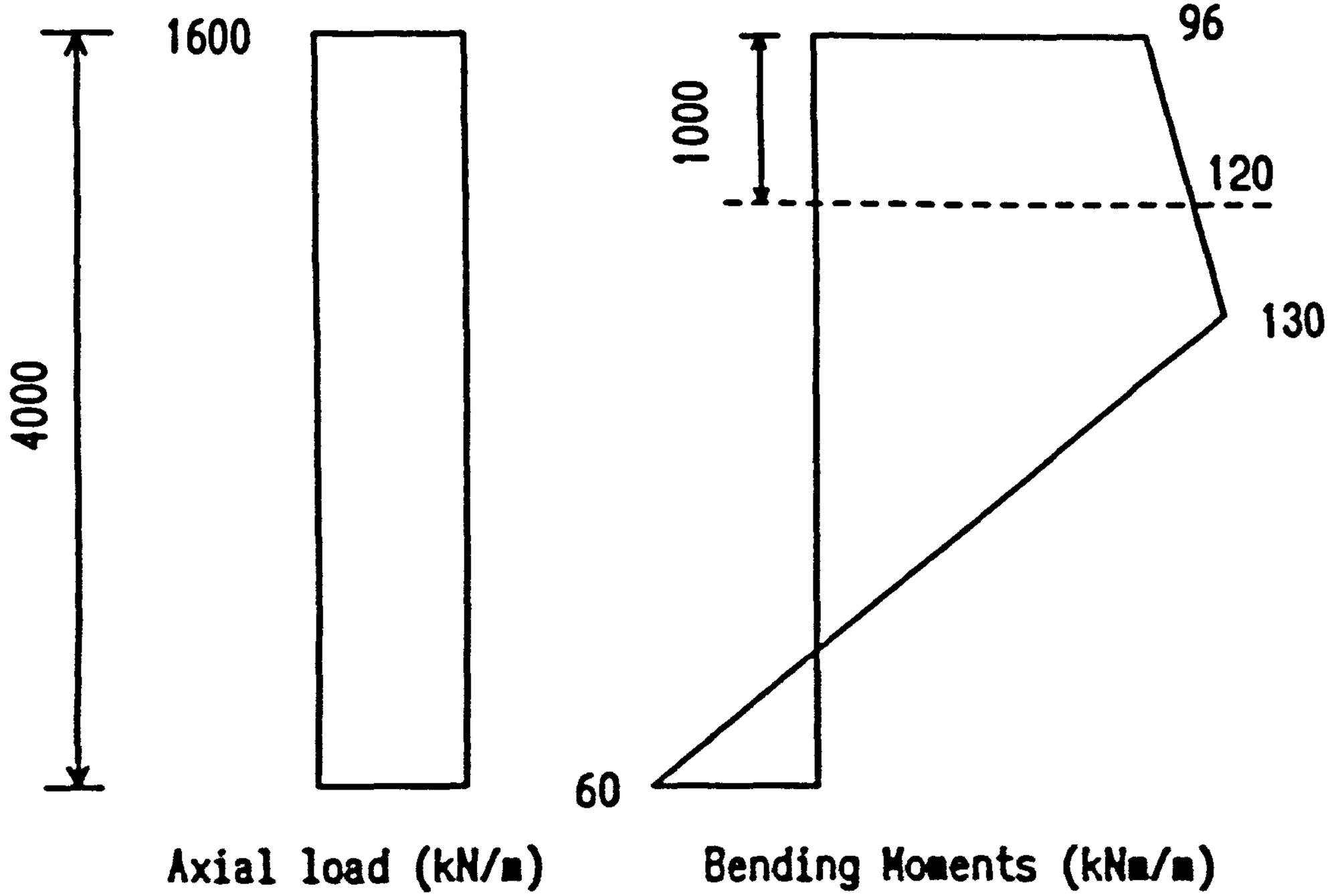

Loading Diagrams

Figure 9.5

Chapter 10 Conclusions

10.1 Introduction

This thesis has studied the viability of composite walls employing profiled steel sheeting with a concrete core. The main aspects of performance considered were

a. The performance of the steel sheeting as vertical formwork, supported by internal ties and lateral bracing, subjected to lateral concrete pressure, and

b. The behaviour of the composite walls under concentric axial loading with various heights and reinforcing details.

The investigations were initially performed on four full-scale experiments on which the lateral concrete pressures and ultimate capacities were measured. However, analytical and numerical studies followed with particular attention given to the nature of the interface bond between the steel and concrete layers. These studies gave an indication of the effects of partial interaction on the capacity of slender composite elements and the load transfer behaviour at the boundaries.

Finally, possible design methods were developed from the previous studies in line with the current British and European recommendations.

This concluding chapter will summarise the previous work from earlier chapters and detail the major findings and recommendations arising from it. Final conclusions will be present together with proposals for further investigations in this field.

10.2 Summary of Research and Main Conclusions

10.2.1 Introduction

The proposed composite walling system was introduced in Chapter 1. The main advantages of composite floor construction over traditional reinforced concrete floors were highlighted including the decreased construction time, combined permanent

formwork and reinforcement, easier services, stability, and weight reductions. The different types of decking and geometric details incorporated in the profiles to achieve interface bond were also briefly described. Based on these benefits the concept of composite walling was introduced as a logical development of composite floors with similar benefits and cost reductions over traditional reinforced walls. The possible applications of the walls were mentioned together with the few disadvantages that may be encountered in certain applications. The chapter concluded with the aims of the thesis and brief contents of the subsequent chapters.

10.2.2 Design of Loading Frame

It was essential for the axial loading tests on the composite walls that a loading frame capable of crushing the composite walls was designed and built. Chapter 2 detailed the frames construction and the various parameters affecting the final design proposal.

The main constraints on the design, that the frame be self-straining, be capable of supplying an axial load of 3000kN, and of sufficient dimension to permit the testing of slender specimens were discussed. These conditions led to a comparison of the merits of various proposals with different steelwork and hydraulic jack arrangements until a final design emerged, primarily dependent on the minimisation of cost.

The details of the selected design were mentioned with reference to the design drawings followed by mention of the shakedown trials performed to establish the performance of the loading frame was consistent with the specification. This chapter concluded by stating that the main influence on design was the limit on the total cost of £15,000 which reduced the possible design choices to a minimum.

10.2.3 Wet Concrete Tests

The experimental studies commenced in Chapter 3 with an investigation of the lateral concrete pressure produced behind the permanent formwork constructed from the Superholorib decking.

A review of previous work was initially discussed, starting with Rodin(1952) who suggested that certain factors affected the concrete pressure such as rate of pour, vibration, concrete temperature and dimensions and shape of the form. The pressure envelope he proposed is still the basis of the current design practice in United Kingdom and United States of America. Although some theoretical work was also discussed, notably by Schojdt (1955), this apparently has not receive wide acceptance due to the method's complexity and problems in determining the strength properties of fresh concrete. As a result, the design of formwork remains empirically based and dependent on many factors. The review suggested that the reason for the pressure drop behind narrow forms is not fully understood as the explanation through arching of the mix has been challenged, more recently, by the pore pressure results form Harrison (1983 A). The design recommendations of ACI Commitee 347 (1988) were found to be extremely conservative, suggesting where concrete types other than Type 1 were employed, they should be designed for the hydraulic pressure. The factors that appeared to have the greatest effect on the maximum lateral concrete pressure were considered to be the rate of placing, slump, temperature, minimum dimension and vibration depth.

The experimental investigation itself examined the lateral concrete pressures and the form deformations developed by the mix behind the permanent formwork.

A direct measurement of concrete pressure was obtained by locating a vibrating wire pressure cell approximately 200mm above the base of the 1.9m and 3.4m high walls during the casting process. The measurements of pressure at the end of each batch was plotted against the concrete head. As expected the pressure increased linearly to a maximum value before declining slightly with greater depths of concrete. The results particularly for the first two 1.9m walls showed good agreement with the CIRIA (1985) predictions. The pressures obtained from the 3.4m walls gave reduced pressures which appeared to have resulted from internal mesh and bar reinforcement directly carrying some of the mix. The results from the lateral displacement measurements showed maximum deflections of approximately 4mm occurring

between the lateral tie supports.

The chapter concluded that the system for constructing the composite walls with lateral supports secured by internal ties was reliable and could be designed according to the current CIRIA (1985) standard. The centrally located join in the profile was shown experimentally to give no problems and appeared to be self-sealing in this case.

10.2.4 Ultimate Tests

Chapter 4 described a series of four ultimate tests on the composite walls of 1.9m and 3.4m height investigating the local buckling and loss of bond at the steel-concrete interface.

A review was performed of related research including plain concrete beams reinforced by external flat steel plates, bonded to the surface with epoxy resin, or fixed with shear studs. This included both double and single skin beams and columns. Although there was no directly related experimental or analytical work found, the closest program of research appeared to be the ASP wall proposed by Yerushalmi (1988) studied for blast resistance and other applications by the United States and Israeli Military.

The initial test performed on a 1.9m composite wall showed a brittle failure between the concrete and steel surfaces with the steel slipping upwards and bearing on the loading beam. This produced local buckles in the profile at the top of the wall, as the plywood loading plate crushed under increasing load. There also appeared to be a gradual transfer of load from the concrete into the steel sheeting when moving away from the boundaries.

Although the wall showed some composite action with a ultimate load slightly greater than the concrete crushing load, the sheeting deformation and slight bursting of the concrete at the top of the wall required some modifications incorporated in the

second test.

Applying a high alumina cement mortar on the bearing surface allowed the loading of only the concrete top surface in the second test. This resulted in a lower failure load than the previous wall because after the interface failure no bearing occurred on the steel boundaries.

After the second test was performed it became clear that the reason for only the concrete crushing strength being achieved was interface bond failure between the steel sheeting and concrete faces. To prevent this mode of failure in the following 3.4m composite wall specimen mesh was welded to the ribs of the profile to provide bond in the critical boundaries of the profile.

During the third test local buckling was observed during the tests with larger strains recorded than previously observed in the first two tests. Despite the increased bond transfer failure occurred close to the top of the wall by concrete crushing at a similar load to the previous test. This was a result of the transfer of load not being sufficiently rapid to prevent concrete crushing at the boundary. This type of failure was prevented in the final test by providing bar reinforcement located internally at the ends of the wall.

The fourth test as a result achieved a maximum load with a concrete crushing failure combined with local buckling of the steel sheeting where the reinforcement terminated.

The main conclusions from this chapter were :

a. The axial loading of composite walls produces a fundamentally different response than composite slabs. If a rapid distribution of load from the concrete to the steel sheeting giving uniform strain distribution is not achieved, concrete crushing at the wall boundaries will result.

b. Local buckling of the steel sheeting between the ribs significantly reduces the ultimate capacity of the walls although this may be prevented by reducing the rib spacing or increasing the profile thickness.

c. Providing a stronger bond between the steel and concrete at the boundaries increases the rate of load transfer and prevents brittle failure of the interface bond. Unfortunately, the unstrained steel boundary condition requires the addition of internal reinforcement to prevent concrete crushing at the ends.

d. At present, composite walls may be designed with existing profiles as reinforced concrete walls if local buckling is accounted for and increased bond provided. Where this is not the case they may be designed as plain concrete walls.

10.2.5 Linear Analysis of Composite Elements

The experiments of the previous chapter revealed the lack of understanding of the interface bond behaviour in axial compressive situations, particularly where a uniform load distribution could not be assumed or achieved.

In Chapter 5 an analytical study was undertaken to obtain an understanding of the effect of partial interaction on the strain transfer, particularly at the boundaries, and also the critical buckling load of double skin composite elements.

A review of the previous work revealed that although a large amount of research had been focused on the effect of partial interaction on the lateral displacements and resulting stresses, little research had been performed on the effect of axial loading. The most relevant investigation was performed by Girhammer and Gopu (1991) who investigated the stability of composite steel/timber beam-columns.

The present analysis was performed by constructing one-dimensional linear elastic equations expressed in terms of the axial and lateral displacements in each of the

three layers. By performing a substitution, the resulting dependent differential equations were uncoupled producing two independent differential equations in γ_1 and γ_2, representing the axial and bending displacements respectively.

From these equations, solutions were derived for

1. The critical buckling load of a double skin composite element.
2. The displacements, slips, stresses and strains produced by various load boundary conditions.

Most of these equations were written in non-dimensional form, where possible, which allowed a simplification and graphical representation of complex behaviour.
From this analysis it was concluded that

a. the greater the values of interface stiffness and length, the closer the critical buckling load including partial interaction comes to the fully-interactive Euler Load.

b. if the level of interaction is low and the steel remains unloaded, the steel stress distribution is generally parabolic with a maximum stress at the centre.

c. if the level of interaction is high and the steel remains unloaded, the steel stress increases rapidly away from the boundaries until a uniform strain distribution is approached and the stress becomes constant.

d. the linear derivation of the equations was more suited to composite columns than composite walls as the brittle interface behaviour produced in the composite experiments does not appear.

10.2.6 Non-linear Analysis of Composite Elements

To obtain a better understanding of the interface behaviour of the composite walls,

a non-linear numerical model was developed in Chapter 6. The analysis incorporated non-linear material and interface behaviour, the second-order P-Δ effect, and the ability to vary the axial boundary conditions. It was also possible to include internal bar reinforcement at the boundaries.

As only simply supported members were considered the Finite Difference Method was implemented to solve the resulting system of non-linear equations. A computer program, written in Pascal named DSCW, was also written capable of incorporating various non-linear material and interface models.

The analysis was finally checked for convergence against the Newmark (1952) solution for the linear case, the Euler buckling solution for a fully composite section, and the critical buckling load, and linear stresses and strains derived in Chapter 5. The results showed that satisfactory convergence was obtained with the exact solutions.

10.2.7 Analytical and Numerical Analysis of Composite Elements

In Chapter 7, the analytical and numerical techniques developed in the previous two chapters were applied, to verify the accuracy of the non-linear modelling, and obtain a better understanding of the interface behaviour observed in the pilot tests presented in Chapter 4.

The performance of DSCW was shown to be particularly accurate when analyzing the behaviour of a double skin composite beam previously tested by Oduyemi and Wright (1988). However, when comparing the DSCW analysis with a double skin beam/column results, there were significant differences. This was considered a consequence of the complicated boundary conditions existing at the ends of the beam/column, which to accurately model were impossible.

The second, third and fourth composite wall tests were then examined by constructing a numerical model of a single bay with non-linear steel, concrete and

various interface relationships. These analyses suggested that

a. the program DSCW is unsuitable for analysis, in conditions where a brittle failure occurs followed by a large drop in interface capacity.

b. the interface failure observed during the axial capacity tests was a brittle chemical failure with the large ductile capacity of the profile never mobilised.

c. welding mesh to the profile ribs reduces the effects of the brittle interface failure but increases the distance from the ends required to produce a uniform strain distribution.

d. internally reinforcing the ends of the walls prevented concrete crushing at the ends increased the effective stiffness reducing the amount of load transferred in this portion.

A further investigation, with the equations developed in Chapter 5, gave an indication of the interface behaviour on the buckling capacity of the composite walls. This suggested that

e. the buckling capacity of this type of composite wall would be reduced by interface slip between the concrete and steel faces.

f. if the brittle failure at the interface was ignored the ductile response observed in composite slab tests would not increase the axial capacity.

10.2.8 Design of Double Skin Composite Columns

Although the work contained in this thesis was primarily directed towards studying the behaviour of composite walls, the research also had a direct bearing on the design of double skin composite columns.

In Chapter 8 a review was performed of the design methods in the current codes of practice concerning the design of composite columns. This indicated that the current methods make no attempt to estimate the effects of partial interaction, where a full connection is not achieved.

Possible design methods were therefore proposed, allowing inclusion of the effects of partial interaction in the design of connections and estimation critical buckling capacity. The reductions proposed, accounting for member slenderness were in accordance with the methods currently applied in the European and American Standards.

Although these methods were fully justified from the analytical studies it was suggested that further work by experimentation was required to verify the effectiveness and accuracy.

10.2.9 Design of Composite Walls

Chapter 9 assembled the finding from the experimental, analytical and numerical studies carried out and suggested a possible design method based on the requirements of BS 8110 with some modifications.

The main assumptions of the proposed method were that

a. the steel in compression was assumed to have no capacity.

b. the steel in tension was fully mobilised.

c. the design strength at a particular section could be based on a limiting bond stress and anchorage length resistance of the profile.

Three critical design sections were identified for a composite wall spanning a single bay height.

The effects of slenderness on composite walls were accommodated by modifying the current BS 8110 equations to reflect the fact, that composite elements normally deflect to greater curvatures before ultimate failure.

The chapter concluded by suggesting that limiting the axial strength to only the compressive strength of the concrete would be a significant drawback although the option of welded mesh at the boundaries would increase the unit costs.

10.3 Viability of the Composite Walling Concept

This thesis has endeavoured to answer the following question;

" Is the idea of composite walling a viable concept, offering similar benefits over traditional construction, to those seen in composite slabs ? "

The experiments performed suggest that from an ease of construction standpoint, composite walls could be easily constructed without requiring a highly skilled labour force to assemble the permanent formwork. The casting would be no more difficult than suggested by the tests, as the steel sheeting provides reliable formwork with little leakage, as the profile joins are self-sealing. In practice trapezoidal sections would allow greater distances between the lateral supports than the Superholorib decking in the experiments. The lateral pressures envelope developed by the fresh concrete behind the formwork could be designed in accordance with the current CIRIA (1985) method which proved reasonably accurate during the wet concrete tests. The steel sheeting, once fixed in position, would provide windbracing and stability to steel frames bays before casting and subsequent hardening of the concrete.

Unfortunately, these are not the only factors considered in assessing the feasibility of concept. The structural performance of the composite walls must also be considered in any evaluation.

In the investigation, ultimate tests and theoretical studies have clearly shown the

brittle interface connection between the steel and concrete surfaces. The nature of the axial loading is to produce brittle chemical failure at the interface, with complete loss of bond, without sufficient strain to mobilise the strong ductile force developed by the embossments.

This produces four alternative approaches to the design of composite walls.

The first option is to assume the steel sheeting provides no structural support to the wall, serving as permanent formwork during the construction of the wall and perhaps providing an aesthetically pleasing finish. Although this option is possible, it is likely to be unacceptable in practice, where it would be perceived as expensive permanent formwork.

The second possibility is to allow the steel sheeting to provide external reinforcement on only the tension face as the strain may be sufficient at the ultimate state to mobilise the ductile strength. This solution provides some increase in the bending capacity but does not provide any increase in axial capacity under concentric loading.

The third choice is to weld mesh and fix internal reinforcement to the ends of the steel sheeting, providing a sufficient increase in bond strength, to obtain the full axial and bending capacity of the wall. The main drawback is the increased cost of production from fixing the mesh and reinforcement to the profile surfaces.

The fourth and final option is to design a profile capable developing a ductile response preventing concrete crushing results on the bearing surface. Although an increase in the interface bond is possible, it is not likely in this authors opinion, to be increased to an extent where concrete crushing at the boundaries is prevented. It may therefore still be necessary to provide internal bar reinforcement at the ends of the wall.

Overall the best solution is that proposed in option four as the maximum performance

would be achieved without the increase in the labour cost seen in the third proposal. At present with only four pilot tests performed it is difficult suggest firm design guidance for composite walls, but there is no reason at this stage in the research process, to suspect that the it is fundamentally impossible. It is obvious that further tests are desirable and these are currently being undertaken at Strathclyde University.

10.4 Future Tests

Although, the work contained in this thesis provides a platform for understanding the behaviour of composite walls, it is important to recognise those areas, in this author's opinion, requiring further research.

The critical feature identified by the pilot tests and subsequent theoretical studies was the apparent brittleness of the interface bond between the steel and concrete surfaces. This reduced the axial capacity of the walls to the concrete compressive strength permitting no structural benefit from the steel sheeting. Though the later experiments avoided this problem, by fixing internal reinforcement and mesh to the profile surface, more effective solutions may be possible. It would be of some benefit to perform push-out tests on various profiles and investigate the relationship between the brittle and ductile behaviour under displacement control.

One potential solution, requiring further study, is the possibility of applying epoxy resin to the steel surfaces close to the boundaries, providing a sufficiently high increase in bond strength, to prevent failure at the loading point.

Alternatively, other research may be conducted towards finding a simple method of providing a mechanical connection between the steel and concrete surfaces. This may be performed by locating alternative types of connectors or embossments in critical areas.

The other major cause of the reduction in capacity during the tests was local buckling of the steel sheeting between the re-entrant ribs. This failure mode, in this authors

view, is more readily prevented but perhaps further work may be conducted into finding the correct geometry and rib spacing to allow the steel sheeting to obtain yield before buckling under the compressive stress. The performance of various profile geometries is also of interest.

Further tests on composite walling funded by the Science and Engineering Research council are currently in progress investigating a larger variety of profiles under different loading conditions. This work will include a study of composite walls under combined axial and bending conditions and the effects of slenderness on axial capacity.

A study concerning the capacity of the composite walls under in-plane shear was outwith the scope of this thesis, but is currently under study at Strathclyde University. This work should provide information on the suitability of composite walls as shear walls, particularly in steel framed buildings. It is possible that similar problems to those encountered in this thesis due to brittle interface failure and local buckling may occur, although the interface behaviour will be more complicated. Openings in composite shear walls, to permit services and access need to be studied, not only structurally but also from a constructional standpoint as well.

Finally, a cost comparison between composite and traditional reinforced concrete walls, considering the various factors affecting the overall construction cost must be undertaken at some stage. There must be some justification for the system, from considering the total costs, otherwise the system will never find a market in the construction industry.

References

Abdel-Sayed, G., Composite cold-formed steel-concrete beams, Proc. ASCE Journal of the Structural Division, Vol. 108, No. ST11, November 1982.

Abdel-Sayed, G. and Chung, K., Composite cold-formed steel-concrete columns, Canadian Journal of Civil Engineering, 14, pp. 295-301, 1987.

ACI, Buildign Code Requirements for Reiunforced Concrete (ACI 318-83), Detroit, MI, 1983.

ACI Committee 347, Pressures on formwork, ACI Journal **30**(2), 1958.

ACI Committee 347, Guide to Formwork for Concrete, ACI Structural Journal, pp. 530-562, September-October 1988.

American Institute of Steel Construction, LRFD Specifications for the Design, Fabrication and Erection of Structural Steel for Buildings, Chicago IL, 1986.

Ansourian, P., and Roderick, F., Analysis of composite beams, Proc. ASCE Journal of the Structural Division, **104** (ST10), October 1978.

Arizumi, Y., Hamada, S. and Kajita, T., Elastic-plastic analysis of composite beams with incomplete interaction by finite element method, Computers and Structures, Vol.14, No. 5-6, pp. 453-462, 1981.

Basu, A.K. and Sommerville, W., Derivation of formulae for the design of rectangular composite columns, Proc. Instn Civ. Engrs, **Suppl.**, pp. 233-380, 1969.

Benson, A.S. and Mayers, J., General instability and face wrinkling of sandwich

plates - Unified theory with applications, AIAA, Vol 5, No. 4, pp. 729-739, April 1967.

Bresson, J., Reinforcement par collage d'armatures du passage inferieur due CD 126 sous l'autoroute du sud. Annales de L'institute technique du batiment est dus travaux publics, supplement au No. 297, serie Beton-Beton Arme, No. 122, 1-30, September 1972.

British Standards Institution, BS 5400, Concrete and Composite Bridges, Part 5, Code of Practice for Design of Composite Bridges, London 1979.

British Standards Institution, BS 5950, Strutural use of steelwork in building, Part 4, Code of practice for design of floors with profiled steel sheeting, London 1982.

British Standards Institution, BS 5950, Strutural use of steelwork in building, Part 5, Code of practice for design in cold formed sections, London 1987.

British Standards Institution, BS 8110, Structural use of concrete, London 1985.

CIRIA. The pressure of concrete on formwork. Civil Industries Research and Information Association. London. England. Research Report No. 1

Clear, C.A., and Harrison, T.A., Concrete pressure on formwork, CIRIA Report No. 108, Concrete Industry Research and Information Association, London, 32 pp, 1985.

Daniels, B.J., Shear bond pull-out tests for cold-formed-steel composite slabs, Rapport d'essais, publication ICOM 194, Juin 1988.

Douglas, B., Saiidi, M., Hayes, R. and Holcomb, G., Field measurement of lateral pressures of concrete wall forms. Concrete International, 56-62, November 1981.

European Convention for Constructional Steelwork, Composite Structures, Chapter 16 Composite Columns, 1985.

Eurocode 4, Composite Steel and Concrete Structures, Final Draft, 1992.

Gardner, N.J., Concrete pressure on formwork. Proc. Instn Civ. Engrs., 145-159, Part 1, 80, February 1986.

Gardner, N.J., Formwork pressures and cement replacement by fly ash. Concrete International, 50-55, October 1984

Gardner, N.J., Pressure of concrete against formwork. ACI Journal, 279-286, July-August 1980.

Gardner, N.J. and Ho, P.T.-J., Lateral pressure of fresh concrete. ACI Journal, 76 No.7, 809-820, July 1979.

Gardner, N.J. and Quereshi, A.R., Internal vibration and the lateral pressure exerted by fresh concrete. Canadian Journal of Civil Engineering, 592-600, 6, 1979.

Girhammar, U.A. and Gopu, V.K.A., Analysis of P-Δ effect in compoiste concrete/timber beam-columns, Proc. Instn Civ. Engrs, Part 2, 91, pp. 39-54, Mar. 1991.

Hamoush, S.A, and Ahmad, S.H., Debonding of steel plate-strengthened concrete beams. Journal of Structural Engineering ASCE, Vol 116, No.2, February 1990.

Harrison, T.A., Form pressures : theory and field measurements. Concrete International, 23-28, December 1983.

Harrison, T.A., Formwork pressures. Concrete, 27-29, May 1983.

Hirst, M.J.S. and Yeo, M.F., The analysis of composite bemas using standard finite element programs, Computers and Structures, Vol. 11, pp. 233-237, 1980.

Johnson, R.P. and Molenstra, N., Partial shear connection in composite beams for buildings, Proc. Instn Civ. Engrs, Part 2, **91**, pp. 679-704, 1991.

Kountouris, G., Design charts for double skin composite elements. Dissertation, University of Wales College of Cardiff, April 1990.

L'Hermite, R. and Bresson, J., Beton arms d'armatures colles. Rilem colloque international, theme 2, Paris, September 1967.

Lerchental, C.M., Bonded Sheet metal reinforcement for concrete slabs. Rilem bulletin, 263-270. December 1967.

Levitsky, M., Form pressure and relaxation in formwork. Journal of the Engineering Mechanics Division, ASCE, 267-277, Vol. 101, N0. EM3, June 1974

MacDonald, M.D., The flexural behaviour of concrete beams with bonded external reinforcement. Transport and Road Research Laboratory supplementary report 415. Crowthorne England 1978.

Mays, G.C. and Smith, D.W., Slab of the future. Concrete, pp. 13-16, June 1980.

Narayan N., Wright H.D., Evans H.R. and Francis R.W., Double skin composite construction for Submerged Tube Tunnels. Steel Construction Today, **1**, pp. 187-189, 1987.

Newmark, N.M., Siess, C.P. and Viest, I.M., Tests and Analysis of Composite Beams with incomplete interaction, Proc. Soc. Exper. Stress Analysis, 9(1), pp. 75-92, 1951.

Oduyemi, T.O.W. and Wright, H.D., The behaviour of Double Skin Composite Beams. Report DS1, University of Wales College of Cardiff 1988.

Oduyemi, T.O.W. and Wright, H.D., The behaviour of double skin composite columns, Report DS2, University of Wales College of Cardiff 1989.

Oduyemi, T.O.W. and Wright, H.D., The behaviour of Double Skin Composite Beam-columns, Report DS3, University of Wales College of Cardiff 1990.

Ong, K.C.G., Mays, G.C. and Cusens, A.R., Flexural tests of steel-concrete open sandwiches. Magazine of concrete research, Vol. 34, No. 120, 130-138, September 1982.

Patrick, M., The slip block test - experience with some overseas profiles (part A), Melbourne Research Laboratories, BHP Research and New Technology, Australia, June 1990.

Plum, D.R. and Horne, M.R., The analysis of continuous composite beams with partial interaction, Proc. Instn Civ. Engrs, Part 2, 59, pp. 625-643, Dec. 1975.

Roberts, T.M., Finite Difference Analysis of Composite Beams with Partial Interaction. Computers and Structures, Vol 21, No. 3, pp.446-473, 1985

Rodin, S., Pressure of concrete on formwork. Proc. Instn. Civ. Engrs. Paper No. 5863, Part 1 (6), 709-746, 1952.

Schjodt, R., Calculation of pressure of concrete on forms. Proc. ASCE, 81, Paper No. 680, 1-16, 1955.

Solomon, S.K., Smith, D.W. and Cusens, A.R., Flexural tests of steel-concrete-steel sandwiches. Magazine of concrete research, Vol 28, No. 94, 13-20, March 1976.

Schuster, R.M., Composite steel-deck concrete floor systems. Proc. ASCE Journal of the Structural Division, **102** (ST5), pp. 899-917, 1976.

Taylor, R., Composite reinforced concrete. Concrete, pp. 23-25. August 1976.

Taylor, R., Mills, P.E. and Rankin, R.I., Tests on concrete beams with mixed types of reinforcement. Magazine of concrete research, Volume 30, No. 103, pp. 73-88, June 1978.

Viest, I.M., Review of Research on Composite Steel-Concrete Beams. Proc. ASCE Journal of the Structural Division, 86 (ST6), pp. 1-21. June 1960.

Wegmuller, A.W. and Amer, H.N., Nonlinear Responce of Composite Steel-Concrete Bridges, Computers and Structures, Vol. 7, pp. 161-169, 1977.

Wright, H.D., The buckling of long thin plates in contact with a rigid medium. Technical report HDWB1, University of Wales College of Cardiff, UK, 1989.

Wright, H.D., The use of Profiled Steel Sheeting in Floor Construction. Journal of Constructional Steel Research, 7, pp. 279-295, 1987.

Wright, H.D. and Oduyemi T.O.S., partial interaction analysis of double skin composite beams, to be published

Wright, H.D., Oduyemi T.O.S. and Evans, H.R., The design of double skin composite elements. Journal of Constructional Steel Research, 19, pp. 111-132, 1991.

Yam, L.C.P. and Chapman, J.C., The inelastic behaviour of simply supported composite beams of steel and concrete, Proc. Inst. Civ. Engrs, 41, pp. 651-683, 1968.

Yarushalmi, Y., Tests performed on the ASP construction system. The ASP Group, Washington D.C.

Bibliography

Allen, H.G. and Bulson, P.S., Background to Buckling, McGraw-Hill Book Company (UK) Limited, London 1980.

Bathe, K.J., Finite element procedures in engineering analysis, Prentice-Hall Inc. Englewood Cliffs, New Jersey, 1982.

Fung, Y.C., Foundations of Solid Mechanics, Prentice-Hall Inc. Englewood Cliffs, New Jersey, 1965.

Greenberg, M.D., Advanced Engineering Mathematics, Prentice-Hall Inc. Englewood Cliffs, New Jersey, 1988.

Hilderbrand, F.B., Advanced Calculus for Applications, Prentice-Hall Inc. Englewood Cliffs, New Jersey, 1976.

Johnson, R.P., Composite structures of steel and concrete, volume one, Crosby Lockwood Staples, London 1975.

Kong, F.K. and Evans, R.H., Reinforced and Prestressed Concrete, Van Nostrand Reinhold (UK) Co. Ltd, 3rd edition, 1987.